

Novel High Capacity Oligomers for Low Cost CO₂ Capture

Final Technical Report

Reporting period: 10-01-08 to 09-30-10

Robert J. Perry
Teresa A. Grocela-Rocha
Michael J. O'Brien
Sarah Genovese
Benjamin R. Wood
Larry N. Lewis
Hubert Lam
Malgorzata Rubinsztajn
Grigorii Soleveichik
Sergei Kniajanski

December 2010

Department of Energy

DE-NT0005310

GE Global Research, 1 Research Circle, Niskayuna, NY 12309

Robert M. Enick, J. Karl Johnson, Hong-bin Xie, Deepak Tapriyal, Department of
Chemical and Petroleum Engineering, University of Pittsburgh, Pittsburgh, PA,
15261

Sam Draper, Ravi-Kumar Vipperla, GE Energy, 300 Garlington Road, Greenville, SC,
29615

Disclaimer

This report was prepared as an account of work sponsored by an agency of the United States Government. Neither the United States Government nor any agency thereof, nor any of their employees, makes any warranty, express or implied, or assumes any legal liability or responsibility for the accuracy, completeness, or usefulness of any information, apparatus, product, or process disclosed, or represents that its use would not infringe privately owned rights. Reference herein to any specific commercial product, process, or service by trade name, trademark, manufacturer, or otherwise does not necessarily constitute or imply its endorsement, recommendation, or favoring by the United States Government or any agency thereof. The views and opinions of authors expressed herein do not necessarily state or reflect those of the United States Government or any agency thereof.

Abstract

The novel concept of using a molecule possessing both physi-sorbing and chemi-sorbing properties for post-combustion CO₂ capture was explored and mixtures of aminosilicones and hydroxy-terminated polyethers had the best performance characteristics of materials examined. The optimal solvent composition was a 60/40 blend of GAP-1/TEG and a continuous bench-top absorption/desorption unit was constructed and operated. Plant and process models were developed for this new system based on an existing coal-fired power plant and data from the laboratory experiments were used to calculate an overall COE for a coal-fired power plant fitted with this capture technology. A reduction in energy penalty, from 30% to 18%, versus an optimized 30% MEA capture system was calculated with a concomitant COE decrease from 73% to 41% for the new aminosilicone solvent system.

Table of Contents

Title Page	1
Disclaimer	2
Abstract	2
Table of Contents	3
Executive Summary	4
Report Details	6
Introduction	6
Budget	6
Task 1.0 Project management	7
Task 2.0 Screening and Selection of Solvent Classes for CO ₂ Capture	7
Subtask 2.1 Proposed Solvent Classes	8
Subtask 2.2 Selection of Solvent Classes	11
Subtask 2.3 Multi-property Determination of Available Solvents	21
Subtask 2.4 Synthetic Strategy Development	32
Task 3.0 CO ₂ Capture Solvent Synthesis, Optimization and Property Testing	33
Subtask 3.1 High Throughput Method Development and Synthesis	33
Subtask 3.2 Evaluation of Selected Properties	40
Subtask 3.3 Multi-property Modeling of Lead Candidates	47
Subtask 3.4 Multi-property Determinations	47
Subtask 3.5 Bench-scale Lead Solvent Performance Evaluation	58
Subtask 3.6 Degradation/Environmental Testing	65
Task 4.0 Process Modeling and COE Services	66
Conclusions	80
References	81
List of External Presentations	83
List of filed patent applications	83
List of External Articles	83
List of Acronyms	84
Appendix 1 ChemSusChem paper	
Appendix 2 Literature Review	
Appendix 3 MEA Reaction Modeling	
Appendix 4 Plant Oil Experiments	
Appendix 5 Details of Disiloxane Syntheses	
Appendix 6 Aminosilicone Heats of Reaction Modeling	
Appendix 7 MEA Baseline COE Optimization	
Appendix 8 J. Phys. Chem. A paper	

Executive Summary

The novel concept of using a molecule possessing both physi-sorbing and chemi-sorbing properties for post-combustion CO₂ capture was explored. A variety of candidate materials with physi-sorbing backbones and chemically reactive peripheral groups were considered with the final selection primarily focusing on aminosilicones. A small effort was also devoted to derivatized plant oils.

None of the plant oil derivatives were effective in absorbing CO₂ in laboratory experiments. Model reactions suggest that both intra-molecular H-bonding between adjacent hydroxyl and amino groups and potential micelle formation suppressed reactions with CO₂. This route was abandoned in favor of the aminosilicones.

A variety of aminosilicones with differing architectures and type and placement of amine groups were examined both experimentally and computationally for physical properties as well as CO₂ capture efficacy. Modeling indicated that the heat reaction of sterically hindered amines with CO₂ was lower than for unhindered amines and that less basic amines also decreased the heat of reaction. This provided options to tune the heat of reaction for optimal plant performance. Physical property predictions were also made for viscosity, vapor pressure, density and CO₂ solubility. Limited experimental data confirmed the accuracy of the density and solubility models as well as trend predictability in heats of reaction. However, viscosity predictions were not accurately modeled and vapor pressure data was unavailable.

Synthetically, GEN 1 aminosilicone solvents with linear, branched, cyclic and star architectures were made that possessed mono and di-amine groups while other solvent candidates had varying degrees of steric hindrance. Oligomers as well as discrete small molecules were prepared and evaluated. These included solvents with covalently bound polyether units. CO₂-capture experiments were performed using both high throughput screening (HTS) techniques as well as small-scale laboratory testing. Mass transfer issues prevented the HTS methodology from being as useful as anticipated. However, efficient mixing on the lab-scale provided reliable data. These experiments also showed that pure solvents did not maintain their desired liquid state on exposure to CO₂. To circumvent this problem, a co-solvent was added. The optimal co-solvent was triethylene glycol (TEG). This material prevented solids formation upon generation of the carbamate salts.

Lab-scale experiments indicated that the aminosilicone designated as GAP-0 provided a CO₂-capture capacity in a 50/50 mixture with TEG commensurate with 30% MEA. Lab-scale absorption and desorption experiments showed complete reversibility of the reaction with CO₂ over several cycles and isotherm data generated indicated a dynamic range (equivalent to net CO₂ loading) of CO₂-capture of 5-6%. This solvent composition was scaled-up and used for further studies.

A continuous absorption system as well as a bench-scale, continuous absorption/desorption system was designed and assembled to validate the lab results seen. Under comparable conditions, the continuous absorber system showed a CO₂ absorption efficiency of >99% for both 50% GAP-0 and 30% MEA. Mass transfer coefficients for that system were of the same order of magnitude. The continuous absorption/desorption system functioned well and provided some initial information on the GAP-0/TEG mixture. However, solid formation during continuous operation was a serious issue. This problem was circumvented by the designed the GEN 2 solvent designated as GAP-1. A 60/40 blend of GAP-1/TEG allowed continuous operation of the absorber/desorber unit with no solid precipitation. Absorption of CO₂ occurred as expected in this system but desorption under pressure was less than expected with a dynamic range of 2.6%.

Corrosion studies comparing 30% MEA and 50% GAP-0 were also conducted and showed that the aminosilicone was equivalent or superior to the organic amine over 3000 hours. Thermal aging at 100 and 120 °C of both GAP-0 and GAP-1 showed little degradation of the materials over 80 days.

Plant and process models were developed for this new system based on an existing coal-fired power plant. Operations taken into account included the steam island, coal handling, boiler and air as well as the environmental treatments and a CO₂ separation unit. Assuming absorber and desorber temperatures and pressures that mimicked the lab-scale continuous system, and using a 60/40 GAP-1/TEG solvent mix, COE and energy penalty calculations showed a reduction in energy penalty from 30% to 18% and a COE decrease from 73% for an optimized 30% MEA base case to 41% for the new aminosilicone solvent system.

Report Details

Introduction

The overall thrust of this program was to develop a novel oligomeric solvent and process for the post-combustion capture of CO₂ from coal fired power plants with 90% carbon capture efficiency, a 25% increase in the capture capacity of CO₂ compared with a 30% aqueous MEA system and less than 35% increase in the cost of energy services. This entailed numerous operations including: identification and modeling of a novel class of capture solvents, synthesizing the materials, developing a screening protocol, evaluating CO₂ capture performance, measuring key physical properties, demonstrating continuous absorption/desorption ability and generating accurate plant and process models with the ultimate goal of assembling a predictive cost of electricity (COE) model to determine the quality of the new solvent system.

These actions were grouped into three tasks. The first was selection and screening of solvent classes. This included identification of the unique solvents, proposed synthetic pathways to make the materials, initial screening for CO₂ absorption and molecular modeling to suggest alternate chemistries to pursue. The second task focused on solvent syntheses, high throughput screening (HTS) of materials, modeling of solvent properties and identification and bench scale evaluation of a down-selected solvent. The final task was building a calibrated power plant model and coupling that to a newly developed process model that would be used to predict the COE of a plant fitted with the new CO₂ capture technology.

This new capture technology was based on the concept of using a non-aqueous solvent that possessed both physical and chemical absorbing properties and had significantly higher boiling point than 30% MEA as well as greater thermal stability. These and other factors were anticipated to result in a substantially lower COE.

Budget

Table 1. Program Budget.

	BP1			BP2			Total		
	Gov't Funding	Cost Share	Total	Gov't Funding	Cost Share	Total	Gov't Funding	Cost Share	Total
GE Global Research	\$982,676	\$317,600	\$1,300,276	\$745,436	\$236,302	\$981,738	\$1,728,112	\$553,902	\$2,282,014
CE Energy	\$241,948	\$0	\$241,948	\$253,102	\$0	\$253,102	\$495,050	\$0	\$495,050
Univ. of Pittsburgh	\$174,553	\$32,194	\$206,747	\$75,447	\$32,194	\$107,641	\$250,000	\$64,388	\$314,388
Total	\$1,399,177	\$349,794	\$1,748,971	\$1,073,985	\$268,496	\$1,342,481	\$2,473,162	\$618,290	\$3,091,452

Baseline Reporting Quarter	Year 1								Year 2							
	Q1		Q2		Q3		Q4		Q1		Q2		Q3		Q4	
	10/1/08 - 12/31/08	1/1/09 - 3/31/09	4/1/09 - 6/30/09	7/1/09 - 9/30/09	10/1/09 - 12/31/09	1/1/10 - 3/31/10	4/1/10 - 6/30/10	7/1/10 - 9/30/10	10/1/09 - 12/31/09	1/1/10 - 3/31/10	4/1/10 - 6/30/10	7/1/10 - 9/30/10	10/1/09 - 12/31/09	1/1/10 - 3/31/10	4/1/10 - 6/30/10	7/1/10 - 9/30/10
Baseline Cost Plan	Q1	Total	Q2	Total	Q3	Total	Q4	Total	Q1	Total	Q2	Total	Q3	Total	Q4	Total
Federal Share	238,305	238,305	378,564	617,889	387,179	1,005,068	394,109	1,399,177	266,938	1,666,115	283,722	1,929,837	269,199	2,199,036	274,126	2,473,162
Non-Federal Share	59,576	59,576	94,896	154,472	96,795	251,267	98,527	349,794	66,735	416,529	85,930	482,459	67,300	549,759	88,531	618,290
Total Planned	297,881	297,881	474,480	772,361	483,974	1,256,335	492,636	1,748,971	333,673	2,082,644	329,652	2,412,296	336,499	2,748,795	342,657	3,091,452
Actual Incurred Cost																
Federal Share	194,157	194,157	437,262	631,419	367,960	999,379	298,869	1,298,248	201,354	1,499,602	163,842	1,663,444	526,978	2,190,422	279,039	2,469,455
Non-Federal Share	48,539	48,539	109,316	157,855	91,990	249,845	67,217	317,062	50,338	367,400	40,961	408,362	131,745	540,107	69,760	609,867
Total Incurred Costs	242,696	242,696	546,578	789,274	459,950	1,249,224	336,087	1,615,310	251,692	1,867,002	204,803	2,071,805	658,723	2,730,529	348,799	3,079,328
Variance																
Federal Share	(44,148)	(44,148)	57,678	13,530	(19,219)	(5,689)	(95,240)	(100,929)	(65,584)	(166,513)	(99,880)	(266,393)	257,779	(8,614)	4,913	(3,707)
Non-Federal Share	(11,037)	(11,037)	14,422	3,383	(4,805)	(1,422)	(31,358)	(32,732)	(16,397)	(49,129)	(24,969)	(74,097)	64,445	(9,652)	1,229	(8,423)
Total Variance	(55,185)	(55,185)	72,098	16,913	(24,024)	(7,111)	(156,549)	(133,661)	(81,891)	(215,642)	(124,849)	(340,491)	322,224	(18,266)	6,142	(12,124)

Total funding for this program was approximately \$3.1 MM including a 20% cost share contributed from each of the participating entities as seen in Table 1. Quarterly variances in spending were due to non-harmonized accounting practices between GE GRC, GEE and U Pitt. However, these mismatches

were anticipated and were fully accounted for by the end of the program. Table 1 indicates that the program was under-spent by \$136M at the end of September 2010. However, fourth quarter report writing and report-outs at conferences brought this number to \$12K which was within 0.4% of the original budget amount.

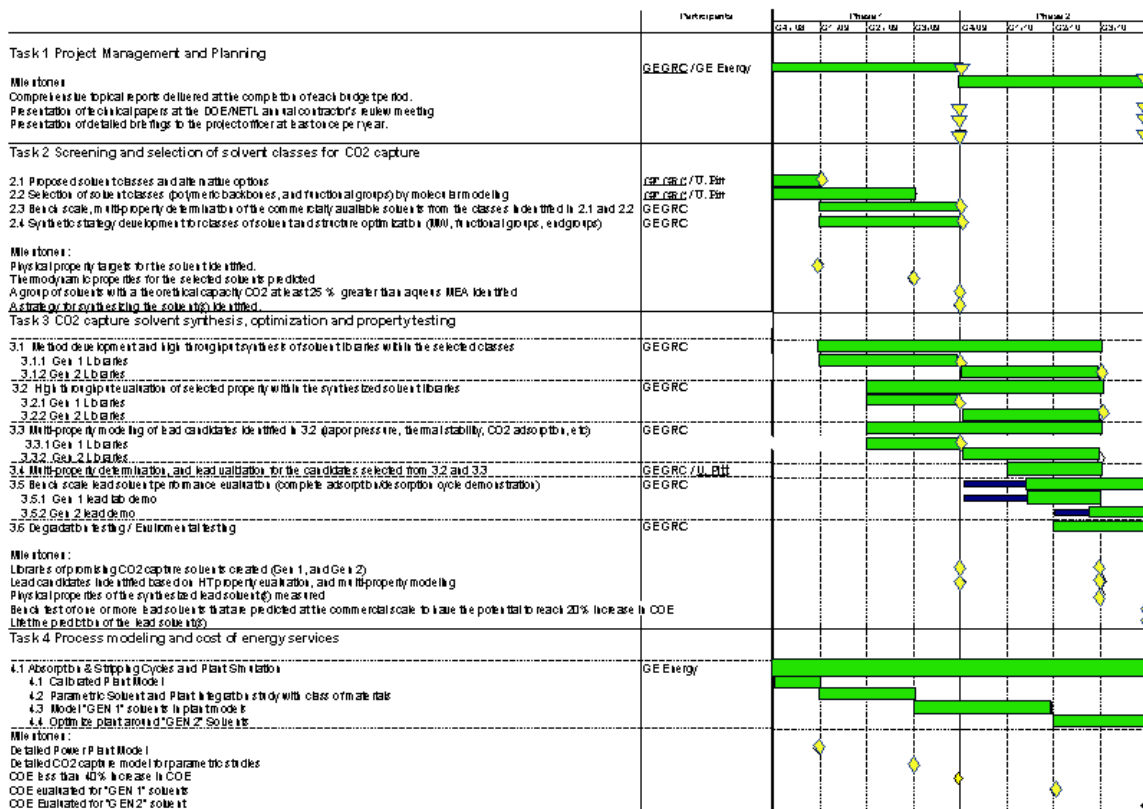


Figure 1. Program Timeline

As seen from the program timeline in Figure 1, numerous activities overlapped and were run in parallel. This final report is organized by task and subtask and as such some results discussed in one section may be founded on data that will be revealed in a subsequent section.

Task 1.0 (Project Management)

This program delivered 8 technical progress reports, one at the end of each quarter of this project. In addition, at the end of budget period (BP) 1 an annual report for continuation of funding was submitted. Numerous seminars were given based on this work which included oral presentations at the 2010 Spring ACS Meeting, 43rd Silicon Symposium, two talks at the 2010 Fall AIChE Annual Meeting and two at the PacifiChem 2010 Congress. In addition, several papers have been published or have been submitted to refereed journals such as ChemSusChem, Journal of Organic Chemistry and Journal of Physical Chemistry, A. A high level review of the program and preliminary experimental results were published in ChemSusChem and are included in Appendix 1. Finally, four patent applications have been filed based on this chemistry and process.

Task 2.0 (Screening and Selection of Solvent Classes for CO2 Capture)

Subtask 2.1 (Proposed solvent classes and alternative options)

A prerequisite for undertaking this program was an understanding of the technologies and chemistries currently employed and being researched in the field of post-combustion capture of CO₂. To this end, a comprehensive search of the open and patent literature was performed. This literature study revealed a sharp rise in activity on liquid CO₂ absorbents through 2007 (Figure 2) with much of the activity centered in Asia and Europe with Mitsubishi Heavy Industries, Alstom and BASF deeply engaged in solvent-based capture technology. (The entire report can be found in Appendix 2). Analysis of this information indicated that our proposed concept of using a material that would possess both chemical and physical absorbing properties had not been reported.

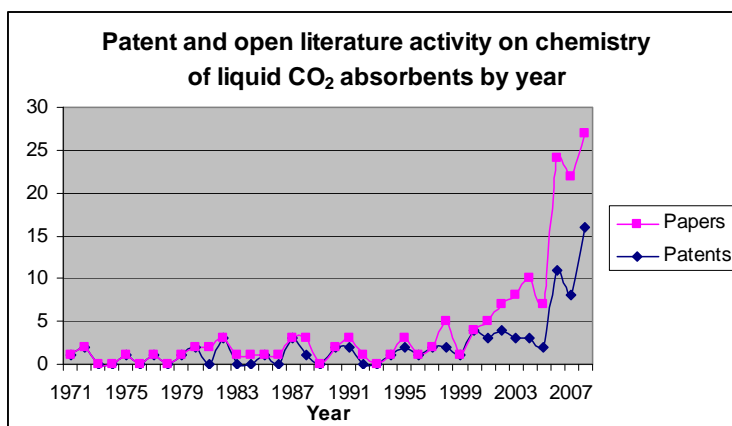


Figure 2. Patent and open literature activity on chemistry of liquid CO₂ absorbents.

A variety of solvent types consisting of various backbones (or core structures) known for CO₂-philic properties and functionalities capable of reacting with CO₂ were considered as candidates for investigation. Table 2 shows the Quality Function Deployment (QFD) matrix employed to down-select the backbones considered most promising. Parameters considered important were low viscosity liquids, relatively low cost, availability in bulk, ease of derivatization, CO₂-philicity in the physico-absorption sense, and stability under the anticipated operating conditions. The highest ranked backbones coming from this analysis, highlighted in green, were the silicones, polyethers, polyamines, polyalkanes, polyamides and polystyrenes. Further down-selection resulted in siloxanes as the top choice with a small effort extended to alkyl chains.

Table 2. QFD for CO₂ Capture Backbones.

backbone	Structure	attribute						total
		physical state	cost (inexpensive)	synthetic availability	ease of derivatization	CO ₂ -philic	stability	
siloxane		9	5	9	9	9	9	50
alkyl ether		9	9	9	5	5	9	46
alkyl amino		5	9	9	5	9	9	46
perfluoroether		9	1	5	1	9	9	34
alkyl		9	9	9	5	1	9	42
aryl ether		1	5	5	5	5	5	26
alkylamido		5	5	9	5	5	5	34
phosphazene		5	1	5	5	5	1	22
Polystyrene		1	9	9	9	1	9	38

physical state
 cost (inexpensive)
 synthetic availability
 ease of derivatization
 CO₂-philic
 must be low viscosity liquid
 should be < \$10/lb
 able to be made on large scale
 must be easily functionalized
 physisorption
 9=liquid, 5=viscous liquid, 1=solid
 9=<\$10/lb, 5=\$10-2-/lb, 1=>\$20/lb
 9=commercial, 5 = small scale, 1 = laboratory
 9=easy, 5 = moderate, 1 = difficult
 9=high, 5=moderate, 1=low

Inspection of the literature indicated that functional groups that most readily reacted with CO₂ were nitrogen-based. With this information, another analysis was performed to evaluate possible N-containing functional groups that could be appended to the backbone or core structure. Table 3 shows the QFD analysis results from such an evaluation. Primary and secondary amines were the most reactive and multiple nitrogen atoms in the same group were thought to be advantageous due to lower entropy factor and formation of intramolecular vs. intermolecular hydrogen bonds to reduce the product viscosity.

As with the backbones, a number of factors were considered in choosing the functional groups. CO₂ capacity was of primary importance as was the rate at which CO₂ would react with the amine and the heat of the reaction. The ease of derivatizing the backbone with the amine group and the cost of the functional group also impacted the selection.

Table 3. QFD Analysis of N-Containing Functional Groups.

Functional Group	Structure	attribute					Total
		CO2 capacity	Heat of reaction	Kinetics	Ease of attachment	Cost	
Aminoethyl		5	5	9	5	9	33
Aminopropyl		5	5	9	9	9	37
Aminoethylaminopropyl		9	9	9	9	9	45
Bis(aminoethyl)aminopropyl		9	9	9	9	9	45
Imidazole		1	1	1	9	5	17
Histamine		5	9	1	5	1	21
Isocytosine		5	5	5	5	1	21
5-Azacytosine		9	5	5	5	1	25
Piperazine		9	9	9	9	5	41
Urea		5	5	1	5	9	25
Acetamide		1	5	1	5	5	17
Guanidine		9	5	9	1	5	29
Amidine		9	5	9	9	5	37
Benzylamine		5	9	5	9	5	33

CO2 capacity
Heat of reaction
Kinetics
Ease of attachment

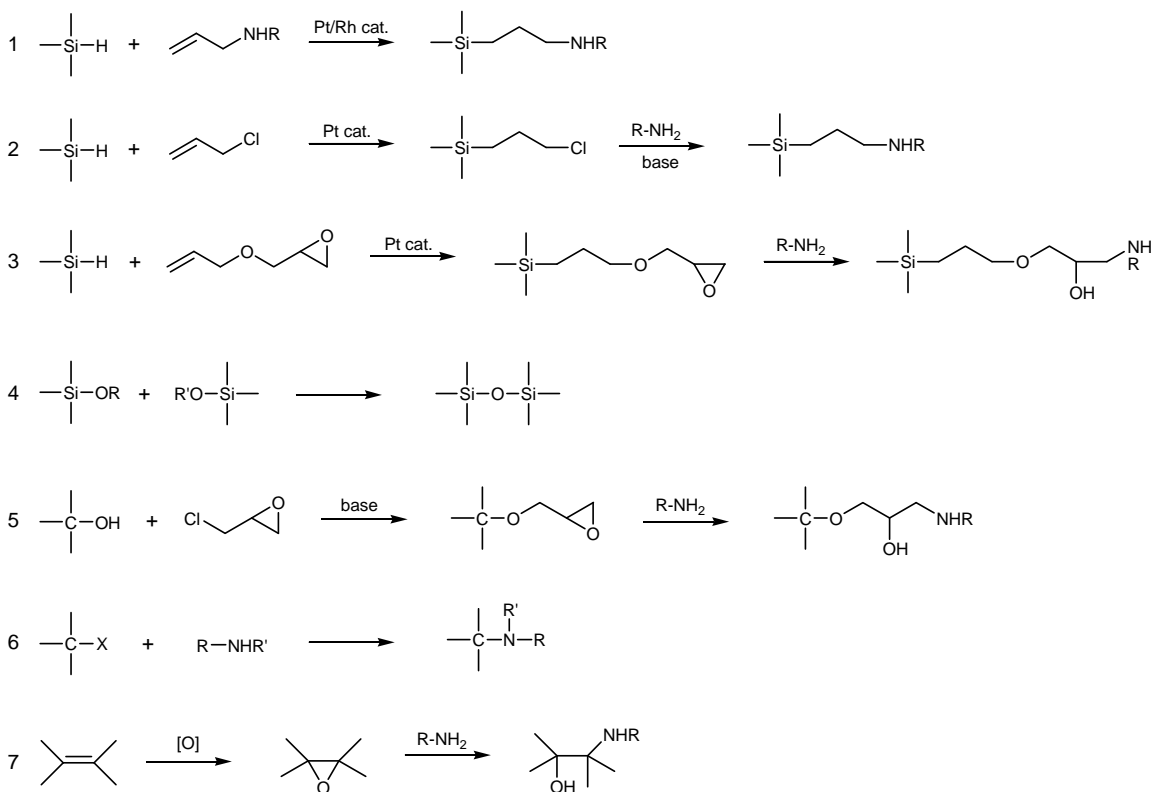
9=high, 5=moderate, 1=low
9=moderate, 5=low, 1=high
9=fast, 5=moderate, 1=slow
9=easy, 5=doable, 1=difficult

(reaction with CO2)

The most promising amino groups (as determined by the numerical ranking) are highlighted in green with others of interest colored yellow. These classes of amino groups were considered as functional groups to be initially explored for their efficacy. While originally designated as second tier choices (ie yellow coded), primary amines without adjacent secondary amino groups (ie aminoethyl and aminopropyl groups in Table 3) were elevated as a class to preferred status due to either their availability and/or their sterically uncongested reactive nitrogen center.

Uniting the backbone choice with the CO₂-reactive functional group would entail various chemistries. While many options were available, only those strategies that were few in steps, high yielding, and amenable to large-scale operations were considered. Scheme 1 shows the general reaction strategies that were likely choices for appending the desired functional groups to the chosen backbones.

Scheme 1. Derivatization Chemistry Reaction Strategies.



Numerous hydride-functional silanes and silicones are available commercially or could be readily prepared. These materials were proposed to undergo hydrosilylation reactions to generate aminosilicones directly (eq. 1), or provide intermediates which could then react with an N-based group to form the product (eqs. 2, 3). Hydrolysis and condensation of appropriate alkoxy silanes (eq. 4) also offers a facile route to a variety of siloxane substitution patterns. Likewise, carbon-based cores can be utilized. Alcohols can react with epichlorohydrin to provide intermediate epoxides that can be converted to the desired amines (eq. 5). Direct displacement of a suitable leaving group by an amine is also a viable synthetic option (eq. 6). Finally, olefins may be oxidized to their corresponding epoxides and, in manner similar to eqs. 3 and 5 converted to products (eq. 7).

Subtask 2.2 (Selection of solvent classes by molecular modeling)

Mechanistic study of the reaction of MEA + CO₂

Detailed reaction mechanism information about the most basic reaction of MEA with CO₂ in aqueous solution was considered as a foundation for designing new amine-based solvents for capturing CO₂. To this end, a detailed mechanistic study on the reaction of MEA + CO₂ was performed at the B3LYP/6-311++G (d,p) level with CPCM (see Appendix 8 for full computational results). In addition, the effect of explicit water on the reaction is considered. Results from the calculations are shown in Figure 3. One can see from Figure 3 that the reaction pathway that forms carbamic acid (red dotted line) is not competitive with other two reaction paths due to its high total reaction energy barrier (33.2 kcal/mol).

The remaining two pathways have similar reaction process. These two paths involve two steps, the only difference being when the second MEA molecule is involved in the reaction. The pathway starting

with one MEA+CO₂ is designated as R (green circle) and the one starting with 2 MEA + CO₂ as R' (blue circle).

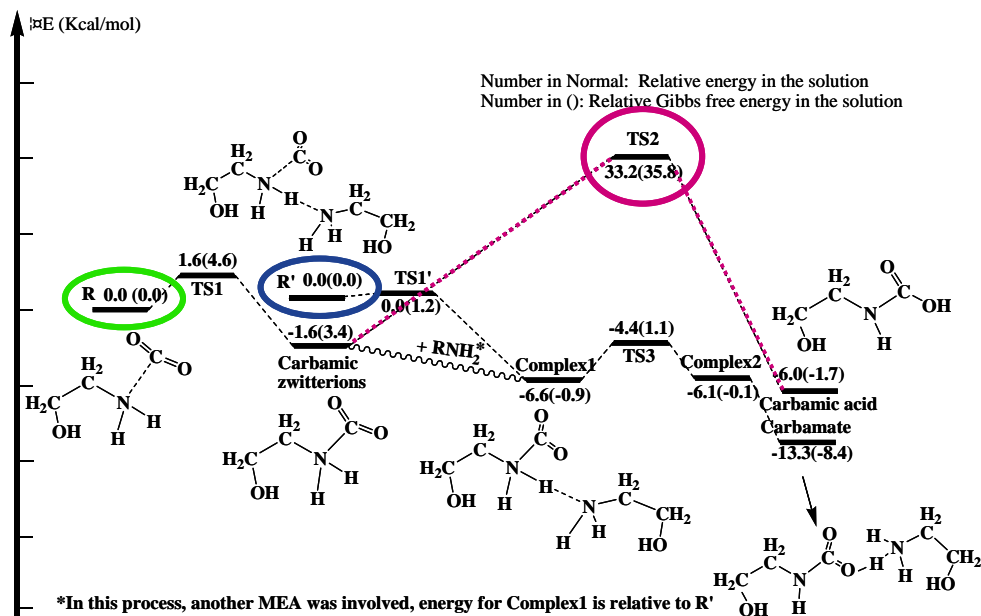


Figure 3. Reaction Coordinate Diagram For MEA + CO₂.

The Gibbs free energy for the carbamic zwitterion formed via path R is 3.4 kcal/mol higher than the reactants although the relative energy (-1.6 kcal/mol) is slightly lower than reactant starting materials. It was also found that Gibbs free energy for carbamic zwitterions is even a little higher than corresponding transition state between R and carbamic zwitterions as explicit waters are added. So, the reaction from zwitterions to R should be *spontaneous* ($\Delta G < 0$ between zwitterion and R) and the rate should be fast (ΔG close to 0 or < 0 between zwitterion and TS1). This indicates that carbamic zwitterions would rather return back to reactants R if no other MEA molecule quickly reacts with it. In contrast to path R, the Gibbs free energy (-0.9 kcal/mol relative to R') for complex 1 is a little lower than one of R' in the R' path, which indicates another MEA can stabilize the zwitterion. This result further indicates that, for CO₂ to react with MEA, another MEA molecule must be present. Once complex 1 is formed from both steps, it needs to overcome an energy barrier of 2.2 kcal/mol to transform to carbamate via TS3. The reaction energy barrier for this process is decreased to 0.3 kcal/mol when water is present.

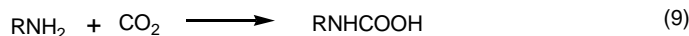
Based on the analysis above, reaction of MEA and CO₂ will not occur via the R pathway if there is not another MEA in the vicinity. If another MEA is in the vicinity, the R pathway is equal to R' pathway. So, we can conclude that formation of carbamate via a single-step, third-order and small-barrier R' pathway is most feasible. (see Appendix 3 for a more complete description of this study).

Impact of substituents on the heat of reaction for MEA-derived molecules.

To design novel primary amines with lower heats of reaction, a calculation of substituent effects on the parent MEA molecule was undertaken. The reaction of CO₂ with an amine will likely involve both reactions given in equations 8 and 9. Moreover, the carbamate and carbamic acid species should be in thermodynamic equilibrium if the proton transfer step is facile, which could be the case for aqueous phase reactions. Hence, carbamate will be main product if its heat of reaction is more exothermic than carbamic acid, and vice versa. It may therefore be possible to change the reaction product distribution by modifying the relative heats of reaction for carbamate and carbamic acid products. Furthermore, it

seemed likely that the relative heats of reaction could be changed by adding substituent groups onto an amine.

To test this hypothesis, ab initio methods at the MP2/aug-cc-pVDZ level were used, coupled with geometries generated from B3LYP/6-311++G(d,p) density functional theory along with the conductor-like polarizable continuum model to compute the heats of reaction. Two possible reaction products were considered: carbamate, having a 2:1 amine:CO₂ reaction stoichiometry, and carbamic acid,



having a 1:1 stoichiometry. Substitution with CH₃, NH₂, OH, OCH₃ and F groups at both the α- and β-carbon positions in MEA were considered (Figure 4).

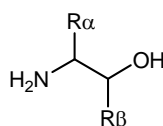


Figure 4. Substituted MEA.

While the exact details of the reaction mechanism between MEA and CO₂ are not known, there is general agreement that Lewis acid-base interactions between amine and CO₂ are important in both carbamate and carbamic acid reactions. Therefore, the basicity of an amine should have a significant influence on the heat of reaction. The relative basicity of each of the substituted MEAs was calculated and is shown in Table 4. Note that the substitution site has an important influence on the change in basicity. The relative basicities of NH₂-MEA and OH-MEA for α site substitution are 277.8 and 275.5 kcal/mol, respectively, which is lower than that of the parent molecule MEA (279). However, relative basicities of the corresponding β site substituted species are 279.5 and 281.3 kcal/mol, respectively, which are higher than the basicity of MEA.

Table 4: Relative basicity (kcal/mol) of substituted MEA.

Species	Relative basicity	Species	Relative basicity
MEA	279.0	α-OH-MEA	275.5
α-CH ₃ -MEA	277.9	β-OH-MEA	281.3
β-CH ₃ -MEA	278.9	α-OCH ₃ -MEA	273.4
α-NH ₂ -MEA	277.8	β-OCH ₃ -MEA	278.7
β-NH ₂ -MEA	279.5	α-F-MEA	266.7
		β-F-MEA	275.9

A plot of the relative basicity of substituted MEA as a function of the electronegativity of the substituent group is shown in Figure 5 with the α- and β-substituted compounds are plotted separately. The α-substituted MEA derivatives show a monotonic decrease in basicity with increasing electronegativity, but the decrease is highly non-linear. Conversely, the basicity of β-substituted compounds initially increases and then decreases with increasing electronegativity. Hence, there is no simple relationship between electronegativity and basicity. Our findings are in agreement with the observation that several factors affect the basicity of a molecule in solution, including inductive or polarization effects, solvation free energy, ability to form intra-molecular hydrogen bonds, and so forth.¹

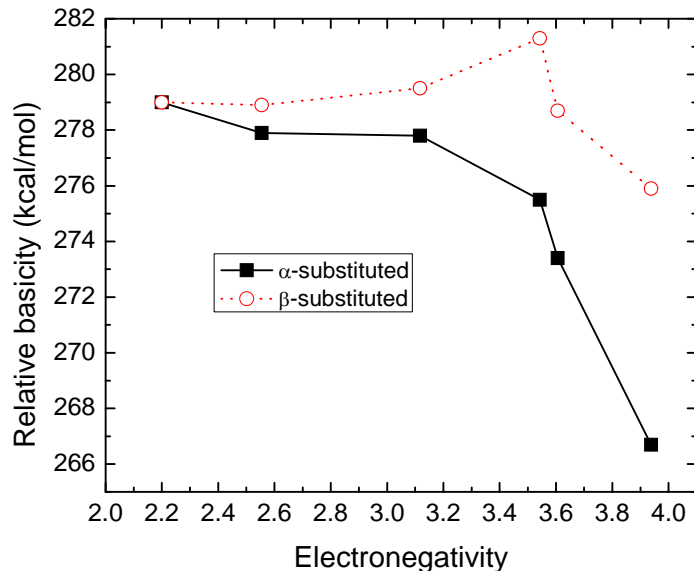


Figure 5: Relative basicity plotted as a function of the electronegativity of the substituent group for α -substituted (filled squares) and β -substituted (open circles) MEA. Lines are drawn as a guide to the eye.

Inspection of Table 5 shows that the carbamic acid heats of reaction do not change a great deal as the substituent group is changed, except for α -F-MEA. The heat of reaction is 4.8 kcal/mol less exothermic for α -F-MEA relative to MEA; the next largest change is 2.2 kcal/mol less exothermic for α -OH-MEA.

The heat of reaction for carbamic acid as a function of the amine basicity is plotted in Figure 6. A roughly linear relationship between the heat of reaction and the relative basicity of the substituted amine was found with a correlation coefficient of $R^2=0.85$. Notwithstanding the scatter about the linear fit to the data, it is clear from inspection of the data that generally speaking, the stronger the base the more exothermic the heat of reaction.

Plotting the carbamate heats of reaction as a function of the basicity of the amine in Figure 6 one observes that the heats of reaction are a linear function of the amine basicity. The correlation coefficient is $R^2=0.976$, indicating a good fit of the data. Hence, one can say with a good deal of confidence that the more basic the amine the more exothermic the heat of reaction. This observation provides a design tool for modifying ΔH and a method for screening candidate amines.

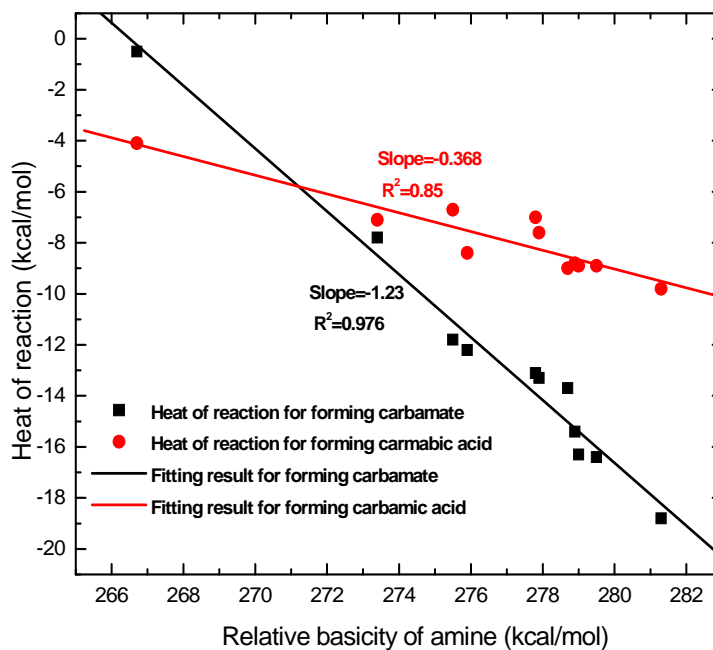


Figure 6: Heats of reaction for forming carbamate and carbamic acid as a function of the relative basicity of the substituted MEA.

Table 5: Computed heats of reaction (kcal/mol) for carbamic acid.

Species	ΔH	Species	ΔH
MEA	-8.9	α -OH-MEA	-6.7
α -CH ₃ -MEA	-7.6	β -OH-MEA	-9.8
β -CH ₃ -MEA	-8.8	α -OCH ₃ -MEA	-7.1
α -NH ₂ -MEA	-7.0	β -OCH ₃ -MEA	-9.0
β -NH ₂ -MEA	-8.9	α -F-MEA	-4.1
		β -F-MEA	-8.4

Table 6: Heats of reaction (kcal/mol) for the first step, $\Delta H1$, the second step, $\Delta H2$, and the total reaction for carbamate formation with substituted MEA. *

Species	$\Delta H1$	$\Delta H2$	ΔH
MEA	-9.7	-6.6	-16.3
α -CH ₃ -MEA	-7.1	-6.2	-13.3
β -CH ₃ -MEA	-8.9	-6.5	-15.4
α -NH ₂ -MEA	-7.9	-5.2	-13.1
β -NH ₂ -MEA	-10.7	-5.7	-16.4
α -OH-MEA	-6.1	-5.7	-11.8
β -OH-MEA	-11.6	-7.2	-18.8
α -OCH ₃ -MEA	-2.3	-5.5	-7.8
β -OCH ₃ -MEA	-7.8	-5.9	-13.6
α -F-MEA	7.4	-7.9	-0.5
β -F-MEA	-5.3	-6.9	-12.2

*The first step is: $2RH_2(sol) + CO_2(sol) \rightarrow RNH_3^+(sol) + RNHCO_2^-(sol)$

*The second step is: $RNH_3^+(sol) + RNHCO_2^-(sol) \rightarrow RNH_3^+RNHCO_2^-(sol)$

The heats of reaction for MEA, and both α - and β -CH₃-substituted MEA were measured in order to test the predictions of the model. Quantitative agreement between the predictions and experiments was seen (Table 7). The relative basicities of the substituted amines were computed and showed that the heats of reaction for both carbamate and carbamic acid products are linearly correlated with the computed relative basicities; weaker basicities result in less exothermic heats of reaction. Heats of reaction for carbamates are much more sensitive to changes in basicity than those for carbamic acids. This leads to a crossover in the heat of reaction so that carbamic acid formation becomes thermodynamically favored over carbamate formation for the weakest bases. This provides a method for tuning the reaction stoichiometry from 2:1 to 1:1.

Table 7: Comparison of calculated and experimentally determined heats of reaction (kcal/mol) for carbamate formation with substituted MEA.

Species	Calculated ΔH	Experimental ΔH
MEA	-16.3	-17.3 \pm 1.3
α -CH ₃ -MEA	-13.3	-12.9 \pm 1.2
β -CH ₃ -MEA	-15.4	-15.6 \pm 1.3

CO₂ Solubility

As described in task 2.3, incorporation of a co-solvent to maintain liquidity through the CO₂ capture and desorption processes was critical. The potential for having a co-solvent that physi-sorbed CO₂ together with a chemi-sorbing solvent seemed attractive. The calculated solubility of carbon dioxide in four physical solvents using the Conductor-like screening model for real solvents (COSMO-RS) formalism was compared to experimental phase behavior.

The oligomers (Figure 7) studied were polyethyleneglycol dimethylether (PEGDME), polypropyleneglycol dimethylether (PPGDME), perfluoropolyether (PFPE), and polydimethylsiloxane (PDMS), and had repeat units ranging from 2 to 5. The solubility data are presented in pressure composition (P \times) diagrams at 25°C. The important region of the phase diagram for CO₂ capture is the oligomer-rich side of the phase diagram. The CO₂ solubility in each of the oligomers is plotted for the 80 to 100 wt% region in Figure 8 for calculations and Figure 9 for experiments. Compared to experimental data, one can see that the COSMO-RS formalism is able to qualitatively and to some extent quantitatively describe solubilities of CO₂ in each of the oligomers.

The pressure required to dissolve a specified amount (wt%) of CO₂ in the PFPE-CO₂ pseudo-binary system is far greater than that required by the three other solvents, PPGDME, PEGDME, and PDMS. This is unexpected, given that fluorinated polymers are widely known to have lower miscibility pressures in CO₂ than non-fluorinated analogs. The performance of PPGDME, PDMS, and PEGDME were comparable; therefore these solvents were considered promising solvents for CO₂ physi-sorption.

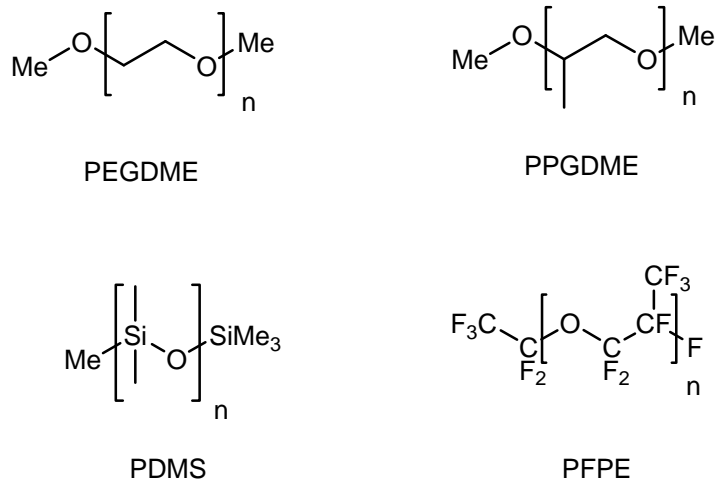


Figure 7. Structures of the four CO₂-philic oligomers used in this study.

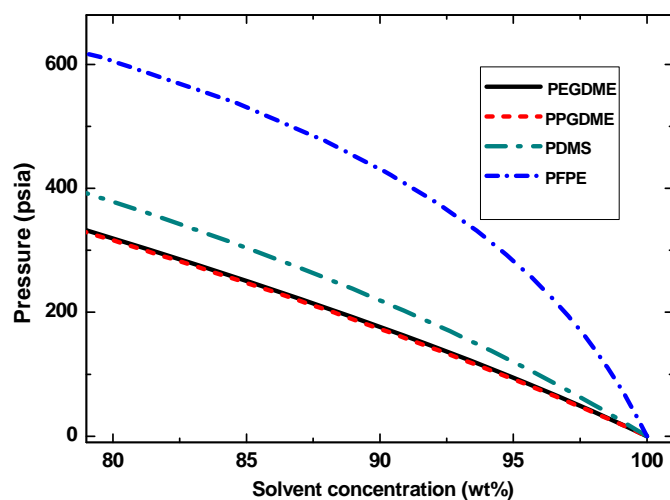


Figure 8. Comparison of the phase behavior of CO₂ in oligomers (PEGDME n=5, PPGDME n=3, PDMS n=2, PFPE n=5) on the solvent rich side, predicted with COSMOtherm.

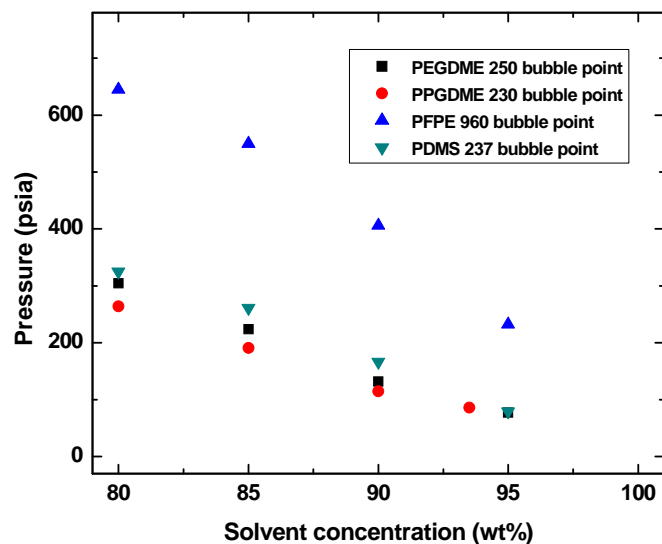


Figure 9. Comparison of the phase behavior of CO₂ in oligomers on the solvent rich side, experimentally determined.

Several other materials were examined as potential physi-sorbing co-solvents for this program. Vapor liquid equilibrium calculations for CO₂ and various oligomers and small molecules were performed. The structure of each oligomer or molecule was optimized at the BP86/def-TZVP level of theory within the Turbomole package. The thermodynamic properties were then predicted with the COSMOtherm package. During the modeling, only one parameter, i.e., experimental vapor pressure of CO₂, was specified in the COSMOtherm calculations. Theoretical modeling was performed at room temperature, 25°C.

As shown in Figure 10, the linear and branched polybutylene glycol diacetate (PBGDAC) with repeat unit of 6 have a similar ability to capture CO₂. However, both of them are worse than polyethylene glycol dimethylether PEGDME (n=6) and polypropylene glycol dimethylether PPGDME (n=7), which were reported above.

Five different small molecules with high boiling points were considered as possible co-solvents for CO₂ capture. The structures of these molecules are shown in Figure 11, and the VLE plots are shown in Figures 13 and 14. 2-Butoxy ethyl acetate was predicted to perform the best among these six molecules. This material was also compared to N-formyl morpholine (NFM), 1,4-dioxane and glyceryl triacetate. Figure 12 shows that the performance of 2-butoxy ethyl acetate was predicted to be very similar to 1,4-dioxane and to perform better than NFM, which is used commercially to absorb CO₂.

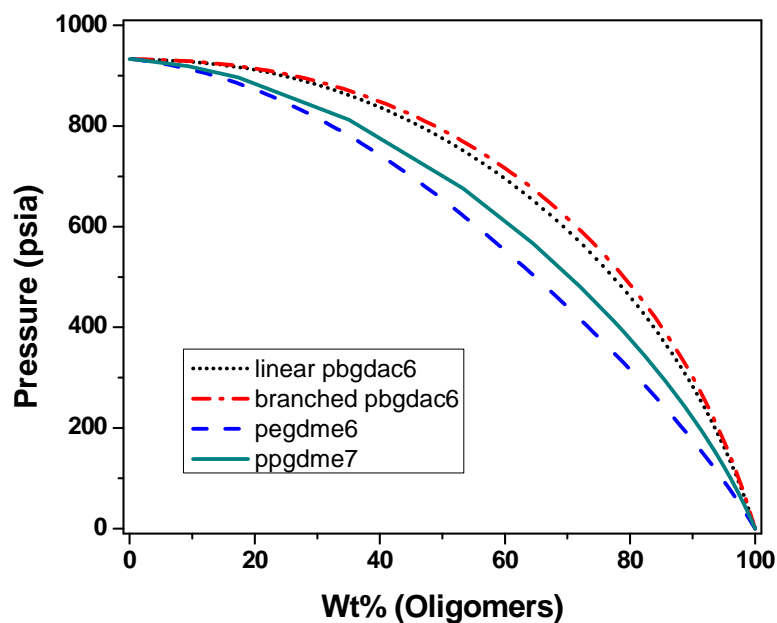


Figure 10. Vapor liquid equilibrium of CO₂ and linear (and branched) PBGDAC based on predictions (repeat units n of 6), and compared to PEGDME and PPGDME.

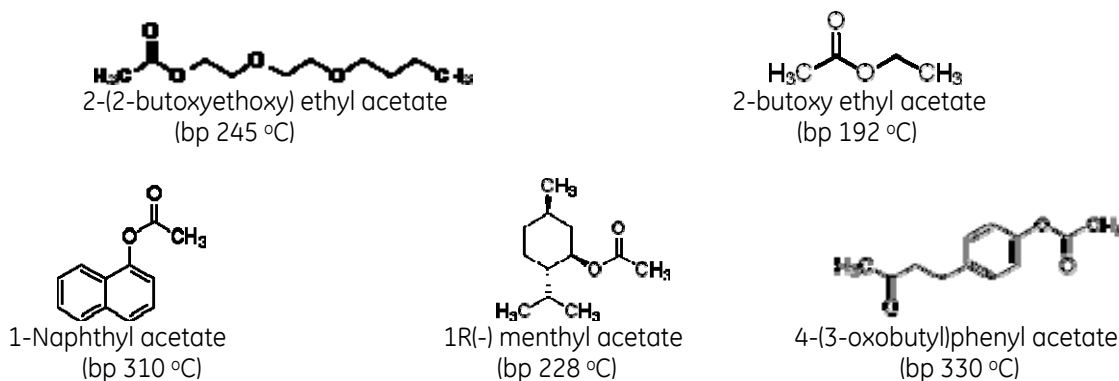


Figure 11. Structures of six small molecules.

Poly(3-acetoxy oxetane) (PAO) was a final co-solvent considered for physi-sorption of CO₂. It contained multiple sites for the Lewis acid:lewis base interactions that typically characterize highly CO₂ philic polymers. This material was synthesized with approximately 3 repeat units as shown in Figure 12.

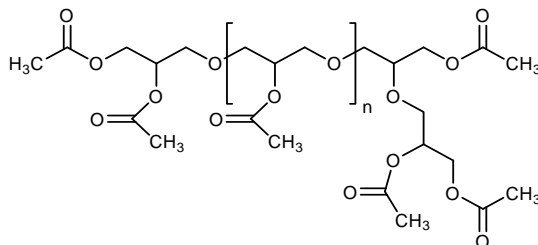


Figure 12. Poly(3-acetoxy oxetane)

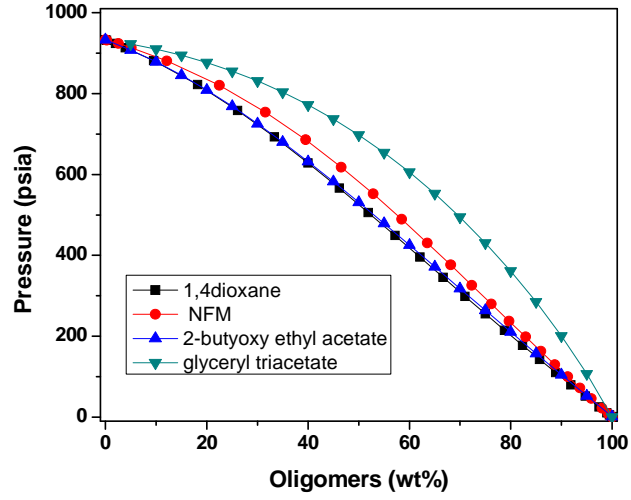


Figure 13. Vapor liquid equilibrium of CO₂ and four small molecules based on predictions.

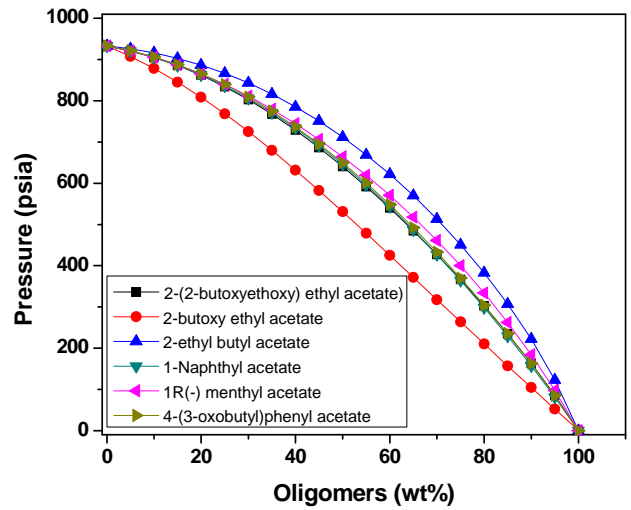


Figure 14. Vapor liquid equilibrium of CO₂ and six small molecules.

Figure 15 illustrates the performance of PAO as a solvent for CO₂ absorption relative to other CO₂ solvents.

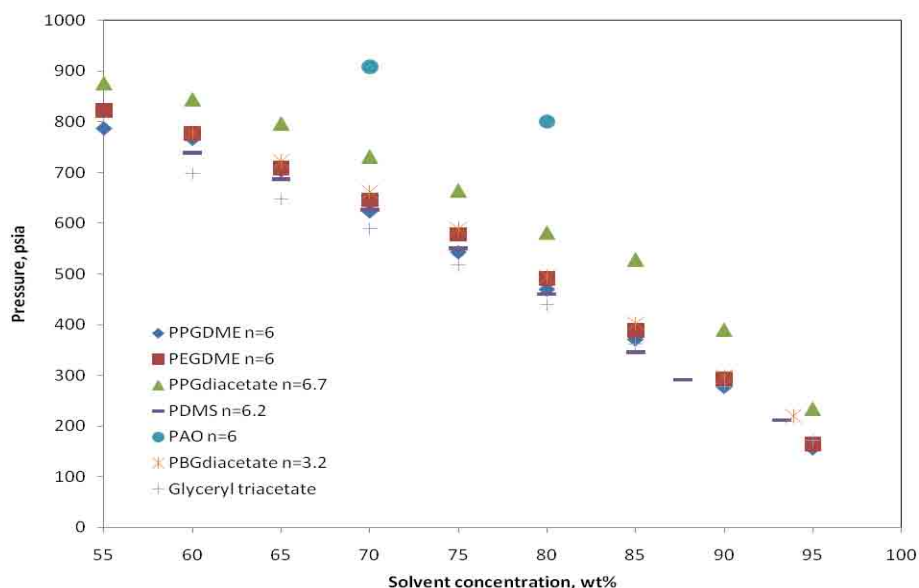


Figure 15. Oligomeric CO₂ Solvents, polypropyleneglycol dimethylethers(PPGDME), polyethyleneglycol dimethylethers (PEGDME), polypropyleneglycol diacetate, polydimethyl siloxane (PDMS), poly(3-acetoxy oxetane) (PAO), linear polybutyleneglycol diacetate (PBGdiacetate), glycerol triacetate (this solubility data collected as part of an IAES project on oligomeric CO₂ solvents).

From the experimental results seen in Figure 15, PAO was a very poor solvent for CO₂. Contrary to prediction, glycerol triacetate is an excellent CO₂ solvent relative to other oligomers tested. Although glycerol triacetate may be a very promising solvent for pre-combustion CO₂ capture, it is not apparent that this compound can be readily modified to incorporate amine functionalities for low pressure CO₂ capture in a post-combustion setting.

Subtask 2.3 (Bench scale, multi-property determination of available solvents)

Plant Oils

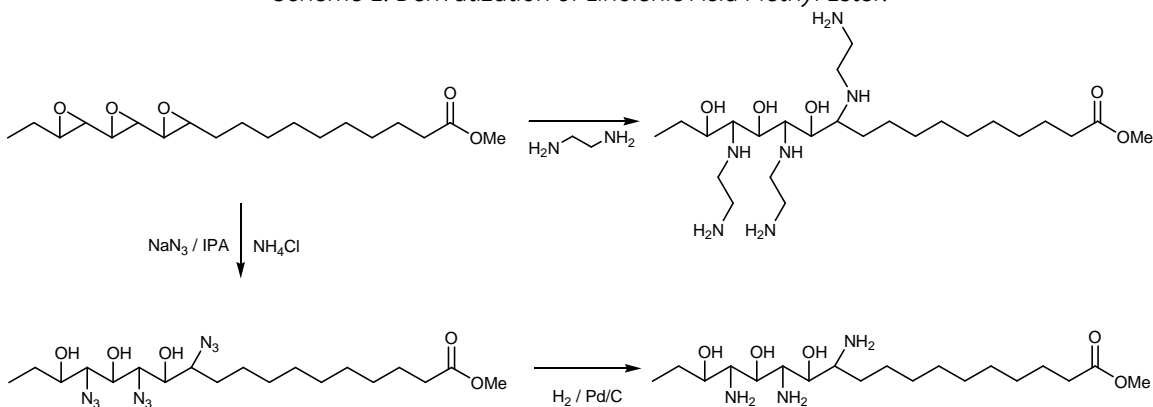
Other than water and petroleum there are no larger liquid sources on earth than plant and animal fats². The strategy adopted in this research was to prepare amine-containing derivatives of large volume plant oils. Two general approaches were considered. Plant oils with the highest degree of unsaturation were converted to their corresponding epoxide. The epoxidized oil was then reacted directly with a diamine to produce hydroxyl amine derivatives³ or the epoxide was reacted in two steps to produce amine by first converting the epoxide to an azide and then reducing to produce the amine⁴.

Typical plant oils are C₁₈ triglycerides with one, two or three unsaturated groups per chain. For this program, a high degree of unsaturation was desired in order to maximize the final amine content. Thus flax oil, with as many as three double bonds per chain (linolenic acid residue) was selected for study. Fortunately epoxidized flax oil (EFO) was commercially available as well. Furthermore, the individual carboxylic acid or ester with olefin units (linolenic acid or linolenic acid methylester) were also commercially available and likewise could be converted to the corresponding epoxide using *m*ClBPA.

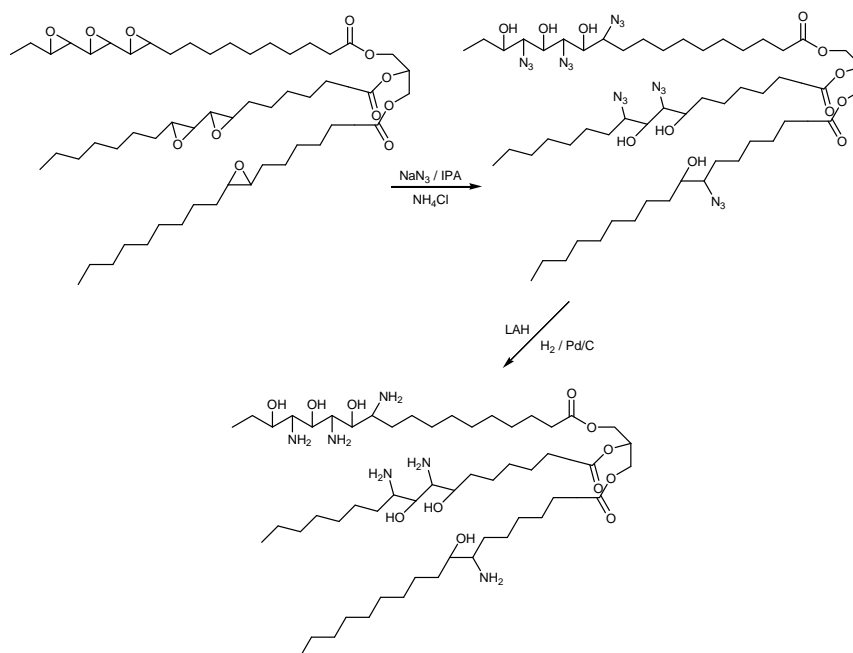
As shown in Scheme 1, the epoxidized linolenic acid ester was easily converted to either amino alcohol in one or two steps. Flax oil was similarly treated and formed the desired amine derivatives (Scheme 2).

Unfortunately, reaction with CO₂ either neat or in a co-solvent did not show any appreciable CO₂ uptake.

Scheme 1. Derivatization of Linolenic Acid Methyl Ester.



Scheme 2. Derivatization of Flax Oil.



A working hypothesis of the poor CO₂ uptake of the amine-hydroxy materials was that intra-molecular hydrogen bonding of the amine to the hydroxide competes with reaction of CO₂ with the amine. To test this hypothesis, we added a step whereby we capped the hydroxide. To further determine why the amino alcohol derivatized plant oils performed poorly in reactions with CO₂, several model compounds were made. These were designed to separate the effects of potential H-bonding between adjacent OH and NH₂ groups and the influence of a hydrocarbon chain. To this end, MEA, aminododecane and compounds 4 and 6 were examined for their reactivity in 50% TEG (triethylene glycol) and as neat materials.

MEA was commercially available as was 1-aminododecane. Compounds **4** and **6** were synthesized as shown in Scheme 1. Epoxidation of 1-decene gave epoxide **2**, which was followed by ring opening with sodium azide to give a 9:1 mixture of azido alcohols **3**. These azides were either reduced directly to the corresponding amines **4** or the alcohol groups capped with an ethyl group and then reduced to **6**.

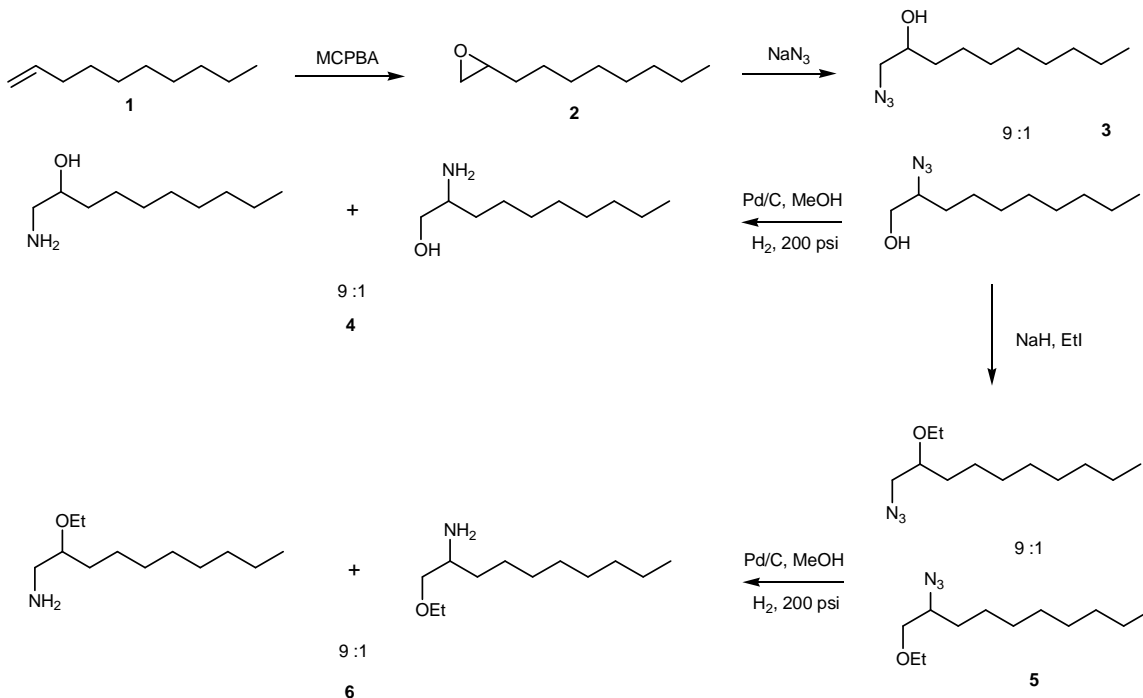
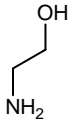
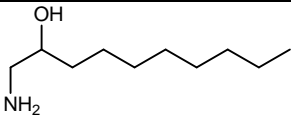
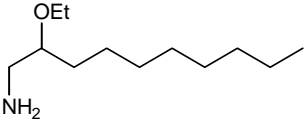
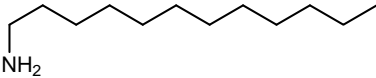


Table 8 shows the results of exposure of these compounds to CO_2 . As expected, MEA readily reacted with CO_2 both neat and as a 50% solution in TEG. When a hydrocarbon rich chain was added to MEA, as in compound **4**, there was a significant decrease in the CO_2 capture ability of the molecule. This result suggested that the non-polar tail of **4** prevented efficient reaction of CO_2 with the polar amino alcohol; perhaps in a fashion similar to micelle formation with non-polar tails surrounding a core of polar groups.

When the hydrogen-bonding ability of the hydroxy group was removed by forming the ethoxy derivative **6**, CO_2 capture efficiency increased significantly over **4**. The results comparing **4** and **6** also intimated that the potential for H-bonding between adjacent amine and hydroxyl functionalities could suppress reaction with CO_2 . The proposed micelle effect was still present when aminododecane was allowed to react with CO_2 . A CO_2 loading higher than **4** but less than **6** was observed. These results support the theory that the long hydrocarbon rich chains of the plant oils may hinder the ability of CO_2 to access the polar amine groups. In addition, the potential for H-bonding in the amino alcohols present also suppress the reactivity of the entire system towards CO_2 absorption.

Table 8. Reactivity of MEA Derivative with CO₂.

Compound	Structure	% CO ₂ Weight Gain	
		Neat	50% TEG
MEA		105	104
4		81	72
6		95	91
aminododecane		86	85

Given these results, this avenue was discontinued and all efforts were directed towards amino silicones. (Full details of the plants oil experiments are in Appendix 4).

Amino Silicones

Several structural classes of aminosilicones were proposed for study. They were linear, branched and cyclic. Among the linear materials, incorporation of physi-sorbing CO₂-philic moieties was considered as well as varying lengths of siloxane backbones and placement and number of the amine functionalities.

One of the more available amino-derivatized disiloxanes was 1,3-bis(3-amoniopropyl) tetramethyl-disiloxane or GAP-0. This material could be obtained from commercial sources in hundred gram quantities and served as a working model for a number of investigations.

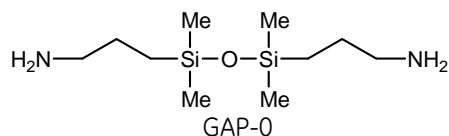
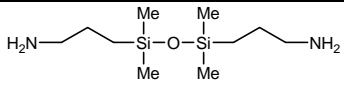
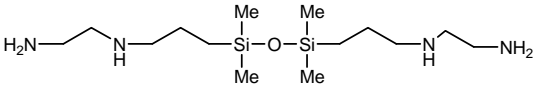
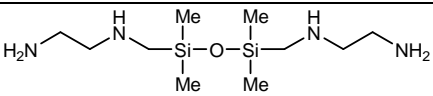
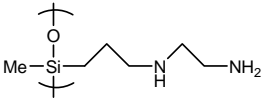
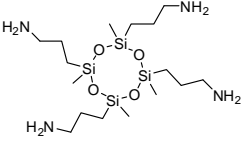
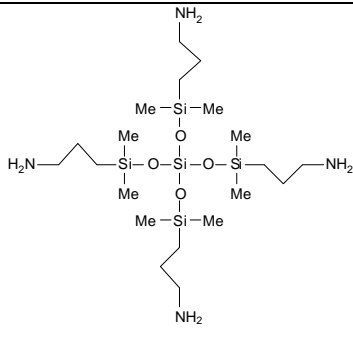
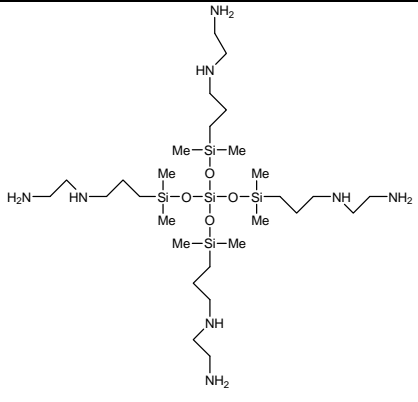
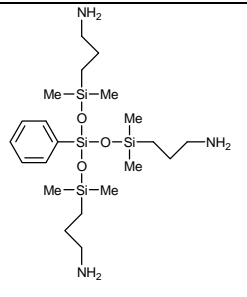
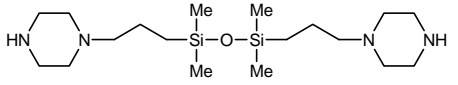
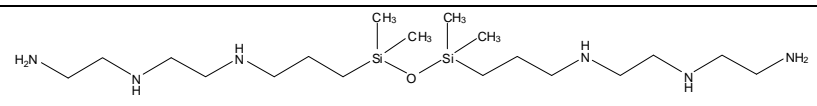
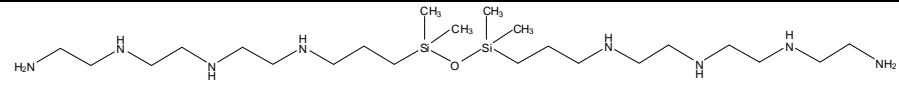
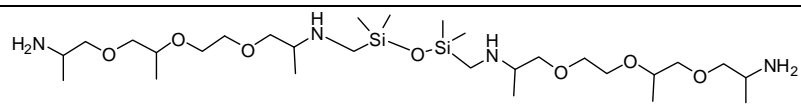


Table 9 shows the results of allowing neat CO₂ capture solvents to react directly with 100% CO₂. Mechanical stirring was employed to facilitate efficient mass transfer of the gas through the solvent. In all cases, the solvents solidified or became extremely viscous. Weight gain was defined as the weight of CO₂ absorbed divided by the original sample weight. The theoretical weight took into account the need for 2 amine groups to neutralize one CO₂ molecule.

Table 9. Weight Gain by Neat CO₂ Capture Solvents in 100% CO₂.

Entry	Structure	Wt Gain (%)	Theoretical Gain (%)	% of Theory
7		17.3	17.7	98
8		16.7	26.3	63
9		14.6	31.6	46
10		10.2	27.5	37
11		5.6	18.8	30
12		13.8	15.8	87
13		6.3	24.2	26

14		7.3	13.2	55
15		3.0	11.4	27
16		2.0	31.4	6
17		6.3	34.7	18
18		6.1	14.0	44

As seen in the table, even with mechanical agitation, very poor uptake of CO₂ was realized. This was a result of poor mass transfer of gaseous CO₂ into and through a solid or very viscous phase. As this program was predicated on maintaining a liquid state for ease of material transportation through the absorber and desorber units, means to solubilize the carbamate salt products were investigated.

There are several solvents currently used for the physi-sorption of CO₂ among which is Selexol, a mixture of dimethylethers of polyethyleneglycols. It was thought that a mixture of a physi-sorbing solvent (such as a glycol) and a silicon-based amine might provide a suitable solution. This selection was also based on the predictions from task 2.2 that indicated PEG oligomers could serve as physi-sorbing co-solvents.

Initial experiments using triethyleneglycol dimethylether as the solvent did not serve to solubilize the reaction products (exp 2 and 3, Table 6). However, the uncapped triethylene glycol (TEG) did serve as a useful co-solvent and allowed >100% theoretical capture of CO₂ based on the amine content of the mixture. This was likely due to enhanced physi-sorption of CO₂ by the much more polar and CO₂-philic solvent mixture, especially as carbamate moieties were formed.

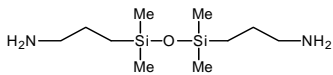
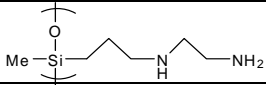
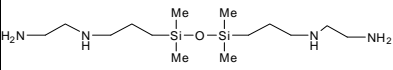
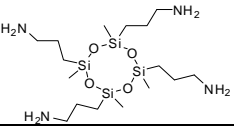
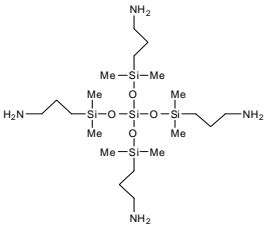
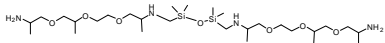
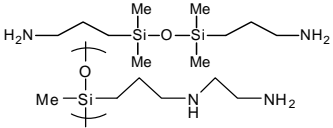
Table 10. Efficacy of Capped vs Uncapped Triethylene Glycol as Co-solvent for CO₂ Capture.

Experiment	Amine	Co-Solvent	Wt ratios (amine:solvent)	CO ₂ uptake (% of theoretical)	% wt gain	physical state
1		none	100:0	71	17.3	S
2			50:50	83	6.8	S
3			33:67	99	5.9	S
4			50:50	114	10.1	L
5			0:100	-	<0.5	L
6			67:33	113	13.2	S
7			33:67	118	6.9	L

A variety of other silicon-based amines were examined to determine if the triethylene glycol co-solvent performed similarly. Table 11 shows the original GAP-0 results (entries 1, 4) as well as an oligomeric amino silicone hydrolyzate (entries 8, 9), cyclics (12, 13), star (14, 15), and other disiloxanes (10, 11, 16, 17). 30% MEA is also shown for comparison. Entry 9 was a 33:67 mixture of amine:co-solvent as a 50:50 mix resulted in the formation a solid. A 1:1 mixture of GAP-0 and hydrolyzate without a co-solvent still produced a solid product (entry 19).

While many of the neat materials absorb significantly higher levels of CO₂ than the benchmark MEA solution, the mass transfer of CO₂ into the neat capture solvent is much slower than that in a low viscosity liquid medium. Even at 50% dilution entries 4, 11 and 13 showed similar or better CO₂ uptake than MEA (entry 18). Dilution ratios were not optimized and likely several of the mixtures could be increased in amino silicone content to raise the CO₂ capture efficiency.

Table 11. Solubilizing Ability of Triethylene Glycol as Co-solvent for CO₂ Capture.

Experiment	Amine	50:50 TEG/Amine	% Theoretical wt gain	% wt gain	Physical State
1		No	98	17.3	S
4		Yes	114	10.1	L
8		No	81	11.3	S
9		Yes	87	7.9	L
10		No	64	16.7	S
11		Yes	90	11.8	L
12		No	30	5.6	S
13		Yes	154	14.2	L
14		No	87	13.8	S
15		Yes	116	9	L
16		No	44	6.1	S
17		Yes	41	2.8	L
18	MEA	30% in water	94	10.2	L
19		No	95	21.4	S
20		Yes	94	10.7	L

Other co-solvents were also investigated for their ability to help solubilize the CO₂ reaction products and maintain a liquid solvent mixture. Table 12 shows the solvents examined. All were tested in a 50:50 ratio with GAP-0. In almost all cases where a hydroxyl-containing co-solvent was employed, the reaction products with CO₂ were soluble. The one exception was poly(propylene) glycol (entry 25). Endcapped polyethers like SF1488 (entry 23) and triethylene glycol dimethylether (entries 2 and 3) did not provide sufficient solvating power to maintain liquidity, nor did sulfolane (entry 34). Hydroxy compounds in the form of liquid phenols were also found to be capable of providing the desired solvating effect (entries 28, 33, 35 and 36). Finally, the cyclic amide (N-methyl caprolactam) was determined to be too volatile for use.

Table 12. Various Co-solvents for CO₂ Capture.

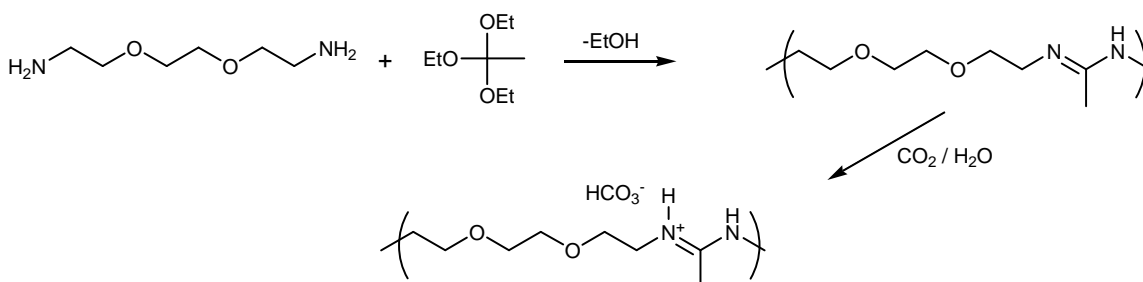
Experiment	Solvent	CO ₂ Uptake (%Theory)	% Wt Gain	Comments
21	triethylene glycol	111	9.8	L
22	SF1488 Momentive Silicone polyether	76	6.7	S
23	a hydrosilylation reaction product of 1,1,3,3-tetramethyldisiloxane and trimethylolpropane allyl ether	97	8.6	L
24	tetraethylene glycol	116	10.2	L
25	poly(propylene) glycol (MW=725)	93	8.2	S
26	3:1 Tetra EG: Diol M'M'	111	9.7	L
27	trimethylolpropane allyl ether	107	9.7	L
28	eugenol	94	8.3	L
29	trimethylolpropane-ethoxylate (4/15 EO:OH) Mn = 170	101	9.0	L
30	pentaerythritol ethoxylate (3/4 EO/OH) Mn = 270	108	9.4	L
31	2:1 tetraethylene glycol:eugenol	107	9.4	L
32	N-methyl caprolactam	-	-7.2	-
33	isoeugenol	96	8.4	L
34	sulfolane	89	7.9	S
35	4-allyl-6-methylphenol	76	6.8	L
36	2-allylphenol	80	7.0	L

Amidine materials

Polyamidines as CO₂ capture oligomeric materials were also explored briefly. These materials were anticipated to be liquids, which would facilitate flow in absorption columns, have low vapor pressures to reduce evaporative losses, have high CO₂ loading capacity and be capable of remaining liquid after reaction with CO₂.

To maintain liquidity, the typical alkyl diamine used to make these oligomers was replaced with an alkylether diamine, 2'2'ethylenedioxy bis ethylamine (Scheme 4). The amidine functionality was selected because it exhibits a 1:1 molar binding with CO₂ rather than the 2:1 binding associated with primary amines, thereby increasing the theoretical CO₂ loading.

Scheme 4. Oligomeric Amidine Synthesis.



This poly(amidine) was indeed a liquid, but was very viscous at ambient temperature. Scheme 4 illustrates the reaction associated with this material's ability to bind CO₂ by forming a bicarbonate salt in the presence of water.

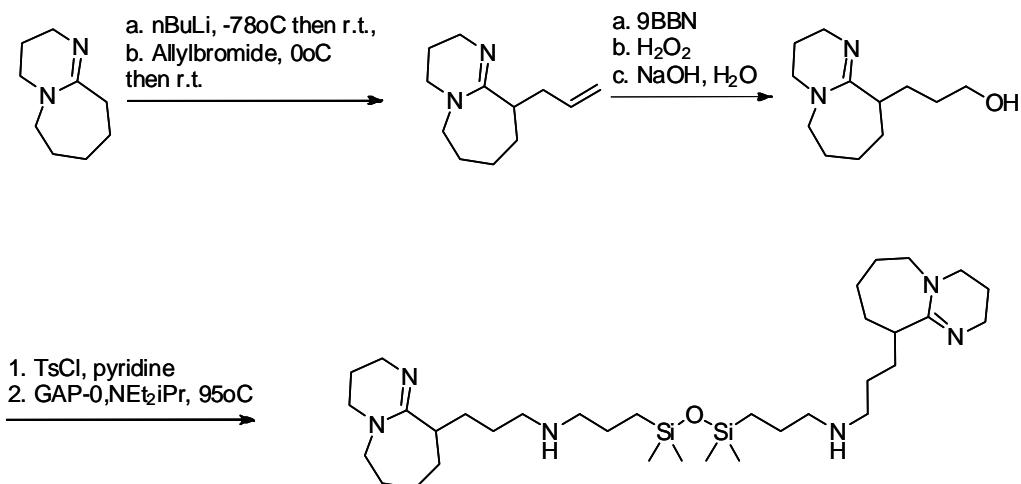
This bicarbonate salt of the polyamidine has a theoretical capacity, assuming a 1:1 molar reaction of the CO₂ with the amidine group, of 19 wt% CO₂. When CO₂ was bubbled through this polyamidine, it became more viscous. Although the product remained a transparent liquid, its viscosity was so high that it was not a feasible solvent for CO₂ absorption in a column. It should be noted that this viscosity increase occurred even in the absence of water, therefore some unreacted 2'2'ethylenedioxy bis ethylamine may have been present in the polyamidine product (the primary amines of the 2'2'ethylenedioxy bis ethylamine can react with CO₂ in the absence of water to form carbamates). Alternately, primary amines at the terminal position of the polyamidines, could have reacted with the CO₂ in the absence of water.

Mixtures of triethylene glycol and the polyamidine were then prepared to lower the solution viscosity, thereby allowing vigorous mixing during contact with CO₂ bubbles to occur. Upon reaction with bubbling CO₂ for 30-60 minutes at ambient temperature and pressure in the absence of water, only ~50% of the mass increase was observed. Once again a substantial portion of this weight gain was accomplished in the absence of water. In summary, this polyamidine did not appear to hold promise as a CO₂ absorption solvent because of its high viscosity, which increases upon reaction with CO₂.

Siloxane amidines

In the light of these results, our target molecule was modified to include a siloxane backbone (GAP-0) and a DBU (1,8-Diazabicycloundec-7-ene) derived amidine (Scheme 5). Allylation of DBU was followed by a hydroboration of the corresponding alkene. Further activation of the alcohol as a toluenesulfonate and coupling with GAP-0 will give access to the GAP-0/DBU hybrid system.

Scheme 5: Towards the synthesis of GAP-0-DBU adduct.



The DBU-Alcohol and GAP-0 /DBU Adduct were tested in the high throughput screening conditions described in task 3.1 using standard conditions (2h, 1.2 mL/min CO_2 , 250-300 μL of sample, triplicates, 40° or 55°C). TEG (Triethylene glycol) was used as a co-solvent. As before, we also investigated the effect of adventitious water in the system.

In this set of CO_2 adsorption experiments, no significant weight uptake was observed. TEG did not seem to have any effect in CO_2 uptake, nor the presence of adventitious water, as seen in Table 13. Given these results, further research into the use of amidines was terminated.

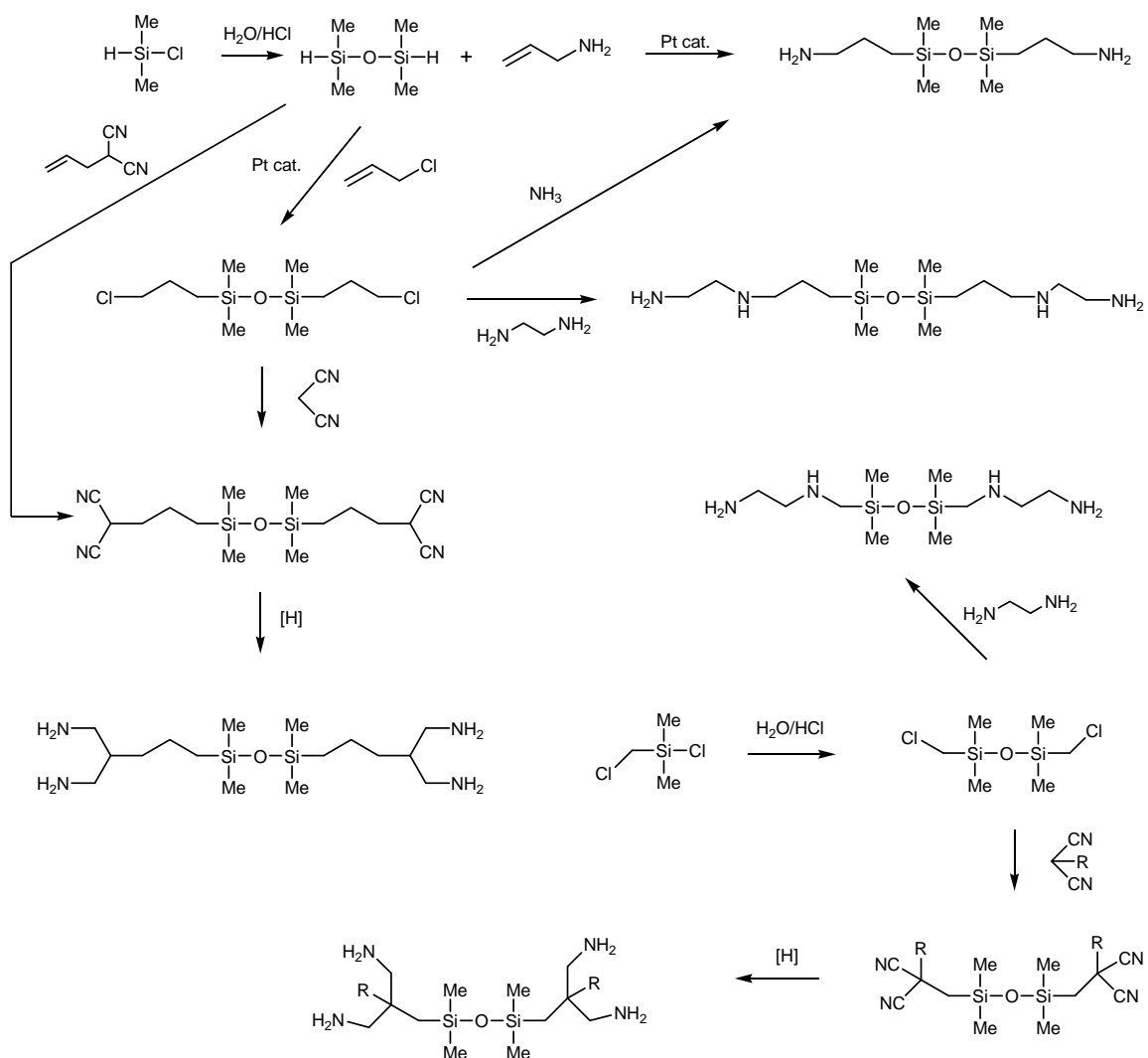
Table 13. CO_2 Absorption Studies with DBU-alcohol and GAP-0/DBU Adduct.

Compound	Co solvent	Additive	Max Theoretical yield (%)	Temperature ($^\circ\text{C}$)	CO_2 weight uptake after 2 h (%)
DBU-alcohol	None	None	0	40	-4.8-0
DBU-alcohol	None	1% H_2O	9.67	40	-2
DBU-alcohol	TEG (50%)	None	n/a	40	-2
DBU-alcohol	TEG (50%)	1% H_2O	9.67	40	-3
DBU-alcohol	None	None	0	55	-4.8-0
DBU-alcohol	None	1% H_2O	9.67	55	-2
DBU-alcohol	TEG (50%)	None	n/a	55	-2
DBU-alcohol	TEG (50%)	1% H_2O	9.67	55	-3
GAP-0/DBU Adduct	None	None	10.5	40	-0.7
GAP-0/DBU Adduct	None	1% H_2O	10.5	40	-2
GAP-0/DBU Adduct	TEG (50%)	None	10.5	40	0.1
GAP-0/DBU Adduct	TEG (50%)	1% H_2O	10.5	40	-3
GAP-0/DBU Adduct	None	None	10.5	40	-0.7
GAP-0/DBU Adduct	None	1% H_2O	10.5	40	-2
GAP-0/DBU Adduct	TEG (50%)	None	10.5	40	0.1
GAP-0/DBU Adduct	TEG (50%)	1% H_2O	10.5	40	-3

Subtask 2.4 (Synthetic Strategy Development)

Successful synthetic strategies were developed throughout the duration of this program as witnessed by the large number and variety of materials made and tested. Scheme 6 shows that several common precursors allowed for a divergent approach to a number of disiloxane core derivatives for evaluation.

Scheme 6. Synthetic Strategy for Preparation of Amino Silicone Capture Solvents.



This and other approaches described in task 3.1 formed the basis for the synthetic work performed. Given the nature of the solvents desired for testing and the amounts of materials needed, high throughput synthesis was not applicable in this case. However, the goal of producing 5 or more structural variations was easily realized with the routes employed.

Task 3.0 (CO₂ Capture Solvent Synthesis, Optimization and Property Testing)

Subtask 3.1 (High Throughput Method Development and Synthesis of Solvents)

High throughput screening (HTS) was envisioned as a suitable method to evaluate numerous solvent samples under a variety of conditions in a rapid manner. The initial screening method used a 48-well reactor with each vial containing solvent exposed to a CO₂ purge via a needle. Flow rates were monitored by a mass flow controller and sample weighing at timed intervals was accomplished with a robotic sampling device. Initial results with pure solvents showed consistently low CO₂ uptakes for all materials examined, whether control amines or candidate solvents. Visual observation of the vials showed all materials transformed into gums, waxes or solids which severely suppressed mass transfer of CO₂ into unreacted solvent. Much of this issue was mitigated by using larger vials and smaller sample sizes. This increased the surface area of the material and showed more consistent performance. Figure 16 shows the 27-well reactor and the robotic balance.

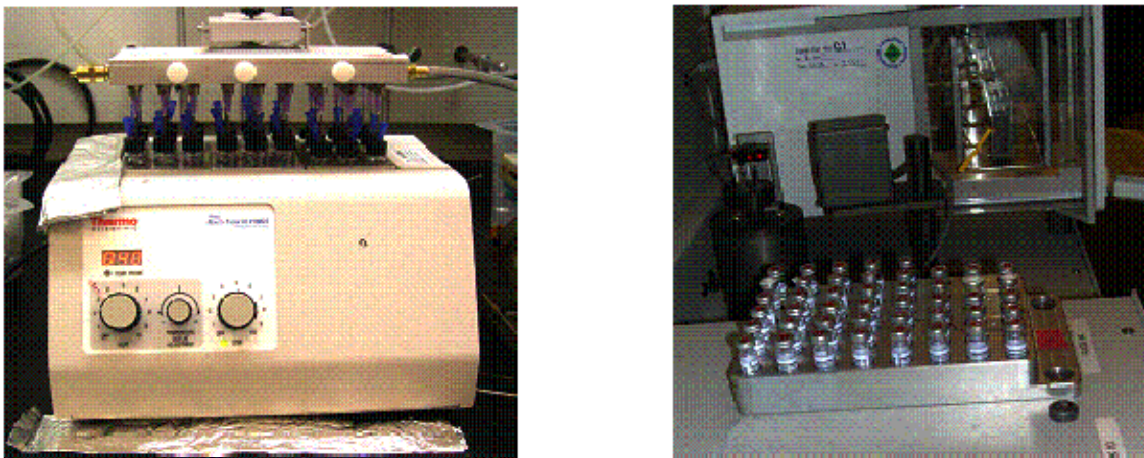


Figure 16. 27-Well Rapid Throughput Reactor and Robotic Balance.

With the new protocol in place, additional screening of both organic amines and candidate capture solvents continued. Tables 14-16 below show 3 differing sets of materials examined, from benchmark organic amines to amino silicones to hybrid amino ether siloxanes. In all cases, poor CO₂ uptake was still observed. Even with the increased surface area and stirring, poor mass transport still plagued the technique. This issue was observed at temperatures of 40, 55 and 70 °C as well as at time intervals of 1, 2 and 4 hours.

Table 14. HTS of Neat Selected Organic-based Amines for CO₂ Absorption at 40 °C, 100% CO₂ and 2 h.

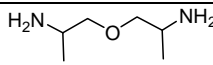
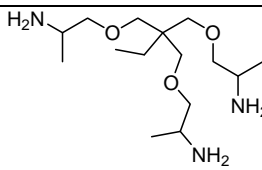
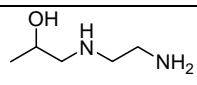
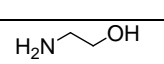
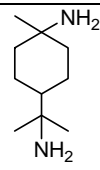
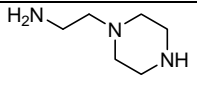
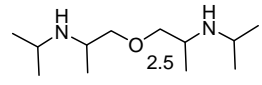
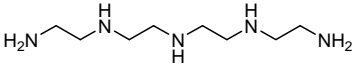
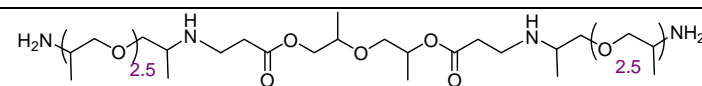
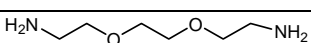
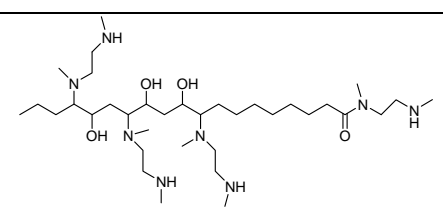
Entry	Structure	Theoretical yield (%)	CO ₂ uptake (%)	% Theoretical Uptake
1		33.3	15.8	47
2		21.6	5.8	27
3		37.2	21.4	58
4		36.0	31.5	88
5		25.8	10.5	41
6		34.0	12.5	37
7		20.4	2.3	11
8		58.2	14.5	25
9		17.3	6.1	48
10		29.7	20.9	73
11		22.0	1.9	9

Table 15. HTS of Neat Jeffamine Derived Solvents for CO₂ Absorption at 40 °C, 100% CO₂ and 2 h.

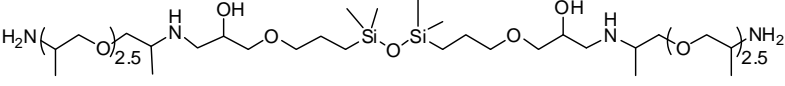
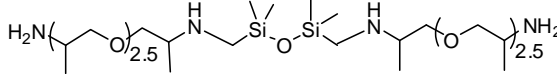
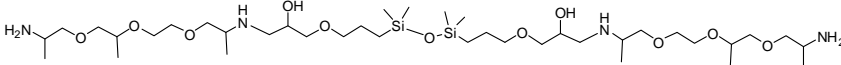
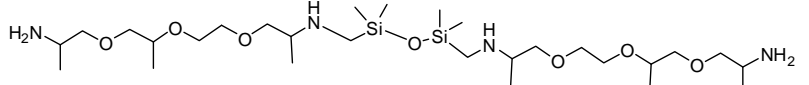
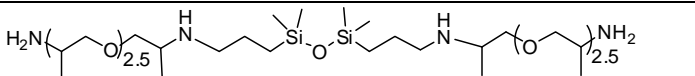
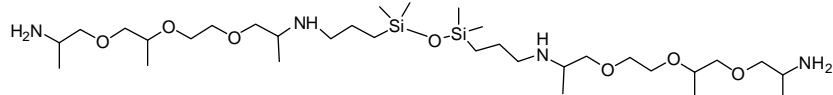
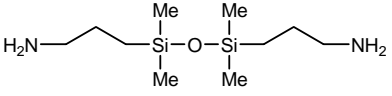
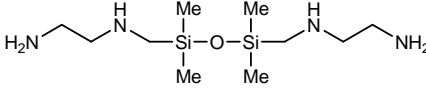
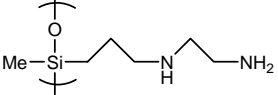
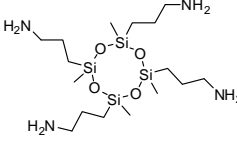
Entry	Structure	Wt Gain (%)	Theoretical Gain (%)	% of Theory
12		3.7	14.0	26
13		9.1	20.8	42
14		4.4	10.6	42
15		8.8	14.0	63
16		10.0	18.4	54
17		7.3	12.9	56

Table 16. HTS of Neat Amino Silicones for CO₂ Absorption at 40 °C, 100% CO₂ and 2 h.

Entry	Structure	Wt Gain (%)	Theoretical Gain (%)	% of Theory
18		15.1	17.7	85
19		13.3	31.6	42
20		6.8	27.5	25
21		3.5	18.8	19

As described in task 2.3, addition of a co-solvent was found to mitigate much of the mass transfer problem observed during CO₂ absorption with larger scale mechanical stirring. The same technique was employed with HTS. Again, temperatures of 40 and 55 °C were explored as well as weight gains at timed intervals and gas composition (ranging from 10% CO₂ in N₂ to 100% CO₂). Table 17 showed that

as more co-solvent was added, the theoretical amount of CO₂ absorbed increased. However, the absolute values were still very low, in most cases, which implied that a mass transfer problem still existed.

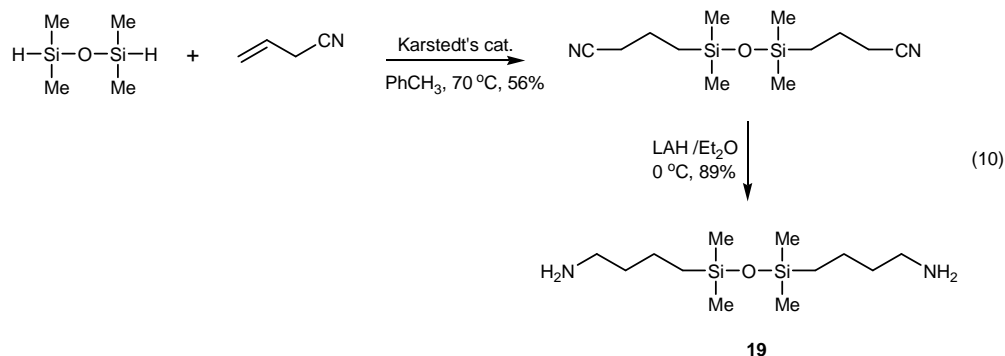
Table 17. Effect of TEG Co-solvent on CO₂ weight uptake for Aminosilicones at 40 °C and 1.5 h.

Entry	Solvent	Ratio of Solvent/TEG	CO ₂ concentration	Weight Gain (%)	% of Theory
22		100:0	10%	11.8	37
23	"	75:25	10%	10.8	45
24	"	50:50	10%	10.5	66
25	"	100:0	100%	18.1	50
26	"	75:25	100%	13.3	56
27	"	50:50	100%	10.6	67
28		100:0	10%	14.0	79
29	"	75:25	10%	12.0	90
30	"	50:50	10%	9.5	107
31	"	100:0	100%	17.1	97
32	"	75:25	100%	13.2	99
33	"	50:50	100%	11.7	131
34		100:0	10%	3.7	13
35	"	75:25	10%	2.6	13
36	"	50:50	10%	4.3	31
37	"	100:0	100%	6.8	25
38	"	75:25	100%	12.4	60
39	"	50:50	100%	5.0	36

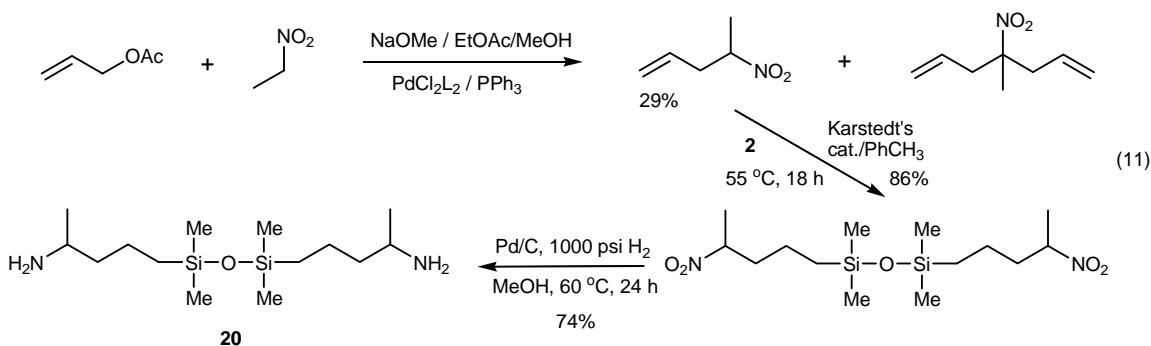
Different co-solvents like TEG, NMP (N-methyl pyrrolidone) and TGDME (tetraglyme dimethylether) were also examined with no improvement. Exploration of multiple components and even the addition of potential promoters such as isoquinoline, triethanolamine and DBU (diazabicycloundecene) had no positive effect on increasing the absorption properties of the capture solvents. With these results in hand, it was determined that mechanical agitation of the reaction mixtures was paramount in order to ensure that best possible mixing was obtained and the mass transfer issues would be minimized.

Based on the CO₂ capture results seen above, and especially in Tables 9-12, it appeared that amino-disiloxanes or closely related species offered the most potential as CO₂-capture solvents. Further optimization of this class of compounds through structural variations followed. For these selected solvents, high throughput synthesis was not necessary.

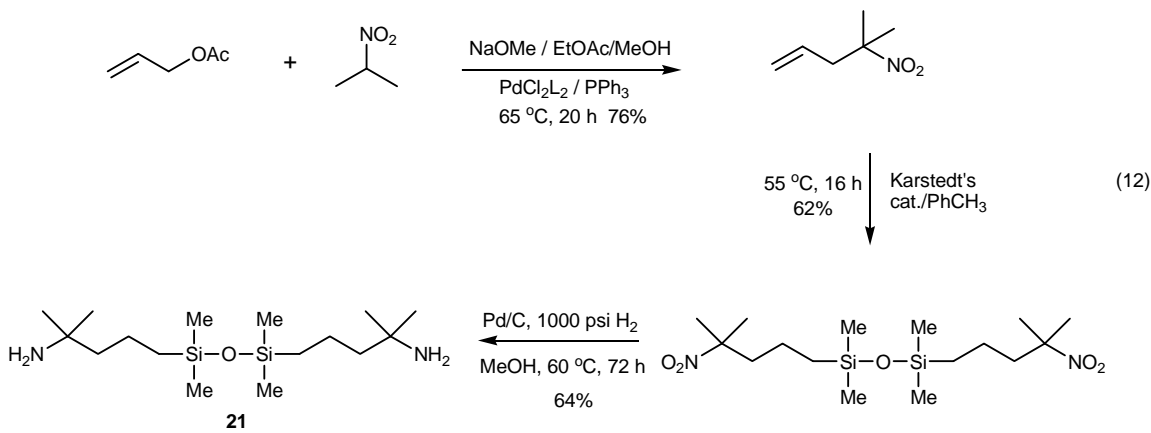
Few aminodisiloxanes are commercially available and a wider range of structural variants needed to be explored in order to gauge their efficacy in CO₂ capture. Hindered amines have been reported to be more effective in capturing CO₂ than their unhindered counterparts.⁵ To test this concept, a series of compounds **19**, **20** and **21** were synthesized with increasing steric bulk. Aminobutyl derivative **19** was made as shown in equation 10. Hydrosilylation of tetramethyldisiloxane with allyl cyanide gave a dinitrile which was subsequently reduced with lithium aluminum hydride (LAH).



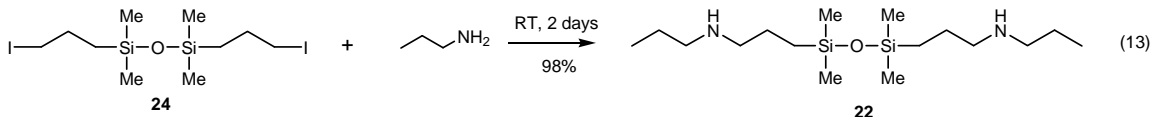
Synthesis of the methyl-substituted derivative **20** proceeded through a nitro functional disiloxane intermediate as shown in equation 11



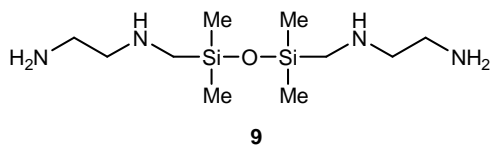
A similar approach was taken for the dimethyl analog **21** as shown in equation 12.



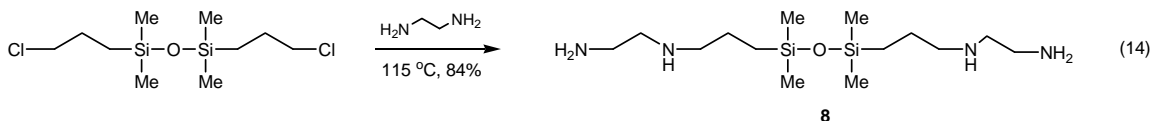
To this point, the aminosiloxanes synthesized contained only primary amino groups. Compound **22** was made to determine what effect a purely secondary amine containing disiloxane would have on CO₂ capture. N-Propylamine readily displaced iodide from **24** to give the propylaminopropyl derivative in nearly quantitative yield.



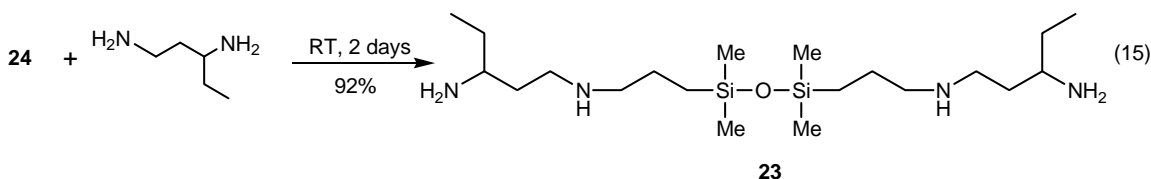
In addition to simple structural variants, some multi-functional derivatives were prepared designed to determine whether higher CO₂ capacity could be obtained. The first approach was to explore compounds with multiple amines in the side chains. These materials contained a mixture of primary and secondary amine functionality.



The aminoethylaminomethyl derivative, **9**, was commercially available but the corresponding aminoethylaminopropyl disiloxane, **8**, required preparation as shown in equation 14.

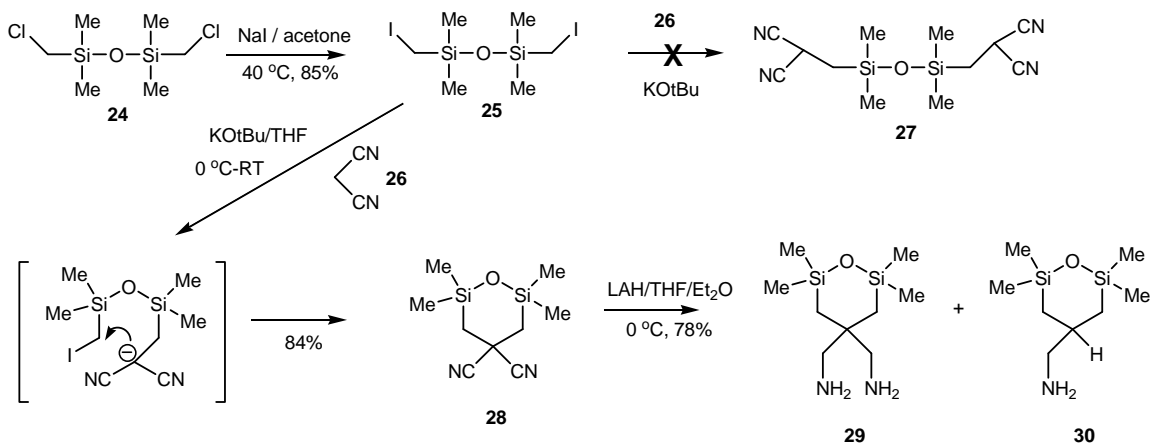


A tetrafunctional hindered amine disiloxane **23** was prepared via the reaction of 1,3-diaminopentane with **24**.

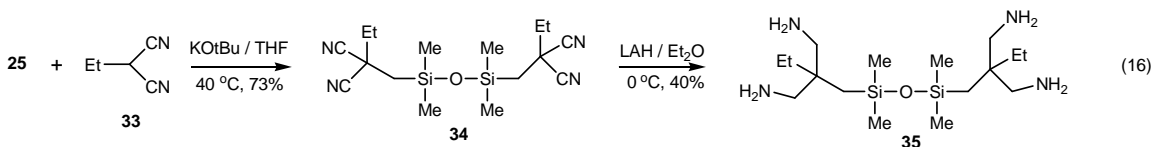


Another series of tetraamino derivatives were targeted where all of the amines were primary. These were envisioned to be available via reaction of haloalkyl disiloxanes with the anion of malononitrile, followed by reduction of the subsequent tetranitriles. As a first example, synthesis of a malononitrile derivative **27** was targeted (Scheme 7). However, it was quickly determined that reaction of malononitrile **26** with bis(iodomethyl)tetramethyl disiloxane **25** using potassium *t*-butoxide as base, did not give the anticipated product **27**, but rather the solid cyclic compound **28**, via intramolecular cyclization. Interestingly this result was obtained even with excess malononitrile. In fact, it was subsequently determined that when the reaction was done on-stoichiometry, that lower yields were obtained. This was due to the formation of more side products, which appeared to arise from attack by potassium *t*-butoxide on the siloxane linkage. LAH reduction of **28** gave a mixture of the mono and diamine materials **29** and **30**.

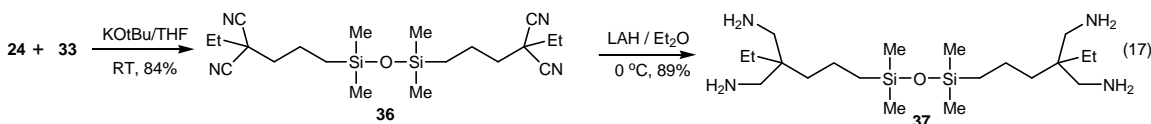
Scheme 7 Preparation of Malononitrile Derivatives.



The intramolecular cyclization that led to **28** could be eliminated by using monoalkylated 2-ethyl malononitrile anion as nucleophile as shown in equation 16. Bisalkylation of iodomethyl functional **25** at 40°C resulted in 73% isolated yield of the solid tetracyano compound **34**. LAH reduction allowed for isolation of the final tetraamine, **35** in 40% yield. In this case, no trace of products derived from reductive decyanation was observed.



2-Ethyl malononitrile was also reacted with bis(3-iodopropyl) tetramethyldisiloxane to give tetranitrile **36** (equation 17). The reaction in this case was more facile than with the iodomethyl disiloxane, and excellent yields of product were obtained after reaction for a couple of hours at room temperature. Subsequent reduction with LAH in ether provided tetraamine **37** in high yield and good purity.



A final tetraamine synthesis was attempted as shown in equation 18. Reaction of the malononitrile anion with **16** gave tetracyano disiloxane **38**. Clean reduction of this material to the corresponding tetraamine **39** proved to be difficult. The acidic methine protons of unsubstituted or monoalkylated malononitrile derivatives have been reported to be the cause of poor yields during reduction.⁶ Chemical reductions using $\text{NaBH}_4/\text{BF}_3\text{-Et}_2\text{O}$, $\text{NaBH}_4/\text{NiCl}_2$ ⁸, LAH⁹ or LAH/ AlCl_3 ¹⁰ did not proceed cleanly, nor did catalytic reduction using PtO_2 in $\text{EtOH}/\text{CHCl}_3$.¹¹ Hydrogenations with Pd/C in EtOH or in an acidic medium¹² were also unsuccessful; even with the possibility of side reactions of amines with partially reduced imine intermediates¹³ being suppressed.

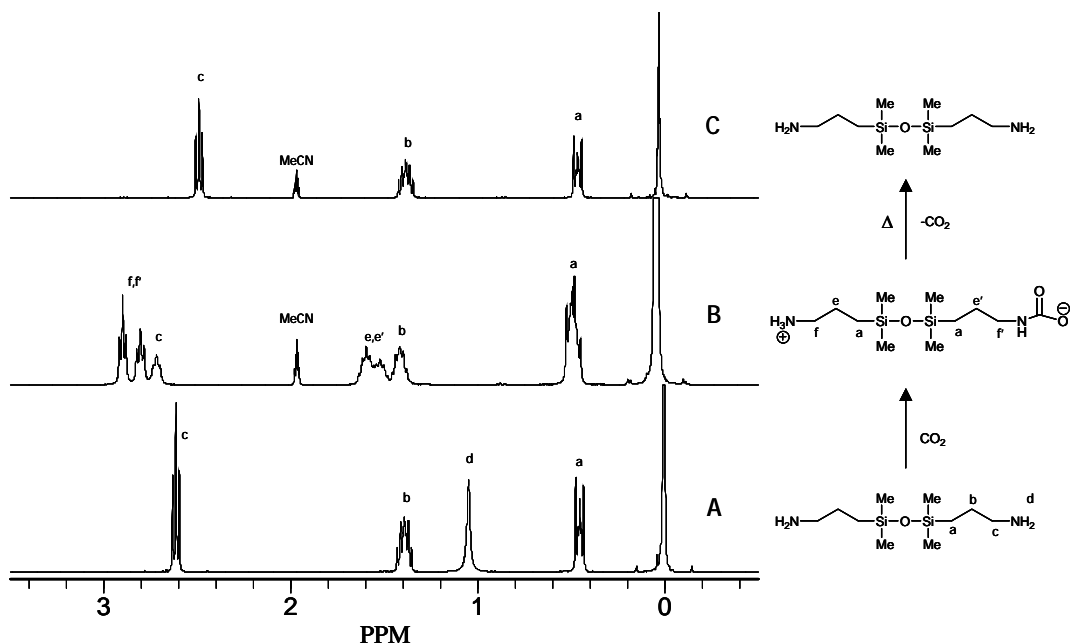


Figure 17. Regeneration of GAP-0 from carbamate salt.

The next step was to prove this could be accomplished in a cyclic manner. Figure 18 shows 6 absorption/desorption cycles run with a 50/50 mixture of GAP-0/TEG under 100% CO₂ at atmospheric pressure and 40 °C.

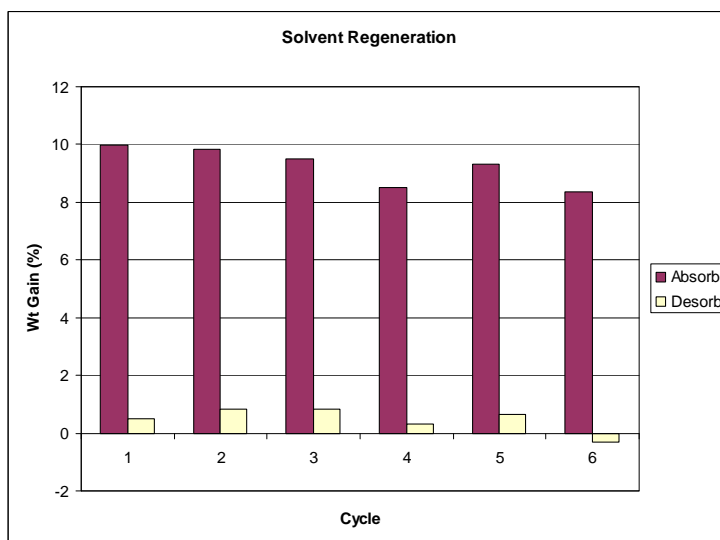


Figure 18. Cyclic regeneration of GAP-0.

Desorption occurred at 120 °C and 1 atmosphere. One can see that 8.5-10% weight increase was seen during the absorption cycles and that, after desorption, 1% or less of the weight gain remained. The downward drift of the plot is due to the slight volatility of the TEG and GAP-0 solvents. No effort was made to capture this solvent although that would need to be taken into account in the plant design.

The viscosity of the GAP-0/TEG mixture at various loadings of CO₂ was also determined and is shown in Figure 19. The lower the viscosity the easier for fluid movement but even at the highest loading and lowest temperature, the viscosity is only ~4500 cP; a value readily handled by appropriate pumps.

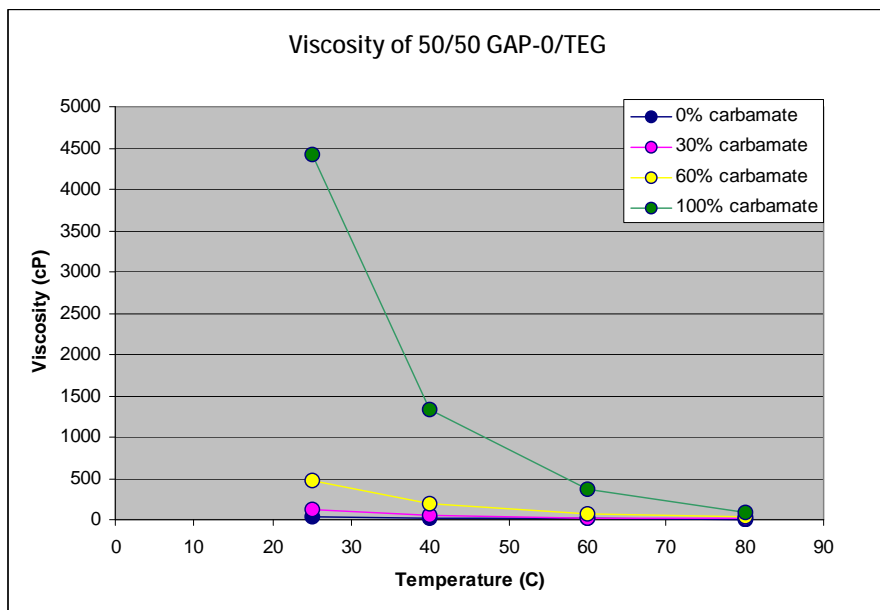


Figure 19. Viscosity change vs temperature for 50/50 GAP-0/TEG solvent mixture.

Density changes over temperature for the same 50/50 blend were also determined as shown in Figure 20. As expected as the solvent mixture becomes richer in carbamate, the density increases due to the presence of oxygen atoms.

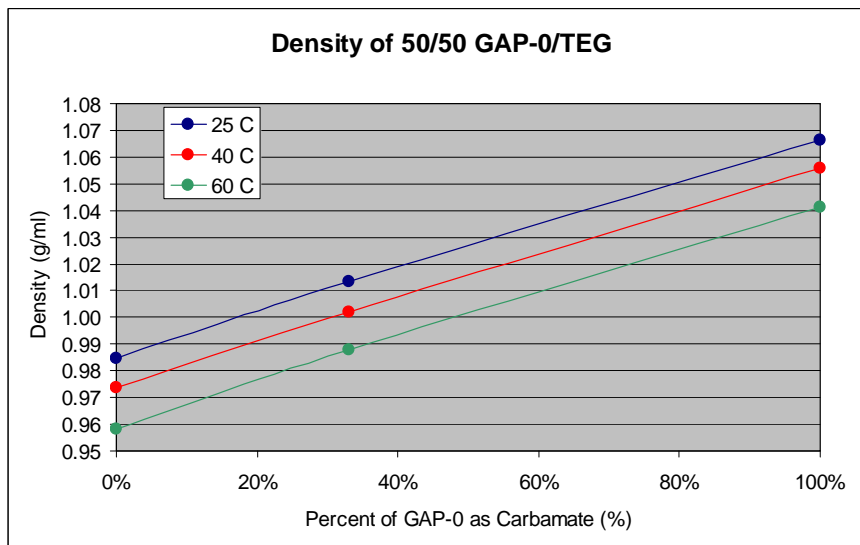


Figure 20. Density Change vs Temperature for Various Compositions of TEG and GAP-0 Carbamate.

The CO₂ absorption profile of a 50/50 weight mixture of GAP-0 and TEG was run at several temperatures to determine the equilibrium value of weight gain (Figure 21). At 1 atmosphere of CO₂,

the amount of CO₂ absorbed ranges from 10.6% at room temperature (22 °C) to 6.2% at 100 °C (blue symbols). At 10% CO₂ (0.1 bar), conditions closer to the composition of flue gas, the CO₂ capture capacity decreased as seen by the yellow symbols. The total overall absorption capacity could be increase by elevating the ratio of GAP-0: TEG. A 60/40 mixture showed that a 2% increase in CO₂ capture capacity was realized at both 100% CO₂ and 10% CO₂.

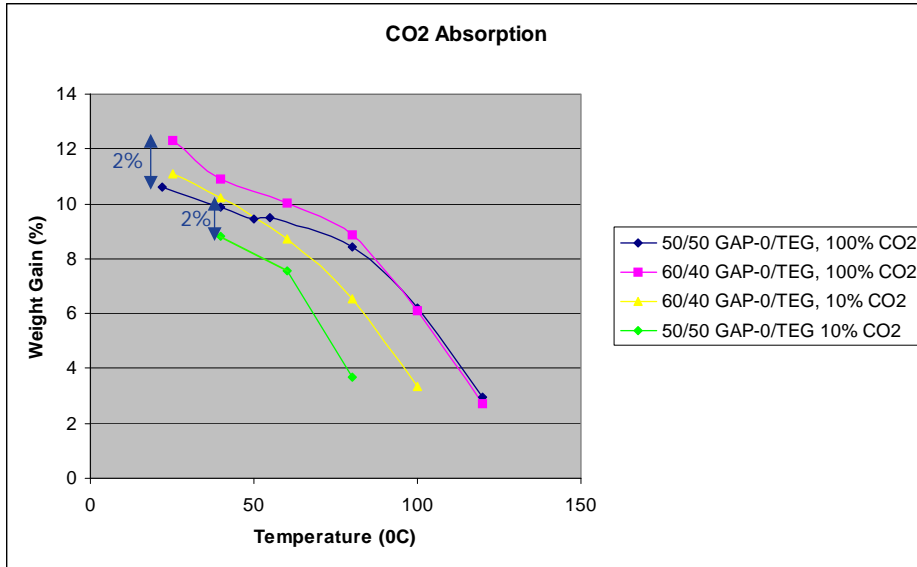


Figure 21. CO₂ capture for 50/50 and 60/40 mixtures of GAP-0 and TEG.

To confirm this result and obtain the isotherms needed for the parametric model, the 60/40 mix was evaluated at six temperatures and pressures. The data are seen in Figures 22 and 23. At the greater weight % loading of GAP-0 an increase of approximately 1 weight % was seen.. Concomitant with that increase is also an increase in viscosity.

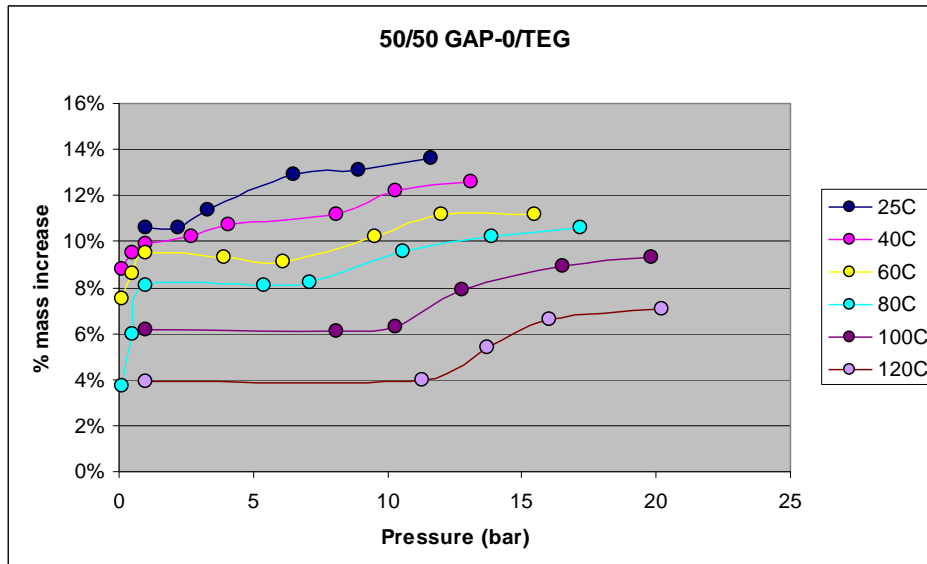


Figure 22. Isotherms for 50/50 GAP-0/TEG.

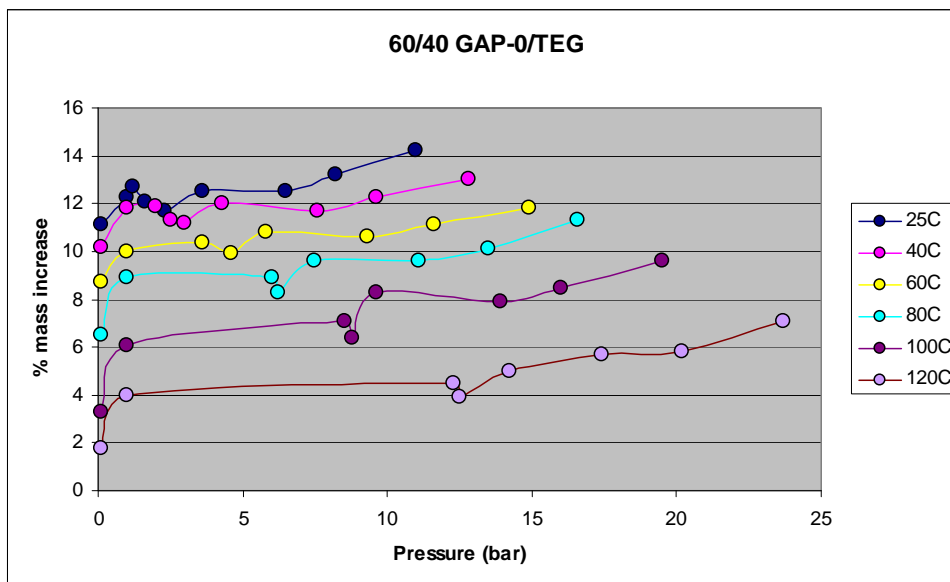


Figure 23. Isotherms for 60/40 GAP-0/TEG

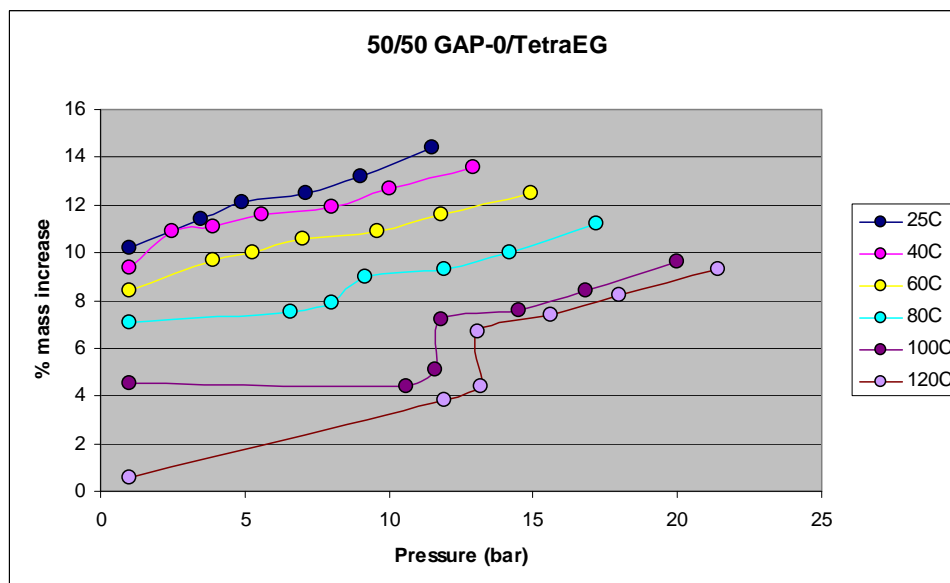


Figure 24. Isotherms for 50/50 GAP-0/tetraethylene glycol.

The same isotherm measurements were taken for 50/50 GAP-0 in tetraethylene glycol. This is a solvent with essentially the same properties as TEG but with a higher boiling point (285 vs 310 °C) Figure 24 shows at higher temperatures there was less CO₂ uptake than seen in the TEG co-solvent.

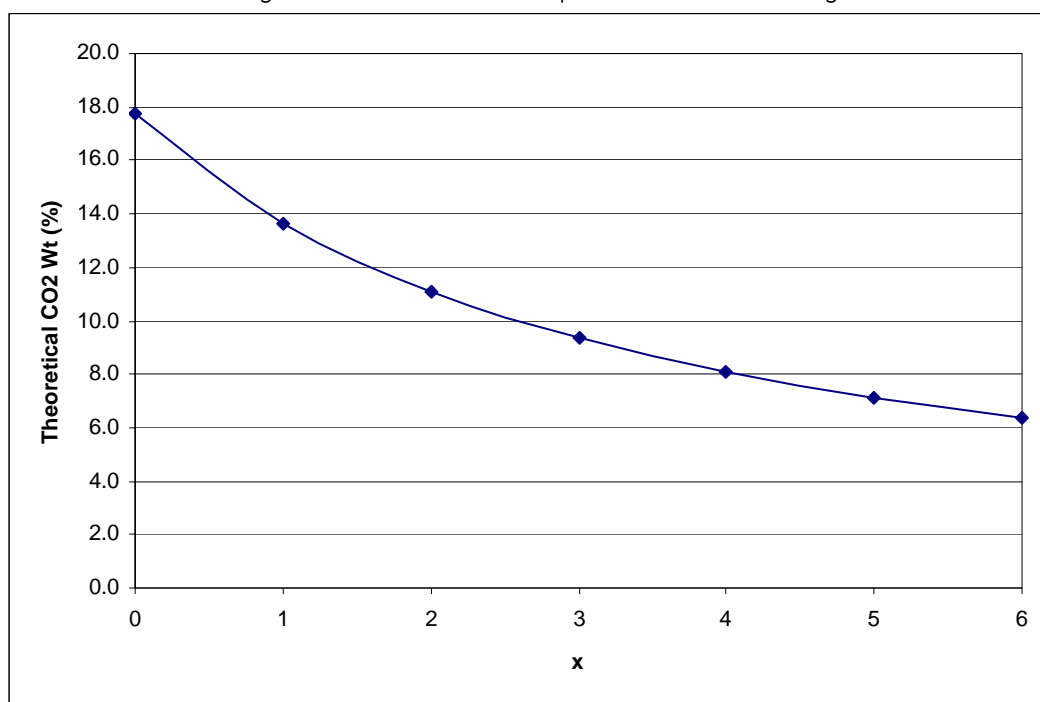
Further elaboration of low molecular weight silicone-based solvents was undertaken with emphasis placed on trimers and tetramers and associated co-solvents. Focus was placed on maximizing CO₂ uptake and solvent boiling point, while minimizing solvent viscosity and amount of co-solvent needed.

GAP-0 Oligomer/TEG Blends

While GAP-0 gave impressive CO₂ uptake experiments, it exhibited a couple of minor shortcomings. First, it is somewhat volatile so that some weight loss may be observed in a continuous process of CO₂ absorption followed by desorption. In addition many of the GAP-0 carbamate/co-solvent blends had a tendency to solidify on standing at room temperature. It was postulated that GAP oligomers might be able to overcome these issues. Thus a series of materials were synthesized and evaluated in blends with TEG.

The simplest approach would be to make linear oligomers of the M'D_xM' type.¹⁵ However, x would need to be kept fairly small so that the theoretical CO₂ uptake would not diminish to too large an extent. Included in Figure 25 is plot of theoretical CO₂ uptake vs x, which shows that in order to maintain an acceptable CO₂ capacity, x could not be much above 2.

Figure 25. Theoretical CO₂ Uptake for Linear GAP Oligomers



A couple of linear materials were synthesized via reaction of GAP-0 with octamethylcyclotetrasiloxane (D₄) using tetramethylammonium hydroxide (Me₄NOH) as catalyst. The first was targeted at x=2, which after stripping gave a material that proton NMR showed to be closer to x= 2.5. Given this, the rest of the materials were not stripped as much. The other linear material that was prepared was M'DM'.

Two branched, low molecular weight oligomers were also prepared. The first material was prepared by reaction of GAP-0 with 3-aminopropyl triethoxysilane, once again using Me₄NOH as catalyst. After heating at 60 °C., water was charged to the mix and after hydrolysis, toluene was added and water and ethanol were azeotroped out under vacuum (so that the temperature could be kept at 90°C, thus minimizing catalyst degradation). The average structure was M'₃T'. The second polymer was made similarly except that D₄ was also added up front. This oligomer had an average composition of M'₃D₅T'.

Finally, a linear copolymer was prepared containing some aminopropyl D groups (D') as well. 3-Aminopropylmethyl-diethoxysilane was used as the source of D'. An average structure was M'D'D₃M' was targeted.

With five different oligomers in hand, CO₂ uptake experiments were begun. Each of these materials turned to solids upon exposure to CO₂. M'DM' and M'₃T' both gave hard powdery solids, M'D_{2.5}M' gave more of a wax, and the M'₃D₅T' and M'D'D₃M' reacted to give glassy materials. Interestingly, three of the five materials (M'D_{2.5}M', M'₃T', and M'₃D₅T') also exhibited % weight gain values >100% of theoretical (103-108%), while both M'DM' and M'D'D₃M' ended up at 96%.

Next, blends of these materials with various amounts of TEG were evaluated. The results of these studies are summarized below in Table 18.

Table 18. CO₂ Uptake of Aminosiloxanes and TEG

Structure	% TEG	% Wt Gain	% of Theory	Final Form
M'D _{2.5} M'	0	10.9	107	Semi-solid
"	17	9.3	110	Flowable oil
"	10	10.1	110	Very viscous oil
M'DM'	0	13.1	96	Hard solid
"	20	11.9	109	Very viscous oil
"	30	10.4	109	Flowable oil
M' ₃ T'	0	18.8	103	Hard solid
"	50	9.8	107	Flowable oil
"	30	13.9	109	Very viscous oil
M' ₃ D ₅ T'	0	11.1	108	Glassy solid
"	16	8.7	100	Very viscous oil
M'D'D ₃ M'	0	10.8	96	Glassy solid
"	20	9.7	108	Viscous oil

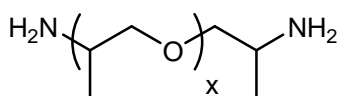
As can be seen, as with GAP-0, TEG was an effective co-solvent. In each case the siloxane/TEG blends were oils. However, several of these blends were very viscous. Addition of more TEG was able in all cases to lower the viscosity such that the blends were flowable. Interestingly, this point always seemed to occur when the overall weight gain on CO₂ exposure was in the 9-10.5% range. This is also in line with the results with GAP-0 and TEG.

The majority of the aminosiloxane oligomer-based carbamate salt solutions in TEG above all appeared to remain liquid on standing. The only exception was the M'DM' blend with 20% TEG which exhibited some solid formation. However, even in this case the bulk of the material looked to remain a viscous oil.

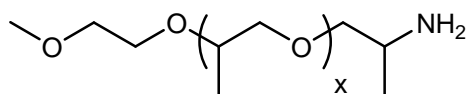
GAP Oligomer/Jeffamine Blends

Another series of blends were explored based on combinations of M'D_{2.5}M' and Jeffamine polyetheramines. This particular GAP oligomer was chosen as the carbamate salt solution formed via reaction of CO₂ with this material was the closest to being an oil as opposed to a solid. With respect to the Jeffamines, the D series materials are difunctional while the M series is monofunctional. Typically, the number in the Jeffamine product name is the rough molecular weight of the material.

Jeffamine Structures



Difunctional



Monofunctional

For example, Jeffamine D-230 is a difunctional product with an approximate molecular weight of 230. All of the materials used were primary amine terminated polyethers except for Jeffamine SD-231, which has secondary amines at the chain ends. Included in Table 19 are the results from CO₂ uptake experiments from a number of these types of blends.

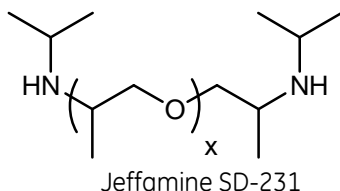


Table 19. CO₂ Uptake Data for M'D_{2.5}M'/Jeffamine Blends

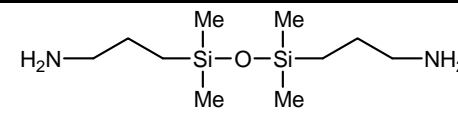
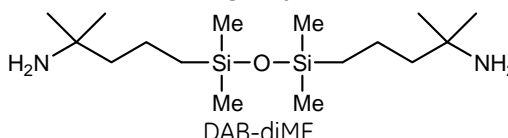
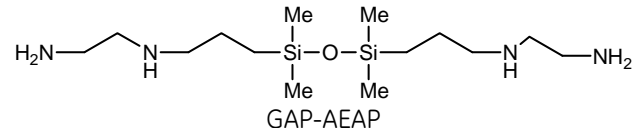
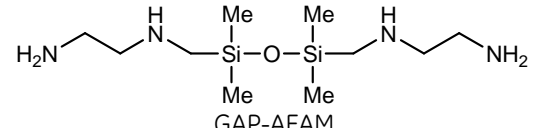
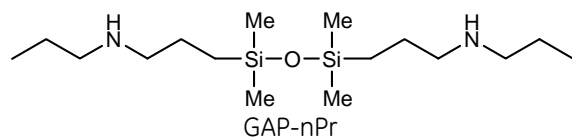
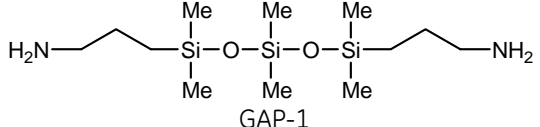
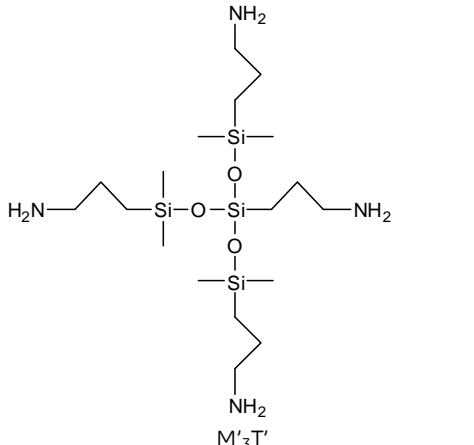
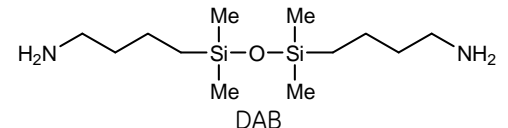
Jeffamine	% Jeffamine(s)	% Wt Gain	% of Theory	Final Form
D-230	50	15.4	105	Very viscous oil
SD-231	41	8.9	76	Flowable oil
D-230/SD-231	50 (25/25)	12.2	92	Slightly flowable
D-230/D-2000	34 (17/17)	11.6	113	Viscous oil
D-400	50	11.3	111	Very sl. Flowable
D-400/SD-231	50 (25/25)	10.1	91	Flowable oil
M-600	15	10.5	115	Soft wax

As can be seen, the results here are similar to those above- flowable carbamate salt blends were observed when the weight gain on CO₂ exposure was less than approximately 11%. The one exception was the blend with the monofunctional M-600, which ended up a soft wax even though the weight gain was 10.5%. One other conclusion was clear from these results- blends containing the secondary amine based SD-231 did not match the theoretical weight gain based on the total amine concentration (amine from the siloxane and the Jeffamine).

Tasks 3.3 and 3.4 (Multi-property Modeling and Property Determination of lead candidates)

The conductor-like screening model for real solvents (COSMO-RS) was used to predict the physical properties of silicon amines including viscosity, density and vapor pressure. This method is widely used to predict thermodynamic properties of fluids. Table 20 presents the viscosities and densities from calculation and those determined experimentally for the aminosilicones. The table shows that viscosities predicted by COSMO-RS are much higher than those from experiments. Also, viscosity trends for silicon amines from calculation do not agree with those from experiment. This indicates that COSMO-RS is a poor predictor of aminosilicone viscosity.

Table 20. Viscosities and Densities for Silicon Amines from COSMO-RS Calculations and Experiments.

Solvent	Viscosity (cP) (Theory) (25 °C)	Viscosity (cP) (Experiment) (25 °C)	Density (g/cm ³) (Theory) (25 °C)	Density (g/cm ³) (Experiment) (22°C)
 GAP-0	40.1	4.4	0.931	0.893
 DAB-diME	66.4	9.1	0.891	0.866
 GAP-AEAP	410.5	22.0	0.961	0.929
 GAP-AEAM	61.1	11.0	0.969	0.938
 GAP-nPr	74.7	5.8	0.890	0.865
 GAP-1	120.3	4.4	0.951	0.913
 M' ₃ T'	1666.5	18.3	0.983	0.965
 DAB	79.6	5.5	0.918	0.898

Viscosity values for aminosilicones were determined using a Brookfield DV-II + Pro Programmable viscometer. This cone-and-plate device was equipped with temperature control and had a small sample holder (~1cc) which was ideal for testing small amounts of these novel compounds. Figures 26 and 27 illustrate the viscosity of GAP-0 and GAP-1, respectively, at 25, 46, 60 and 80°C over the entire range of shear rates available for this apparatus. The “poly” curves represent polynomial fits of the data. These polynomials illustrate that GAP-0 and GAP-1 are essentially shear rate-independent over this temperature and shear rate range, which is not surprising given the relatively low MW of these compounds.

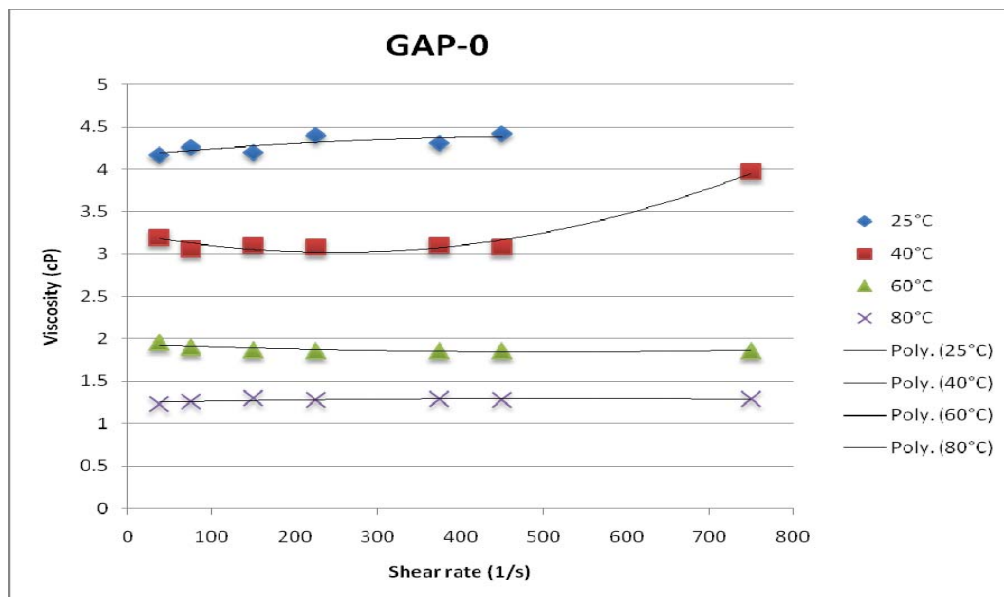


Figure 26. Viscosity of GAP-0 as a Function of Temperature and Shear Rate.

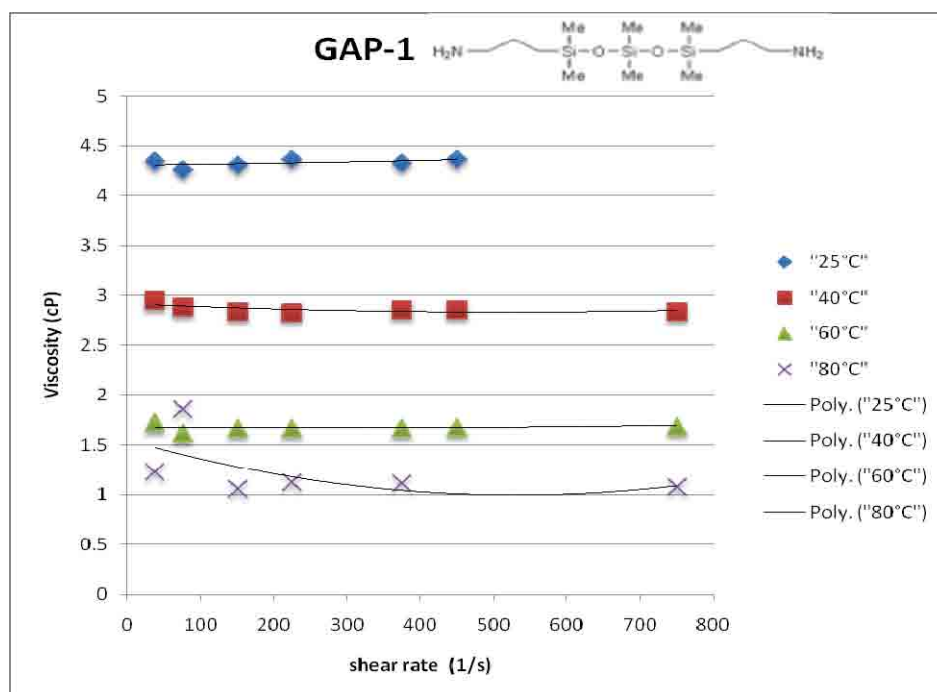


Figure 27. Viscosity of GAP-1 as a Function of Temperature and Shear Rate.

Similar shear-rate independent results were obtained for all of the aminosilicones, therefore in the following plot (Figure 5) the average viscosity of the aminosilicone was plotted as a function of temperature. As expected, viscosity decreases with temperature and increases with the MW and number of amines in the compound.

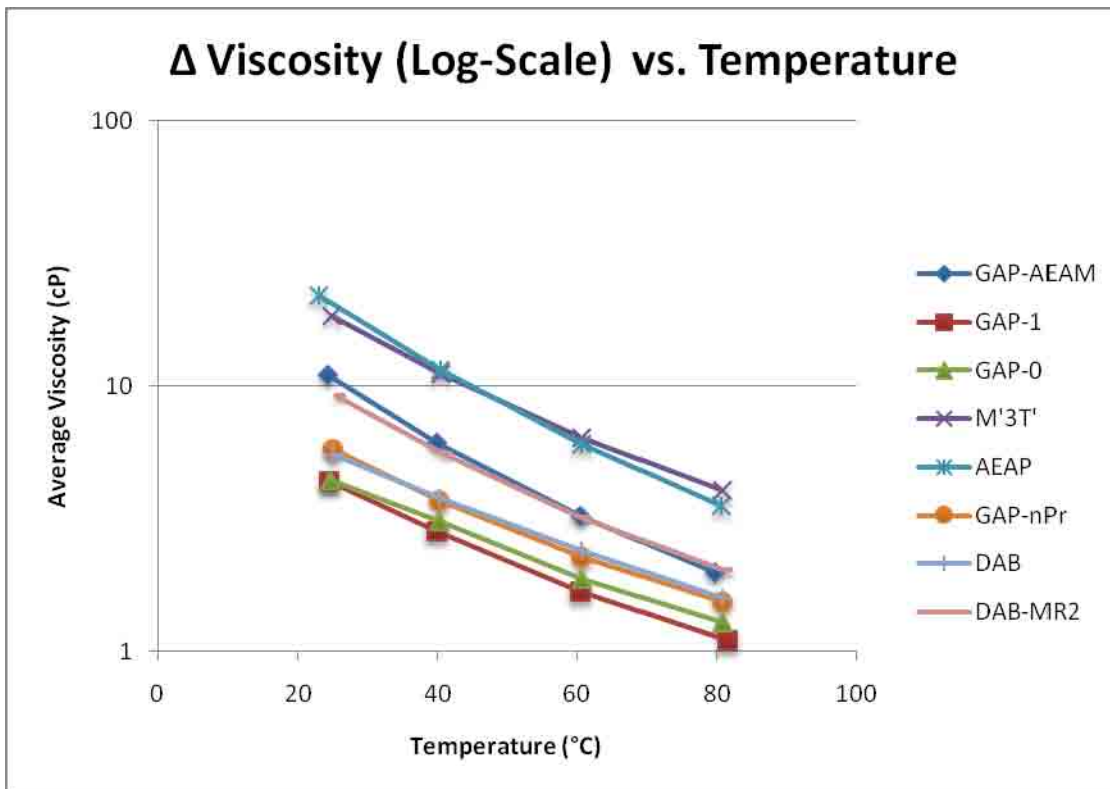


Figure 28. Temperature Dependence of Amino Silicones on Viscosity.

For all aminosilicones considered, densities predicted by COSMO-RS were about 2%-4% higher than those experimentally determined. Density trend M'3T > GAP-AEAM > GAP-AEAP > M'DM' > GAP-0 > DAB-0 > DAB-diME > GAP-nPr predicted by COSMO-RS is in good agreement with that from experiments (Figure 6). The one outlier was GAP-Dytek, in which COSMO-RS closely predicted the experimental value. Also note that the actual temperature in the experimental data is a little different from that used for calculations.

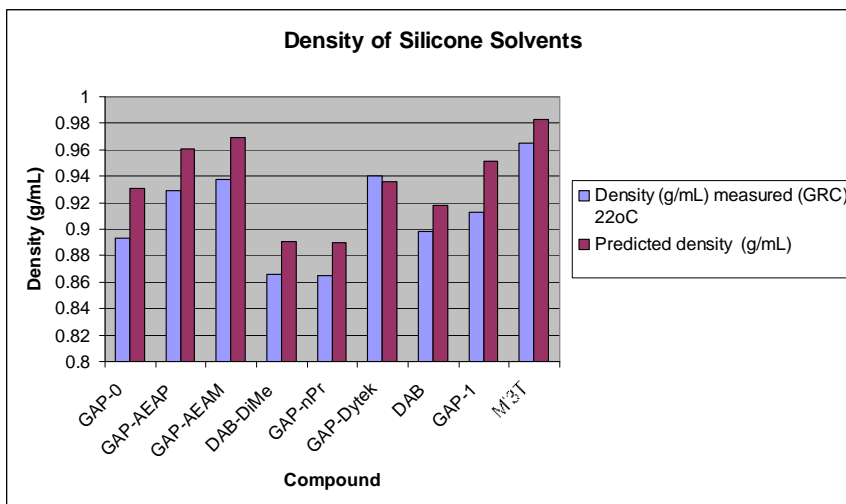


Figure 29 Measured vs. Predicted Values of Density for Aminosilicones.

At this time, there is no experimental data for the vapor pressure of aminosilicones. To validate the model, the vapor pressure of MEA (from literature) was compared to the COSMO-RS calculation. From Figure 30, the vapor pressure of MEA predicted by COSMO-RS is in reasonable agreement with experiment. Validation of this technique is in progress to confirm that COSMO-RS is effective in predicting vapor pressure for other amines. The trend of vapor pressure predicted by COSMO-RS is GAP-Dytek < GAP-AEAP < M'3T < GAP-nPr < GAB-DiMe < M'DM' ≈ DAB-0 ≈ GAP-AEAM < GAP-0.

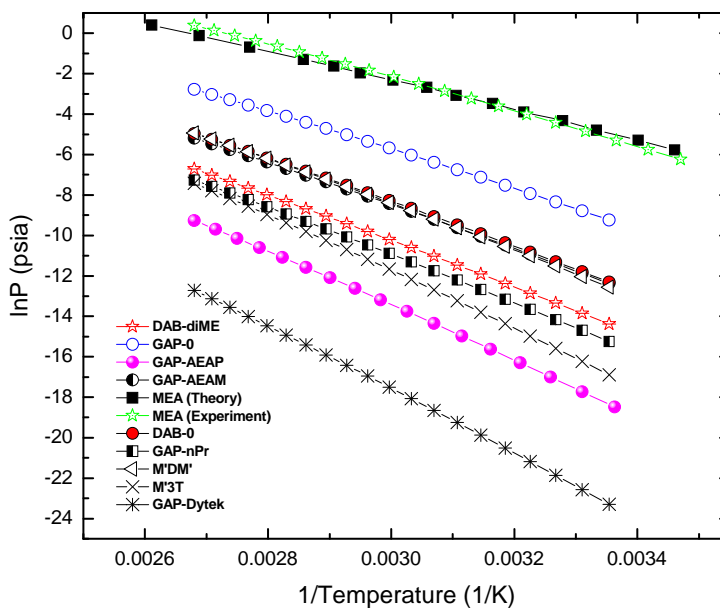


Figure 30. Predicted Vapor Pressures for Aminosilicones.

As described in task 3.5, the CO₂-rich solvent mixture of GAP-0 and TEG solidified on standing. This was a major issue when considering the operation of a full-scale power plant with this capture technology. To circumvent this, it was found that a 60/40 mixture of GAP-1/TEG suppressed any solid formation and provided a comparable capture capacity to the original GAP-0/TEG composition. To this end, the

isotherm plot of the new mixture is seen in Figure 31. These data were incorporated into the GEN 2 COE model in task 4.

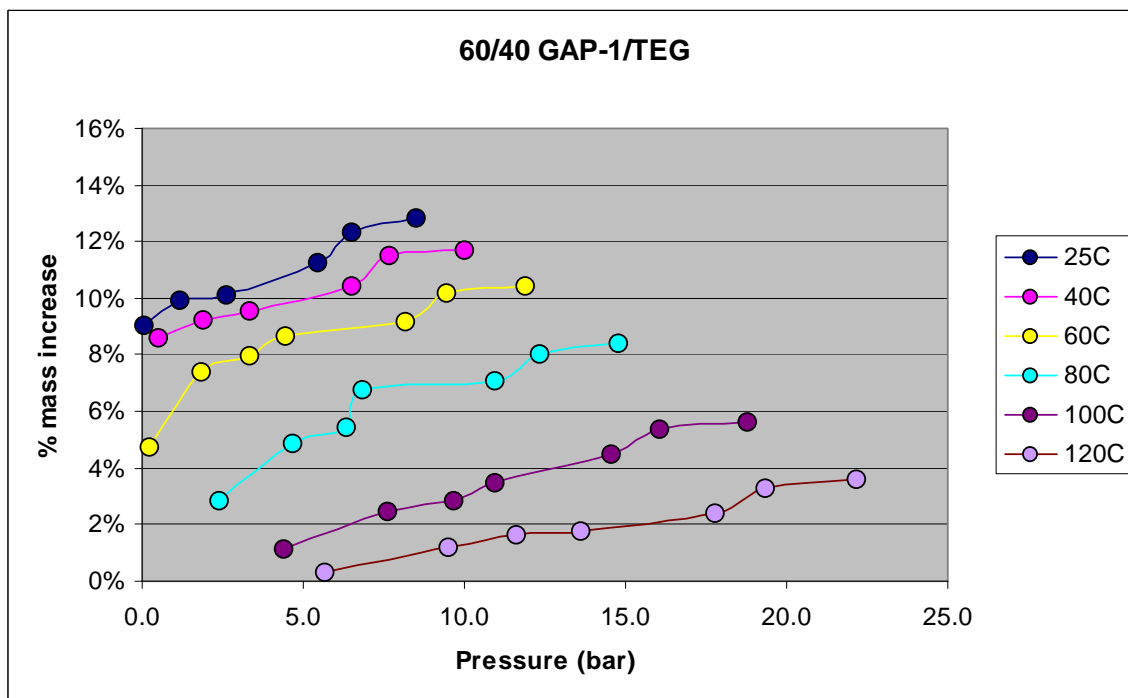


Figure 31. Isotherm Plots for 60/40 GAP-1/TEG.

As described above, successful syntheses of a series of disiloxanes with varying steric hindrance around the amine functional group and amine position were realized. Table 21 shows these solvents and their CO₂ uptake capacities.

Table 21. CO₂ Absorption of Aminodisiloxanes.

Cmpd	Structure	% CO ₂ Wt Gain (Neat)	% of Theory	% CO ₂ Wt Gain (1/1 TEG)	% of Theory
1		17.3	98	10.2	115
5		14.6	92	8.6	108
11		13.5	94	8.2	116

15		9.5	72	5.4	84
18		7.1	54	3.3	50
19		21.8	69	15.9	101
21		16.7	64	11.8	90
23		16.5	79	9.9	95
29		15.5	82	6.5	69
30		12.7	117	6.1	111
32		NT	NT	4.6	63
35		4.8	20	11.4	90
37		13.4	64	9.9	95

Preliminary evaluation of these aminodisiloxanes proceeded by exposing the neat materials at 40°C in a flask with mechanical stirring, to a stream of dry CO₂. Mechanical agitation was necessary to improve the mass transfer of the gas through the reaction medium and 40°C is the approximate

temperature that flue gas would enter a CO₂ absorber column. The first column of Table 1 shows the weight gain recorded for the neat compounds after 2 h exposure to CO₂. The second column indicates the percentage of theoretical pickup to which this weight gain corresponds. Theoretical weight gain values were calculated based on the amine equivalent weight of each compound and the assumption that two amines were required per carbon dioxide molecule as shown in Equations 1 and 2. As can be seen, few of the materials reached their theoretical capacity in the neat state. However, many were in the 70-90% range. This was especially encouraging as almost all the aminodisiloxanes turned into solids during reaction with CO₂. Significantly, the only exception was the monoamine **30**, which remained liquid during CO₂ uptake, and as such was the only neat material to exceed 100% of the theoretical uptake value. This higher than theoretical value was presumably due to some physisorption of gas, as well as formation of bicarbonate salts from adventitious water present in the system.¹⁶

A closer look at the structural variations and their effect of CO₂ absorption revealed that the best materials were the linear primary amine containing solvents **1**, **5**, **11** and **30**. Increased steric hindrance around the primary amine with alkyl groups (compounds **15**, **23**, **35** and **37**) or a ring (**29**) substantially reduced the CO₂ capture capability. Multiple amines on a chain as seen in aminoethyl derivatives **19** and **21** did enhance CO₂ pickup on a weight % basis, but were less impressive on a molar or theoretical basis. Presumably, the secondary amines were less reactive than the primary ones. This latter supposition was born out by the relatively poor reactivity of secondary amine functional disiloxane **18**.

To further facilitate the mass transfer of CO₂ to the reactive amine sites, use of a co-solvent was also explored. Triethylene glycol (TEG) was found to be a suitable candidate for this purpose.¹⁷ First, it has low volatility and thus did not readily evaporate during testing. Furthermore, it solubilizes most carbamate salts formed from the reaction of the aminodisiloxanes with CO₂. Exposure of 50/50 mixtures of each of the disiloxanes with TEG for 2 h at 40 °C generated the results seen in column 3 of Table 1. Theoretical CO₂ uptake increased significantly and in several cases exceeded 100%. In all cases of increased weight gain, the reaction mixtures were homogeneous liquids. Secondary amine **18** did not show any improvement in CO₂ weight gain and compound **29** showed a decrease. In the latter case, the carbamate mixture in TEG was a waxy gel that suppressed rapid CO₂ reaction. The dicyclic triamine **32** was only tested in TEG as it was a solid at 40 °C. Even diluted, the reaction product with CO₂ gave a very thick waxy solid that only absorbed 63% of the theoretical amount of CO₂. Again, poor reactivity was likely a result of poor mass transfer

Interestingly, the stability of the absorbed CO₂ was evidenced by the fact that no appreciable loss of weight was seen with samples absorbing over 100% even after standing at ambient temperature for several days.

Thermal stability studies of both GAP-0 and GAP-1 were completed with the results shown in Figures 32-34. Figure 32 shows the GC analysis of GAP-0 held at 100 °C over 80 days. There was a decrease in GAP-0 content after 15 days but the by-product appeared to be the next higher homologue, GAP-1. Two other components were produced but in concentrations less than 1%. The same effects were seen in the 120 °C exposure (Figure 33). Again, >92% of the original GAP-0 remained after 85 days.

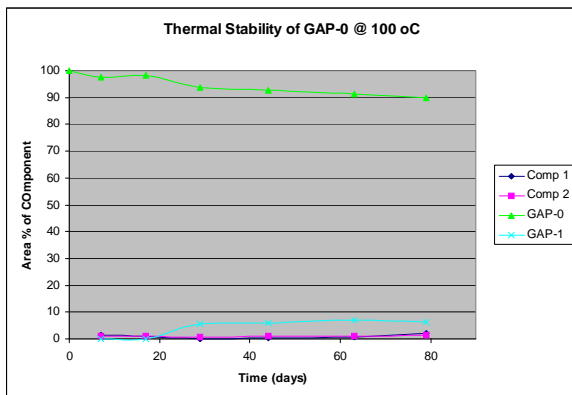


Figure 32. GAP-0 stability at 100 °C

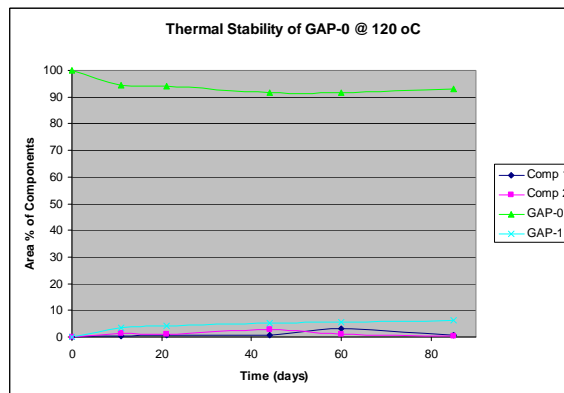


Figure 33. GAP-0 stability at 120 °C

The stability of GAP-1 is shown in Figure 34. There was some variation in the GC analysis of this material with time but there was essentially no change in composition over nearly three months at 100 °C.

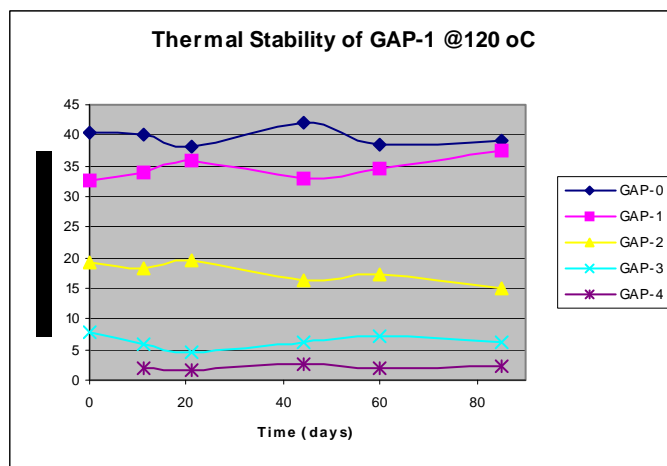


Figure 34. GAP-1 stability at 100 °C

The aminosilicones selected as likely candidates for further investigation contained over 40 atoms. For a system with so many atoms, it was computationally expensive to perform high-level calculations such as MP2 level of theory. Therefore a computational model was developed for aminosilicones that retained the important functional moieties while reducing the number of atoms in the calculation. The model is shown in Figure 35. (Appendix 6 provides details of the assumptions and calculations) Heats of reaction for forming carbamate were calculated using a two-step scheme as denoted in Table 6.

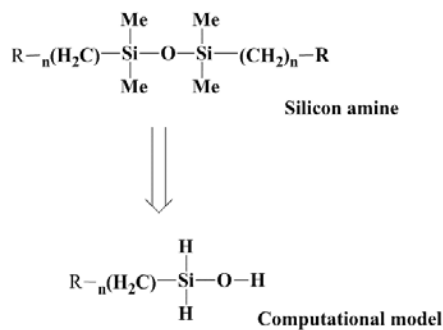


Figure 35. Computational Model used for Heats of Reaction Calculations.

The heats of reaction for GAP-0, DAB-0, DAB-Me and DAB-diMe are -14.5, -15.0, -13.0 and -11.5 kcal/mol at MP2/aug-cc-PVDZ//B3LYP/6-311++G(d,p) with UAHF radii, respectively, which is a less exothermic than corresponding values -16.7, -16.7, -14.6 and -12.6 kcal/mol at MP2/aug-cc-PVDZ//B3LYP/6-311++G(d,p) level with Bondi radii. At both levels, order of the heats of reaction for primary silicon amine is GAP-0 \approx DAB-0 > DAB-Me > DAB-diMe. This is in good agreement with our previous conclusion that the substitution of methyl group at α -site makes the basicity of amino group weaker and therefore makes the heat of reaction less exothermic. From GAP-0 to DAB-0, it just increases one more CH₂ spacer, which will have little influence on the heat of reaction and therefore heat of reaction almost did not change. From DAB-Me to DAB-diMe, one more methyl group is introduced into the α -site, which will further decrease the basicity of amino group and make the heat of reaction less exothermic relative to DAB-Me. More importantly, heats of reaction for these silicon amines are less exothermic than that of MEA, which could decrease the energy cost of the regeneration process in the CO₂ capture.

GAP-AEAM includes two different amino groups -NH and -NH₂. Therefore, when CO₂ reacts with GAP-AEAM, the product could be an inter-molecular or intra-molecular carbamate. However, the heat of reaction for forming intra-molecular carbamate is less exothermic than forming inter-molecular carbamate. So, if GAP-AEAM is in the reaction in an excess, the main product could be inter-molecular carbamate from the view of thermodynamics; if CO₂ is excess, the intra-molecular carbamate could be main product because CO₂ will continue to react with another vacant -NH or -NH₂ group in ammonium cations and carbamate anions to form intra-molecular carbamate. There is also a possibility to form ammonium dication and carbamate dianion. However, it should be unfavorable relative to form neutral intra-molecular carbamate because ammonium dication and carbamate dianion are generally unstable as Brennecke et al. suggested in their recent paper.¹⁸

Table 22 shows a comparison between the experimental and calculated heats of reaction data for some aminosilicones. The general trend of greater steric hindrance leading to lower ΔH_{rxn} is seen as was predicted but interestingly the GAP-0 solvent showed a similar ΔH_{rxn} to that of MEA. Adding a methylene spacer (in DAB) was not predicted to have much effect, but was found experimentally to reduce the ΔH_{rxn} by 4.5 kcal/mol. Most encouraging was the observation that GAP-1 was also substantially lower than MEA which would lower the energy needed for CO₂ desorption.

Table 22 Experimental and Calculated Heats of Reactions for Aminosilicones.

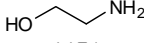
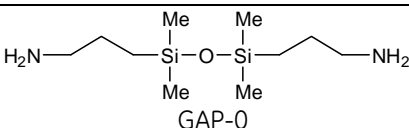
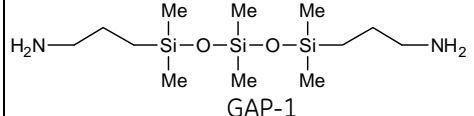
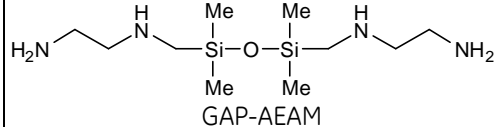
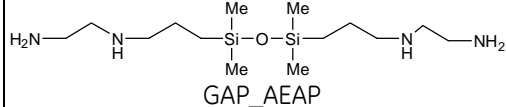
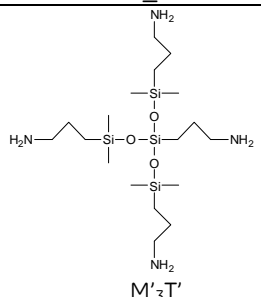
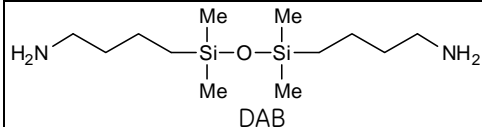
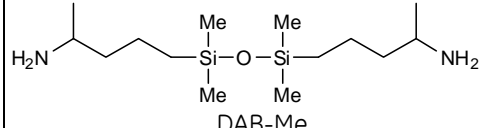
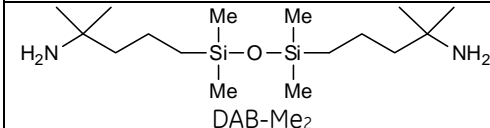
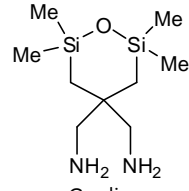
Structure	Experimental			Calculated	
	ΔH_{rxn} (kcal/mol)	Std. Dev.	DSC data (kcal/mol)	B3LYP (UAHF)	B3LYP (BONDI)
 MEA	17.3	1.3	17.2	16.3	17.8
 GAP-0	17.3	1.2	16.8	14.5	16.7
 GAP-1	13.0	1.1	-	-	-
 GAP-AEAM	12.4	0.6	12.3	14.5	15.4
 GAP_AEAP	12.4	0.3	-	-	-
 M'3T'	8.5	1.1	-	-	-
 DAB	12.8	0.3	13.7	15.0	16.7
 DAB-Me	11.4	0.8	12.8	13.0	14.6
 DAB-Me ₂	7.9	0.1	11.6	11.5	12.6
 Cyclic	11.3	-	-	-	-

Table 23 shows some of the physical properties of the GEN-1 and GEN-2 solvents compared to 30% aqueous MEA. The boiling points of both aminosilicones are substantially higher than MEA (especially obvious when all boiling points are normalized to atmospheric pressure). Densities of both aminosilicones are lower than MEA but the attendant viscosities are slightly higher, although still within an acceptable range. Interestingly, the heats of reaction with CO₂ for both GAP-0 and MEA were found to be identical while that for GAP-1 was substantially lower. This was a favorable factor in the COE calculations described later. The CO₂ uptake observed for both aminosilicones was comparable to 30% MEA and greater than expected. This was likely due to some physio-sorption of CO₂ in the solvent mixture as well as some bicarbonate formation from adventitious water in the solvent. The freezing points of the aminosilicones were substantially below that for MEA as was the heat capacity.

Table 23 Solvent Properties.

Property	GAP-0	GAP-1	30% MEA
Molecular Weight (Daltons)	248.1	322.5	61.1
Boiling point (°C/mm Hg) (pure solvent)	132-9/11	145-155/5	170/760
Boiling point (°C at 1 atm) (pure solvent)	265	310	170
Density (g/cm ³) (pure solvent)	0.893	0.913	1.0
Viscosity (25 °C) (pure solvent)	4.4	4.4	1.0
ΔH _{rxn} (kcal/mol CO ₂ absorbed) (pure solvent)	17.3	13.0	17.3
CO ₂ Uptake (wt % in TEG)	10.2 (50% in TEG)	9.1 (60% in TEG)	10.2
Theoretical CO ₂ Uptake (wt % in TEG)	9.8 (50% in TEG)	8.2 (60% in TEG)	10.8
Freezing Point (°C) (pure solvent)	-85	-90	10.5
Thermal Stability (pure solvent)	>150	>150	122
Heat Capacity (cal/g °C) @ 25 °C	0.56 (50% in TEG)	0.58 (60% in TEG)	0.89*

*Weiland, R. H.; Dingman, J. C.; Cronin, D. B., *J. Chem. Eng. Data* **1997**, *42*, 1004.

Subtask 3.5 (Bench Scale Lead Solvent Performance Evaluation)

Mass Transfer Experiments

Experiments were performed for both a 50:50 wt % mixture of GAP-0 and TEG and a 30 wt% mixture of monoethanol amine (MEA) and water. The absorption system is shown in Figure 36. The absorbent to be tested was placed in the liquid reservoir, which was purged with nitrogen to ensure that the absorbent did not absorb any CO₂ from the atmosphere during the experiment. For the case of the experiment with GAP-0/TEG this reservoir was initially heated to 110 °C for 30 minutes under a N₂ purge to remove any CO₂ or water. The mixture was then cooled to 90 °C. At the beginning of each experiment the absorbent was pumped by a Masterflex peristaltic pump at a flow rate of 0.9 ml/min from this reservoir to the top of a jacketed Ace Glass chromatography column. The column had an inside diameter of 11 mm and was packed with 30 ml of 2 mm diameter glass beads. The column was heated to 60 °C by flowing water through the jacketing. The absorbent trickled down through the bed of glass beads and into a second liquid reservoir at the bottom of the column. Simulated flue gas with 10% CO₂/balance N₂ at 50 ml/min was initially set to flow directly from the source gas cylinders to an MKS Cirrus mass spectrometer where the concentration of CO₂ in the gas stream was monitored. After 10 minutes of monitoring this baseline amount of CO₂ in the gas stream, the gas flow was switched so that the gas flow was introduced at the bottom of the column. The gas flowed countercurrent to the liquid flow and exited at the top of the column. The gas then flowed to the mass spectrometer, where the resulting concentration of CO₂ was measured. Brooks Instrument model 5850E mass flow controllers metered the gas flow rates.

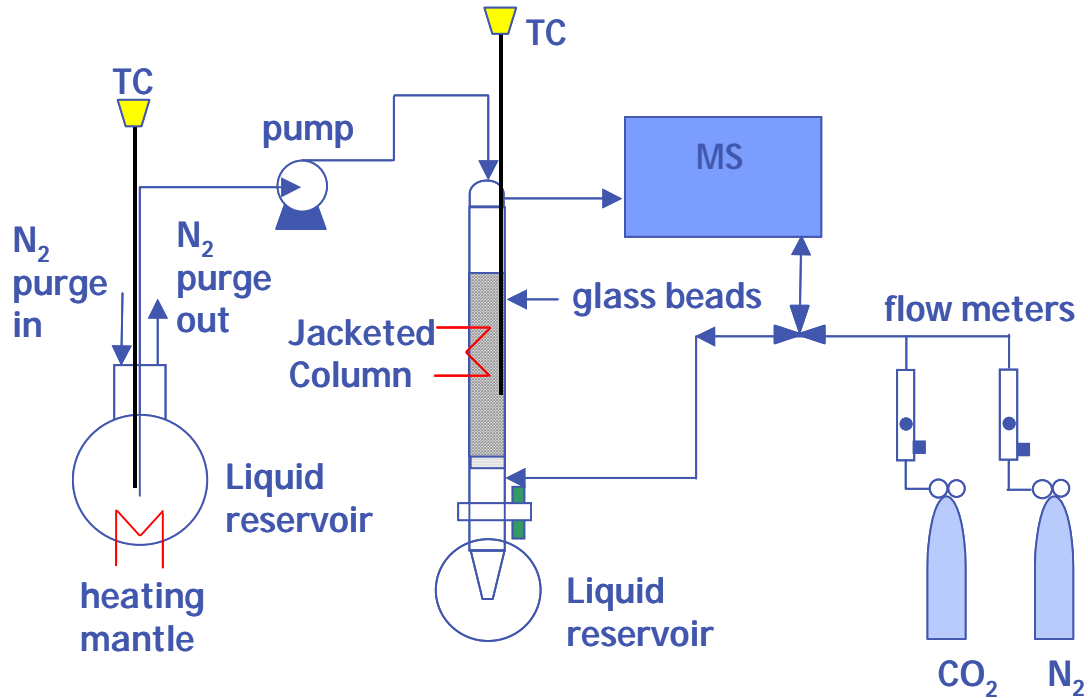


Figure 36. Process flow diagram of absorption system used for mass transfer experiments

The results of the experiments for 1:1 (wt/wt) GAP-0 :TEG and 30 wt% MEA/H₂O are shown in Figure 37. For both experiments, the simulated flue gas was initially set to bypass the absorption column and flow directly to the mass spectrometer to obtain a baseline measurement of the simulated flue gas that will be introduced into the absorption column. Several minutes are required after starting the measurements for the CO₂ concentration to stabilize, as the simulated flue gas travels through the process lines from the source cylinders to the mass spectrometer. After 10 minutes with the flue gas flow set to bypass the column, the gas is directed to the inlet at the bottom of the column. Several minutes after this switch, the CO₂ concentration begins to drop as the liquid absorbent starts to absorb CO₂. After switching the flow to the column, the experiment was continued for an additional 30 minutes to ensure that the process had come to steady state. As shown in Figure 37, both 1:1 (wt/wt) GAP-0 :TEG and 30 wt% MEA/H₂O gave similar results with slightly superior performance for 30 wt% MEA/H₂O. Using the assumption that the concentration of CO₂ in the simulated flue gas was dilute and that the reaction is irreversible under the experimental conditions, Equation 19 was used to calculate the overall mass transfer coefficient based on the gas phase. For 1:1 (wt/wt) GAP-0 :TEG the mass transfer coefficient, under the conditions of the experiment, was calculated to be 5.3 mol/m²h, while for the 30 wt% MEA/H₂O it was calculated to be 8.4 mol/m²h. These experiments indicate that the GAP-0 based absorbent results in mass transfer rates similar to that of MEA based absorbents.

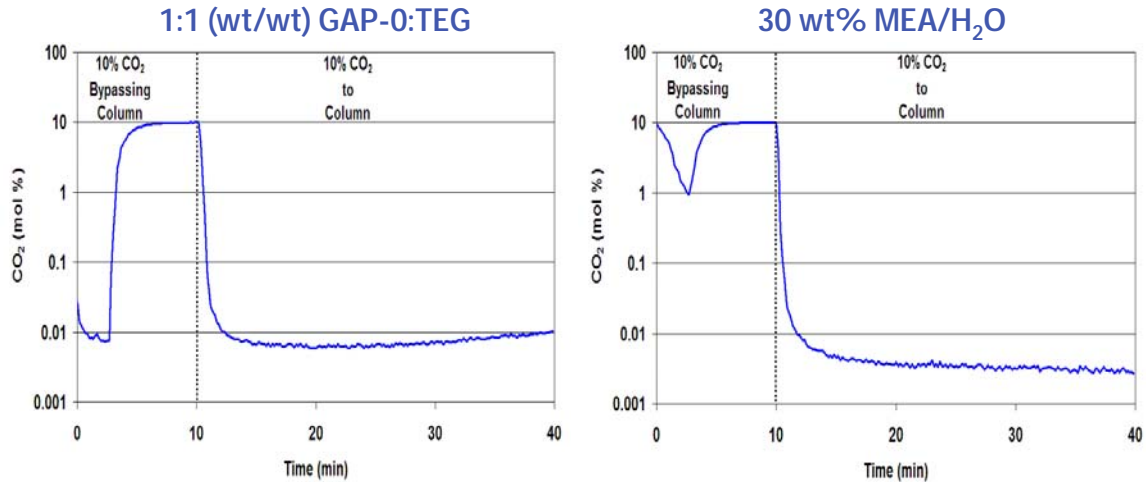


Figure 37. Experimental results from absorption mass transfer experiments with 1:1 (wt/wt) GAP-0:TEG and 30 wt% MEA/H₂O.

$$Z_T = \frac{\left(\frac{V}{S}\right)}{K_y a} \ln\left(\frac{y_{in}}{y_{out}}\right) \quad (19)$$

Z_T = packing height

V = molar flow rate of gas

S = cross-sectional area of column

K_y = overall mass-transfer coefficient based on gas phase

a = gas/liquid interfacial area

y_{in} = mole fraction of CO₂ in gas phase at inlet

y_{out} = mole fraction of CO₂ in gas phase at outlet

Continuous CO₂ Capture System

Construction of the continuous CO₂ capture system was completed in the second quarter of 2010. The first test with the system was performed on the 14th of May of this year. The first tests, were performed using a 50/50 (by weight) mixture of bis(3-aminopropyl) tetramethyl disiloxane (GAP-0) and triethylene glycol (TEG). Subsequent experiments utilized a 60/40 mixture of GAP-1/TEG.

A process flow diagram of the continuous CO₂ capture system is shown in Figure 38. The system's primary unit operations are an absorption column and a high-pressure desorber. The absorption column is a glass, jacketed absorption column with a 50 mm inside diameter packed with 2.5 liters of 5×5 mm glass Raschig rings from Ace Glass. The desorber is an Autoclave Engineers pressure vessel with a volume of 500 ml. This vessel is capable of temperatures in excess of 120 °C and pressures greater than 20 bar.

During operation, simulated flue gas, stored in a gas cylinder, is metered to the process by an Alicat mass flow controller. The flue gas first flows to the bottom of the absorption column, where it flows up through the column, exiting the top, and then flows through an Alicat mass flow meter and to a multi-channel MKS Cirrus mass spectrometer for compositional analysis. Lean absorbent is pumped by a low-pressure, Masterflex peristaltic pump to the top of the absorption column, where it trickles down through the packing, counter-current to the flue gas flow. CO₂-rich absorbent flows from the bottom of the column and drains into the rich-absorbent reservoir. The rich absorbent is then pumped by a high-pressure Eldex pump into the desorber, which is maintained at 120 °C. In the desorber, the absorbent, which is thoroughly mixed by a stirrer, is maintained at a volume of 250 ml. The CO₂ that desorbs from the heated absorbent in the desorber is maintained at elevated pressure by an Alicat back-pressure regulator on the desorber gas-exit line. The CO₂ exiting the desorber passes through the back-pressure regulator, then through a mass flow meter, before flowing to the mass spectrometer. The lean absorbent flows from the desorber and then through a throttling valve where the absorbent's pressure is reduced to atmospheric before flowing into a lean-absorbent reservoir. The completed continuous CO₂ capture system is shown in Figure 39.

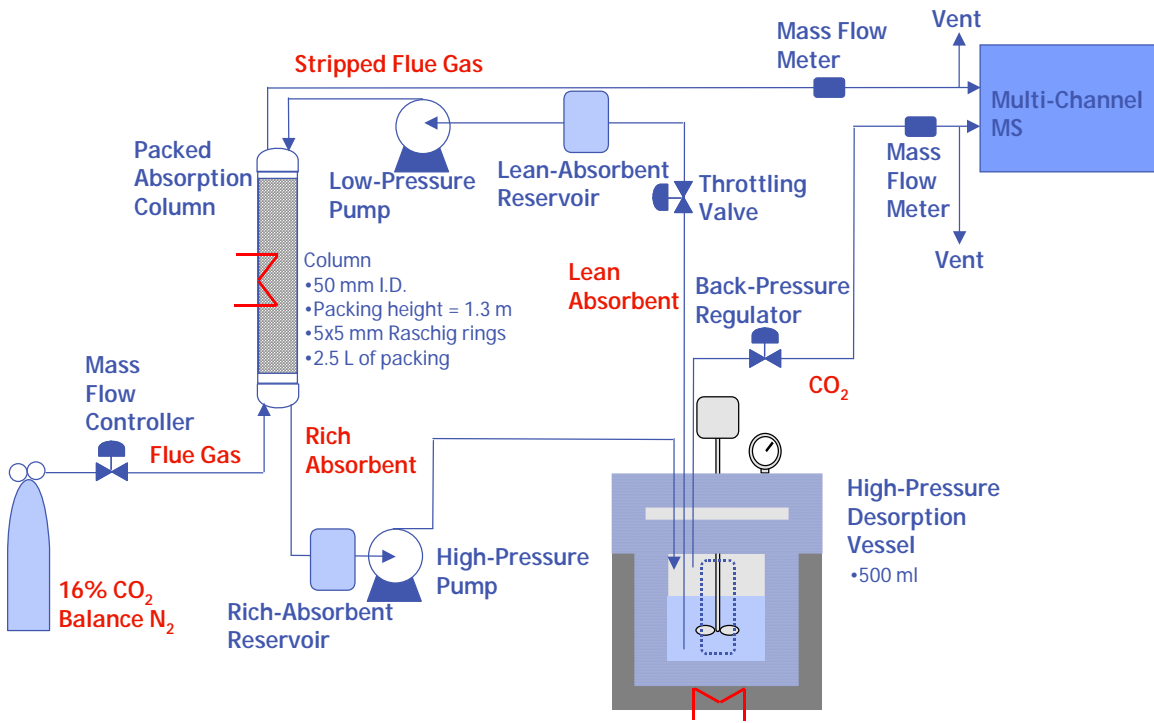


Figure 38. Process flow diagram for continuous CO₂ capture system.

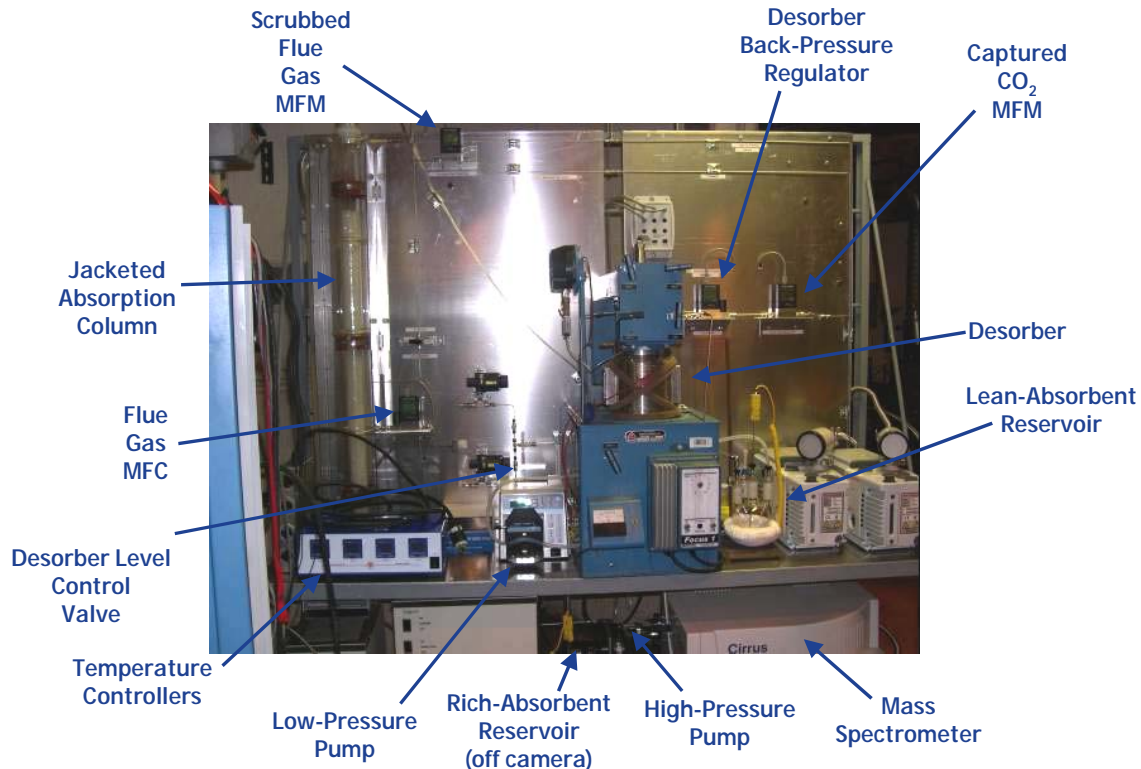


Figure 39. Completed continuous CO₂ capture system.

During initial attempts to operate the CO₂ capture system continuously, a number of system improvements were identified and implemented. In early experiments, it was found that the absorbent viscosity resulted in performance issues with several components in the system. The absorbent in the desorber had a tendency to not flow readily through the liquid outlet and into the lean-absorbent reservoir. To remedy this, the piping between the desorber and the lean-absorbent reservoir was shortened and simplified to decrease the pressure drop required to generate acceptable liquid flow rates. It was also determined that the high-pressure pump was not generating the anticipated flow rates. It was determined that, because of the high liquid viscosity, cavitation was occurring when the piston attempted to draw the absorbent into the pump. In order to remedy this, the diameter of the piping leading from the rich reservoir to the high-pressure pump was increased.

It was found that at the design flow rates of flue gas (2.7 LPM at 1 bar and 25 °C) and absorbent (22 ml/min), the column had a tendency to flood as the absorbent became enriched in CO₂ and its viscosity therefore increased. To combat this, the flow rates of the flue gas and absorbent were decreased significantly and the tubing leading from the bottom of the column to the rich-absorbent reservoir was shortened.

The system was designed so that the desorber could be operated at elevated pressures (up to 20 bar) so that the CO₂ desorbed would require less compression in preparation for sequestration. Isotherm experiments performed with the 50/50 (by weight) mixture of GAP-0 and triethylene glycol indicated that the solvent could desorb CO₂ at these pressures at 120 °C. However, it was found that much lower pressures were generated in the desorber at 120 °C (<3 bar, gauge). Because of this, in later experiments, the desorber back-pressure regulator was set to maintain the desorber at lower pressures (0.5 bar, gauge) during continuous operations.

After making the previously described modifications to the system, the CO₂ capture system was successfully operated continuously. In this initial experiment a 50/50 mixture (by weight) of GAP-0 and TEG was used and the column temperature was maintained at 40 °C using heating water flowed

through the jacketing on the column. The flue gas (16% CO₂/balance N₂) was set to flow to the column at 0.54 LPM (at 1 bar and 25 °C) and the absorbent was set to cycle at 4.4 ml/min. The desorber back-pressure regulator was set to 0.5 bar (gauge). The system was operated continuously for several hours. After operating continuously for this duration, the percent of CO₂ captured by the system was measured using two different methods. In the first, the concentration of CO₂ in the stripped flue gas was measured by mass spectrometry and the percent of CO₂ captured was calculated to be 90%. The amount of CO₂ captured was also determined by the difference in flow rate between the flue gas delivered to the column and the flow rate of the stripped flue gas leaving the top of the column, measured by the mass flow meter. Based on this method, the percent of CO₂ captured was 80%. Analysis of the gas leaving the desorber by mass spectrometry determined that most of the gas leaving the desorber was CO₂ (87%) with most of the balance being N₂ and a small amount of water. This was the most successful experiment from the standpoint of avoiding column flooding and system clogging.

During the experiments in the continuous CO₂ capture system with the 50/50 (by weight) mixture of GAP-0 and triethylene glycol, it was found that this material had a tendency, upon exposure to CO₂, to solidify in the unheated portions of the system. This caused a number of operating problems with the system. The solids were a significant issue during system start-up at the beginning of each experiment, since the solids tended to clog the piping throughout the system, requiring heating of the lines to melt the solids. Solid particles had a tendency to plug the check valves in the high-pressure pump during operation causing the pump to fail. However, the most problematic issue was that solids tended to form over time in the spaces in the column packing. This was identified as a major contributing factor in the flooding observed in the column. Because of this issue, it was decided to switch to new materials that do not solidify for future experiments.

Subsequent experiments with the continuous CO₂ capture system used a 60/40 (by weight) mixture of GAP-1 and triethylene glycol as the absorbent. Testing showed that this absorbent composition would not solidify in the continuous CO₂ capture system, thus avoiding many of the operating challenges faced during the experiments with the 50/50 (by weight) mixture of GAP-0 and triethylene glycol.

A series of experiments was conducted with the 60/40 (by weight) mixture of GAP-1 and triethylene glycol in which the liquid absorbent flow was maintained at a constant rate, and the simulated flue gas flow rate was varied. In these experiments, the column temperature was maintained at 40 °C using heating water flowed through the jacketing on the column. The flue gas (16% CO₂/balance N₂) was set to flow to the column at various rates from 0.59 to 1.77 LPM (each flow rate being a separate experiment at 1 bar and 25 °C) and the absorbent was set to cycle at 10 ml/min. The desorber back-pressure regulator was set to 0.5 bar (gauge). The system was operated continuously for several hours. After operating continuously for this duration, the percent of CO₂ captured by the system was measured using two different methods. The first method was to take samples of the liquid absorbent from both the lean- and rich-reservoirs and analyze these samples by NMR to determine the fraction of the GAP-1 that had reacted to form carbamate. Figure 40 shows the results of the NMR measurements. Based on the carbamate loading in the lean- and rich-liquid absorbent samples, the liquid absorbent flow rate, and the flue gas flow rate and initial CO₂ concentration, the percent of CO₂ captured was calculated. The second method used the multi-channel mass spectrometer measurements of the CO₂ loading in the simulated flue gas, before and after passing through the absorption column, as well as the flow rate of the simulated flue gas before and after the absorption column, to calculate the percent of CO₂ captured. The calculated CO₂ capture percents based off of both methods are shown in Figure 41.

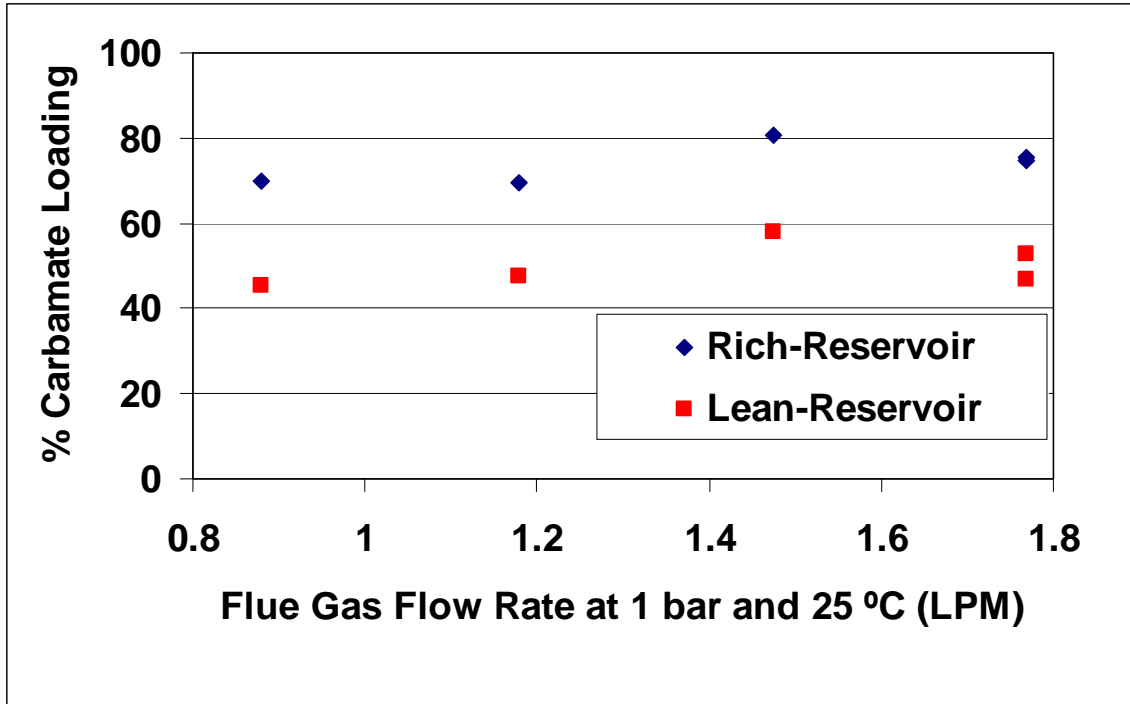


Figure 40. Percent carbamate loading of 60/40 (by weight) mixture of GAP-1 and triethylene glycol at various simulated flue gas flow rates.

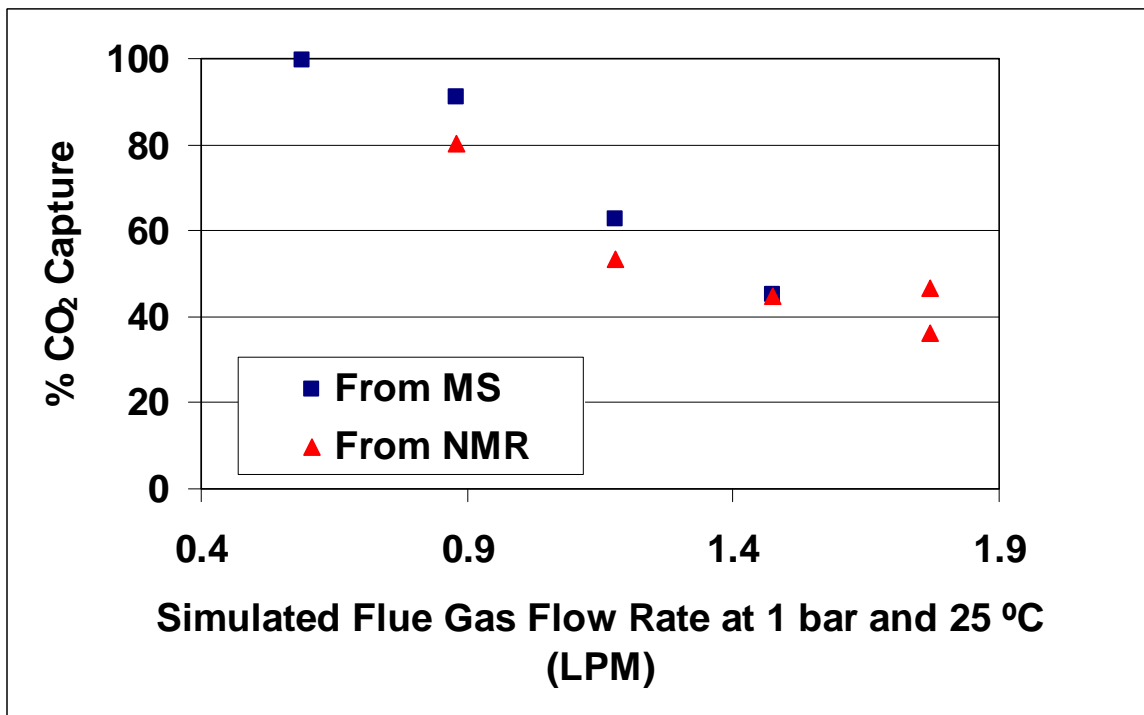


Figure 41. Percent CO₂ capture at various simulated flue gas flow rates measured by mass spectrometry and NMR.

Examination of Figure 40 shows that, within the error of the experiment, the percent of carbamate loading in the rich- and lean- liquid, respectively, is largely independent of the flue gas flow rate. This suggests that, under the conditions run, the liquid absorbent flowing through the absorption column is coming to saturation at a percent carbamate loading of approximately 70-80% (where 100% carbamate loading corresponds to the amount of carbamate formed if one GAP-1 molecule reacted with one CO₂ molecule). The additional CO₂ feed at the higher flow rates passes through the column unreacted. As shown in Figure 41, the percent CO₂ captured measured by mass spectrometry and NMR are generally in good agreement. At the lowest simulated flue gas flow rate, the liquid absorbent captures almost 100% of the CO₂. As the flow gas flow rate is increased, the percent of CO₂ captured decreases, consistent with the observation that the rich-liquid absorbent does not capture additional CO₂ at the higher flow rates.

Subtask 3.6 (Degradation/Environmental testing)

Corrosion studies were completed with evaluation of two metals (340L stainless steel and C1018 high carbon steel), three temperatures when appropriate (50, 100, 150 °C) and 4 compositions (neat GAP-0, 50/50 GAP-0/TEG, 30% MEA in TEG and 30% aqueous MEA) with weight loss data collected for 3000 hours.

Neat GAP-0 (Figure 42a) and the 50/50 mixture of GAP-0 and TEG (Figure 42b) show essentially no change in weight over 3000 hr, with the exception of the 150 °C high carbon steel coupons both GAP-0 solutions. However, the percent weight losses were still less than 0.2%.

30% aqueous MEA also shows very little weight change over 3000 hours at temperatures up to 100 °C (Figure 42d). In contrast, the C1018 samples in 30% MEA /TEG show a relatively large weight loss at 100 and 150 °C (Figure 42c). At 150 °C, nearly 0.4% weight is lost from the original samples.

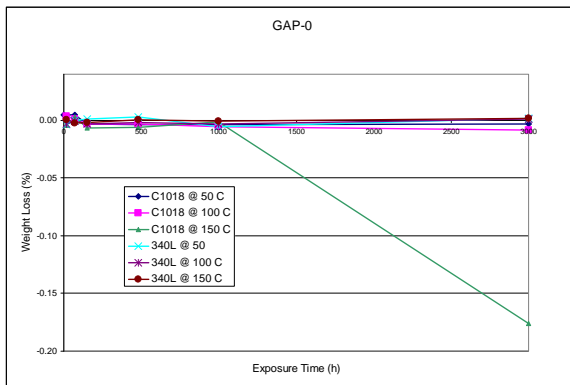


Figure 42a. Metal Coupons in Neat GAP-0

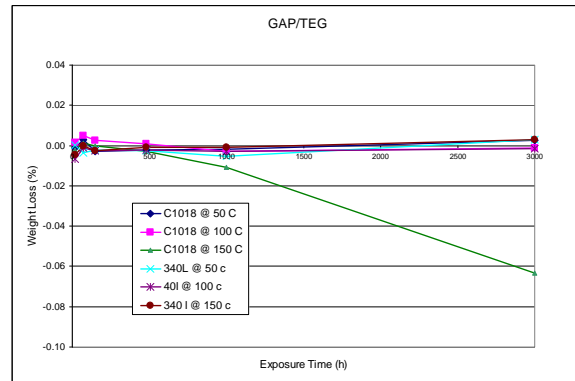


Figure 42b. Metal Coupons in 50/50 GAP-0/TEG

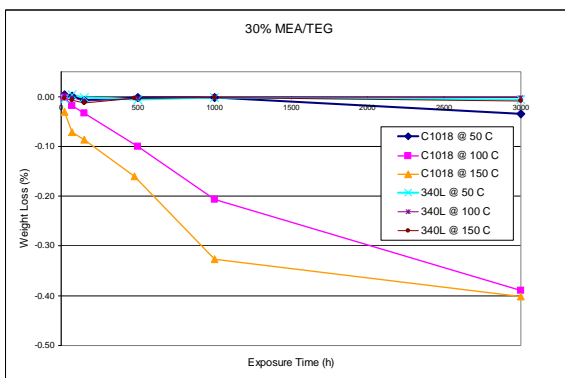


Figure 42c. Metal Coupons in 30% MEA/TEG

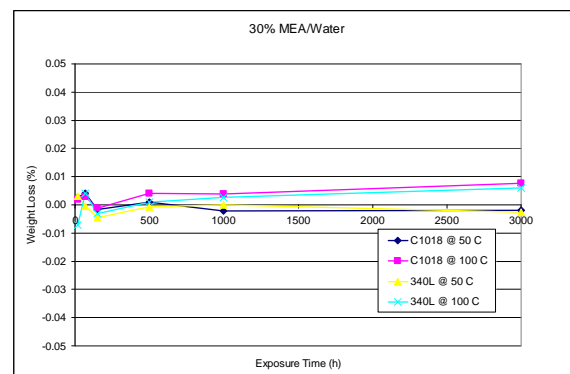


Figure 42d. Metal Coupons in 30% MEA/Water

Metal samples of C-1018 and S304 in GAP-0/TEG (Figure 43b) and MEA/Water saturated with CO₂ (Figure 43a) were also tested. Again, the 340L stainless steel samples were stable under these conditions as was the C-1018 carbon steel sample in the presence of GAP-0 carbamate. However, a noticeable weight loss (~0.2%) was seen with C-1018 coupons in the MEA solution after 3000 hours. GAP-0/TEG samples demonstrated equivalent or superior performance to 30% MEA samples.

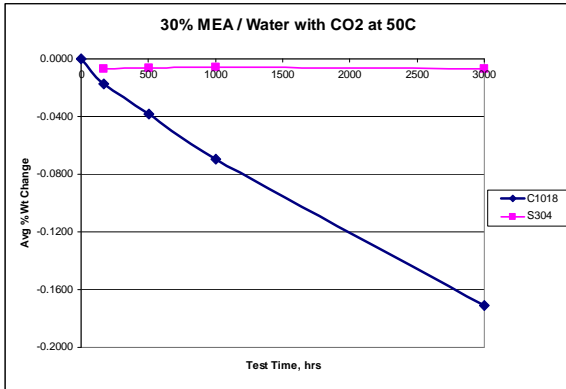


Figure 43a. Metal Coupons in 30% MEA/TEG

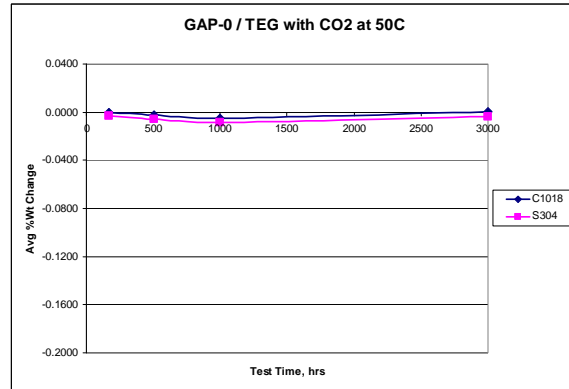


Figure 43b. Metal Coupons in 30% MEA/Water

Task 4.0 (Process Modeling and Cost of Energy Services)

Approach

The pulverized coal boiler power plant and temperature swing monoethanol amine (MEA) based CO₂ separation processes are well developed, and they are outlined in "Cost and Performance baseline for Fossil Energy Plants, DOE/NETL-2007/1281, Volume 1: Bituminous Coal and Natural Gas to Electricity Final Report, May 2007". The assumptions from this DOE report were used for the power plant.

A process model was developed for the CO₂ separation unit to calculate the mass and energy balances and the system performance. The process model was calibrated with lab-scale experimental data, which were presented earlier in this report. The model accounts for capture of CO₂ by GAP-1 and the capture of water by TEG. The model accounts for heat input needed to vaporize the water in the desorber, heat input needed to desorb the CO₂ and the heat input needed for sensible heating of the solvent. The model also accounts for parasitic loads such as power plant compressors, power plant pumps, exhaust blower, CO₂ solvent pumps and CO₂ compressor. The mass and energy balances were used to calculate the system performance (efficiency).

The direct capital costs and O&M costs for the power plant and CO₂ compression unit were taken from the DOE bituminous baseline report. The direct capital costs and O&M costs for the CO₂ separation unit were estimated using a similar methodology. The engineering costs were estimated as a certain fraction of the total direct cost and contingency was added to determine the fully installed capital cost for the CO₂ separation and compression unit. The fuel and O&M costs were levelized over the life of the plant. The cost of electricity was then calculated using a capacity factor of 85% and a capital recovery factor of 17.5% for plants with CO₂ capture.

Process Description

A simplified block diagram of the power plant and CO₂ separation system is shown in Figure 44. The pulverized coal boiler generates steam, which is sent to the steam turbines. The flue gas is sent through a selective catalytic reduction (SCR) unit to reduce nitrogen oxides (NO_x), a bag house to remove fly ash and a flue gas desulfurizer (FGD) to remove sulfur dioxide. The flue gas is then sent through the carbon dioxide separation unit before venting the flue gas.

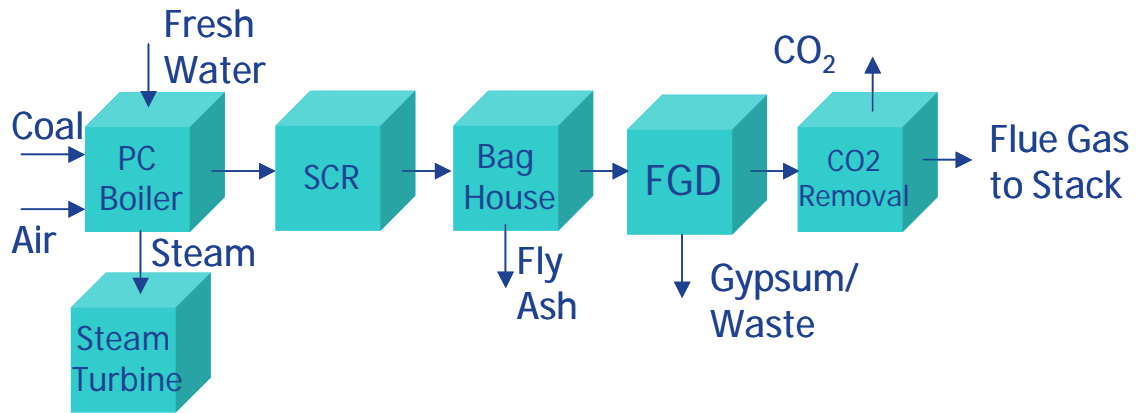


Figure 44. System Block Diagram.

Power Plant Sub System

A process flow diagram for the power plant is shown in Figure 45. This subsystem includes:

- Steam Island
 - High pressure (HP), intermediate pressure (IP) & low pressure (LP) turbines
 - Steam extraction points
 - Feed water heaters & pumps
 - Condenser & cooling tower
- Coal Delivery, Air Delivery and Boiler Burners in boiler
 - Air heaters
 - Pulverizer, conveyor & stacker/reclaimer
- Environmental Treatment
 - SCR, FGD, bag house and CO₂ Separator

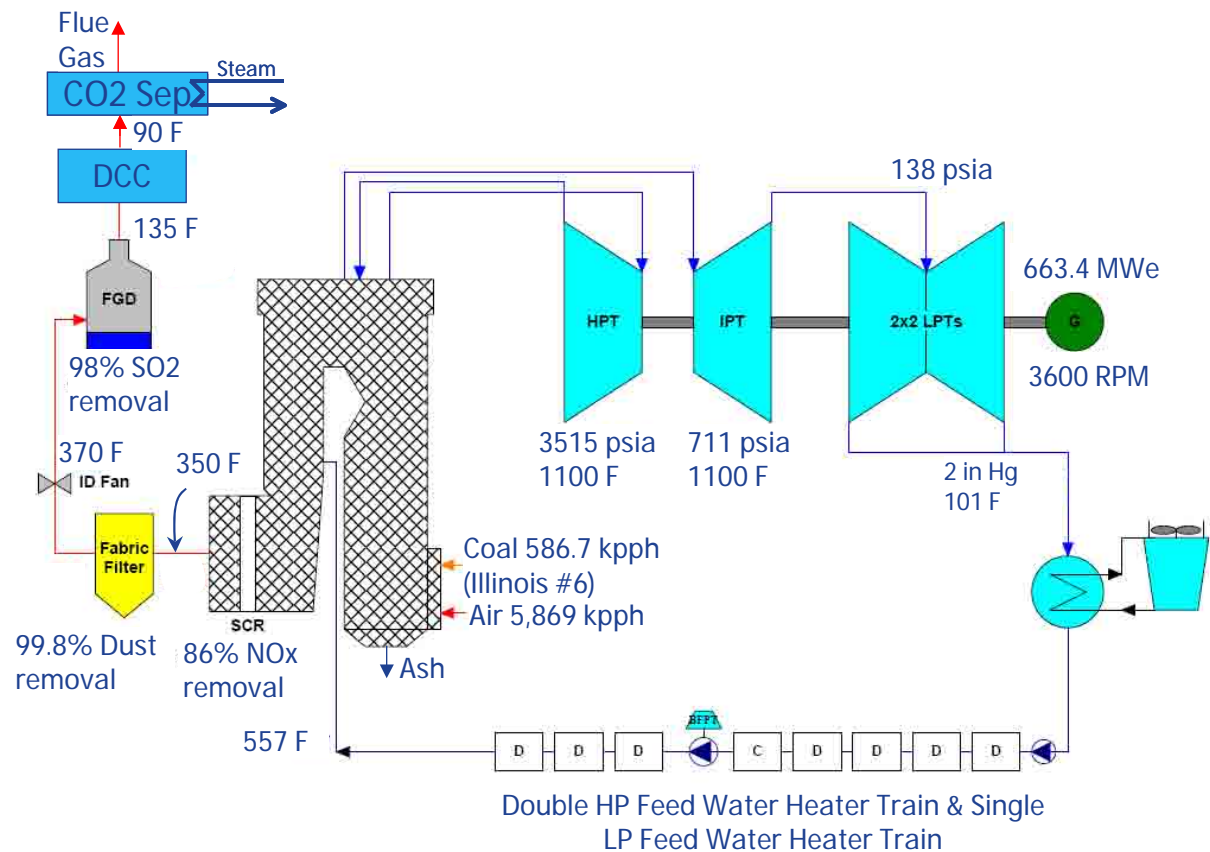


Figure 45. Power Plant Process Flow Diagram.

CO₂ Separation Unit

The CO₂ separation unit utilizes four key processes: CO₂ Absorption, CO₂ Desorption, Solvent Handling, and CO₂ Compression.

The flue gas from the power plant is processed in a direct contact cooler to reduce the temperature to 90F and then enters the bottom of the absorber and flows up through the column counter current to the lean solvent, as shown in Figure 46. The lean solvent enters from the top of the absorber and captures most of the CO₂ from the flue gas and the rich solvent leaves from the bottom of the absorber. The CO₂ absorption increases the temperature of the solvent by about 20-40°F. The absorber is operated at temperatures of around 100-150°F and at atmospheric pressures.

The rich solvent from the rich-lean heat exchanger is fed to the rich-lean heat exchanger and heated to temperatures of 200-300°F before being fed to the desorber (stripper) for separation of the absorbed CO₂. The lean solvent from the desorber is passed through the other side of the rich-lean heat exchanger.

The rich solvent is fed to the desorber and then routed to the desorber reboiler. Steam is supplied to the desorber reboiler to provide heat, which releases CO₂ from the rich solvent. Steam is supplied from the low pressure (LP) section of the steam turbine in the power plant sub-system. The hot vapor from the top of the desorber consisting of CO₂ and steam is cooled in a heat exchanger utilizing water. The stream then flows to a desorber reflux drum where the vapor and liquid are separated. The CO₂ gas is removed from the reflux drum and then delivered to the CO₂ product compressor. The condensed liquid from the bottom of the reflux drum is returned back to the desorber as reflux.

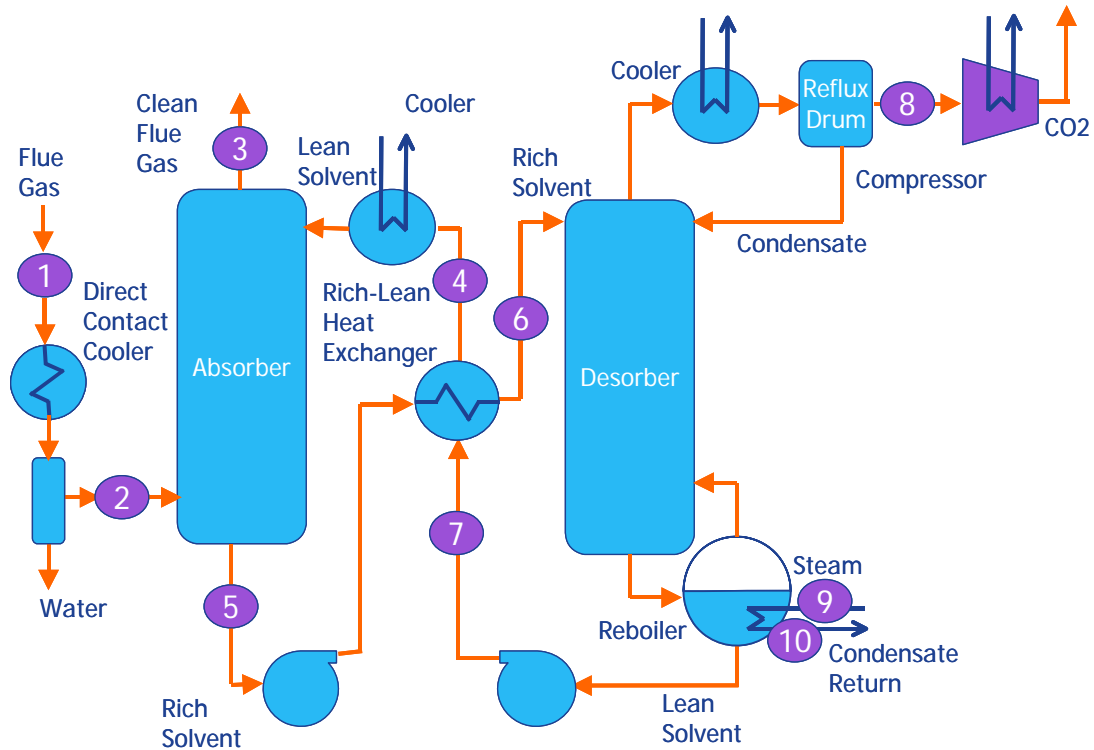


Figure 46. CO₂ Separation Sub-System.

The lean solvent from the desorber is pumped through the rich-lean heat exchanger to the absorber. The lean solvent is cooled further before being fed to the absorber in order to increase the loading of CO₂ in the absorber.

System Layout

Unigraphics was used for the physical plant layout, which is shown in Figure 47. The model includes the boiler, coal handling and crushing, limestone preparation, gypsum production, fans, pumps and blowers, an ammonia SCR unit for NO_x removal, cooling tower, slag and ash handling, and steam turbines.

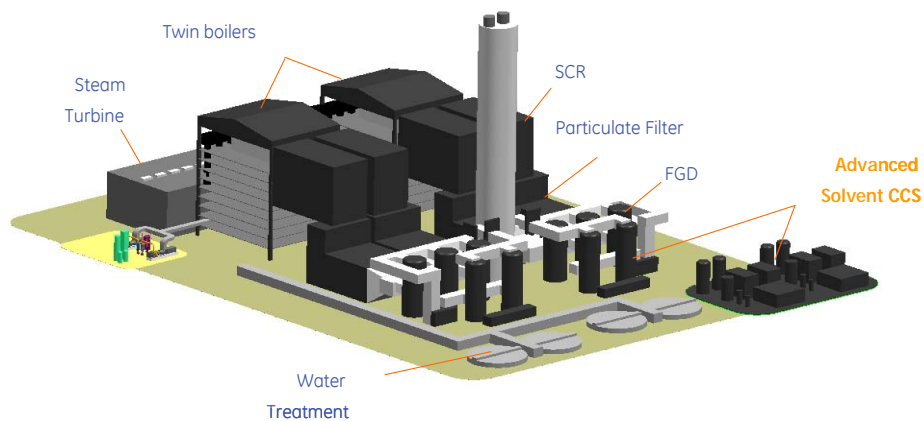


Figure 47. System Layout.

Key System Assumptions

Power Plant Assumptions

The key system assumptions for the power plant are consistent with “DOE Bituminous baseline report” and are shown in Table 24. The gross thermal input was kept constant at 2,007 MW_{th} for all the case studies presented in this report. The higher heating value (HHV) and lower heating value (LHV) for the coal are 30,506 kJ/kg (13,126 Btu/lb) and 29,544 kJ/kg (12,712 Btu/lb).

The pulverized coal subsystem model was built in Thermoflow and calibrated against the DOE bituminous baseline report. All of the unit operations in the plant and capture models are changeable, and could be swapped out for alternate units, for example, an electro-static precipitator (ESP) can be used in place of the bag house.

The energy needed by the CO₂ separator is provided by extraction of steam from the steam turbines. The extracted steam would otherwise pass through the steam turbine and provide electrical energy. The conversion of that heat into electrical energy does not occur at 100% efficiency, and the efficiency of that conversion is a function of the temperature of the required steam extraction. The steam will pass through the desorber reboiler, and must have a condensation temperature as high as the temperature in the desorber. Previous GE studies and Alstom reports show an advantage for taking lower temperature steam from the steam turbine. Figure 48 shows the effect of reducing the steam extraction temperature on the amount of electrical power utilized within the plant. If the temperature in the desorber could equal the temperature in the condenser of ~100F, there would be no penalty for using that heat, while in the range of interest (250°F to 350°F), the penalty will range from 22% to 28% of the steam energy extracted. However, if the CO₂ separation unit is a retrofit of an existing pulverized coal plant the steam conditions are fixed by the location from which the steam must be extracted. In this case, the steam will be extracted in the crossover pipe between the medium pressure (MP) and low pressure (LP) steam turbines.

Table 24 Key System Assumptions for the Power Plant.

Steam Cycle, Bar/ °C/°C (psia/°F/ °F)	241/593/593 (3515/1100/1100)
Coal	Illinois #6
Gross Thermal Input, MWth	2007
Condenser pressure , mm Hg (in Hg)	50.8 (2)
Boiler Efficiency, %	89%
Cooling water to condenser, °C (°F)	16 (60)
Cooling water from condenser, °C (°F)	27 (80)
SO ₂ Control	Wet Limestone Forced Oxidation
FGD Efficiency, %	98%
NO _x Control	Low NO _x Burner, with Over Fired Air and SCR
SCR Efficiency	86%
Particulate Control	Fabric Filter
Fabric Filter Efficiency	99.8%
Mercury Control	Co-benefit capture
Mercury Removal Efficiency	90%
CO ₂ Capture	90%

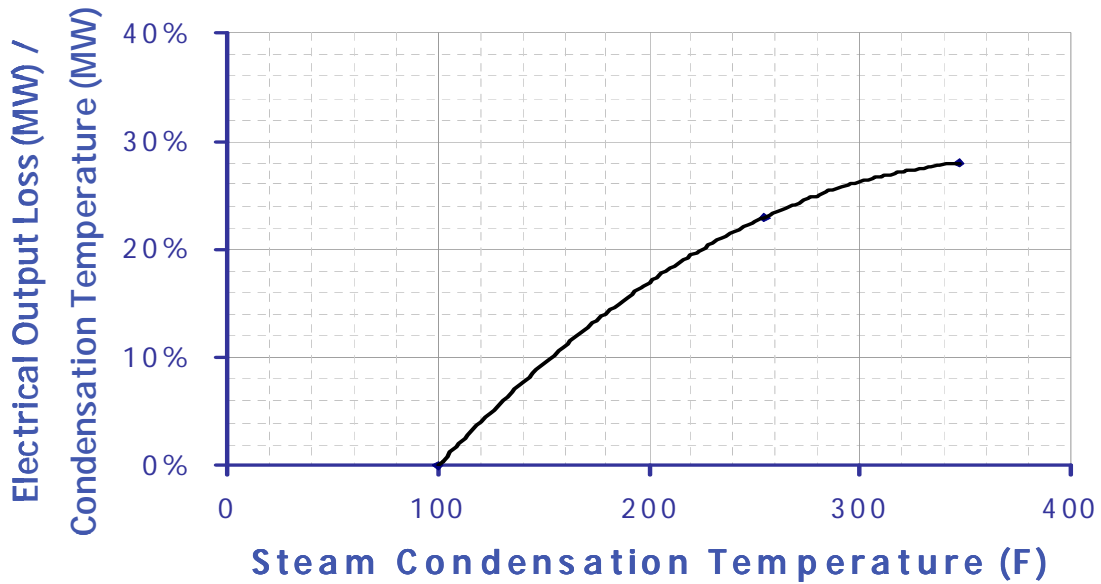


Figure 48. Effect of Steam Plant Extraction Temperature on Loss in Electrical Output.

CO₂ Separation Unit Assumptions

The detailed MEA baseline model is based on the Fluor's Econamine temperature-swing solvent separation process, which was reported in the 2004 IEA report and the 2007 DOE report (see Appendix 7 for details of an optimized MEA model). The system has four process variables that dominate the performance with a given solvent and they are: absorber temperature, desorber reboiler temperature, desorber pressure, and rich/lean heat exchanger approach temperature. The system model accounts for the major energy penalties for CO₂ separation, and they include the energy required:

- (1) for vaporization of water,
- (2) to desorb the carbon dioxide (i.e., reaction energy), and
- (3) for sensible heating of the solvent.

The energy is supplied by feeding steam to the reboiler in the desorber column. The model also accounts for CO₂ compression energy and auxiliary loads.

The *solvent rich loading* is defined as the weight % of CO₂ in the rich solvent leaving the absorber column. The *solvent lean loading* is defined as the weight % of CO₂ in the lean solvent leaving the desorber column. The *solvent net loading* is defined as the difference between the *rich loading* and the *lean loading* and is obtained from lab-scale experiments.

The key assumptions for the CO₂ separation unit utilizing the GAP-1/ triethylene glycol (TEG) solvent are listed below in Table 25:

Table 25. Assumptions for CO₂ Separation Unit.

Temperature of flue gas after direct contact cooler, °C (°F)	32 (90)
Absorber temperature, °C (°F)	49 (120)
Absorber pressure, bar (psia)	1.03 (15.2)
Desorber temperature, °C (°F)	127 (260)
Desorber pressure, bar (psia)	2.87 (42.2)
Rich-lean heat exchanger temperature approach, °C (°F)	5.6 (10)
Solvent-to-Gas Mass Ratio kg/kg	7.9

In the DOE bituminous report, the partial pressure of CO₂ in the stream from the power plant to the CO₂ separation unit is 0.139 bar (2.02 psia). The lab-scale absorption isotherm data was used to estimate the *rich loading* at this partial pressure and 49°C (120°F) for the Gap-1/TEG solvent. The *lean loading* was measured at 2.87 bar (42.2 psia) and 127 °C (260 °F) for the solvent. The *net loading* from the current experimental data is ~2.63%. Further optimization of the operating pressures, temperatures and flow rates of the experimental system and better contact between the solvent and flue gas in the absorber column may increase the net loading for the GAP-1/TEG solvent. Also, other amino-silicone solvents could potentially be developed with higher loadings. The current model does not account for mass transfer and reaction kinetics in the absorber and desorber. GE may develop more detailed models if the technology development is continued.

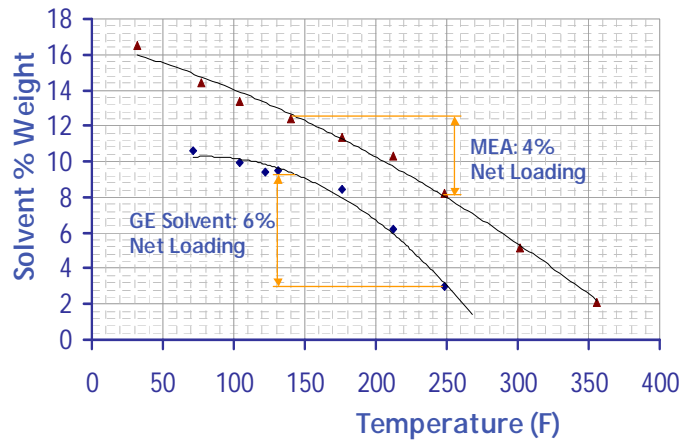


Figure 49. GE Solvent and MEA Solvent Loading.

Figure 49 shows the loading isobar at 1 atmosphere for the GE solvent compared to the MEA solvent. The lower-temperature region of the chart, between 120°F and 140°F, shows the potential rich loading, and that the GE solvent has a lower rich loading potential. The high temperature side shows the desorber potential. The high curvature of the GE solvent makes the loading fall rapidly as temperature increases, making the potential lean loading lower than that of MEA. These effects result in a higher potential for net loading for the GE amino-silicone solvent. However, in the lab-scale continuous experiments the net loading was only 2.63% for the amino-silicone solvent.

As explained earlier, the Gap-1/TEG solvent utilizes less energy than the MEA solvent due to:

- Low water in the solvent mixture
- Low heat of absorption of CO₂
- Low specific heat of the solvent

The effect of these parameters is described in more detail below:

Low H₂O

The model accounts for absorption of water in the flue gas by the solvent and the vaporization of the water in the desorber column. The baseline MEA solvent concentrations are limited to 20-30% and the remaining is water due to viscosity and corrosion issues. The water in the solvent necessitates significant amount of energy due to sensible heat as well as vaporization of the water. For the plant shown in Figures 45 and 46, about 190 lb/s of water is vaporized in the desorber for the MEA solvent.

In the GE system, TEG is added to the Gap-1 solvent to avoid formation of solids and to reduce viscosity. The exhaust of coal-fired power plants is ~ 16.7% by volume water vapor at the exit of the FGD. Gap-1 does not absorb water, but TEG is a well known desiccant. It is imperative that any solvent remains in contact with power plant exhaust. The flue gas is processed in a direct contact cooler (DCC) and the water is separated before being fed to the absorber. The temperature reduction in the DCC reduces the water content in the exhaust to ~ 4.6% by volume or ~2.74% by mass. If we assume that all of this water is absorbed by TEG, the mass fraction of the water in the Gap-1/TEG mixture is only 0.36%. The amount of water that is vaporized in the desorber for the Gap-1/TEG mixture is only 48 lb/s, which is much lower than the baseline MEA solvent and that improves the energy efficiency.

In the MEA process, the top of the absorber houses a water-wash section used to collect evaporated MEA and return it to the system. This water-wash is a source of water to the system. The amino-silicone solvent has low vapor pressure, which eliminates the need for the water wash and eliminate the path for additional water to enter the system. Figure 50 shows that the GE solvent, has less than 10% of the vapor pressure of MEA. Hence, the net loss of

solvent from the top of the absorber without the water wash will be less than MEA with the water wash.

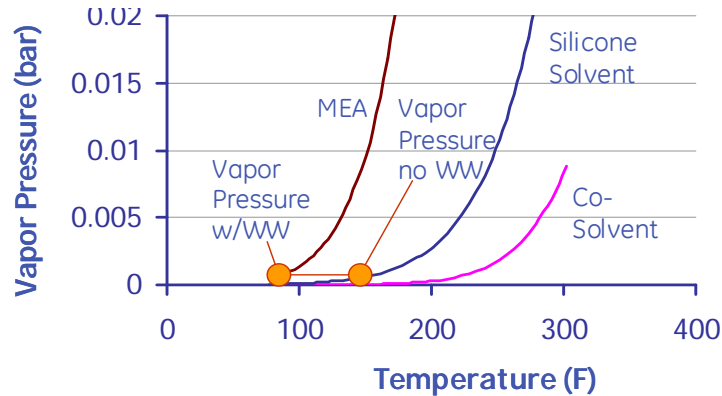


Figure 50. Low Solvent Vapor Pressure.

Low Heat of Absorption of CO₂

The model includes new experimental data for the heat of absorption of CO₂. The heat of absorption of CO₂ for the 60% Gap-1/40% TEG mixture is 1,211 kJ/kg (521 Btu/lb) while the heat of absorption for MEA is 1,635 kJ/kg (703 Btu/lb). The lower heat of absorption of CO₂ for the Gap-1/TEG solvent improves the energy efficiency.

Low Specific Heat

The specific heat of 60% Gap-1/40% TEG mixture is 2.43 kJ/kg-°C (0.58 Btu/lb-°F) while the specific heat of MEA is 3.73kJ/kg-°C (0.89 Btu/lb-°F). The lower specific heat for the Gap-1/TEG solvent improves the energy efficiency.

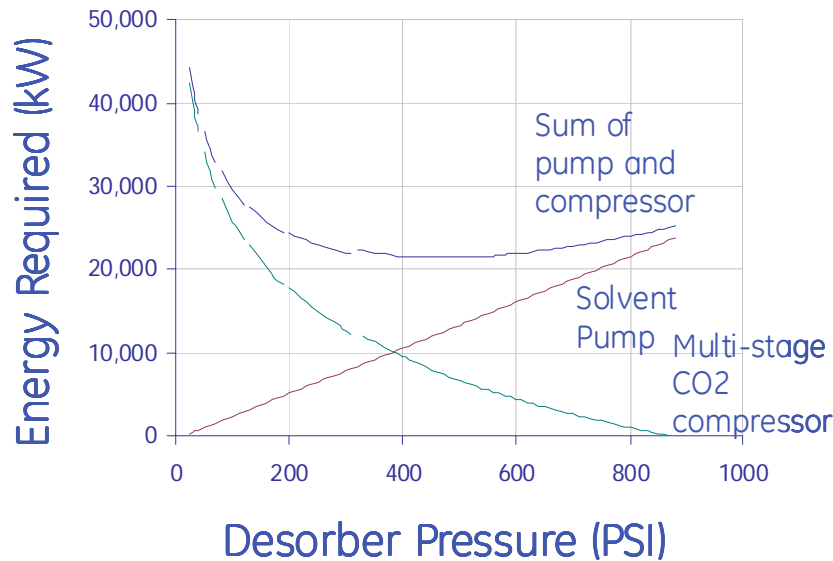


Figure 51. Compression and Pump Energy at 4% Net Loading.

The electrical loads for the entire system are listed below:

- Power plant auxiliaries – 42.95 MW
- Exhaust blower – 28 MW
- Solvent Pumps – 1.15 MW
- CO₂ Compression – 29.8 MW

Increasing the desorber pressure reduces the energy required to compress the separated gaseous CO₂ stream. A barrier to raising the pressure in the desorber is the energy required to pump the solvent to the desorber pressure. While the energy required to pump the CO₂ liquid is much lower than that required to compress the CO₂ gas, the net loading in many solvent systems is about 2-6%, making the pumping requirements of the solvent much higher than those of pumping only liquid CO₂. Figure 51 shows the liquid pump energy and the CO₂ gas compression energy at 4% net loading. The compression curves are broken where the number of stages in the compressor will drop, starting at six and ending at one, as the desorber pressure is raised utilizing the solvent pump. The net loading reduction due to high pressure in the desorber pushes the optimum pressure to a much lower value than indicated in Figure 51.

If the net loading is increased (as in the dry system without TEG), the optimum pressure increases and the energy required decreases, and the system is able to better approach the optimum. Figure 52 shows the potential of a dry solvent to reach higher desorption pressures, at 10% net loading.

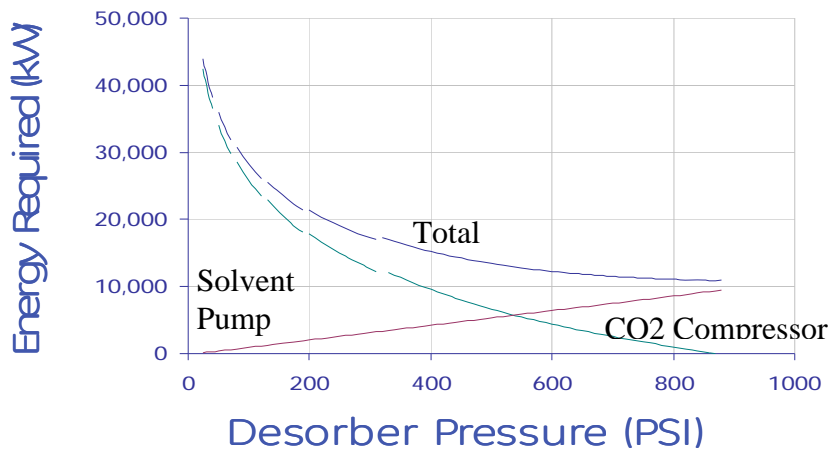


Figure 52. Compression and Pump Energy at 10% Net Loading.

System Analysis Results

The energy penalty water fall chart for 90% carbon capture and sequestration is shown in Figure 53. The energy penalty is normalized relative to the net electrical output from a plant without carbon capture.

The water fall charts presented in this report were constructed by changing one parameter at a time. For example in Figure 53, the first column is the baseline MEA solvent and accounts for higher amount of water used along with the MEA solvent and the second column accounts for reducing the water content to a value that corresponds to the GAP-1/TEG solvent, but the other solvent parameters were left unchanged and correspond to the MEA solvent. Changing one parameter at a time allows quantifying the effect of each parameter. This approach helped GE develop specifications for a solvent that has the potential to improve the performance and thus guide the experimental development. However, it is pointed out that the intermediate columns do not correspond to a real MEA or real GAP-1/TEG solvent.

The first column in this figure is the base case MEA solvent. The next three columns show the advantage of reducing water content, heat of absorption of CO₂ and specific heat of the solvent. The next two columns are the kinetic desorber and modularization, which account for faster reaction kinetics in the desorber and plant modularization. The kinetic desorber and modularization do not

improve the energy efficiency. But, they reduce capital cost and hence will reduce cost of electricity (COE), as will be outlined below. The last two columns are based on lab-scale isotherm data and lab-scale continuous system data and they also account for system optimization of the CO₂ separation system based on GE solvent. The advanced solvent reduces the energy penalty for carbon capture down to ~ 17%.

The net electrical efficiency for 90% carbon capture is shown in Figure 54. The first column shows the efficiency for the baseline MEA solvent. The next three columns show that the benefit of reducing water content, heat of absorption of CO₂ and specific heat of the solvent as 2.05 pt, 0.93 pt and 0.89 pt, respectively. The amino-silicone solvent is about 5.2 pts more efficient than the baseline MEA solvent. The gross electric output of the plant was 765.7 MWe, the net HHV efficiency was 33.1% and net power was 663.8 MWe.

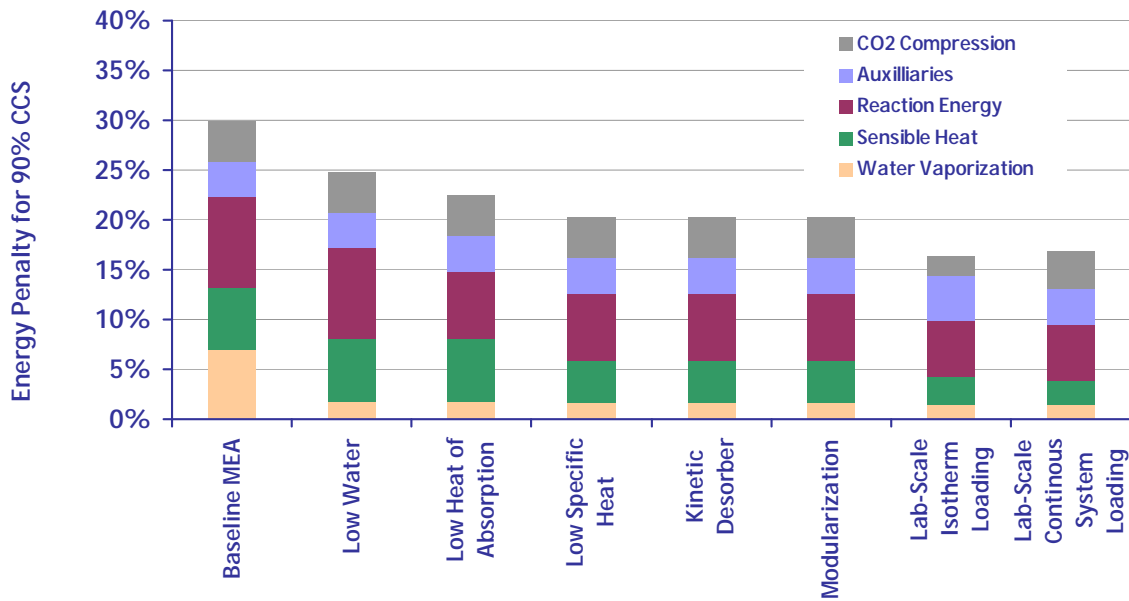


Figure 53. Water fall for energy penalty.

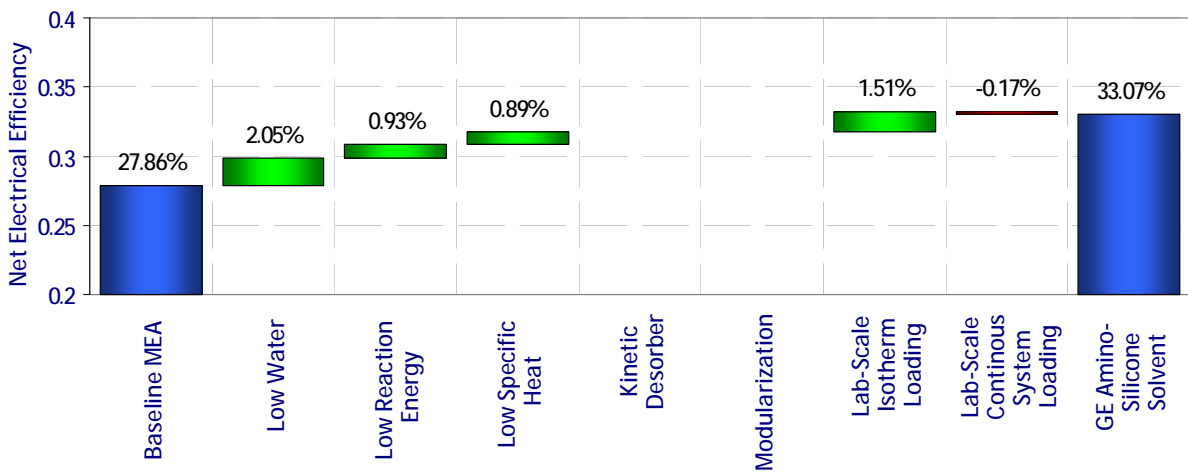


Figure 54. Waterfall for net electrical efficiency.

Table 26 summarizes the performance and parasitic loads for the GAP-1/TEG solvent based CO₂ separation unit.

Table 26. Summary of performance and parasitic loads for the GAP-1/TEG solvent.

Gross Thermal Input	MWth	2007
Gross thermal efficiency		41.9%
Gross theoretical output	MWe	841
Thermal need for CO ₂ Separation (supplied with steam)		
Water vaporization	MWth	49.3
Solvent sensible heat	MWth	80.7
Heat of desorption of CO ₂	MWth	191.4
Total	MWth	321.4
Loss in electrical output due to steam extraction	MWe	75.3
Gross electric output (accounts for steam extraction)	MWe	765.7
Power Plant, CO ₂ Separation and CO ₂ Compression Auxiliaries		
Power Plant Auxiliaries	MWe	42.95
Exhaust Blower	MWe	28.00
CO ₂ Solvent Pumps	MWe	1.15
CO ₂ Compression	MWe	29.77
Total	MWe	101.87
Net electrical output	MWe	663.8
Net electrical efficiency	%	33.1%

Economics

The COE waterfall is shown in Figure 55. The data shows that the GE amino-silicone solvent is significantly better than the baseline MEA solvent. The effects of lower water content, lower heat of absorption of CO₂ and lower specific heat of the solvent on COE are shown. The kinetic desorber and modularization result in lower capital cost for the CO₂ separation sub-system and that lowers the COE. The last two columns are based on lab-scale isotherm data and lab-scale continuous system data. Further optimization of lab-scale systems may reduce the COE. (Calculations relating to optimization of the MEA system are found in Appendix 7)

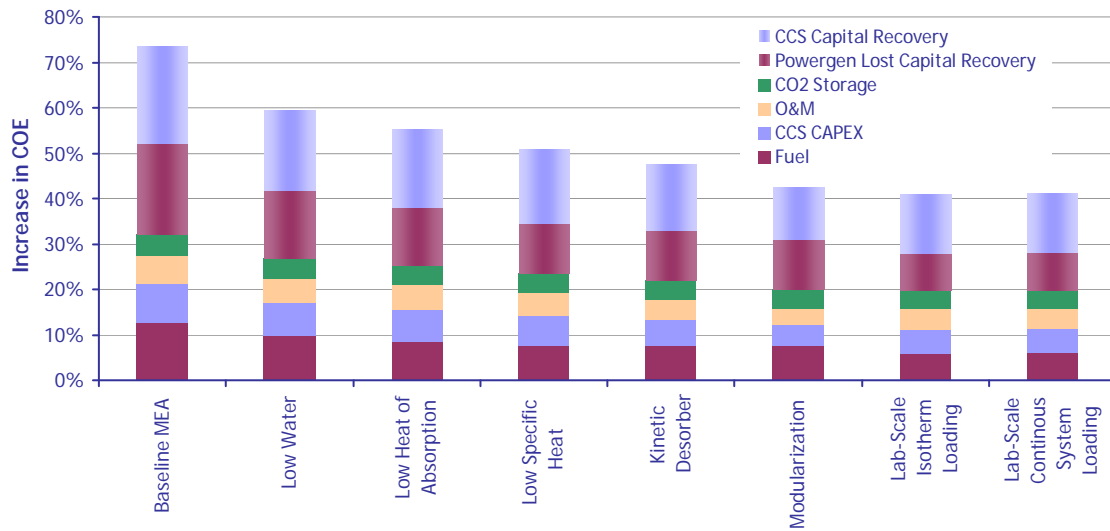


Figure 55. Waterfall Diagram for Cost of Electricity (COE) Calculations.

The low water decreases the COE from 73.3% to 59.4%. (In the DOE bituminous report the increase in COE for the base case MEA solvent was 86%, since there are some differences between GE assumptions and DOE bituminous report; however, it is more important to look at the relative differences presented in this report between the baseline MEA solvent and the Gap-1/TEG solvent) In the earlier sections it was pointed out that only 48 lbs/s can be absorbed by the TEG solvent. If no water was absorbed the COE will be decreased to 56.3%. So, the small amount of water in the Gap1-/TEG mixture leads to only 3.1% increase in COE.

The US CAP 2050 goal of 80% reduction in CO₂ emissions over 2005 levels will required near complete carbon capture on all existing coal plants, and certainly on any new coal plants. The deployment of carbon avoidance technologies should occur in order of their cost in \$/ton avoided. Figure 56 shows the \$/ton of CO₂ avoided for the waterfalls shown in Figures 53-55.

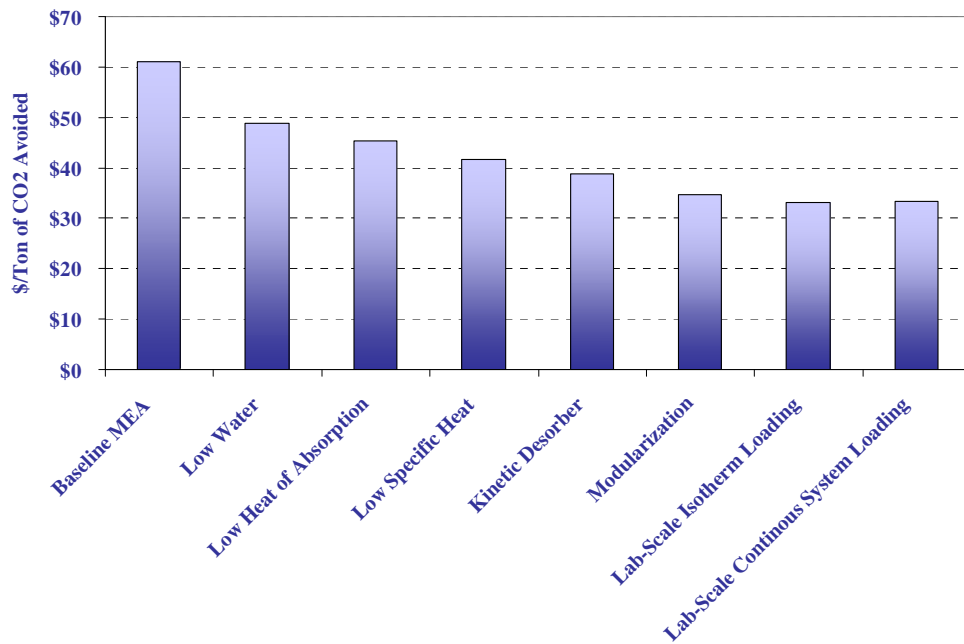


Figure 56. Waterfall Diagram for \$/Ton of CO₂ Avoided.

Conclusions

A variety of aminosilicones were examined as potential CO₂-capture solvents and a number of physical properties of this class of materials were both modeled and experimentally determined. Of the myriad structural variations examined, GAP-0 was initially chosen as the desired aminosilicone for GEN 1. Physical properties measurements showed good CO₂ uptake, high boiling point, lower heat of reaction compared to MEA, and lower heat capacity. Corrosion and thermal stability testing of this material also indicated good performance with no corrosion in stainless steel samples and carbon-steel corrosion only at 150 °C and thermal stability up to 120 °C.

However, carbamate formation from GAP-0/TEG mixtures resulted in precipitation of the salts over time. To mitigate this issue, a GEN 2 solvent was developed and tested. A 60/40 weight ratio of GAP-1 with a TEG co-solvent was found to be optimal. This avoided the precipitation problem seen with its lower molecular weight analog GAP-0. Similar physical properties were measured and a dynamic CO₂ uptake range of 5-6% was initially determined during batch isotherm experiments. Continuous absorption/desorption experiments only showed a 2.6% range. Even with this diminished overall CO₂ capacity, the models constructed indicated a reduction in CO₂ capture energy penalty from 30% to 18%. The increase in COE over the baseline plant without carbon capture changed from 73% for an optimized 30% MEA base case to 41%. Although the target of 35% increase in COE over the non-capture plant was not realized with these data, a huge benefit was realized with the new solvent system.

There are several steps that should be taken to build on these encouraging results. First, additional experiments need to be run in the continuous system to generate additional data at varying absorption and desorption temperatures and pressures. Raising the temperature of desorption by 10 °C may offer a significant increase in dynamic CO₂ capture capacity. Collecting data at different flow rates will also offer insight into the scalability of the system. Data also needs to be collected to determine rates of reaction.

While there are gaps in the available data for this new system, the initial results are extremely promising and further development will be able to answer many of the existing questions. However, from an original concept to demonstration of a continuous absorption/desorption system that has the potential to reduce COE to 41% from the original MEA baseline in two years is a tremendous accomplishment.

References

1. Kawata, M.; Ten-no, S.; Kato, S. H., F.; *Chem. Phys.* **1996**, *203*, 53.
2. Meier, M. R.; Metzger, J. O.; Schubert, U. S., *Chem. Soc. Rev* **2007**, *36*, 1788.
3. Tellez, G.L.; Viguera-Santiago, E.; Hernandez-Lopez, S.; Bilyeu, B., *Designed Monomers and Polymers*, **2008**, *11*, 435.
4. Momose, T.; Muraoka, O.; Shimada, N.; Tsujimoto, C.; Minematsu, T., *Chem. Pharm. Bull.*, **1989**, *37*, 1909.
5. (a) Yoshida, K.; Mimura, T.; Shimojo, S.; Karasaki, M.; Iijima, M.; Mitsuoka, S. US 6689332 to Kansai Electric Power Co., Inc and Mitsubishi Jukogyo Kabashika Kaisha, **Feb 10, 2004**. (b) Yoshida, K.; Mimura, T.; Shimojo, S.; Karasaki, M.; Iijima, M.; Mitsuoka, S. EP 588178 to Kansai Electric Power Co., Inc and Mitsubishi Jukogyo Kabashika Kaisha, **Jan. 21, 1998**. (c) Yoshida, K.; Mimura, T.; Shimojo, S.; Karasaki, M.; Iijima, M.; Seto, T.; Mitsuoka, S. EP 588175 to Kansai Electric Power Co., Inc and Mitsubishi Jukogyo Kabashika Kaisha, **Aug. 6, 1997**. (d) Tontiwachwuthikul, P.; Wee, A. G. H.; Idem, R.; Maneeintr, K.; Fan, G.-J.; Veawab, A.; Henni, A.; Aroonwilas, A.; Chakma, A. US 20080050296 to University of Regina, Ca., **Feb. 28, 2008**. (e) Sartori, G.; Savage, D. W., *Ind. Eng. Chem. Fundam.* **1983**, *22*, (2), 239-49.
6. (a) Haddenham, D.; Pasamansky, L.; DeSoto, J.; Eagon, S.; Singaam, B., *J. Org. Chem.* **2009**, *74*, 1964. (b) Ohsawa, T.; Kobayashi, T.; Mizaguchi, Y.; Saitoh, T.; Oishi, T. *Tetrahedron Lett.* **1985**, *26*, 6103. (c) Sieveking, H. U.; Luttke, W. *Angew. Chem. Int. Ed Engl.* **1969**, *8*, 458.
7. Hutchins, R. O.; Maryanoff, B. E., *Org. Syn.*, **1973**, *53*, 21.
8. Xie, X.; Liotta, C. L.; Eckert, C. A. *Ind. Eng. Chem. Res.* **2004**, *43*, 7907
9. Takiguchi, T.; Amagai, K.; Kawabata, H., *Bull. Chem. Soc. Jpn.*, **1979**, *52*, 1871.
10. Kida, T.; Isogawa, K.; Morishima, H.; Zhang, W.; Masatuma, A.; Nakatsuji, Y.; Ikeda, I., *J. Jpn. Oil Chem. Soc.*, **1998**, *47*, 41.
11. Mikata, Y.; Inaba, Y.; Morioka, M.; Yano, S., *Tetrahedron Lett.*, **2004**, *45*, 8785.
12. Yu, S.-B.; Droege, M.; Downey, S.; Segal, B.; Newcomb, W.; Sanderson, T.; Crofts, S.; Suravajjala, S.; Bacon, E.; Earley, W.; Delecki, D.; Watson, A. D. *Inorg. Chem.*, **2001**, *40*, 1576.
13. Rylander, P. N. in "Catalytic Hydrogenation in Organic Syntheses," Academic Press, New York, **1979**, pgs 138-145.
14. Tudge, M.; Mashima, H.; Savarin, C.; Humphrey, G.; Davies, I. *Tetrahedron Lett.* **2008** *49*, 1041.
15. The M, D, T, Q nomenclature is commonly used in silicone chemistry. M denote a silicon atom with 3 oxygen bonds and one carbon bond. D is two oxygen and two carbon bonds, T is one oxygen and three carbon bonds and Q is four oxygen bonds. The prime denotes some reactive functional group.
16. ¹³C NMR spectra of the carbamate from **1** showed evidence of a bicarbonate resonance at ~160 ppm vs carbamate resonance at ~164.5 ppm. See Tomizaki, K.-y.; Kanakubo, M.; Nanjo, H.; Shimizu, S.; Onoda, M.; Fujioka, Y. *Ind. Eng. Chem. Res.* **2010**, *49*, 1222.
17. Perry, R. J.; Grocela-Rocha, T. A.; O'Brien, M. J.; Genovese, S.; Wood, B. R.; Lewis, L. R.; Lam, H.; Soloveichik, G.; Rubinsztajn, M.; Kniajanski, S.; Draper, S.; Enick, R. M.; Johnson, J. K.; Xie, H.-b.; Tapriyal, D. *ChemSusChem*, **2010**, *3*, 919.

18. Gurkan, B. E.; de la Fuente, J. C.; Mindrup, E. M.; Ficke, L. E.; Goodrich, B. F.; Price, E. A.; Schneider, W. F.; Brennecke, J. F. *J. Am. Chem. Soc.* **2010**, *132*, 2116.

Summary of External Presentations:

ACS National Meeting, March 24, 2010 "Novel Aminosilicone Solvents for CO₂ Capture"
43rd Silicon Symposium, May 21, 2010 "Aminosilicone Solvents for Low Cost CO₂ Capture"
2010 NETL CO₂ Capture Technology Meeting, September 15, 2010 "Novel High Capacity Solvents for CO₂ Capture"
AIChE Meeting, November 8, 2010 "Characteristics of Aminosilicones for CO₂ Capture"
AIChE Meeting, November 12, 2010 "CO₂-Capture Process Using Aminosilicone-Based Absorbents"
PacifiChem 2010, December 17, 2010 "Aminosilicones as CO₂-Capture Solvents"

Summary of Patent Applications Filed:

Docket 238260: "LIQUID CARBON DIOXIDE ABSORBENT AND METHODS OF USING THE SAME" July 28, 2009.
Docket 237591: "CARBON DIOXIDE ABSORBANT AND METHOD OF USING THE SAME" July 28, 2009.
Docket 238253: "A SPRAY PROCESS FOR THE RECOVERY OF CO₂ FROM A GAS STREAM; AND A RELATED APPARATUS" October 28, 2009.
Docket 242793: "CARBON DIOXIDE ABSORBANT AND METHOD OF USING THE SAME" June 15, 2010.

Summary of External Articles:

"Novel Aminosilicones for CO₂ Capture," Fuel Preprints, 2010, 55(1), 282.
"Aminosilicones Solvents for CO₂ Capture," ChemSusChem, 2010, 3, 919.
"A Computational Study of the Heats of Reaction of Substituted Monoethanolamine with CO₂," J. Phys. Chem. A (accepted).
"Aminosilicones for CO₂ Capture," Energy & Fuels. (submitted)
"A combined experimental and computational study on the heat of reaction for amino silicones with CO₂," (to be submitted)

Acronyms

GE GRC – General Electric Global Research Center
GEE – General Electric Energy
U Pitt – University of Pittsburgh
ACS – American Chemical Society
AIChE – American Institute of Chemical Engineers
QFD -Quality Function Deployment
MEA – Monoethanol Amine
TS – Transition State
 ΔG – Gibbs Free Energy
 ΔH_{rxn} – Heat of Reaction
PEGDME – polyethyleneglycol dimethyl ether
PPGDME – polypropyleneglycol dimethyl ether
PFPE – poly(tetrafluoro)ethylene
PDMS - poly(dimethyl)siloxane
NFM – N-formyl morpholine
PAO – poly(acetoxyoxetane)
MCIBPA – meta-chloroperbenzoic acid
TEG – Triethylene glycol
GAP-0 – 1,3-bis(3-aminopropyl)-1,1,3,3-tetramethyldisiloxane
DBU – 1,8-diazabicycloundec-7-ene
nBuLi – n- butyl lithium
r.t. – room temperature
9-BBN – 9-borobicyclo[3.3.1]nonane
TsCl – para-toluene sulfonylchloride
HTS – High throughput screening
NMP- N-methyl pyrrolidinone
LAH- Lithium aluminum hydride
THF – Tetrahydrofuran
DAB – 1,3-bis(4-aminobutyl)-1,1,3,3-tetramethyldisiloxane
DAB-DiMe – 1,3-bis(4-amino-4-methylpentyl)-1,1,3,3-tetramethyldisiloxane
DAB-Me - 1,3-bis(4-aminopentyl)-1,1,3,3-tetramethyldisiloxane
GAP-nPr - 1,3-bis(propylaminopropyl) -1,1,3,3-tetramethyldisiloxane
GAP-AEAP - 1,3-bis(3-(2-aminoethyl)aminopropyl)-1,1,3,3-tetramethyldisiloxane
GAP-AEAM - 1,3-bis(3-(2-aminoethyl)aminomethyl)-1,1,3,3-tetramethyldisiloxane
M'DM' – 1,5-bis(3-aminopropyl)-1,1,3,3, 5,5-hexamethyldisiloxane
M'3T' – tris(3-aminopropyldimethylsiloxy)-3-aminopropylsilane
GAP-Dytek - 1,3-bis(3-(2-aminobutyl)aminopropyl)-1,1,3,3-tetramethyldisiloxane
PLM – liters/minute
MS – mass spectrometry
NMR – nuclear magnetic resonance
SCR – selective catalytic reduction
PC – pulverized coal
FGD – flue gas desulfurization
NOx – nitrogen oxides
HPT – high pressure turbine
IPT – intermediate pressure turbine
LPT – low pressure turbine
kpph – kilo pounds per hour
psia – pounds per square inch absolute
rpm – revolutions per minute
MWe – megawatt (electric)
LP – low pressure
HP – high pressure
COE – cost of electricity

DOI: 10.1002/cssc.201000077

Aminosilicone Solvents for CO₂ Capture

Robert J. Perry,^{*,[a]} Teresa A. Grocela-Rocha,^[a] Michael J. O'Brien,^[a] Sarah Genovese,^[a] Benjamin R. Wood,^[a] Larry N. Lewis,^[a] Hubert Lam,^[a] Grigorii Soloveichik,^[a] Malgorzata Rubinsztajn,^[a] Sergei Kniajanski,^[a] Sam Draper,^[b] Robert M. Enick,^[c] J. Karl Johnson,^[c] Hong-bin Xie,^[c] and Deepak Tapriyal^[c]

This work describes the first report of the use of an aminosilicone solvent mix for the capture of CO₂. To maintain a liquid state, a hydroxyether co-solvent was employed which allowed enhanced physisorption of CO₂ in the solvent mixture. Regeneration of the capture solvent system was demonstrated over 6 cycles and absorption isotherms indicate a 25–50% increase

in dynamic CO₂ capacity over 30% MEA. In addition, proof of concept for continuous CO₂ absorption was verified. Additionally, modeling to predict heats of reaction of aminosilicone solvents with CO₂ was in good agreement with experimental results.

Introduction

Coal is an important source of global energy, with nearly 1500 generators in the US alone producing 315 GW of electricity in 2007,^[1] however, it was also estimated that nearly 2.8×10^9 tonnes of CO₂ were released to the atmosphere from these same plants.^[2] Given the elevated concern over global warming and the role CO₂ may play in such a scenario, numerous pieces of legislation have been proposed and significant funding has been provided to design processes that will capture CO₂ from coal-fired power plants.^[3]

Post-combustion CO₂ capture processes have been demonstrated at various scales using chilled ammonia,^[4] cryogenics,^[5] carbonates,^[6] organic amines,^[7] and ionic liquids.^[8] However, none are in full-scale commercial use and all suffer from one or more deficiencies, including high energy costs for cooling, poor regeneration, low working capacity, or slow kinetics.

Our research has been focused on achieving targets set by the Department of Energy (DOE) for post-combustion capture of CO₂, namely: 90% CO₂ capture efficiency and less than a 35% increase in cost of electricity (COE) versus a plant with no CO₂ capture.^[9] This is in contrast to a calculated COE increase of 83% for the MEA process. We have concentrated on a solvent-based route and this paper describes our methodology for tackling the problem as well as preliminary experimental results directed towards these goals.

Results and Discussion

Numerous tactics have been used to address the challenge of post-combustion CO₂ capture. Our initial approach to the problem was to work backwards from the final COE numbers to the material properties. Figure 1 shows a schematic of this method. This reverse-engineering method required an accurate COE model and a fully integrated plant and process model. Having these in hand would permit prediction of solvent parameters necessary to achieve the 35% COE target.

The COE model simulates the economics of operation of a carbon capture plant retrofitted to an existing SCPC (super-critical pulverized coal) plant in the mid-western United States. The carbon capture process simulation is an integrated series of parametric models for a temperature- and pressure-swing solvent system consisting of an absorber, desorber, heat exchangers, and CO₂ compressors. The model accounts for heat additions for reaction energy, sensible heat changes, and steam stripping, and electrical loads for exhaust blowers, CO₂ compressors, and solvent pumps. Operational costs including solvent degradation are also modeled. Detailed Aspen process models linked to Icarus cost estimations provide the data that is parameterized into the COE model.

Given a set of solvent characteristics, the parametric plant operation is optimized to identify the operational characteristics that produce the lowest cost of electricity. The model produces optimized operational characteristics for MEA plants that are in good agreement with available literature data for key parameters, and produce similar cost of electricity penalties to the US DOE Bituminous Coal report.^[10]

Theoretical solvent parameters were created and new optimizations run to identify characteristics of the solvent that reached the DOE goals and were realistic based on the class of solvents under investigation. It was found that the non-aque-

[a] Dr. R. J. Perry, Dr. T. A. Grocela-Rocha, Dr. M. J. O'Brien, S. Genovese, Dr. B. R. Wood, Dr. L. N. Lewis, Dr. H. Lam, Dr. G. Soloveichik, M. Rubinsztajn, Dr. S. Kniajanski
GE Global Research
1 Research Circle, Niskayuna, NY, 12309 (USA)
Fax: (+1) 518 387 7403
E-mail: robert.perry@crd.ge.com

[b] S. Draper
GE Energy
300 Garlington Rd, Greenville, SC, 29615 (USA)

[c] Prof. R. M. Enick, Prof. J. K. Johnson, Dr. H.-b. Xie, Dr. D. Tapriyal
Department of Chemical and Petroleum Engineering
University of Pittsburgh, Pittsburgh, PA, 15261 (USA)

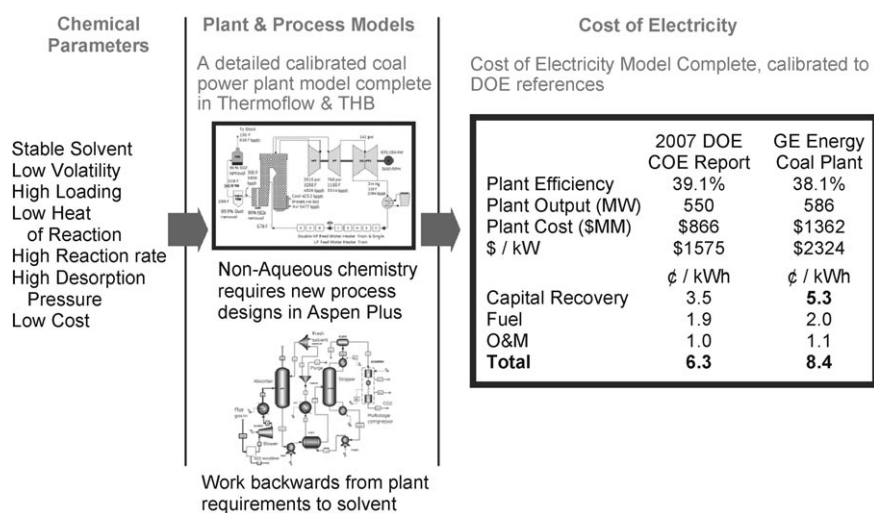


Figure 1. Program methodology.

ous nature of the proposed solvent was a key characteristic, in that it eliminated crucial temperature limits in the desorber and heat exchanger systems. The slope of the isotherms was then recognized as an important parameter, and shallow isotherms were identified as important to the process. The shallow isotherms lead to a focus on chemically complexing solvents, and away from physically absorbing solvents. These isotherms allow for an optimum plant operating condition that permits higher pressure in the desorber. Without the shallow isotherms, the non-aqueous solvent would not be viable.

To achieve the aggressive 35% maximum COE increase goal, analysis suggested that a solvent system with low volatility, high thermal stability, optimal heat of reaction with CO₂, high dynamic capacity, ready availability, and acceptable cost was needed. A solvent with low volatility would decrease the heat load on the condenser system, as would the enhanced thermal stability, leading to lower operational costs. Optimal ΔH_{rxn} would permit minimal energy expenditure during absorption and desorption cycles. A high dynamic CO₂ capacity of the solvent would permit maximum CO₂ capture with minimal solvent, also having a favorable impact on the cost of the system. However, optimization of all these systems parameters is non-trivial.

Given these target properties, we employed the concept of combining both a physisorbing and chemisorbing component in one molecule. The physical absorbing portion of the molecule would reside in the backbone and covalent CO₂ capture would sit on the termini of tethering groups, as shown in Figure 2.

Solvents that physically absorb CO₂ are commonly used today for acid gas scrubbing. For instance the Selexol process utilizes dimethylethers of polyethylene glycol, the Rectisol method uses cold methanol, and Purisol is based on *N*-methylpyrrolidinone.^[11]

We considered the incorporation of one of these or other physical-absorbing species, as shown in Table 1. Using the QFD method^[12] for assessing the quality of each of these classes of

compounds, the scaffolds that were deemed most promising are highlighted. Siloxanes, ethers, perfluoroethers, and amides were highly rated.^[13] Styrene and alkyl derivatives were also considered, based mainly on their cost and availability.

A similar assessment was also done for the chemically reactive functional groups, as shown in Table 2. A survey of the literature indicated that nitrogen-containing materials were optimal for CO₂ reactivity and a variety of amine groups were proposed. Primary and secondary amines were highly rated, as were guanidine and piperazine moieties.

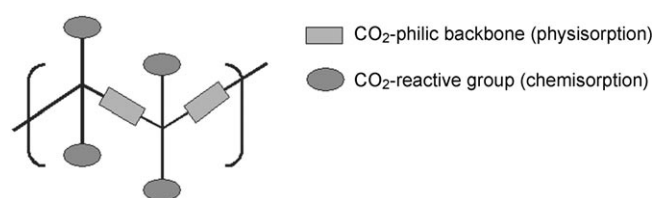


Figure 2. Schematic of novel CO₂ capture solvent.

CO₂ capacity was based on the number of reactive primary and secondary amines present in the structure. Two or more reactive amine groups were ranked highest in this evaluation. Kinetics were qualitatively based on the presence of primary or unhindered amines. These unhindered amines are the least sterically encumbered and would react most quickly. Rapid reaction is important given the large volume of flue gas that would need to be treated in the shortest amount of time. The ability to readily append the reactive amine groups to the backbone was founded on intermediates considered commercially available. Ease of synthesis was also considered in the cost factor. Many of the heterocyclic derivatives considered were found to be made in relatively small volumes.

After considering the synthetic challenges for making some of these materials, further downselection was performed and focused on the siloxane backbone with amino-containing arms. A large number of amino silicones were synthesized or procured from commercial sources and testing was carried out using high-throughput screening (HTS) methodologies.

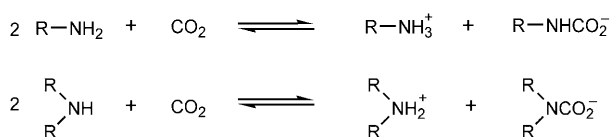
Amino-substituted alkoxy silanes have been explored as CO₂ capture materials. Glassy carbamic acid dimers have been formed at low temperatures from monoamine derivatives^[14] while diamino silanes formed intramolecular complexes.^[15] The intermolecular reaction product of two aminosilanes and CO₂ have been described as ionic liquids.^[16] Mesoporous silica derivitized with aminopropyltrimethoxysilane has also been used

Table 1. QFD Assessment of backbone structures.

Backbone	Structure	Attributes ^[a]			Ease of derivatization	CO ₂ -philic	Stability	Total
		Physical state	Cost	Synthetic availability				
siloxane		9	5	9	9	9	9	50
alkyl ether		9	9	9	5	5	9	46
alkyl amino		5	9	9	5	9	9	46
perfluoroether		9	1	5	1	9	9	34
alkyl		9	9	9	5	1	9	42
aryl ether		1	5	5	5	5	5	26
alkylamido		5	5	9	5	5	5	34
phosphazene		5	1	5	5	5	1	22
polystyrene		1	9	9	9	1	9	38

[a] The physical state must be a low-viscosity liquid: 9=liquid, 5=viscous liquid, 1=solid. Cost should be <\$10 lb⁻¹: 9=<\$10 lb⁻¹, 5=\$10–20 lb⁻¹, 1=>\$20 lb⁻¹. Synthetic availability refers to ability of being made on a large scale: 9=commercial, 5=small scale, 1=laboratory. Ease of derivatization refers to easy functionalization: 9=easy, 5=moderate, 1=difficult. CO₂-philic physisorption: 9=high, 5=moderate, 1=low.

as a CO₂-capture adsorbant^[17] as has silica functionalized by ring-opening polymerization of aziridine.^[18] An example of aminosilicone polymers used in CO₂ capture has also been reported.^[19]



The reaction of amines with CO₂ is well documented and is the basis for several large-scale pilot or slipstream processes being explored. It is well-established that primary and secondary amines react with CO₂ to form carbamates, as shown in Equations (1) and (2) and, under anhydrous conditions, two moles of amine are required to capture one mole of CO₂.^[20]

HTS allowed a rapid determination of the CO₂ capacities of a multitude of materials under various conditions. Table 3 is a summary of the screening results of the neat aminosilicone capture solvents at 40 °C for 2 h under an atmosphere of 100% CO₂. The CO₂ weight uptake is compared to that ob-

tained with the benchmark 30% aqueous MEA solution. Any material exhibiting a weight gain over 10% was considered promising. Testing was done under 100% CO₂ with triplicate samples tested at 1, 2, and 4 h to ensure complete reaction and at 40 and 55 °C to determine the effect of temperature on the capture capacity. These temperatures were chosen to bracket those typically found in flue gas stacks.

Table 3 shows the results of the aminosilicone materials tested as CO₂ capture solvents. Linear, cyclic, and branched solvents containing primary and secondary amine groups were examined as well as some compounds with ether or hydroxyl functionalities.

Compound 1 exhibited a nearly quantitative CO₂ loading, with a 16.5% weight gain. While not close to pure MEA (entry 18), it was better than the benchmark 30% aqueous MEA solution that showed 10.2% (entry 19). The diamine derivatives 2 and 3 were expected to display a substantially higher CO₂ uptake given twice the amine functionality per mole, but less than half of the theoretical loading was observed. Aminosilicone oligomer 4 also showed poor CO₂ pickup, despite the high amine loading. In contrast, oligomer 5 absorbed 84% of the theoretical limit of CO₂ but the absolute value of CO₂ uptake was less than 5%. Piperazine derivative 6 and the two cyclic materials 7 and 8 exhibited very poor CO₂ uptake. The branched and star materials (9–11) performed better but their CO₂ uptake percentage was still only about half of the expected value.

In most cases, the neat materials being tested either solidified or became very viscous liquids upon reaction with CO₂. Formation of solid product was almost always accompanied by a lower than theoretical uptake of CO₂ based on chemisorption; likely the result of poor mass transport of the CO₂ through the medium. The negative effect of formation of solid product of amine with CO₂ was evident by comparing reaction of CO₂ with compounds 4 and 5, with 4 turning into a paste while 5 was a moderately viscous liquid. While not solidifying, the Jeffamine derivatives 12–17 did form viscous oils which also accounted for their modest absorption.

Little difference was noted between the 1, 2, and 4 h points, indicating that whatever reaction was occurring, happened relatively quickly. Likewise, examination of these neat solvents at

Table 2. QDF assessment of reactive functional groups.

Functional group	Structure	Attribute ^[a] CO ₂ capacity	Heat of reaction	Kinetics	Ease of attachment	Cost	Total
aminoethyl		5	5	9	5	9	33
aminopropyl		5	5	9	9	9	37
aminoethylaminopropyl		9	9	9	9	9	45
bis(aminoethyl)aminopropyl		9	9	9	9	9	45
imidazole		1	1	1	9	5	17
histamine		5	9	1	5	1	21
isocytosine		5	5	5	5	1	21
5-azacytosine		9	5	5	5	1	25
piperazine		9	9	9	9	5	41
urea		5	5	1	5	9	25
acetamide		1	5	1	5	5	17
guanidine		9	5	9	1	5	29
amidine		9	5	9	9	5	37
benzylamine		5	9	5	9	5	33

[a] CO₂ capacity: 9 = high, 5 = moderate, 1 = low. Heats of reaction 9 = moderate, 5 = low, 1 = high. Kinetics (reaction with CO₂): 9 = fast, 5 = moderate, 1 = slow. Ease of attachment: 9 = easy, 5 = doable, 1 = difficult.

the two temperatures showed a small effect on CO₂ uptake. There were two competing processes contributing to the overall level of absorption. At higher temperatures, less CO₂ is absorbed at equilibrium but this was offset by a decrease in viscosity, which facilitated the mass transfer of CO₂ through the medium and allowed more complete reaction.

Table 4 illustrates the change in absorption with temperature for several of the aminosilicones. The only material that showed a significant change in absorbance was **7**. At 55 °C, cyclic aminosilicone **7** showed an increase in CO₂ uptake, commensurate with the observation that at the higher temperature the sample was a viscous liquid while at 40 °C the material was a solid. All other solvents remained either solids or very viscous liquids at either temperature.

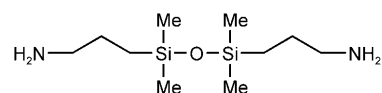
To mitigate the problem of hindered mass transfer and efficient reaction with CO₂, use of a co-solvent was employed. The co-solvent served to lower the viscosity of reaction medium as

well as provide for additional physisorption of CO₂. Table 5 illustrates the effect that triethylene glycol (TEG) had on the CO₂ uptake in several systems. Other hydroxy-terminated glycol-like co-solvents were also identified as promising co-solvents for these systems.

Although the absolute amount of CO₂ absorbed was decreased over that of the pure compound, the percentage of theoretical loading was substantially increased. Values over 100% were indicative of high levels of chemisorption as well as a substantial amount of physisorption in the reaction medium. In all cases, the final reaction product was a flowable liquid as opposed to a solid for the neat material. For comparison, the CO₂ uptake for 30% MEA was measured at 10.2 wt% using this method. Control experiments were also run on neat TEG. These indicated that physisorption by this co-solvent produced a weight gain in the range of 0.15–0.95% at 45 °C and 1 bar CO₂. The higher than theoretical yield may be accounted for by a combination of some physisorption as well as some bicarbonate formation from adventitious water present in the system.^[21]

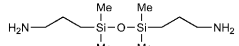
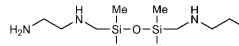
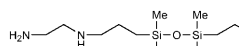

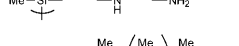
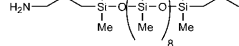
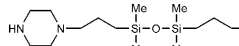
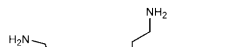
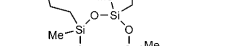
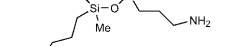

In light of these experiments, 1,3-bis(3-aminopropyl)-1,1,3,3-tetramethyldisiloxane, compound **1** (GAP-0), was chosen among a few promising candidates as the prototype for the aminosiloxane portion of the solvent and TEG as the co-solvent. This combination of GAP-0 and TEG had > 10% CO₂ absorption, maintained a very flowable state on reaction with CO₂, and could be readily made from available starting materials or purchased commercially.

With the solvent system chosen, physical properties needed



to be measured to feed into the process and COE models for validation. One of the first properties was reversibility of CO₂ absorption. To this end, a 50:50 mixture of GAP-0 and TEG was treated with CO₂ at 40 °C for 2 h and then heated to 120 °C for

Table 3. CO₂ capture performance of aminosilicones from HTS.

Compound	Structure	CO ₂ gain [wt %]	Theoretical CO ₂ gain [wt %]	Percentage of theoretical value [%]
1		16.5	17.7	94
2		15.3	31.6	48
3		10.9	26.3	41
4		8.5	27.5	31
5		4.6	5.5	84
6		3.8	11.4	33
7		3.5	18.8	19
8		2.0	27.5	7
9		7.5	13.2	57
10		10.4	15.8	66
11		15.1	24.2	62

Compound	Structure	CO ₂ gain [wt %]	Theoretical CO ₂ gain [wt %]	Percentage of theoretical value [%]
12		9.8	10.4	94
13		4.1	9.0	46
14		9.2	14.0	66
15		7.7	12.9	60
16		4.6	10.6	43
17		9.0	13.5	67
18	MEA	28.0	36.0	78
19	30% aqueous MEA	10.2	10.8	94

Compound	CO ₂ absorption @40 °C [wt %]	CO ₂ absorption @55 °C [wt %]
7	3.5	8.5
8	2.0	2.5
10	10.4	10.3
11	15.1	15.1
12	9.8	8.3
14	9.2	8.4
16	4.6	6.5

Aminosilicone	1:1 TEG/GAP-0	Theoretical gain [wt %]	Gain [wt %]	Physical state ^[a]
1	No	97	17.3	S
	Yes	114	10.1	L
2	No	69	21.8	S
	Yes	101	15.9	L
3	No	64	16.7	S
	Yes	90	11.8	L
7	No	30	5.6	S
	Yes	108	10.1	L
10	No	87	13.8	S
	Yes	116	9	L
MEA	30% in water	94	10.2	L

[a] S = solid, L = liquid.

15 min, and the sequence was repeated over 6 cycles. Figure 3 shows the % weight pickup for the absorption and desorption cycles.

Gravimetric measurements were made at the end of each half cycle to determine the total weight of CO₂ remaining in the system. The average dynamic range at 1 bar CO₂ was

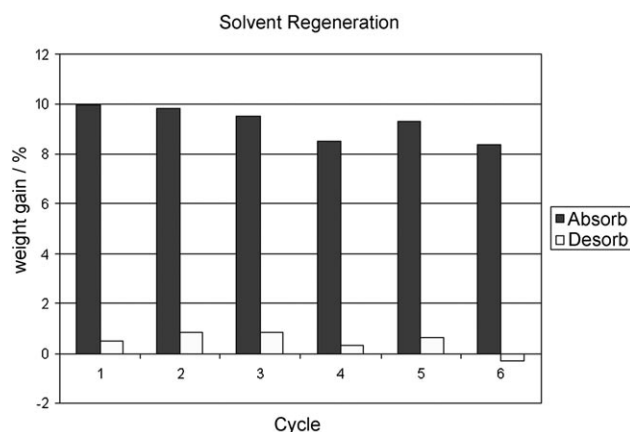


Figure 3. CO₂ weight uptake for a 50:50 GAP-0/TEG mixture over 6 cycles.

9.2%. The slight downward trend noted for weight gain and the negative weight remaining during the 6th desorption cycle in Figure 5 was due to evaporation of small amounts of the solvent and/or co-solvent. NMR analysis of the mixture after 6 cycles showed no observable decomposition of the aminosilicone.^[22]

A more accurate measure of the dynamic capacity of the solvent system was obtained through generation of absorption isotherms. In an ideal system, the solvent should absorb large quantities of CO₂ at flue gas temperatures (ca. 45 °C) and pressures (ca. 0.15 bar) and then readily release CO₂ at higher temperatures and pressures. The higher the pressure, the less parasitic energy would be needed to compress the CO₂ into a liquid for transport and sequestration. The larger the difference in CO₂ loading between the absorption and desorption stages, the greater the working capacity.

As seen in Figure 4, approximately 9 wt% CO₂ is absorbed at 0.1 bar and 45 °C. At 120 °C, and 10 bar CO₂ pressure, less than

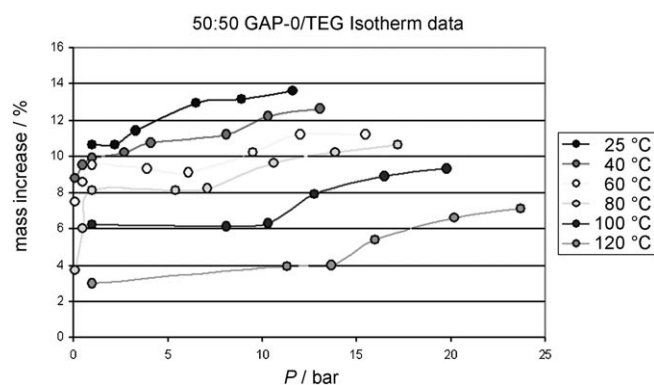


Figure 4. Experimentally measured isotherms for 50:50 GAP-0/TEG solvent.

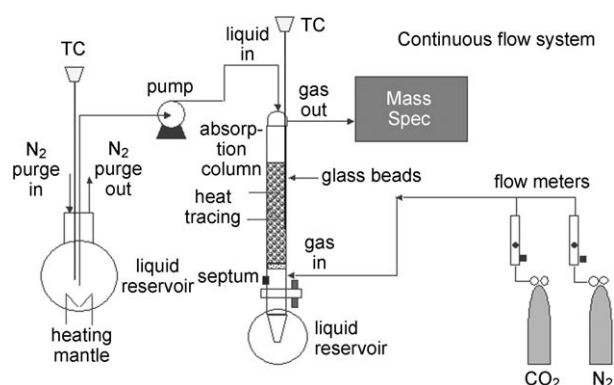


Figure 5. Continuous absorption apparatus for CO₂ capture.

4% CO₂ remained in solution. The absorption data provided a 5+ % dynamic capacity for this aminosilicone mixture. In contrast, 30% MEA has been reported to only have a 4% capacity under optimal conditions.^[23] The cause of the second plateau at elevated pressures observed in the isotherms shown in Figure 4 is unknown. One possibility is that the capacity of the solution for physically absorbing CO₂ increases as the concentration of polar carbamate species increases in the liquid phase. Other possibilities include phase changes in the chemical system at elevated pressures that result in increased CO₂ absorption capacity. An alternate possibility is that a secondary reaction is occurring and its isotherm is superimposed on the carbamate isotherm, resulting in a discontinuity in the curve at higher pressures. Because the isotherm experiments were performed in a sealed metal reactor, it was not possible to observe the chemical system during the experiments to determine if any phase changes occurred. At elevated pressure, a fraction of the carbamate species may precipitate, altering the solubility of CO₂ in the liquid phase. Or the liquid phase may have separated into two phases, with one of the phases exhibiting an increased capacity for CO₂ absorption. There is an error of approximately 0.2% in the weight measurements that would account for the slightly negative slopes seen in the 60 and 80 °C data at moderate pressures.

A favorable heat of reaction of CO₂ with the capture solvent was also a significant factor. There is an optimum value of the heat of reaction due to a competition between the equilibrium constant and the energy required for regeneration. A highly exothermic value of ΔH_{rxn} leads to a large equilibrium constant, but requires a large amount of heat to regenerate the solvent. On the other hand, low magnitude ΔH_{rxn} values allow facile regeneration, but an unfavorable equilibrium constant. The ΔH_{rxn} for CO₂ with MEA, GAP-0, and two other aminosilicones were measured and the results are shown in Table 6.

Table 6. Heats of reaction with CO₂.

Compound	Average ΔH_{rxn} [Jg ⁻¹ CO ₂]	Std dev [Jg ⁻¹ CO ₂]
1	-1596	118
2	-1168	53
3	-948	57
18 (MEA)	-1852	93

These data are based on amount of CO₂ reacted. The reaction was deemed complete when the rate of mass change was zero. A typical run took several hours. Using the TGA/DSC method described in the experimental section, the ΔH_{rxn} for CO₂ and MEA was $-1852 \pm 93 \text{ Jg}^{-1}$ which is in good agreement with the literature value of $1896 \pm 43 \text{ Jg}^{-1}$.^[24] GAP-0 showed a slightly lower ΔH_{rxn} than MEA while those of bisamines 2 and 3 were substantially lower.

We also computed ΔH_{rxn} from first-principles modeling. The purpose of these calculations was to validate the modeling by comparison with experiments so that modeling could be used as a way of predicting ΔH_{rxn} for molecules not yet synthesized. All calculations were carried out by using the Gaussian 03 package.^[25] Implicit solvent effects were taken into account by exploiting the conductor-like polarizable continuum model (CPCM) formalism, with the dielectric constant of water, $\epsilon = 78.39$, in the geometry optimizations and vibrational frequency calculations. The reference state for the energy calculations was taken as the isolated amines and CO₂. Although the molecules involved in these calculations have considerable conformational degrees of freedom, only a single configuration was used for each species in these calculations. We randomly constructed the initial configurations for the amines and optimized each to a local minimum. We constructed the initial configurations for carbamates by keeping the backbone of amines unchanged. Three different levels of theory were used to carry out the calculations for MEA: B3LYP/6-311++G(d,p) is a standard density functional theory (DFT) method using a large basis set. BHANDHLYP is considered to be a more accurate DFT method, and the same 6-311++G(d,p) basis set was used for these calculations. Finally, the MP2/6-31+G(d,p) level of theory was employed to account for electron correlation in a more rigorous way. A smaller basis set was used for these calculations because of unfavorable scaling.

In Table 7 the magnitude of ΔH_{rxn} for MEA is underestimated to a large degree (> 40%) by B3LYP/6-311++G(d,p) compared

Table 7. Calculated heats of reaction for compounds 1, 3, and 18 (MEA) in J g^{-1} .			
Compound	B3LYP/6-311++G(d,p)	BHANDHLYP/6-11++G(d,p)	MP2/6-31+G(d,p)
1	-1150	-1558	NA
3 (NH)	-475	-827	NA
3 (NH_2)	-1045	-1425	NA
18 (MEA)	-1074	-1549	-1729

with the value of 1896 J g^{-1} reported in the literature.^[24] The BHANDHLYP/6-311++G(d,p) level of theory gives a ΔH_{rxn} about 18% too small, whereas the MP2/6-31+G(d,p) method is within 9% of the experimental value. The modeling results indicated that the BHANDHLYP/6-311++G(d,p) method was a reasonable compromise between accuracy and efficiency. It is computationally prohibitive to compute the heat of reaction for larger molecules at the MP2/6-31+G(d,p) level of theory because of the very unfavorable scaling of the MP2 method. Therefore, only the B3LYP and BHANDHLYP methods were used for compounds 1 and 3. Although the value of ΔH_{rxn} for 1 from the BHANDHLYP/6-311++G(d,p) method is in excellent agreement with experimental values in Table 6, the trend from MEA to 1 is not reproduced. The lack of agreement with experiment is probably not a defect of the BHANDHLYP method, but rather an artifact of using only a single configuration to represent the reactant and product states. Conformational effects on ΔH_{rxn} are currently being investigated and will be the subject of a future publication. The ΔH_{rxn} for compound 3 that has both primary and secondary amines was also calculated. The values of ΔH_{rxn} for the secondary amines in 3 are much less exothermic than for the primary amines in the same molecule. Given the large differences in these heats of reaction, it is reasonable to assume that other secondary amines with silicone backbones will also be less exothermic than primary amines. Note that the heats of reaction for 1 and 3 predicted by the B3LYP/6-311++G(d,p) method are much less exothermic than those from the BHANDHLYP/6-311++G(d,p) theory of level, indicating a general trend.

It should be noted that the results presented to this point were based on batch reactions of solvents with CO_2 . However, a commercial process would need to be operated on a continuous basis. Thus, in order to evaluate the GAP-0/TEG system in a more realistic manner, a benchtop continuous absorption apparatus was assembled, as shown in Figure 5.

The heated (60°C) solvent mixture was introduced at the top of a heated (60°C) packed column at a rate that would accommodate the flow of simulated flue gas (10% $\text{CO}_2/90\% \text{ N}_2$) introduced at the bottom of the column. The effluent gas composition was monitored by mass spectrometry (MS). Preliminary measurements indicated that a 50:50 mixture of TEG/GAP-0 at equilibrium (Figure 6a), captured >99% of the CO_2 in the gas stream, as did 30% MEA (Figure 6b). Although the flow rates are not commensurate with power plant emissions, it demonstrates the first use of an aminosilicone as a CO_2 capture material in continuous mode.

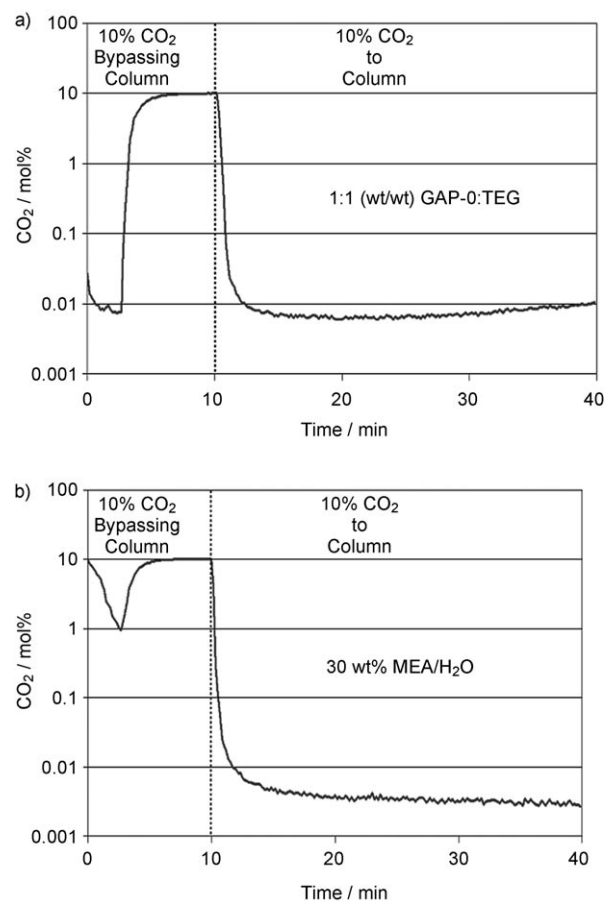


Figure 6. Continuous CO_2 capture for a) 1:1 GAP-0/TEG, compared to b) 30% MEA.

From these experiments, mass transfer coefficients were calculated and found to be $5.3 \text{ mol m}^{-2} \text{ h}^{-1}$ for the aminosilicone solvent system vs $8.4 \text{ mol m}^{-2} \text{ h}^{-1}$ for 30% MEA. These and other data were used to predict a COE that is shown in the waterfall diagram in Figure 7.

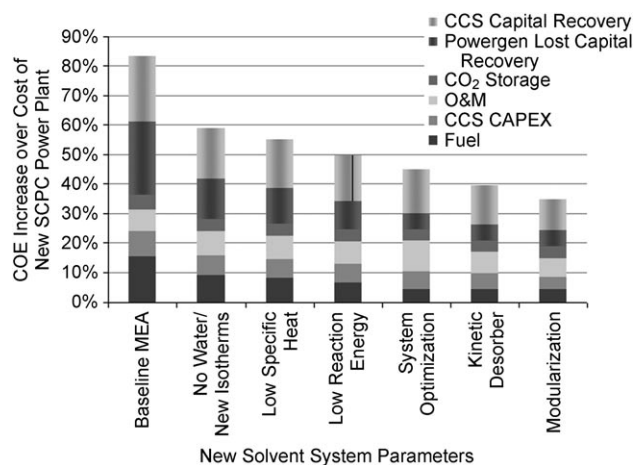


Figure 7. Waterfall diagram indicating contributions of various solvent attributes to COE.

The largest impact was removal of water from the system with over 20% reduction in COE predicted. Another 10% was projected to come from the lower specific heat and the decreased reaction energy of the new solvent system. These parameters alone were calculated to bring the COE to 50% for GAP-0/TEG from the 83% for aqueous MEA. Additional energy savings were projected to come from optimization of the entire system, including new desorber designs and modularization and standardization of unit operations.

Conclusions

This paper describes the first report of the use of an aminosilicone solvent mix for the capture of CO₂. To maintain a liquid state, a hydroxyether co-solvent was employed which allowed enhanced physisorption of CO₂ in the solvent mixture. Regeneration of the capture solvent system was demonstrated over 6 cycles and absorption isotherms indicate a 25–50% increase in dynamic CO₂ capacity over 30% MEA. In addition, a proof-of-concept for continuous CO₂ absorption was demonstrated. Additionally, modeling to predict heats of reaction of aminosilicone solvents with CO₂ was in good agreement with experimental results.

Further exploration of this system is in progress with thermal stability and corrosivity studies underway as well as further optimization of the amino silicone substrate. Finally, a laboratory-scale continuous absorption/desorption unit is under construction, which will provide needed kinetic data.

Experimental Section

General

Monoethanol amine and triethylene glycol were purchased from Aldrich and bis(3-aminopropyl)-1,1,3,3-tetramethyldisiloxane (**1**), bis(aminomethyl)-1,1,3,3-tetramethyldisiloxane (**2**) and oligomer **5** were obtained from Gelest. Oligomer **4** was obtained from Momentive Performance Materials. All materials were used as-received.

Synthesis of aminosilicone solvents

Compound 3. 1,3-bis(3-(2-aminoethyl)aminopropyl)-1,1,3,3-tetramethyldisiloxane: Ethylenediamine (155 g, 2.58 moles) was charged to a 500 mL three-necked flask equipped with a magnetic stirbar, reflux condenser, addition funnel, and nitrogen sweep. The flask was then heated using an oil bath. Once the temperature reached about 95 °C, 1,3-bis(3-chloropropyl)-1,1,3,3-tetramethyldisiloxane (73 g, 254 mmols) was added dropwise over about 2 h. During this time the temperature of the oil bath was allowed to increase to about 110–115 °C. Once addition was complete, the reaction mix was allowed to continue at this temperature for 2 h at which time proton NMR indicated that the reaction was complete. The mixture was cooled, and then some of the excess ethylenediamine was stripped off. At this point the material was cooled to room temperature, partitioned between chloroform and 10% NaOH, and then the organic phase was washed with deionized water and saturated sodium chloride and dried over anhydrous potassium carbonate. After filtration, solvent was removed on a rotary evaporator affording 71.2 g (84%) crude product which was purified by fractional

distillation at 130–135 °C/0.18–0.25 mm Hg. ¹H NMR (CDCl₃): δ = 2.79 (t, *J* = 6.0 Hz, 4H); 2.65 (t, *J* = 6.0 Hz, 4H); 2.58 (t, *J* = 7.3 Hz, 4H); 1.49(m, 4H); 1.31 (br 6H); 0.49 (m, 4H); 0.03 ppm(s, 12H). ¹³C{¹H} NMR (CDCl₃): 53.1, 52.7, 41.9, 23.9, 15.8, 0.3 ppm. FT-IR (neat): 3366, 3285, 2929, 2877, 2807, 1604, 1495, 1455, 1345, 1301, 1257, 1176, 1127, 1054, 841, 795 cm⁻¹.

Compound 6. 1,3-bis(3-*N*-piperazinopropyl)-1,1,3,3-tetramethyldisiloxane: A stirred suspension of bis(3-chloropropyl)tetramethyldisiloxane (4.2 g, 14.6 mmol), piperazine (6.28, 73 mmol) in acetone (50 mL), and sodium iodide (5.47 g, 36.5 mmol) was heated to 70 °C for 3 days. The resulting yellow orange suspension was then filtered through a pad of celite and further washed with diethyl ether (2 × 50 mL) and toluene (30 mL). The reaction was monitored by GCMS (100 μL aliquots were taken from the reaction mixture and diluted 10 times in acetone and the resulting mixtures were injected in the GCMS over the course of 3 days). After refluxing for 3 days, the corresponding mixture was then filtered over a pad of celite and taken to dryness using a rotavap (5 mm Hg, dry ice trap). The resulting residue was then redissolved in hot toluene (100 mL) to room temperature and further filtered twice using a 450 nm syringe filter. The filtrate was then subjected to rotary evaporation (5 mm Hg, dry ice trap) to afford a clear viscous orange oil. Yield: 5.0 g, 89%. ¹H NMR (CDCl₃): δ = 0.06 (s, 12H), 0.50 (app t, 4H, *J* = 8 Hz), 1.49–1.56 (m, 4H), 2.34–2.38 (m, 4H), 2.51–2.80 (br, 13H), 2.96–3.05 (m, 5H) ppm.

Compound 7. 1,3,5,7-tetrakis(3-aminopropyl)tetramethylcyclotetrasiloxane: A solution of 20 g 1,3,5,7-tetramethylcyclotetrasiloxane in 100 mL dry toluene and 0.5 mL of Karstedt catalyst (5% in xylenes), was treated with allylamine (32 g, 0.533 mol), and heated to reflux at ~80 °C for 2 h. The volatiles were removed in vacuo. The residue was distilled at 130 °C/0.1 mm Hg to give 47.4 g of colorless viscous liquid. ¹H NMR (CDCl₃): δ = 2.64 (t, 8H, *J* = 6.8 Hz); 1.76 (br. s, 8H); 1.46 (m, 8H); 0.51 (m, 8H); 0.07 (s, 12H) ppm.

Compound 8. 1,3,5,7-Tetrakis[*N*-(2-aminoethyl)-3-aminopropyl]tetramethylcyclotetrasiloxane: Aminoethyl aminopropyl dimethoxymethylsilane (25 g, 121 mmol) was added to excess water in 1 L of THF and stirred over 72 h. The initially clear solution became turbid. The pot contents were transferred to a separation funnel and allowed to separate overnight to give a small portion of a yellow oil and clear THF solution. The THF layer was separated and the volatiles were removed under reduced pressure. Drying in vacuum afforded ~14 g of yellowish viscous product. ¹H NMR ([D₆]DMSO): δ = 2.56 (m, 8H); 2.46 (m, 16H); 2.40 br s (12H); 1.44 (m, 8H); 0.49 (m, 8H); 0.05 (s, 12H) ppm.

Compound 9. Tris(3-aminopropyl dimethylsiloxy)phenyl silane: A solution of PhSi(OSiMe₂H)₃ (10 g, 30 mmol) in 40 mL dry toluene and 0.5 mL of Karstedt catalyst (5% in xylenes), was treated with allylamine (6.5 g, 108 mmol), and heated to reflux at ~80 °C for 2 h. The volatiles were removed in vacuo to give 16.1 g of dark viscous liquid that starts to decompose in vacuo at ~100 °C. ¹H NMR (CD₂Cl₂): δ = 7.62 (m, 2H); 7.4 (m, 3H); 2.62 (t, 6H, *J* = 6.8 Hz); 1.45 (m, 6H); 1.05 (br. s, 6H); 0.60 (m, 6H); 0.16 (s, 18H) ppm.

Compound 10. Tetrakis(3-aminopropyl dimethylsiloxy)-silane: To a solution of Si(OSiMe₂H)₄ (10 g, 30.5 mmol) in 40 mL dry toluene and 0.5 mL of Karstedt catalyst (5% in xylenes), was added allylamine (7.95 g, 132 mmol). The mixture was heated to reflux for 2 h. The volatiles were removed in vacuo to give 16.5 g of dark viscous liquid that starts to decompose at ~100 °C in vacuo. ¹H NMR (CD₂Cl₂): δ = 2.64 (t, 8H, *J* = 7.1 Hz); 1.47 (m, 8H); 0.98 (br. s, 8H); 0.58 (m, 8H); 0.13 (s, 24H) ppm.

N-allylethylenediamine: Allylbromide (20 g, 165 mmol) was rapidly added dropwise to 5-fold excess of cooled (ice bath) and vigorously stirred ethylenediamine (50 g, 826 mmol). After 10 min of stirring, the mixture was heated to reflux for 1 h under N₂ then cooled down to room temperature. 1 equiv of NaOH (50 wt% aqueous solution) was added, stirred for 15 min, then refluxed for 1 h. The mixture was slowly distilled with the product collected between 155–158 °C. ¹H NMR ([D₆]DMSO): δ = 5.82 (m, 1H); 5.13 (ddt, 1H, *J* = 17.2; 2.0; 1.8 Hz); 5.01 (ddt, 1H, *J* = 10.4; 2.0; 1.3 Hz); 3.12 (dt, 2H, *J* = 5.8; 1.5 Hz); 2.57 (t, 2H, *J* = 6.1 Hz); 2.46 (t, 2H, *J* = 6.1 Hz); 2.06 (br s, 3H) ppm.

Compound 11. Tetrakis[*N*-(2-aminoethyl)-3-aminopropyl-dimethylsiloxy]silane: To a solution of Si(OSiMe₂H)₄ (8 g, 24.4 mmol) in 40 mL dry toluene and 0.5 mL of Karstedt catalyst (5% in xylenes), was added *N*-allylethylenediamine (9.76 g, 97 mmol). The solution was heated for 7 h at reflux. The volatiles were removed in vacuo to give 17.5 g of dark viscous liquid. ¹H NMR (CD₂Cl₂): δ = 2.61 (t, 8H, *J* = 5.5 Hz); 2.48 (m, 16H); 1.40 (m, 8H); 0.92 (br s, 12H); 0.47 (m, 8H); 0.0 (s, 24H) ppm.

Compound 12. Jeffamine D-230/bis(chloro-methyl)tetramethyldisiloxane adduct: 12.0 g of Jeffamine D-230 was heated to approximately 90 °C under nitrogen. 3.0 g of bis(chloromethyl)tetramethyldisiloxane (M^{CM}M^{CM}) was then added drop-wise. After addition was complete, the reaction mixture was maintained at this temperature for another 5 h. At this point the material was cooled to room temperature and diluted with chloroform. The resulting solution was then washed once with 5% sodium hydroxide, four times with water, and then once with NaCl solution. After drying over anhydrous K₂CO₃, filtration, and stripping on the rotary evaporator, 5.91 g (73% yield) of product was obtained as a low viscosity yellow oil. ¹H NMR (CDCl₃): δ = 0.08 (s, CH₃Si), 0.9–1.1 (multiplets, CH₃s), 1.40 (m, NHs), 1.78 (multiplets, NCH₂Si), 2.66 (CHN), 3.0–3.8 (multiplets, CH_xOs) ppm.

Compound 13 Jeffamine D-230/bis(glycidoxy-propyl)tetramethyldisiloxane adduct: To 10.0 g of Jeffamine D-230 was added with stirring under nitrogen 4.0 g of bis(glycidoxypropyl)tetramethyldisiloxane (M^{CP}M^{CP}). The result was heated to approximately 90 °C for 4 h. At this point, the material was cooled to room temperature, diluted with chloroform and then transferred to a separatory funnel. It was then washed five times with deionized water to remove excess Jeffamine. Next the organics were washed a single time with saturated NaCl solution and dried over anhydrous potassium carbonate. After filtering out the drying agent, the solvent was removed on a rotary evaporator yielding 8.15 g of product (90% yield) as a yellow oil. ¹H NMR (CDCl₃): δ = 0.01 (s, CH₃Si), 0.47 (m, CH₂Si), 0.98 (m, CH₃), 1.10 (m, CH₃), 1.3–1.8 (br multiplets, NHs), 1.55 (multiplets, CH₂CH₂CH₂), 2.4–2.9 (br multiplets, CH₂Ns), 3.0–3.9 (br. multiplets, CH_xOs) ppm.

Compound 14. Jeffamine HK-511/bis(chloro-propyl)tetramethyldisiloxane adduct. 3.0 g of M^{CP}M^{CP} was added drop-wise to 11.5 g of Jeffamine HK-511. The result was allowed to react as above for 3 h at 110–115 °C. After workup, 6.44 g of product was obtained (94% yield) as a low viscosity yellow oil. ¹H NMR (CDCl₃): δ = 0.02 (s, CH₃Si), 0.48 (t, *J* = 8 Hz, CH₂Si), 0.99 (m, CH₃), 1.12 (m, CH₃), 1.2–1.6 (br multiplets, NHs and CH₂CH₂CH₂), 2.4–2.9 (br multiplets, CH₂Ns), 3.0–3.7 (br. multiplets, CH_xOs) ppm.

Compound 15. Jeffamine HK-511/bis(chloro-methyl) tetramethyldisiloxane adduct: 14.3 g of Jeffamine HK-511 was heated to approximately 75 °C under nitrogen. 3.0 g of M^{CM}M^{CM} was then added drop-wise. The temperature was allowed to climb to 80–85 °C where the reaction was kept for 3 h. The material was cooled to

room temperature, diluted with CHCl₃, washed five times with deionized water then with saturated NaCl solution, dried over K₂CO₃, filtered, and concentrated to give 4.98 g of product (64% yield) as a light yellow oil. ¹H NMR (CDCl₃): δ = -0.06 (s, CH₃Si), 0.85–1.2 (multiplets, CH₃s), 1.39 (m, NHs), 1.76 (m, NCH₂Si), 2.6–2.6 (CHN), 3.0–3.7 (m, CH_xOs) ppm.

Compound 16 Jeffamine HK-511/bis(glycidoxy-propyl)tetramethyldisiloxane adduct: 8.4 g Jeffamine HK-511 was reacted with 6.0 g of M^{CP}M^{CP} at 90 °C for 2 h. The material was cooled to room temperature and diluted with CHCl₃, washed with 5% NaOH, four times with water and once with brine, dried over K₂CO₃, filtered, and concentrated to give 11.3 g of material (85% yield) was obtained as a yellow oil. ¹H NMR (CDCl₃): δ = -0.01 (s, CH₃Si), 0.43 (m, CH₂Si), 0.96 (m, CH₃), 1.07 (m, CH₃), 1.3–2.0 (br multiplets, NHs), 1.55 (m, CH₂CH₂CH₂), 2.4–2.9 (br multiplets, CH₂Ns), 3.0–3.9 (br. multiplets, CH_xOs) ppm.

Compound 17. Jeffamine D-230/bis(chloro-propyl)tetramethyldisiloxane adduct: 4.0 g of bis(chloropropyl) tetramethyl-disiloxane (M^{CP}M^{CP}) was added to 12.8 g of Jeffamine D-230 and heated to 105–110 °C under nitrogen for 7 h. The mixture was worked up as described for Compound 15. This gave 8.77 g of product (93% yield) as an orange oil. ¹H NMR (CDCl₃): δ = -0.03 (s, CH₃Si), 0.43 (t, *J* = 8 Hz, CH₂Si), 0.94 (m, CH₃), 1.08 (m, CH₃), 1.2–1.5 (br multiplets, NHs and CH₂CH₂CH₂), 2.3–2.9 (br multiplets, CH₂Ns), 2.95–3.6 (br. multiplets, CH_xOs) ppm.

High-throughput screening protocol

Experiments were carried out using a 27 well parallel reactor (React Vap III) from Pierce and a Symyx Core Module for automated weighing in 8 mL glass vials. The experiments were run using technical grade CO₂ at 1 atm and the flow was set at 1.2 mL min⁻¹ by using a MKS mass flow controller. Each formulation was tested in triplicate. Each vial was loaded with a stirrer bar and pre-weighed using the Symyx Core module. The vials were then loaded with the corresponding compound (200–300 μL) and the corresponding amount of co-solvent where applicable. The contents were treated with CO₂ gas (1 atm) for 60–120 min at the desired temperature (40 and 55 °C). After the CO₂ treatment, the reactor block was cooled down to room temperature and all the vials were transferred to the Symyx Core Module for automated weighing. The physical state of each vial was visually inspected and recorded. The CO₂ adsorption performance was reported as an average of the % weight gain after each CO₂ treatment.

Laboratory reactions

Experiments were performed in a 25 mL, three-neck, round-bottom flask equipped with a mechanical stirrer, gas inlet, and bubbler. The candidate solvent (and co-solvent as appropriate) were added, the entire flask assembly was pre-weighed and then allowed to react at 40 °C while being exposed to a constant stream of dry CO₂ generated from dry ice and passed through a drying column. Periodically, the flask was weighed to determine the total weight gained. For desorption experiments, the flask was heated to 100–120 °C for 15–30 min.

Heats of reaction

Thermogravimetric analysis was performed on a Mettler Toledo TGA/DSC1 instrument. The sample was analyzed as received in

9 mm diameter platinum sample pans. The sample was held in a scintillation vial and the headspace was purged with argon after taking aliquots for analysis. Gas flow was 190 mL min⁻¹ N₂ held 30 min then 190 mL min⁻¹ CO₂ held 90 min followed by 190 mL min⁻¹ N₂ held 30 min. Calibration was performed with respect to the melting point and heat of fusion of a biphenyl standard under a carbon dioxide purge. The measured melting point was within 2 °C of the expected value and the heat of fusion was within 3 J g⁻¹ of the expected value (122 J g⁻¹).

Isotherm measurements

The isotherms were measured by using a 100 mL Parr reactor system fitted with a magnetically coupled mechanical stirrer and a pressure transducer. The reactor of known volume was loaded with a known amount of liquid. The reactor was flushed with CO₂ and then pressurized to the desired loading of CO₂. The reactor was weighed to determine the mass of gas loaded in the system. The temperature was set to the initial desired temperature and the system was allowed to come to equilibrium while stirring vigorously. The system was held at equilibrium for at least one hour while data was recorded. The next temperature was then set, and the process was repeated for all desired temperatures at that loading of CO₂. The equilibrium concentrations of CO₂ in the gas and liquid phases were calculated from the equilibrium temperature, pressure, the known reactor and sample volumes, and the known gas loading. Additional CO₂ was then added to the reactor, and the temperature profile was repeated.

Continuous absorption

For these experiments a 50:50 (wt/wt) mixture of bis(3-aminopropyl) tetramethyldisiloxane and triethylene glycol was prepared as was a 30 wt% aqueous solution of MEA. The absorbent to be tested was placed in a liquid reservoir, which was purged with nitrogen. For the case of the experiment with bis(3-aminopropyl) tetramethyldisiloxane and triethylene glycol this reservoir was initially heated to 110 °C for 30 min under a N₂ purge to remove any CO₂ or water. The mixture was then cooled to 90 °C. At the beginning of each experiment the absorbent was pumped by a Masterflex peristaltic pump at a flow rate of 0.9 mL min⁻¹ from this reservoir to the top of a jacketed Ace Glass chromatography column. The column had an inside diameter of 11 mm and was packed with 30 mL of 2 mm diameter glass beads. The column was heated to 60 °C by flowing water through the jacketing. The absorbent trickled down through the bed of glass beads and into a second liquid reservoir at the bottom of the column. A flow rate of 10% CO₂ in N₂ at 50 mL min⁻¹ was initially set to flow directly from the source gas cylinders to an MKS Cirrus mass spectrometer where the concentration of CO₂ in the gas stream was monitored. After 10 min of monitoring this baseline amount of CO₂ in the gas stream, the gas flow was switched so that the gas flow was introduced at the bottom of the column. The gas flowed countercurrent to the liquid flow and exited at the top of the column. The gas then flowed to the mass spectrometer, where the resulting concentration of CO₂ was measured. Brooks Instrument model 5850E mass flow controllers metered the gas flow rates.

Acknowledgements

This report is based upon work supported by the Department of Energy, National Energy Technology Laboratory under Award

Number DE-NT0005310. We also thank Tracy Zhang for ¹³C NMR experiments and Maria LaTorre for TGA analyses. **Disclaimer.** This report was prepared as an account of work sponsored by an agency of the United States Government. Neither the United States Government nor any agency thereof, nor any of their employees, makes any warranty, express or implied, or assumes any legal liability or responsibility for the accuracy, completeness, or usefulness of any information, apparatus, product, or process disclosed, or represents that its use would not infringe privately owned rights. Reference herein to any specific commercial product, process, or service by trade name, trademark, manufacturer, or otherwise does not necessarily constitute or imply its endorsement, recommendation, or favoring by the United States Government or any agency thereof. The views and opinions of authors expressed herein do not necessarily state or reflect those of the United States Government or any agency thereof.

Keywords: absorption · aminosilicones · carbon storage · silicon · solvent effects

- [1] *Existing Capacity by Energy Source, January 2009*, Energy Information Administration, available from <http://www.eia.doe.gov/eneaf/electricity/epa/epat2p2.html> (accessed August 2010).
- [2] a) *Science Daily*, CO₂ Sequestration/Articles/References for Fuel Preprint/Science Daily **2007**, Nov 15.htm, <http://www.sciencedaily.com/releases/2007/11/071114163448.htm>; b) *Intergovernmental Panel on Climate Change: Special report on Carbon Dioxide Capture and Storage*, (Ed.: B. Metz, O. Davidson, H. C. DeConinck, M. Loos, L. A. Meyer), Cambridge University Press, Cambridge, **2005**, available from http://www.ipcc.ch/pdf/special-reports/srccs/srccs_wholereport.pdf; c) M. Mikkelsen, M. Jorgensen, F. C. Krebs, *Energy Environ. Sci.* **2010**, *3*, 43.
- [3] *American Clean Energy and Security Act of 2009*.
- [4] a) G. Valenti, D. Bonalumi, E. Macchi, *Energy Procedia* **2009**, *1*, 1059; b) E. Gal, O. M. Bade, I. Jataweera, G. Krishnan, US Pat Appl. US2009/148930, June 11, **2009** to Alstom Power, Inc; c) R. Peltier, *Power* **2008**, *152*, 38; d) V. Darde, K. Thomsen, W. van Well, E. Stenby, *Chilled Ammonia Process for CO₂ Capture* (Eds.: R. Span, I. Weber), *15th International Conference on the Properties of Water and Steam*, Germany, **2008**.
- [5] *Cryogenic Carbon Capture Technology*, in *Carbon Capture Journal* **2009**, *10*, 18.
- [6] a) T. O. Nelson, D. A. Green, L. J. I. Coleman, R. P. Gupta, J. D. Figueroa, *Proc. Ann. Int. Pittsburgh Coal Conf.* **2008**, *25*, 411/1–411/2; b) E. J. Anthony, *Ind. Eng. Chem. Res.* **2008**, *47*, 1747; c) P. C. Tseng, W. S. Ho, D. W. Savage, *AIChE J.* **1988**, *34*, 922; d) G. R. Say, F. J. Heinzlmann, J. N. Iyengar, D. W. Savage, A. Bisio, G. Sartori, *Chem. Eng. Prog.* **1984**, *80*, 72; e) G. Astarita, D. W. Savage, J. M. Longo, *Chem. Eng. Sci.* **1981**, *36*, 581; f) G. T. Rochelle, E. Chen, B. Oyekan, A. Sexton, J. Davis, M. Hilliard, Q. Xu, D. Van Wagener, J. M. Plaza, in *CO₂ Capture by Absorption with Potassium Carbonate*; DOE Report; University Of Texas at Austin, Austin **2006**.
- [7] a) S. Reddy, D. Johnson, J. Gilmartin, *Fluor's Econamine FG Plus Technology for CO₂ Capture at Coal-fired Power Plants*, in *Power Plant Air Pollutant Control "Mega" Symposium*, August 25–28, **2008**; b) D. W. Bailey, P. H. M. Feron, *Oil Gas Sci. Technol.* **2005**, *60*, 461; c) D. G. Chapel, C. L. Mariz, J. Ernest, *Recovery of CO₂ from Flue Gases: Commercial Trends*, 1999 Canadian Society of Chemical Engineers Annual Meeting, Saskatoon, Saskatchewan, **1999**; d) N. Boucif, E. Favre, D. Roizard *Chem. Eng. Sci.* **2008**, *63*, 5375; e) N. Nsakala, J. Marion, C. Bozzuto, G. Liljedahl, M. Palkes, *Engineering Feasibility Of CO₂ Capture On An Existing US Coal-Fired Power Plant*, First National Conference on Carbon Sequestration, Washington DC, **2001**; f) I. L. Leites, *Energy Convers. Manage.* **1998**, *39*, 1665; g) G. Sartori, D. W. Savage, *Ind. Eng. Chem. Fundam.* **1983**, *22*, 239; h) K. Yoshida, T. Mimura, S. Shimojo, M. Karasaki, M. Iijima, S. Mitsuoka, US 6689332 to Kansai Electric Power Co., Inc., Feb. 10, **2004**; i) R. Idem, M. Wilson, P. Tontiwachwuthikul, A. Chakma, A. Veawab, A. Aroonwilas, D.

- Gelowitz, *Ind. Eng. Chem. Res.* **2006**, *45*, 2414; j) G. T. Rochelle, *Science* **2009**, *325*, 1652.
- [8] a) D. Camper, J. E. Bara, D. L. Gin, R. D. Noble, *Ind. Eng. Chem. Res.* **2008**, *47*, 8496; b) E. D. Bates, R. D. Mayton, I. Ntai, J. H. Davis Jr., *J. Am. Chem. Soc.* **2002**, *124*, 926; c) R. E. Baltus, R. M. Counce, B. H. Culbertson, H. Luo, D. W. DePaoli, S. Dai, D. C. Duckworth, *Sep. Sci. Technol.* **2005**, *40*, 525; d) J. Kumelan, A. Perez-Salado Kamps, D. Tuma, G. Maurer, *J. Chem. Thermodyn.* **2006**, *38*, 1396; e) J. Kumelan, D. Perez-Salado Kamps, D. Tuma, G. Maurer, *J. Chem. Eng. Data* **2006**, *51*, 1802; f) M. J. Muldoon, S. N. V. Aki, J. L. Anderson, J. K. Dixon, J. F. Brennecke, *J. Phys. Chem. B* **2007**, *111*, 9001.
- [9] J. Ciferno, T. Fout, *IOP Conference Series: Earth and Environmental Science* **2009**, *6*, 172016.
- [10] *Cost and Performance Baseline for Fossil Energy Plants*; DOE/NETL-2007/1281. Volume 1: Bituminous Coal and Natural Gas to Electricity. Revision 1, Aug. **2007**.
- [11] R. W. Bucklin, R. L. Schendel, *Acid and Sour Gas Treating Processes* (Ed.: S. A. Newman), Gulf, Houston, **1985**, pp. 42–47.
- [12] QFD stands for “Quality Function Deployment” and is designed to help planners focus on characteristics of a new product from the viewpoint of technology-development needs.
- [13] a) M. B. Miller, D.-L. Chen, H.-B. Xie, D. R. Luebke, J. K. Johnson, R. M. Enick, *Fluid Phase Equilib.* **2009**, *287*, 26; b) S. Li, Y. Li, J. Wang, *Fluid Phase Equilib.* **2007**, *253*, 54; c) J. A. Dzielawa, A. V. Rubas, C. Lubbers, D. C. Stepinski, A. M. Scurto, R. E. Barrans Jr., M. L. Dietz, A. W. Herlinger, J. F. Brennecke, *Sep. Sci. Technol.* **2008**, *43*, 2520; d) V. M. Shah, B. J. Hardy, S. A. Stern, *J. Polym. Sci., Part B: Polym. Lett.* **1993**, *31*, 313; e) M. K. Tham, R. D. Walker Jr, J. H. Modell, *J. Chem. Eng. Data* **1973**, *18*, 385.
- [14] A. Dibenedetto, M. Aresta, C. Fragale, M. Narracci, *Green Chem* **2002**, *4*, 439.
- [15] A. Dibenedetto, C. Pastore, C. Fragale, M. Aresta, *ChemSusChem* **2008**, *1*, 742.
- [16] V. Blasucci, C. Dilek, H. Huttenhower, E. John, V. Llopis-Mestre, P. Pollet, C. A. Eckert, C. L. Liotta, *Chem. Commun.* **2009**, *1*, 116.
- [17] G. P. Knowles, S. W. Delaney, A. L. Chaffee, *Ind. Eng. Chem. Res.* **2006**, *45*, 2626.
- [18] J. C. Hicks, J. H. Drese, D. J. Fauth, M. L. Gray, G. Qi, C. W. Jones, *J. Am. Chem. Soc.* **2008**, *130*, 2902.
- [19] W. A. Starke, M. J. Ziemelis, EP674936 to Dow Corning Corp., Nov. 11, **1998**.
- [20] a) J.-Y. Park, S. J. Yoon, H. Lee, *Environ. Sci. Technol.* **2003**, *37*, 1670; b) R. J. Hook, *Ind. Eng. Chem. Res.* **1997**, *36*, 1779. This 2:1 stoichiometry may be circumvented if a counterion is already present in the system to replace the ammonium ion needed for charge neutralization. See: c) B. E. Gurkan, J. C. de La Fuente, E. M. Mindrup, L. E. Ficke, B. F. Goodrich, E. A. Price, W. F. Schnieder, J. F. Brennecke, *J. Am. Chem. Soc.* **2010**, *132*, 2116.
- [21] Some preliminary ^{13}C NMR evidence indicates a bicarbonate resonance at ca. 160 ppm vs carbamate resonance at ca. 164.5 ppm. See: K.-y. Tomizaki, M. Kanakubo, H. Nanjo, S. Shimizu, M. Onoda, Y. Fujioka, *Ind. Eng. Chem. Res.* **2010**, *49*, 1222.
- [22] A recent report indicates that irreversible urea formation in the presence of dry CO_2 may also limit the recycling ability of an amine solvent: A. Sayari, Y. Belmabkhout, *J. Am. Chem. Soc.* **2010**, *132*, 6312.
- [23] A. L. Kohl, R. B. Nielsen, *Gas Purification, 5th Edition*, Elsevier **1997**, p 65.
- [24] Measured at 40 °C. I. Kim, H. F. Svendsen, *Ind. Eng. Chem. Res.* **2007**, *46*, 5803.
- [25] M. J. Frisch, G. W. Trucks, H. B. Schlegel, G. E. Scuseria, M. A. Robb, J. R. Cheeseman et al., *Gaussian 03 revision C.02 ed.*; Gaussian, Inc: Wallingford, CT **2004**.

Received: March 10, 2010

Revised: May 14, 2010

Appendix 2 Chemical CO₂ capture by liquid absorbents

G.L. Soloveichik

1. CO₂ capture technologies outlook

There is a growing understanding and concern that global warming is mostly caused by carbon dioxide (CO₂) emitted as the result of combustion of fossil fuels. One of the major sources of anthropogenic CO₂ is coal based power generation (about 1/3 of total CO₂ emission). The Department of Energy's Carbon Sequestration Program is established to create new affordable carbon capture and sequestration (CCS) technologies.¹ CO₂ removal processes are not new and are widely used for natural gas sweetening and in food industry. They include absorption processes, for example the UOP Benfield™ process (hot potassium carbonate solutions) and UOP Amine Guard-FS™ and Dow UCARSOL™ processes (amine based solvents); cryogenic processes; adsorption processes, such as pressure swing adsorption (PSA), thermal swing adsorption (TSA); and membrane processes (UOP, Air Products). However, these processes have been developed for the gas streams with high partial pressure of carbon dioxide (pressurized gas or high concentration of CO₂ at ambient pressure) and not well suited for exhaust from combustion engines with low CO₂ partial pressure and high oxygen content.

Three different types of technologies for CO₂ capture for power generation plants are being developed: pre-combustion, post-combustion, and oxy-combustion (oxyfuel combustion).² Recently, a novel chemical looping process where metal oxides (M = Mn, Fe, Ni, Cu) are used as an oxygen carrier has been proposed.³ Currently more than 30 carbon capture and storage pilot scale demonstration projects are being built and tested across the globe, with majority in USA and Norway.

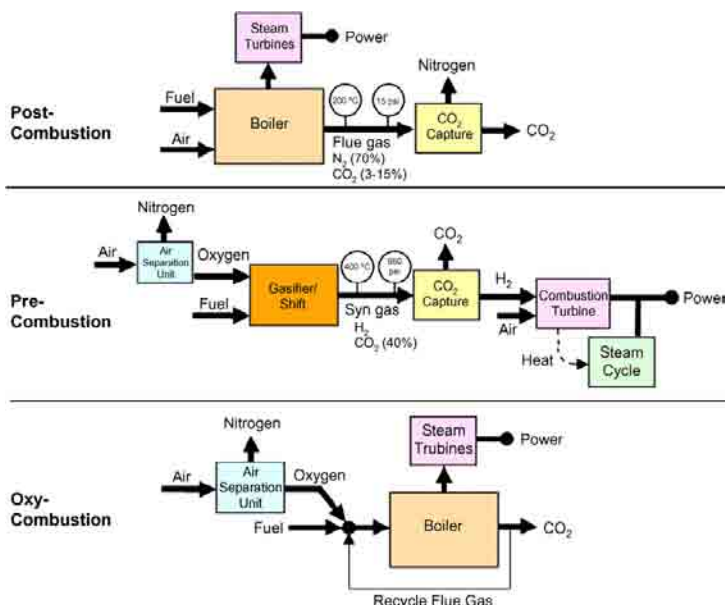


Fig. 1 Block diagrams illustrating post-combustion, pre-combustion, and oxy-combustion systems.¹

Pre-combustion CO₂ removal targets integrated gasification combine cycle (IGCC) power plants where coal is partially oxidized with oxygen (gasified) to generate syngas (H₂ + CO) followed by the water gas shift reaction. The resulting stream is the high-pressure mixture of H₂ and CO₂ that allows the use of physisorption based processes using physical solvents like dimethyl ethers of polyethylene glycol (Selexol™, UOP), refrigerated methanol (Ifpecsol™, Institute Français du Pétrole and Rectisol™, Lurgi AG), and propylene carbonate (Fluor).

In oxy-combustion process coal is burned in almost pure oxygen producing mostly carbon dioxide and water. After water condensation, the flue gas consists of CO₂ diluted with O₂, N₂, SO₂, NO_x that could be inexpensively removed using existing technologies. The major part of the oxy-combustion cost structure is the cost of oxygen separation. Post-combustion processes target the flue gas produced by combustion of fossil fuels in air. In contrast to pre-combustion and oxy-combustion processes, the flue gas has low concentration of CO₂ at ambient pressure (partial pressure of CO₂ is less than 0.15 bar). As the result, physisorption is not as effective, and processes based on chemisorption are required to effectively remove CO₂. It should be noted that retrofitting of existing pulverized coal (PC) power plant that generate 2/3 of the power sector emissions is possible only with the post-combustion technology.

Heat and electrical energy as well as capital cost are the most important factors in the cost structure of liquid absorbent-based CO₂ capture processes.^{4,5} New chemical absorbents with lower energy requirements and higher loading may reduce both steam consumption (operational cost) and absorbent circulation rate (capital cost).⁶ Therefore, search for new absorbents is very important for the development of cost effective industrial processes.

1.1. Membrane separation

Polymeric and porous inorganic membranes were evaluated for CO₂ removal from the flue gas. Polyimide, polyamides and polysulfones demonstrated the highest selectivity in separation of the CO₂/N₂ mixture.⁷ Composite membranes containing amino groups in polymer or in a carrier agent,⁸ for example, made of a thin cationic poly(N,N-dimethylaminoethyl methacrylate) layer and a microporous polysulfone substrate⁹ or polyimide/polyamide blends¹⁰ showed improved permselectivity for CO₂. Inorganic membranes are made of carbon (pyrolyzed thermosetting polymers), mesoporous alumina and silica, and zeolites.¹¹ The most promising is the use of membrane in a hollow fiber membrane contactor where an amine solution is placed outside the membrane tubes.¹²

A systematic parametric study showed that energetic costs of membrane separation may be 5-10 times less than that of amine absorption.¹³ However, the recovery ratio and permeate composition of current materials are not sufficient. Membrane CO₂/N₂ selectivity should be above 100 but selectivity of available membranes does not exceed 50 and can be used only for gas streams containing more than 20% CO₂.¹³

1.2. Adsorption by solid adsorbents

Many solids can capture CO₂ either chemically or by physical adsorption. Sodium¹ or potassium¹⁴ carbonates react with carbon dioxide in the presence of water forming

bicarbonate MHCO_3 , and can be regenerated by a temperature swing. CaO requires higher regeneration temperature and, therefore, is less preferable.¹⁴

Numerous porous materials have been tested as CO_2 sorbents. Zeolites and carbon based molecular sieves selectively adsorb components of the flue gas based on molecular size and show capacity up to 250 mg/g (for example, Zeolite 13X) but only at elevated pressure and are too expensive for large volume processes. Porous alumina and silica have low capacity that can be increased by treatment with carbonates or oxides of Li, Na, K up to 15 mg/g.¹⁵ Sorbents prepared by impregnation with potassium carbonate on activated carbon, TiO_2 , Al_2O_3 , MgO, SiO_2 supports showed excellent CO_2 capture capacity. Depending on the support the reaction products are different - KHCO_3 for activated carbon and titania and $\text{KAl}(\text{CO}_3)_2(\text{OH})_2$, $\text{K}_2\text{Mg}(\text{CO}_3)_2$ for alumina and magnesia, which reflects in different sorbent regeneration temperatures: 130 – 135 °C vs. 350 – 400 °C respectively.¹⁶

Metal–organic frameworks (MOFs) with very high surface area (3000 – 5000 m^2/g) show high CO_2 storage capacity at room temperature but at elevated pressure. The best materials demonstrate about 800 mg/g (MOF-177 at 43 bar¹⁷, MOF-5 at 40 bar¹⁸). New zeolitic imidazolate frameworks show a significant CO_2 capacity even at ambient pressure.¹⁹ Modification of porous materials with amines substantially increases their capacity, especially at lower pressures, and will be discussed later.

It is generally accepted that handling of solids is more difficult than liquids, and such problems as pressure drop, heat transfer within solids and attrition prevent commercialization of solid sorbents for CO_2 capture in a large scale.

1.3. Absorption by liquid absorbents

Processes based on liquid absorbents are the most suited for post-combustion CO_2 capture and close to commercialization (some of them are currently being piloted). Three major methods use amines, aqueous ammonia and carbonates.

1.3.1. MEA process

Ability of amino alcohols to absorb CO_2 from gas mixtures is known for more than 75 years.²⁰ Monoethanolamine (MEA) dissolved in water is the state-of-the-art absorbent for CO_2 capture from flue gas.^{4,6} Kerr-McGee/ABB Lummus Global process uses 15 – 20 % aqueous MEA solution to avoid problems with corrosion and MEA oxidation and has demonstrated capacity up to 720 ton CO_2/day .²¹ Another process using more concentrated solutions (30 % MEA) was developed by Dow Chemical Company and later acquired by Fluor Daniel. Modified MEA process with new absorbent formulation, which includes an oxidation and corrosion inhibitor, (Econamine FG PlusSM) is now commercially offered by Fluor Daniel.⁶ This process removes 85 to 90 % of CO_2 from flue gas generated by fossil fuel-fired boilers and steam reformers and has been in operation for more than 15 years recovering up to 320 ton CO_2/day in a single train. Compared to the ABB Lummus process, the Fluor Daniel process requires less steam and solvent flow rate but MEA

consumption is higher.⁴ Deoxygenation of the solvent by depressurization or stripping of dissolved oxygen with N₂ or CO₂ was patented.²²

Addition of organic solvents as diluents to aqueous MEA allows substantial decreasing of the required process heat up to 50 % for the most efficient tetrahydrofuryl alcohol.²³ CO₂ solubility in such mixtures was lower than in aqueous MEA, but absorptivities remained about equal, for example using N-methylpyrrolidone because of better regeneration.²⁴ Mixtures of MEA with N-methylpyrrolidone, tetrahydrofurfuryl alcohol, benzyl alcohol, and ethylene glycol for CO₂ removing from synthesis gas have been tested in a pilot plant.²⁵

Different di- and polyamines were used to accelerate the absorption rate. Examples are alkylendiamines,²⁶ diethylenetriamine,²⁷ piperazine and piperidine.²⁸ Piperazine accelerates CO₂ absorption by aqueous MEA. Addition of 24 mol% piperazine (of the total amine) decreases CO₂ equilibrium pressure by 50% and enhances the absorption rate by 50 -100 %.²⁹ Imidazole was also used as an additive to MEA.³⁰ Addition of a physical solvent for absorption of acid gases has been proposed for this system.³¹

1.3.2. Hindered amine process

Kansai Electric Power Co. (KEPCO) and Mitsubishi Heavy Industries, Ltd. (MHI) are working on development of new technology for CO₂ recovery from power plant boiler flue gas and gas turbine exhaust gas using proprietary hindered amines.³² Several amines for this purpose have been patented, for example, 2-amino-2-methyl-1-propanol (AMP), 2-(ethylamino)ethanol, 3-amino-3-methyl-2-pentanol, 2,3-dimethyl-3-amino-1-butanol, 2-amino-2-ethyl-1-butanol, 2-amino-2-methyl-3-pentanol, 2-amino-2-methyl-1-butanol, 3-amino-3-methyl-1-butanol, 3-amino-3-methyl-2-butanol, 2-amino-2,3-dimethyl-3-butanol, 2-amino-2,3-dimethyl-1-butanol, and 2-amino-2-methyl-1-pentanol.³³⁻³⁵ Among these, AMP is preferred choice. Hindered amines show higher effective CO₂ loading than non-hindered ones 0.57 – 0.60 mol CO₂/mole amine at 9.8 kPa and absorption temperature 40 °C and desorption temperature 120 °C vs. 0.40 mole/mole for MEA and 0.48 mole/mole for DEA. Aqueous solutions of AMP have a much higher absorption capacity compared to solutions of DEA and diisopropanolamine (DIPA).¹² It was claimed that combination of three different amines has a synergistic effect on CO₂ absorption and desorption.³⁶ Using mixtures of methyldiethanolamine (MDEA) with MEA substantially decreases the process heat load compared to a single MEA absorbent but chemical stability is an issue.³⁷ However, slow reaction rate at low CO₂ partial pressures makes absorption columns prohibitively expensive for the post combustion capture.²²

Piperazine and alkylpiperazines accelerate CO₂ absorption by aqueous hindered amines.³⁸ (2,2-(ethylenedioxy)bis(ethylamine)) NH₂(CH₂CH₂O)_nCH₂CH₂NH₂ (n is 1-12) used as a promoter in hindered amine process accelerates the CO₂ absorption across vapor-liquid interface.³⁹ The mixtures of AMP with piperazine are preferred solvents for the KEPCO-MHI process.⁴⁰

Diaminotoluenes in combination with primary amino alcohols was claimed as CO₂ absorbents.⁴¹ Hydroxyl substituted diamines in water have been patented as CO₂

absorbents.^{42,43} Combination of N,N'-di-(2-hydroxyethyl)piperazine (DIHEP) and N-hydroxyethylpiperazine (HEP) is used in the process developing by Cansolv Technologies, Inc.⁴⁴

To prevent oxidative degradation of hindered amines, the addition of inhibitors like cupric carbonate was used.³²

1.3.3. Chilled ammonia process

Aqueous ammonia reacts with CO₂ according Eqs. 1 - 3 to produce ammonia bicarbonate. This process has less energy requirements than the amine based processes, potentially low cost and no degradation via oxidation and hydrolysis.⁴⁵ However, high ammonia volatility and associated safety hazard makes its commercial use challenging. Addition of alkanolamines reduces the ammonia loss, probably, due to the interactions between ammonia and additives or absorbents and CO₂ via hydrogen bonding.⁴⁶ Another way to mitigate these problems is the reducing of process temperature. Alstom is developing a chilled ammonia process, which uses the same chemistry but at temperatures only slightly above 0 °C.

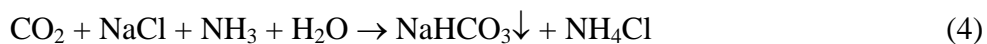


To minimize these problems, so-called chilled ammonia process⁴⁷ is being developed by Alstom in collaboration with the Electric Power Research Institute (EPRI). The flue gas is cooled before absorption to 0 – 10 °C. The liquid phase in the process is not homogeneous and contains slurry of solid ammonia bicarbonate. Alstom designed and constructed the 1.7 MW system that captures CO₂ from a portion of coal-fired boiler flue gas that will operate at coal-fired We Energies' Pleasant Prairie Power Plant.⁴⁸ The technology is targeted for commercialization in 2011. Absorption kinetics is comparable to kinetics of reaction with MEA and DEA and much faster than that with MDEA.⁴⁹ The process modeling predicts a significant reduction of the energy consumption in the desorber compared to that of the MEA process.⁵⁰ However, the equilibrium calculation of the gas phase in the absorber shows a high mole fraction of ammonia thus requiring an additional cleaning system. Chilling the flue gas and absorber requires a lot of energy that reduces the total plant efficiency, and more washing sections to remove ammonia demands higher capital costs. Along with the necessity of mitigating of ammonia slip and problems with slurry transportation and equipment fouling, it makes this process challenging.

Powerspan is working on post-combustion, ammonia-based carbon capture process (ECO₂) licensed from NETL that does not require chilling.^{45,51} The commercialization is anticipated in 2012. Ammonia based processes may be particularly advantageous for plants equipped with ammonia SCR deNO_x emissions control.

1.3.4. Dual alkali process

The Solvay process for the manufacture of sodium carbonate uses reaction between ammonia and carbon dioxide in a saturated sodium chloride solution below 15°C to form a precipitate of sodium bicarbonate. However, the Solvay process is not practical for the CO₂ sequestration due to consumption of limestone used for ammonia regeneration, production of CO₂ (1 mole per 2 mole captured), and extensive energy requirement during calcination. Modified Solvay process (dual alkali process) was suggested, where ammonia was replaced with alkanolamines and regeneration of ammonia (but not alkanolamine yet) was done using reaction of NH₄Cl with an activated carbon.⁵²



1.3.5. Carbonate process

CO₂ absorption by carbonate solutions is promoted by diethanolamine (DEA), piperazines and aminoacids like 2,3-diaminopropionic acid or histidine.⁵³⁻⁵⁵ It was claimed that N-sec-butyl glycine or pipercolinic acid are the best promoters.⁵⁶ Vanadium salts are usually added as a corrosion inhibitor.⁵⁷ The hindered amine solutions increase the mass-transfer coefficient for CO₂ absorption by 2.5 – 3 times and have 30% larger capacity than the DEA promoter.⁵⁸ In addition to promoters, a catalyst for CO₂ absorption, for example, carbonic anhydrase can be added.⁵⁹ It was shown that promotion mechanism for this reaction is similar for inorganic and organic promoters.⁶⁰ The reaction rate is controlled by the rate of proton abstraction from the zwitterion intermediate for high carbonate conversions.⁵⁴ The University of Texas at Austin is developing a process for CO₂ capture that uses aqueous K₂CO₃ solution promoted by piperazine.⁶¹ Compared with the MEA process, the carbonate process has lower energy requirements (by 15 – 20 %) and higher CO₂ capacity (40 % vs. 30 %).⁶² ASPEN modeling showed that this process is better suited for pressurized CO₂ streams while the MEA process is better for low-pressure streams.⁶³

2. CO₂-philic solvents (physical absorption)

As mentioned, physical sorption is used for CO₂ capture from high-pressure streams but not suitable for post-combustion processes. However, combination of physi- and chemisorption may be beneficial in development of new absorbents with low energetic requirements. CO₂ is a weak Lewis acid and could exhibit specific interactions with Lewis bases. However, in contrast to SO₂, solubility of CO₂ in different solvents does not correlate with solvent's basicity expressed as the Gutmann donor number.⁶⁴ Semiempirical analysis of CO₂ solubility in organic solvents showed that two parameters are the most important: the Hildebrand solubility parameter that should be minimized and calculated energy of CO₂ – solvent interaction that should be maximized.⁶⁵ This interaction is caused by sharing of an electronic doublet of basic atoms (O or N) with the C atom of CO₂ (FTIR spectroscopy)⁶⁶ or van der Waals interactions between fluorine atoms and carbon dioxide (¹⁹F NMR)⁶⁷. Equilibrium constants for the interactions of CO₂ with Lewis bases increase in the row triethylamine < pyridine < tributyl phosphate but are by several orders of value smaller than those for the interactions SO₂ – Lewis base.⁶⁶ So, ethers, esters, ketones, tertiary amines, and alkyl phosphates are the most promising solvents for CO₂ physisorption.⁶⁵ Solubility in mass units is maximal for ethers and ketones but in molar units is the highest for alkyl phosphates. Fluorination of solvents

decreases the Hildebrand solubility parameter and therefore might slightly increase the molar solubility of CO₂ but would decrease the mass solubility.

2.1. Fluorinated materials

Fluorinated fluid phases have been attracting attention as gas carriers for biomedical applications in vivo due to high O₂ and even higher CO₂ solubility compared to non-fluorinated analogs. High solubility of fluorocarbons in scCO₂ was demonstrated in 1992 and used for preparation fluorinated polymers.⁶⁸ Since then, fluorinated “ponytails” was being added to many materials, surfactants and catalysts to make them soluble in scCO₂. Conformational analysis showed that spontaneous cavities are larger and more easily formed in the fluorocarbon than in analogous hydrocarbon, but this does not explain the high solubility of carbon dioxide compared to that of other gases.⁶⁹ Unfortunately, fluoro-containing solvents are prohibitively expensive for use in the large scale post-combustion CO₂ capturing.

2.2. Oxygen containing materials

Linear polyethers demonstrate higher CO₂ solubility than branched ones and are comparable to commercial Selexol solvent (a mixture of dimethyl ether of polyethylene glycol homologues).⁷⁰ The enthalpy of CO₂ absorption at infinite dilution for hyper-branched polyethers is about 2–3 kJ/mol less than that for linear polyethers. The replacement of hydroxyl end-capping groups for methyl groups increases the CO₂ solubility by 15%.⁷⁰ Dialkyl carbonate and alkoxyalkylcarbonates have been claimed as physical solvents for CO₂ removal.⁷¹ It was found that poly(ether-carbonate) copolymers have very high solubility in scCO₂.^{72,73} Non-reactive towards carbon dioxide solvents prepared by alkylation of reactive amines like N,N-dialkoxyalkylaminoalkanols and N,N-dialkylaminoalkyl ethers⁷¹ and dimethylaminopropionitrile⁷⁴ and have been also claimed.

Some oxygen containing polymers, for example polymethylmetacrylate and polyvinylacetate, which demonstrate splitting of the bending CO₂ vibration band in films saturated with carbon dioxide, are soluble in scCO₂.⁷⁵ An acetate group is slightly more CO₂-philic than an acrylate group.⁷⁶ Oligomers of vinyl acetate demonstrate CO₂-philic properties similar to fluoropolymers.⁷⁷

Derivatization of glucose with substituted phenyl groups increases its solubility in scCO₂ especially for electron-withdrawing substituents.⁷⁸

2.3. Siloxanes

In the search of materials soluble in supercritical CO₂, which is important in its use as a process solvent, it was found that siloxanes, namely dimethylsiloxane, exhibit CO₂-philic properties. First, the use of silicon oils as absorbents was suggested in 1972.⁷⁹ The use of diethyl-, dimethyl- and the most efficient trifluoropropylmethyl polysiloxane, has been patented.⁸⁰ The gas solubility is decreased by either backbone-chain or side-chain substitutions of functional groups in (Me₂SiO)_x which increase the stiffness of the polymer chains and decrease the specific or fractional free volume of the polymers.⁸¹ Addition of acetate terminal side chains to siloxane causes the dramatic reduction in the phase separation pressure while addition of similar length alkyl side chains raises the cloud point pressures.⁸² Carbon dioxide solubility was enhanced through silicone functionalization with diphosphonate ligands.⁸³ The solubility of silicones modified with side chain esters and phosphine groups in scCO₂ is generally larger than that of

polyethers of the same chain length, and solubility of hydroxyl-ended silicones is better than that of methyl-ended.⁸⁴

2.4. Ionic liquids

Ionic liquids (ILs) are very attractive solvents due to high thermal stability and lack of measurable pressure at elevated temperatures (up to 300 °C). Their stability towards water depends on the anion; for example, salts with PF₆⁻ anion are quite stable in the presence of water. It was found that CO₂ is highly soluble in 1-butyl-3-methylimidazolium hexafluorophosphate ([bmim][PF₆]) at high pressure (mole fraction 0.6 at 80 bar).⁸⁵ Solubility of CO₂ in ILs is much higher than solubilities of most other gases (O₂, N₂, CO, hydrocarbons) except SO₂.⁸⁶ Henry's constants for different ILs are in the range 20 - 60 bar compared with 300 for CH₄, 1700 for O₂, and 3400 for N₂ but 1.5 for SO₂.⁸⁶ Increasing the length of the hydrocarbon chain in 3-position of imidazolium ring increases CO₂ solubility while the replacement of PF₆⁻ anion for BF₄⁻ and NO₃⁻ anions decreases it.⁸⁷ ILs with bis(trifluoromethylsulfonyl)imide or Tf₂N⁻ anion show even the highest CO₂ solubility.^{88,89} CO₂ solubility in bmim-based ILs is determined by the extended Henry's law up to 100 bar pressure and for different anions increases in the row MeSO₄⁻ < PF₆⁻ < [N(CF₃SO₂)₂]⁻ (bis(trifluoromethylsulfonyl)imide or Tf₂N⁻).^{90,91} The highest solubility was observed for ILs with tris(trifluoromethanesulfonyl) C(SO₂CF₃)₃⁻ (methide) anion.⁹² At low CO₂ partial pressures (< 1 bar) the mole fraction of CO₂ is much lower (< 0.03 at 1 bar) but relative CO₂ solubility for different ILs is the same. The presence of water practically does not effect CO₂ solubility when relative humidity is less than 40 %.⁸⁹ Replacement of alkyl groups in the cation for phenyl decreases the solubility while fluorination of alkyl groups substantially (by a factor of 8) increases it.⁸⁹ Additional fluorination of IL's anion by partial replacement of fluorine atoms in the PF₆⁻ anion for fluoroalkyl groups also increases CO₂ solubility.⁹³ The salt [bmim]OAc with the acetate anion shows highly unusual phase behavior with CO₂ demonstrating very low vapor pressure at CO₂ concentrations less than 20 mol %.⁹⁴ Polymeric ionic liquids prepared by radical polymerization of methylacrylate- and vinylbenzyltrialkylammonium salts demonstrated much higher CO₂ sorption than bmim-based and monomeric tetraalkylammonium ILs. At 1 bar CO₂ pressure, the equilibrium capacity was 10.2 and 8.0 mol % of CO₂ for [poly(vinylbenzyltrimethylammonium)] and [poly(methylacrylatetrimethylammonium)] salts with BF₄⁻ anion respectively vs. 1 – 2 % for monomeric ILs.⁹⁵ Interestingly, in the case of polymeric ILs the influence of anion is different from monomeric ILs: salts with Tf₂N⁻ anion show less capacity than with (2.85 mol %) than salts with PF₆⁻ (10.66 mol %) and BF₄⁻ (10.22 mol %) anions.⁹⁵ Comparison of poly(vinylbenzyltrimethylammonium) and poly(1-vinylbenzyl-3-methylimidazolium) salts with BF₄⁻ anion shows much higher CO₂ absorption for tetraalkylammonium salts that points to the effect of cation on CO₂ sorption.⁹⁶ Measured enthalpies of CO₂ absorption are in the range -9 – -14 kJ/mol following an inverse relationship with solubility, and the entropies are in the range -29 – -44 J/K mol.⁹⁷ No specific interactions between CO₂ and IL cations were found but some correlation between CO₂ solubility and liquid molar volume suggests a space-filling mechanism.⁸⁷

Replacement of alkyl chain in imidazolium cation for oligomeric ethylene glycols practically does not change CO₂ solubility but substantially decreases solubility of nitrogen and methane, thus increasing CO₂/N₂ and CO₂/CH₄ selectivities.⁹⁸

Liquid salt tetramethylammonium acetate tetrahydrate demonstrated unusual sorption behavior: it absorbs CO₂ in liquid form (0.15 mol/mol) at elevated temperature and momentarily releases it upon cooling at the point of solidification.⁹⁹

3. Chemical Reactions of CO₂

CO₂ is a very stable molecule and only few reactions with its participation have a negative value of the Gibbs free energy ΔG°. In many such reactions hydrogen or hydrocarbons are participating, which reacts into water and thus make overall thermodynamics favorable. Thermodynamics is also more preferable at elevated temperature and CO₂ pressure.¹⁰⁰ Examples of these reactions are reduction with hydrogen to methanol, formation of carboxylic acids with alkenes, organic carbonates with epoxides, and alkyl formates with alcohols and hydrogen. Unfortunately these reactions cannot be used for reversible post-combustion CO₂ capture due to high stability of reaction products or the presence of coreactants.

3.1. Carbamate formation

Primary and secondary amines react with CO₂ yielding carbamates.



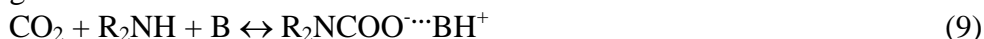
Ion separation in products of reaction (?) was observed in non-aqueous polar solvents while in non-polar solvents ion pairs are predominantly present.¹⁰¹

Tertiary amines react with CO₂ according reactions (7) and (8).



Based on measurements of the rates of homogeneous reaction of mono-, di- and tri-ethanolamine with CO₂, it was proposed that a zwitterion is the intermediate in the formation of carbamate and that the reaction of DEA (but not of MEA) is catalyzed by bases.¹⁰² Kinetics of CO₂ reactions with alkanol amines was recently reviewed.¹⁰³ The zwitterion mechanism describes the reaction between CO₂ and primary/secondary amines over a wide range of conditions and amine concentrations and for blends of amines and sterically hindered amines.^{12,104} The specific rate of CO₂ absorption in solutions of MEA and DEA in ethanol and ethylenglycol showed that reactions were first order with respect to CO₂ and second order with respect to amine except cyclohexylamine in ethylenglycol, which has the first order with respect to amine.¹⁰⁵ There is the Brønsted relationship between the zwitterion-formation rate constant and the acid dissociation constant of the alkanolamine (but not for cyclic amines).¹⁰⁶ The value of k₂ of this reaction can be estimated with the following equation: $\ln k_2 = \text{pK}_a + 17.60 - 7188/T$.¹⁰⁴ For different amines, two classes was found: when the zwitterion formation is rate determining a significant temperature influence is observed whereas only a slight temperature dependence is observed when the zwitterion deprotonation is rate determining.¹⁰⁶

Another, termolecular mechanism assumes that an amine, CO₂ and a base react simultaneously in one step via an amine – base intermediate (Eq. 9) was proposed on the basis of kinetic measurements¹⁰⁷ and *ab initio* calculations.¹⁰⁸ Kinetics of one hindered amine – 2-((2-aminoethyl)amino)ethanol – is described by this mechanism but only at high amine concentrations.¹⁰⁹



Measurement of the difference in CO₂ solubility in 30 wt. % aqueous solutions for different amine compounds as function of amine's pK_a showed a volcano-shaped curve.¹¹⁰ The maximum value depends on CO₂ pressure and equals 7.0, 7.3 and 8.7 for 0.1, 1 and 4 MPa of CO₂ partial pressure respectively.¹¹⁰ It was found that CO₂ molar loading for alkanolamines approximately linearly increases with reducing of HOMO energy.¹¹¹ However, sterically hindered amines demonstrate higher loading due to formation of bicarbonates instead carbamates.¹¹²

Kinetics of CO₂ reaction with cyclic diamines (piperazine, piperidine) is much faster than that for other primary and secondary amines.¹¹³ The reaction is of the first order with respect to both reactants and at high loading results mostly in protonated piperazine carbamate with some presence of dicarbamate.¹¹³

The reaction between CO₂ and tertiary amines occurs via base catalyzed CO₂ hydration.¹¹⁴ The formation of monoalkylcarbonate is not responsible for the reactivity measured in aqueous tertiary amine solutions at low pH. In non-aqueous solvents no reaction occurs. The value of the rate constant k₂ can be estimated with the following equation: $\ln k_2 = 1.3pK_a + 11.48 - 8270/T$.¹⁰⁴ Another equation for prediction of reactivity of tertiary amines with two amino groups is based on comparison of enthalpy of the protonation reaction, which can be estimated using the following equation:

$$\Delta H \cong R^*(pK_1 - pK_2)/1/T_1 - 1/T_2 * \ln(10).$$

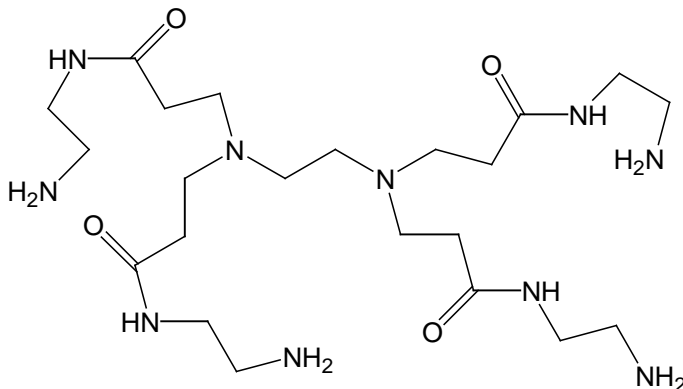
Tertiary amines with higher ΔH (and higher pK₁ in the range 9 – 11) are more suitable for CO₂ capture because they absorb at lower pressures and can be regenerated with a relatively low energy input.

Enthalpy of CO₂ absorption for aqueous MDEA solutions slightly increases with MDEA concentration and temperature (from 49 kJ/mol CO₂ at 40 °C to 58 kJ/mol CO₂ at 120 °C) but independent of the pressure.¹¹⁵

4. Aqueous absorbents for CO₂ capture

Different amino alcohols, for example, methyldiethanolamine (MDEA) and β,β' -hydroxyaminoethyl ether (diglycolamine, DGA) in the form of aqueous solutions have been tried as CO₂ absorbents. Introduction of C₁ – C₄ alkyl groups at the nitrogen atom of MEA generally decreases the absorption rate and capacity.¹¹⁶ However, the replacement of alkyl groups for amino- or hydroxyalkyl groups substantially improves performance. (2-Aminoethyl)ethanolamine (AEEA) was suggested as a potential candidate for the post combustion capturing based on its high capacity and fast absorption kinetics.^{109,117} The heat of absorption for AEEA is similar to that for MEA at the same conditions (for example, about 77 vs. 84 kJ/mol CO₂ at 40 °C for 30 wt. % solutions).¹¹⁸ The reaction rate for AEEA is higher than that for MEA.¹⁰⁹ Aqueous solutions of another hindered amine, 2-amino-2-hydroxymethyl-1,3-propanediol (AHPD), demonstrate higher CO₂ solubility than MEA solutions due to predominant formation of bicarbonate as opposite to carbamate.¹¹⁹ However, the CO₂ solubility for this amine sharply decreases with the CO₂ partial pressure and below 4 kPa at 25 °C becomes lower than that for MEA. The crossover point is observed at higher CO₂ partial pressures when temperature is higher.¹¹⁹

Potassium salts of alpha-amino acids (10 – 30 wt. % aqueous solution) have been proposed as CO₂ absorbents. Serine and alpha-aminobutyric acid potassium salts in combination with piperazine (2.5 wt %) showed better results than MEA solution with the same concentration.¹²⁰



Non-volatile polyamidoamine generation 0 dendrimer (Fig. ?) with four primary, four secondary and two tertiary amino groups was used as 22 vol. % aqueous solution to absorb CO₂ from 5% gas mixture in a hollow fiber membrane contactor.¹²¹ The dendrimer didn't show any capacity decrease in 55 days.¹²¹ Second-generation polyamidoamino dendrimer can be dissolved in water up to 61 wt. % and has enthalpy of CO₂ absorption at infinite dilution (-23.9 kJ/mol), which is intermediate between physical solvents polyethers (-10 – -14 kJ/mol) and MEA (-85.0 kJ/mol for 30 % wt. solution).⁷⁰

Concentrated (85 %) aqueous solution of bis(methyldiethyleneglycol ether)amine is about two times more efficient in removing CO₂ from 35 % gas stream compared to polyethylene glycol dimethyl ether.¹²²

Because the first step of reaction with molecular oxygen is presumably the abstraction of a hydrogen atom by the carbon atom in the α -position to the amino group, resistance of aminoalcohols in which the α -carbon atoms not have hydrogen atoms to oxidative decomposition amines is increased.¹²³

Sterical hindrance in amines with hydroxyl groups destabilizes the carbamate anion formed at the first stage of interaction with CO₂ (CO₂: amine ratio = 1:2) and shifts reaction towards formation of bicarbonate anions (CO₂: amine ratio = 1:1).¹²⁴ However, the CO₂ loading by weight for hindered amines is lower than that for MEA, especially at lower partial CO₂ pressures.¹²⁵ The molar CO₂ loading is highest for N-alkyl substituted amino-2-methyl-1-propanols.¹¹¹ Carboxylate salts amines with α -substituents behave like alcohol amines but solubility of their bicarbonate salts is low leading to formation of slurries. Only MeHNCHMeCOOK demonstrate CO₂ absorption properties comparable with hindered amines.¹²⁴ Replacement methyl groups in 2-amino-2-methyl-1,3-propanediol (AMPD) for hydroxomethyl groups in 2-amino-2-hydroxymethyl-1,3-propanediol (AHPD) substantially increased the CO₂ loading due to higher bicarbonate:carbamate ratio but the loading strongly depends on CO₂ partial pressure.¹¹⁹

Aqueous solutions of tertiary amines (2 M) absorb CO₂ in the presence of catalytic (5 %) amounts of secondary amines, for example N-2-hydroxyethylpiperazine or piperazine-substituted sulfonic acids and an oxygen scavenger.¹²⁶ Tertiary amines preferably have pK_a from 6.5 to 9, and the best amines are N,N'-di-(2-hydroxyethyl)piperazine and triethanolamine, which in combination with N-2-hydroxyethylpiperazine are more effective than the mixture of MDEA with piperazine and can also remove SO₂.⁴⁴ Screening of 25 different tertiary amines as 30 % aqueous solutions showed that the best capacity was observed for molecules with the Me₂NC₂H₄O- fragment (alcohol or symmetric ether) while the highest absorption rate was detected for rather hindered diamine with methylene bridge Et₂NCH₂NEt₂.¹²⁷ Bulky substituents (ⁱPr, ^tBu) and the increase of the number of hydroxyl groups decrease both capacity and absorption rate. Reaction heat is decreased for molecules with ether functionality.¹²⁷ Primary and secondary hydroxyamines amines like MEA¹²⁸ and DEA¹²⁹ also catalyze the reaction between tertiary amines and CO₂. It is assumed that a secondary amine transfers CO₂ to the tertiary amine.^{130,131} For the system AMP – PZ reacting with CO₂, a hybrid reaction rate model including a second-order reaction for the reaction of CO₂ with PZ and a zwitterion mechanism for the reaction of CO₂ with AMP has been proposed.¹³²

Compared with commonly used β-amino alcohols, aqueous α-amino amides have been found to exhibit comparable or better reversible absorption capacity of carbon dioxide.¹³³ It is suggested that in the case of amino acids the zwitterion is stabilized by hydrogen bonding with the second amino acid molecule via carbamate or carboxylic groups.¹³⁴

An amino acid or its salt, for example, potassium taurate dissolved in water absorb CO₂ and H₂S from gas streams forming a precipitate. Heating of the resulting slurry releases CO₂ and regenerates the absorbent.¹³⁵

Different di- and polyamines dissolved on water are effective in absorption. An increase in the linker length between the amine and different functional groups in the absorbent structure results in a increase of the cycling absorption capacity (30 °C, 0.1 atm absorption; 90 °C, 1 atm desorption) but in a decrease of the absorption rate.¹³⁶ The capacity grows with the number of carbon atoms in the linker but levels at n = 6. Side chains decrease the CO₂ capacity. N,N'-dimethyl-1,6-hexamethylenediamine having primary and tertiary amino groups and 1,7-heptamethylenediamine showed the best cycling absorption capacity (0.8 – 0.85 moles CO₂/moles amine for 0.5 M solution) comparable with the capacity of piperazine (0.8 moles CO₂/moles amine).¹³⁷ Interestingly, the CO₂ absorption for these diamines exceeds the anticipated CO₂:N ratio (0.5) reaching 1.3 – 1.5 moles CO₂/moles amine. The increase of the amine concentration in 5 times to 2.5 M decreases the of the cycling absorption capacity almost twice, so the CO₂ removal per cycle still increases.^{137,138} Linear polyamines with pK_a <10.5 have been patented.⁴³ Tetraethylenepentamine (TEPA) demonstrates the highest CO₂ loadings and absorption rate compared to other amines (MEA, AMP and HEP) with the same concentration (about 3 times more CO₂ per cycle than MEA).¹³⁸ However, a viscosity increase makes work with higher TEPA concentrations difficult.

Molecules containing both amino and amido groups, for example, diethylaminoacetamide, 2-(*t*-butylamino)acetamide and 2-dimethylamino-N,N'-

dimethylacetamide show lower CO₂ absorption capacity but desorb CO₂ at lower temperature thus increasing the cycling capacity compared to –2-diethylaminoethanol.¹³⁹

5. Non-aqueous absorbents for CO₂ capture

5.1. Non-aqueous solutions of amine absorbents

The zwitterion mechanism explains the reaction between CO₂ and amines both in aqueous and non-aqueous solutions.¹⁰⁴ Fluorescently active arylamines react with CO₂ in DMSO or DMF to form relatively stable carbamic acids with enhanced fluorescence.¹⁴⁰ These acids lose CO₂ even at room temperature under N₂ bubbling, and generated free amines form carbamate salts with the remaining carbamic acids.^{140,141}

Silylalkylmonoamine H₂N(CH₂)₃Si(OMe)₃ reacts with CO₂ in THF at room temperature in a 2:1 molar ratio to give intermolecular ammonium carbamate but form a glassy dimeric carbamic acid at low temperature (0 °C).¹⁴² The first reaction is complete in 15 min while formation of carbamic acid is much slower (about 1 h). Comparison of mono- and disilylamines H₂N(CH₂)₃Si(OMe)₃ and H₂N(CH₂)₃NH(CH₂)₃Si(OMe)₃ dissolved in THF showed that despite similar reaction stoichiometry (about 0.5 mole CO₂ per N atom), they bind CO₂ in differently - intermolecular and intramolecular respectively.¹⁴³ Therefore, the diamine has higher specific absorbing capacity and, in addition, demonstrates faster kinetics. Dimeric carbamic acids [(RO)₃Si(CH₂)₃NHCOOH]₂ release CO₂ under heating but carbamates (RO)₃Si(CH₂)₃NHCOO⁻NH₃⁺(CH₂)₃Si(OR)₃⁺ undergo complex decomposition above 55 °C without CO₂ release. Their aqueous solutions though are able to release CO₂. Amidoaminosiloxane H₂NC(O)NH(CH₂)₂NH(CH₂)₃Si(OMe)₃ is much less active in reaction with CO₂ (the carbamate yield < 5 %).¹⁴² Interestingly, CO₂ catalyzes reaction of aminosiloxanes H₂NC₃H₆Si(OR)₃ with dimethylcarbonate to yield methyl carbamate esters.¹⁴⁴

The sol-gel hydrolytic condensation of such carbamates synthesized from mono- and diaminosiloxanes occurs without the decomposition of the carbamates.^{145,146} Thermal treatment releases CO₂ to provide aminosilica materials retaining initial lamellar structure.¹⁴⁶

Solutions of fatty amines C_nH_{2n+1}NH₂ (n = 8 –18) in silicon oil and DMSO react with CO₂ to form stable gels due to formation of ammonium carbamates while solutions in fatty alcohols and nitrobenzene remain liquid.¹⁴⁷ Calixarenes modified with amidoamino groups reversibly react with CO₂ in nonpolar solvents at room temperature to yield gels with a three-dimensional network of hydrogen bonds NH³⁺···⁻OC(O)NH⁻, which release CO₂ at 100 °C.¹⁴⁸

Amidines are known to promote different reactions of CO₂ including reduction, coupling and carboxylation. The most commonly used amidine is 1,8-diazabicyclo[5.4.0]undec-7-ene (DBU). Its solution in MeCN reacts with CO₂ in the ratio 1:1 supposedly forming a zwitterionic complex that can be used as a transcarboxylating reagent for preparation of N-alkyl carbamates.¹⁴⁹ The formation of the zwitterionic carbamic complexes of DBU and other amidines, like 1,5-diazabicyclo[4.3.0]non-5-ene (DBN) was proposed on the basis of ¹³C NMR data but crystallization from solutions in MeCN produced the

bicarbonate salt $[\text{DBUH}]^+\text{HCO}_3^-$.¹⁵⁰ Further study showed that interaction between DBU and CO_2 takes place only in the presence of water while in thoroughly dried solution no visual changes observed.¹⁵¹ Interestingly, the decomposition temperature of the adduct of DBN with CO_2 is substantially lower than that for the DBU: CO_2 adduct (30 °C vs. 58 °C).¹⁵⁰

5.2. Neat liquid absorbents

Bubbling CO_2 in liquid polyethyleneimine (PEI) results in the formation of a solid salt while its solutions in an alcohol form a stable gel.¹⁵²

Neat DBU reacts with CO_2 in the presence of water as shown by conductivity measurements and eventual formation of a white precipitate of the bicarbonate salt.¹⁵¹ Reaction does not occur with dry DBU even at high pressure. Proton source may be different from water. It was found that mixtures of amidines or guanidines with alcohols are reversibly binding CO_2 .^{153,154} The free energy of CO_2 binding is relatively small (-9 kJ/mol for DBU and even smaller for guanidines) and slightly depends on the length alcohol's hydrocarbon radical but decreases from linear to *iso* radicals (*tert*-BuOH does not react).^{154,155} Fatty radicals in Roh (like in hexanol-1) keep the reaction products liquid.¹⁵³ The reaction rate is very high and limited by the rate of mass transport of CO_2 from the gas phase into solution.¹⁵⁴ Stoichiometric mixtures of DBU with alcohols have high CO_2 capacity (up to 19 wt. % for MeOH) and selectivity and can be cycled several times without capacity loss.¹⁵⁴ In the presence of water the mixtures of DBU and peralkylguanidines with alcohols form bicarbonate salts with higher decomposition temperatures that is comparable with the MEA process. However, the lower specific heat (less than 50 % of aqueous systems) makes these systems attractive for post-combustion CO_2 capture.¹⁵⁵

Mixtures of DBU and other amidines $\text{RN}=\text{C}(\text{Me})\text{NMe}_2$ with primary and secondary amines reversibly absorb CO_2 at room temperature to form solid or liquid ionic salts.¹⁵⁶ The amidine acts as the proton acceptor, and amine is converted in the carbamate anion. Only primary normal and secondary alkylamines RNH_2 ($\text{R} = n$ -butyl, *sec*-butyl, *n*-hexyl) form liquid products. The presence of water results in formation of solid bicarbonates, but the mixture of *n*-hexyl substituted amidine and *n*-butylamine remained liquid after bubbling CO_2 even in the presence of 3 % water.¹⁵⁶ The amount of absorbed CO_2 is close to theoretical. Mixtures of *N'*-alkyl-*N,N*-demethylacetamide with esters of natural amino acids (1:1) reversibly react with CO_2 forming ILs with amidinium cation and $\text{R}^2\text{OOCCHR}^1\text{NHCOO}^-$ anions.¹⁵⁷ These systems remain liquid upon CO_2 uptake up to equimolar amount of CO_2 and are tolerant to water. Heating to 50 °C releases CO_2 and restores the non-ionic starting material.¹⁵⁷ Combining different sultones, amines and ammonium cations produced a library of liquid and gel- or resin-like compounds that reversibly absorb CO_2 via reaction with aminosulfone anions.¹⁵⁸

Tetramethylguanidine (TMG) reversibly absorbs CO_2 as neat liquid in the presence of traces of water but tri-azabicyclodecene (TBD) requires addition of small amount of solvent (MeCN).¹⁵⁹ Reaction results in formation of two types of products: carbamate (two isomers for TBD) and bicarbonate. Thermal stability of reaction product is higher for TBD (140 °C vs. 75 °C).¹⁵⁹

Trialkoxysilylpropylamines reversibly react with CO₂ at ambient temperature and pressure to form viscous ionic liquids: 3-(trialkoxysilyl)propylammonium 3-(trialkoxysilyl)propylcarbamates.¹⁶⁰ Heating releases 13 wt. % CO₂ at 88 °C for R = Me and 9 wt. % CO₂ at 125 °C for R = Et. These liquids are not applicable to the post combustion CO₂ capture though because of low hydrolytical stability.

Mixtures of diamines (1,2-diaminopropane, 1,6-diaminohexane) and silica react with CO₂ at 25 – 40 °C without a solvent with practically 100 % conversion of diamines to carbamates to produce finely divided powder.¹⁶¹

5.3. Functionalized ionic liquids

Ionic liquids effectively absorb CO₂ only at high pressure (physisorption), so attempts to add a chemical sorption ability to ILs have been made to produce so-called “task – specific” ILs. Functionalization of ionic liquids by addition of amine-containing side chain to the cation substantially increases solubility of CO₂ at low pressures. Addition of aminopropyl group to the 3-position of bmim cation increases the weight gain at CO₂ absorption from 0.09 wt. % for unsubstituted [bmim]PF₆ to 7.4 wt. % for modified IL at room temperature and 1 bar pressure.¹⁶² The ratio CO₂:N in this case close to theoretical value 0.5. ILs with the primary amino group in the side chain and BF₄ anion are more reactive than those with the tertiary one, and comparable with MDEA solutions but worse than MDE and DEA.¹⁶³ ILs with the same cation but with cyanamide anion showed less capacity that correlates with higher surface tension. Compared with unsubstituted analog, [bmim]BF₄, the absorption was improved by a factor of 13.¹⁶³ DFT calculations showed that electron-donating groups attached to amino group raise the energy of frontier occupied MO enhancing the interaction between CO₂ and NH₂ group.¹⁶⁴ It was shown that in the case of terminal NH₂-groups, anions strongly interact with these groups causing the viscosity increase.¹⁶⁵

Amino functionality may be introduced also in IL's anion. IL's with amino acid anions (alanine, lysine and glycine) and PBU₄⁺ cation effectively absorb CO₂.¹³⁴ These ILs react with 0.5 mole CO₂ per mole IL (up to 13 wt. % CO₂ for [PBU₄][Gly]), but in the presence of water (1 wt. %) they absorb equimolar amounts of CO₂. It points out to two different mechanisms – formation of carbamates in anhydrous conditions and bicarbonates in the presence of water.¹³⁴

5.4. Polymers

Styrene-vinylbenzylchloride copolymers aminated with diamines absorb CO₂ at 25 °C from 14 % mixture with N₂ and even air.¹⁶⁶ According TGA, each primary amine binds on average 0.18 CO₂ molecules, secondary - 0.07 molecules. Even tertiary amine moieties bind about 0.02 CO₂ molecules in contrast to non-reactive low molecular weight tertiary amines.¹⁶⁶ Porous cross-linked polymer beads show better capacity than the linear copolymers.

Polyphenylenoxide polymers containing imidazolynium and pyridinium groups were claimed as materials for membrane separation of CO₂.¹⁶⁷

6. Modified solid adsorbents

6.1. Inorganic sorbents with surface modification

Monolith or beads coated with imidazolium, pyridinium, ammonium or guanidinium-based ionic liquids have been patented.¹⁶⁸

Reaction mechanism of silylamines $\text{H}_2\text{N}(\text{CH}_2)_3\text{Si}(\text{OMe})_3$ and $\text{H}_2\text{N}(\text{CH}_2)_3\text{NH}(\text{CH}_2)_3\text{Si}(\text{OMe})_3$ tethered on xerogel with CO_2 is the same as with free amines but the tethered monoamine is much less active than its diamine analog.¹⁴³

Functionalization of mesoporous silica with N-[(3-trimethoxysilyl)propyl]amine, -ethylenediamine and -diethylenetriamine resulted in products with reduced surface area and pore volume but much higher capacity for CO_2 absorption than the starting material.¹⁶⁹ CO_2 absorption capacity increases in the row monoamine < diamine < triamine. The rate of absorption is highest for monoamine and about the same for di- and triamine. The presence of water does not significantly change the capacity of monoamine modified sorbent, but decreases the capacity in the case of di- and triamine containing sorbents by 20 % probably due to competitive water adsorption.¹⁶⁹

Ring-opening polymerization of aziridine on the silica surface resulted in formation of aminosilica with high amine surface loading (7 mmol N/g vs. 2 – 2.5 mmol N/g for silica functionalized with aminosiloxanes).¹⁷⁰ This material showed higher capacity for CO_2 adsorption than traditionally functionalized aminosilicas (by 5 – 8 times). The CO_2 :N ratio was 0.44, also higher than that for other aminosilicas (0.2 – 0.3). The sorption capacity for silicas with physisorbed tetraethylenepentamine and polyethyleneimine (PEI) was close or comparable, but a decrease in the capacity was observed for these physisorbed aminosilicas after several sorption-desorption cycles.¹⁷⁰

6.2. Polymer adsorbents

Polyaryleneoxides and polyimides with imidazolium and quaternary ammonium groups were claimed as materials for absorbing CO_2 .¹⁶⁷

Polycondensation of tetraethylenepentamine with formaldehyde and phenol produced water-soluble polymers with C_2H_4 and CH_2 linkers between nitrogen atoms.¹⁷¹ 25 wt. % aqueous solutions of these polymers are able to absorb more than 30 wt. % CO_2 from rich gas mixture (> 40 vol. % CO_2) but the capacity drops below 10 wt. % for gas streams with CO_2 concentration less than 15 %. ΔH for absorption at infinite dilution is 18.0 kJ/mol.

7. Potential backbones for liquid CO_2 adsorbents

Amino groups in polyamines like pentaethylenhexamine and polyethyleneimine (PEI) adsorbed on activated carbons substantially decrease CO_2 capture due to decreasing the

surface area.¹⁷² This points at predominant physisorption but chemisorption becomes more pronounced at higher temperatures (70 – 90 °C).¹⁷²

Addition of physical solvents to aqueous amine absorbents enhances the CO₂ sorption. As physical solvents, several classes of oxygen containing organic compounds have been claimed: alkylamides,¹⁷³ sulfolanes,^{173,174} and polyethers.

8. Functional groups for CO₂ capture

Comparison of primary (MEA), secondary (diethanolamine, DEA) and tertiary (triethanolamine, TEA) as aqueous solutions shows that affinity for CO₂ increases in the row TEA < MEA < DEA.¹⁷⁵ This indicates that secondary amines are better suited for CO₂ removal from a gas stream, at least at low concentrations. It is considered that the presence of hydroxyl group in ethanolamines is important, but it seems that CO₂ capacity is not directly depends on the quantity of OH-groups. Reaction of MEA with acrylonitrile, which converts it into a secondary amine, provides a large increase in CO₂ removal capacity and makes it comparable with DEA.¹⁷⁵ Solid 1:1 adducts of tetraethylenepentamine (TEPA) and ethyleneamine E-100 (the mixture of ethyleneimine oligomers with n = 4 – 6) with acrylonitrile also show higher cyclic capacities than individual amines.¹⁷⁶ The formation of these acrylonitrile adducts decreases the absorption rate but increases the rate of CO₂ desorption.¹⁷⁶

Diglycolamine catalyzes the CO₂ absorption by aqueous morpholine that is consistent with the zwitterion mechanism.¹⁷⁷

Aqueous solutions of glucosamine have been suggested for CO₂ absorption.^{178,179}

The idea of using a mixture of two amines where one has higher capacity but slower reaction rate has been patented.¹⁸⁰ Blends combining primary, secondary and tertiary amines are advantageous for optimum CO₂ capture compared with single amines or binary mixtures.¹⁸¹

Hexamethylenediamine (HMDA) and N-methyldiethanolamine (MDEA) exhibit catalytic properties like piperazine when blended into 2-amino-2-methyl-1-propanol (AMP). The reaction rate is close from MDEA and piperazine but higher for HMDA.¹⁸²

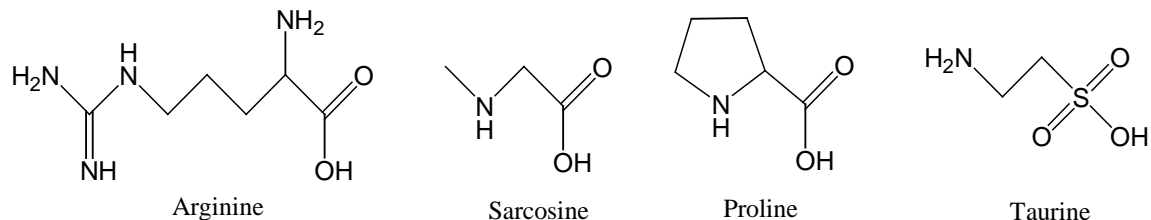
The experimental rate constant for the absorption of CO₂ from flue gas into aqueous 1,5,8,12-tetraazadodecane (APEDA) polyamine is of the same order of magnitude as that for the absorption AMP activated with piperazine, which was found to be the most advanced system.¹⁸³

It was claimed that addition of the amino carboxylic acid or amino sulfonic acid to aqueous amines decreases the amount of energy required for regeneration of the absorbent.¹⁸⁴

A mixture of MDEA and bismethyldiethyleneglycolamine was proposed for separating acid gas components from technical gases.¹⁸⁵

Amine compounds containing all primary, secondary, and tertiary N atoms in a single molecule have been proposed for absorbing both CO₂ or H₂S.¹⁸⁶

CO₂ is absorbed in high concentrated solution of amino acids or their salts with formation of a precipitate.¹⁸⁷ Potassium taurate has been proposed as a suitable amino acid salt.^{135,188} The overall pseudo-first-order constant for potassium salts of sarcosine, arginine and proline is higher than that for MEA.¹⁸⁹ Arylglycine amino acids substantially change the fluorescent response upon absorption of CO₂ and were suggested as CO₂ sensors.¹⁴¹



Hydroxyalkyl and aminoalkyl derivatives of piperazine were used as a carrier for stable permselective membranes for separating CO₂ from a combustion waste gas.¹⁹⁰

It was claimed that aqueous alkanolamines with secondary hydroxyl groups exhibit superior stability compared to alkanolamines with primary hydroxyl groups.¹⁹¹

The use of aqueous solutions of aminoethylene glycol for CO₂ capture has been patented.¹⁹²

Mercaptoimidazoles and/or mercaptobenzimidazoles were used as antioxidants for alkanolamine based CO₂ absorption.¹⁹³

Absorption of CO₂ with amino amides, like diethylaminoacetamide, 2-(tert-butylamino)acetamide, and 2-dimethylamino-N,N-dimethylacetamide, requires less the thermal energy for regeneration of the aqueous solution compared with alkanolamines.¹³⁹

9. Synthetic strategy for liquid CO₂ absorbents design

Based on results of this study and literature data,.

10. Conclusions and recommendations

Calculations of the overall energy consumption based on the heat of reaction and equilibrium constants of formation of carbamate and bicarbonate reaction products showed that there is a minimum in energy demand for these values and higher absorbency should be accompanied by higher reaction heat.¹⁹⁴ CO₂ binding should be weaker than that for MEA and for tertiary amines producing bicarbonates, the equilibrium constant of reaction (7) should be between 10⁹ and 10¹⁰.¹⁹⁴

11. Acknowledgements

I would like to thank Terri Grocela-Rocha, Robert Perry, Mike O'Brien, Larry Lewis, Sergei Kniajanski, Hubert Lam, and Dan Hancu for useful discussion.

12. Distribution list

GE GRC Niskayuna

T. Leib
K. Fletcher
L. Lewis
T. Grocela-Rocha
S. Kniajansky
M.O'Brien
H. T. Lam
J. Lee
M. Idelchik
G. Soloveichik
S. Genovese
B. Wood
R. Perry
D. Hancu

10. References

- (1) Figueroa, J. D.; Fout, T.; Plasynski, S.; McIlvried, H.; Srivastava, R. D. *International Journal on Greenhouse Gas Control* **2008**, *2*, 9 – 20.
- (2) Yang, H.; Xu, Z.; Fan, M.; Gupta, R.; Slimane, R. B.; Bland, A. E.; Wright, I. *Journal of Environmental Sciences* **2008**, *20*, 14-27.
- (3) Rydén, M.; Lyngfelt, A. *International Journal of Hydrogen Energy* **2006**, *31*, 1271-1283.
- (4) Bailey, D. W.; Feron, P. H. M. *Oil & Gas Science and Technology* **2005**, *60*, 461-474.
- (5) Rao, A. B.; Rubin, E. S. *Industrial & Engineering Chemistry Research* **2006**, *45*, 2421-2429.
- (6) Chapel, D. G.; Mariz, C. L.; Ernest, J. 1999 Canadian Society of Chemical Engineers annual meeting, Saskatoon, Saskatchewan, Canada, 1999.
- (7) Powell, C. E.; Qiao, G. G. *J. Membr. Sci.* **2006**, *279*, 1-49.
- (8) Ghosal, K.; Chern, R. T.; Freeman, B. D.; Daly, W. H.; Negulescu, I. I. *Macromolecules* **1996**, *29*, 4360-4369.
- (9) Du, R.; Feng, X.; Chakma, A. *J. Membr. Sci.* **2006**, *279*, 76-85.
- (10) Ho, W. S. W.; UNIV KENTUCKY RES FOUND: US7011694, 2006.
- (11) Shekhawat, D.; Luebke, D. R.; Pennline, H. W. “A Review of Carbon Dioxide Selective Membranes: A Topical Report,” National Energy Technology Laboratory, US Department of Energy, 2003.
- (12) Boucif, N.; Favre, E.; Roizard, D. *Chemical Engineering Science* **2008**, *63*, 5375-5385.
- (13) Bounaceur, R.; Lape, N.; Roizard, D.; Vallieres, C.; Favre, E. *Energy* **2006**, *31*, 2556-2570.
- (14) Hoffman, J. S.; Pennline, H. W. *Journal of Energy and Environmental Research* **2001**, *1*, 90-100.
- (15) Yong, Z.; Mata, V.; Rodrigues, A. E. *Separation and Purification Technology* **2002**, *26*, 195-205.
- (16) Lee, S. C.; Choi, B. Y.; Lee, T. J.; Ryu, C. K.; Ahn, Y. S.; Kim, J. C. *Catalysis Today* **2006**, *111*, 385-390.
- (17) Millward, A. R.; Yaghi, O. M. *Journal of the American Chemical Society* **2005**, *127*, 17998-17999.
- (18) Choi, J.-S.; Son, W.-J.; Kim, J.; Ahn, W.-S. *Microporous and Mesoporous Materials* **2008**, *116*, 727-731.
- (19) Banerjee, R.; Phan, A.; Wang, B.; Knobler, C.; Furukawa, H.; O’Keeffe, M.; Yaghi, O. M. *Science* **2008**, *319*, 939-943.
- (20) BOTTOMS, R. R.; GIRDLER CORP: US 1783901, 1930.
- (21) Nsakala, N. y.; Marion, J.; Bozzuto, C.; Liljedahl, G.; Palkes, M. First National Conference on Carbon Sequestration, Washington DC, 2001.
- (22) Chakravarty, S.; Gupta, A.; Hunek, B. In *First National Conference on Carbon Sequestration* Washington DC, 2001.
- (23) Leites, I. L.; Dymov, V. E.; Selitskii, A. P.; Sichkova, O. P.; Taraba, I. G.; Argunova, V. I.; Targanskaya, M. N.; Tyurina, L. S. *Khimicheskaya Promyshlennost (Moscow, Russian Federation)* **1975**, 599-602.
- (24) Dymov, V. E.; Leites, I. L.; Murzin, V. I.; Yazvikova, N. V.; Tyurina, L. S.; Sukhotina, A. S. *Khimicheskaya Promyshlennost (Moscow, Russian Federation)* **1976**, 221-224.
- (25) Leites, I. L. *Energy Conversion and Management* **1998**, *39*, 1665-1674.
- (26) Asprien, N.; Grossmann, C.; BASF AG: US 6939393, 2005.
- (27) Aksel'rod, Y. V.; Leites, I. L.; Dil'man, V. V.; Furmer, Y. V.; Morozov, A. I.; Khutoryanskii, F. M. SU 486767, 1975.
- (28) Peytavy, J. L.; Le Coz, P.; Oliveau, O.; Societe Nationale Elf Aquitaine (SNEA): US5209914, 1993.
- (29) Dang, H.; Rochelle, G. T. *Separation Science and Technology* **2003**, *38*, 337 - 357.
- (30) Yit, N. E. C.; Texaco Inc.: US 4775519, 1988.
- (31) Grossman, C.; Asprien, N.; BASF AG: US 7374734, 2008.
- (32) Yoshida, K.; Mimura, T.; Shimojo, S.; Karasaki, M.; Iijima, M.; Mitsuoka, S.; The Kansai Electric Power Co., Inc., Mitsubishi Jukogyo Kabushiki Kaisha: US 6689332 2004.
- (33) Yoshida, K.; Mimura, T.; Shimojo, S.; Karasaki, M.; Iijima, M.; Seto, T.; Mitsuoka, S.; Kansai Electric Power Co., Inc., Mitsubishi Heavy Industries, Ltd.: EP 588175, 1997.

- (34) Fujii, M.; Suda, T.; Hotsuta, Z.; Kitamura, K.; Jinno, Y.; Mimura, T.; Shimojo, S.; Iijima, M.; Mitsuoka, S.; Kansai Electric Power Co, Mitsubishi Heavy Industries, Ltd.: JP 2809368, 1998.
- (35) Yoshida, K.; Mimura, T.; Shimojo, S.; Karasaki, M.; Iijima, M.; Mitsuoka, S.; Kansai Electric Power Co., Inc., Mitsubishi Heavy Industries, Ltd.: EP 588178, 1998.
- (36) INOUE, Y.; YOSHIYAMA, R.; OISHI, T.; IJIMA, M.; TANOURA, M.; MIMURA, T.; YAGI, Y.; MITSUBISHI HEAVY INDUSTRIES, LTD.; THE KANSAI ELECTRIC POWER CO., INC.; : WO 2008156085, 2008.
- (37) Idem, R.; Wilson, M.; Tontiwachwuthikul, P.; Chakma, A.; Veawab, A.; Aroonwilas, A.; Gelowitz, D. *Industrial & Engineering Chemistry Research* **2006**, *45*, 2414-2420.
- (38) Suzuki, H.; Hayakawa, A.; Mimura, T.; Shimojo, S.; Shimayoshi, H.; Iijima, M.; Mitsuoka, S.; Iwaki, T.; Kansai Electric Power Co., Inc., Mitsubishi Jukogyo Kabushiki Kaisha: EP 705637, 2001.
- (39) Baek, J. I.; Eom, H. M.; Lee, J. G.; Sim, J. G.; Yoon, J. H.; Korea Electric Power Corporation; Korea Hydro & Nuclear Power Co., Ltd.: KR 2002003962, 2002.
- (40) Yoshida, K.; Mimura, T.; Shimojo, S.; Karasaki, M.; Iijima, M.; Seto, T.; Mitsuoka, S.; KANSAI ELECTRICAL POWER CO INC; MITSUBISHI HEAVY IND LTD: US 6500397, 2002.
- (41) Fujii, M.; Suda, T.; Hotta, Y.; Kitamura, K.; Jinno, Y.; Mimura, T.; Shimojo, S.; Iijima, M.; Mitsuoka, S.; KANSAI ELECTRIC POWER CO; MITSUBISHI HEAVY IND LTD: US5700437, 1997.
- (42) Karasaki, M.; Iijima, M.; Mitsuoka, S.; Mitsubishi Heavy Industries, Ltd.: JP 07313840, 1995.
- (43) Ouimet, M. A. US 20080159937, 2008.
- (44) Hakka, L. E.; Ouimet, M. A.; CANSOLV TECHNOLOGIES INC: US7056482, 2006.
- (45) Resnik, K. P.; Yeh, J. T.; Pennline, H. W. *International Journal of Environmental Technology and Management* **2004**, *4*, 89 - 104.
- (46) You, J. K.; Park, H.; Yang, S. H.; Hong, W. H.; Shin, W.; Kang, J. K.; Yi, K. B.; Kim, J.-N. *The Journal of Physical Chemistry B* **2008**, *112*, 4323-4328.
- (47) Gal, E. WO/2006/022885, 2006.
- (48) Peltier, R. *Power* **2008**, *152*, 38-41
- (49) Derks, P. W. J.; Versteeg, G. F. *Energy Procedia* **2008**, *in press*.
- (50) Dardea, V.; Thomsena, K.; van Wellb, W.; Stenbya, E. 15th International Conference on the Properties of Water and Steam, Berlin, Germany, 2008.
- (51) Yeh, J. T.; Pennline, H. W.; US OF AMERICA DEPARTMENT OF ENERGY: US 7255842, 2007.
- (52) Huang, H. P.; Shi, Y.; Li, W.; Chang, S. G. *Energy Fuels* **2001**, *15*, 263-268.
- (53) Sartori, G.; Thaler, W. A.; Exxon Research and Engineering Co. : US 4405578, 1983.
- (54) Tseng, P. C.; Ho, W. S.; Savage, D. W. *AIChE Journal* **1988**, *34*, 922-931.
- (55) Matsufuji, S.; Matsumiya, N.; Shinno, H.; Haratani, K.; Agency of Industrial Sciences and Technology, Japan; Sumitomo Electric Industries, Ltd.: JP 3096696, 2000.
- (56) Sartori, G.; Savage, D. W.; Exxon Research and Engineering Co. : US 4405577, 1983.
- (57) Hesse, H. J. F. A.; Smit, M. J.; Du Toit, F. J.; Sasol Chemicals Europe Ltd.: US 6312655, 2001.
- (58) Say, G. R.; Heinzelmann, F. J.; Iyengar, J. N.; Savage, D. W.; Bisio, A.; Sartori, G. *Chem. Eng. Prog.* **1984**, *80*, 72-7.
- (59) Svendsen, H. F.; Tobiesen, F. A.; Mejdell, T.; Hoff, K.; Andersen, M. T.; Sinvent AS, Norway: WO 2008072979, 2008.
- (60) Astarita, G.; Savage, D. W.; Longo, J. M. *Chemical Engineering Science* **1981**, *36*, 581-588.
- (61) Cullinane, J. T.; Rochelle, G. T. *Industrial & Engineering Chemistry Research* **2006**, *45*, 2531-2545.
- (62) Rochelle, G. T.; Chen, E.; Oyenekan, B.; Sexton, A.; Davis, J.; Hiilliard, M.; Xu, Q.; Van Wagener, D.; Plaza, J. M. "CO₂ Capture by Absorption with Potassium Carbonate," University Of Texas At Austin 2006.
- (63) Kothandaraman, A.; Nordb, L.; Bollandb, O.; Herzog, H. J.; McRaea, G. J. *Energy Procedia* **2008**, *in press*.
- (64) van Dam, M. H. H.; Lamine, A. S.; Roizard, D.; Lochon, P.; Roizard, C. *Industrial & Engineering Chemistry Research* **1997**, *36*, 4628-4637.
- (65) Gwinner, B.; Roizard, D.; Lapique, F.; Favre, E.; Cadours, R.; Boucot, P.; Carrette, P. L. *Ind. Eng. Chem. Res.* **2006**, *45*, 5044-5049.

- (66) Meredith, J. C.; Johnston, K. P.; Seminario, J. M.; Kazarian, S. G.; Eckert, C. A. *The Journal of Physical Chemistry* **1996**, *100*, 10837-10848.
- (67) Dardin, A.; DeSimone, J. M.; Samulski, E. T. *The Journal of Physical Chemistry B* **1998**, *102*, 1775-1780.
- (68) DeSimone, J. M.; Guan, Z.; Elsbernd, C. S. *Science* **1992**, *257*, 945-947.
- (69) Costa Gomes, M. F.; Padua, A. A. H. *The Journal of Physical Chemistry B* **2003**, *107*, 14020-14024.
- (70) Rolker, J.; Seiler, M.; Mokrushina, L.; Arlt, W. *Industrial & Engineering Chemistry Research* **2007**, *46*, 6572-6583.
- (71) Hong, C. C.; Columbia Gas System Service Corp.: US 4238206, 1980.
- (72) Sarbu, T.; Styranec, T.; Beckman, E. J. *Nature (London)* **2000**, *405*, 165-168.
- (73) Sarbu, T.; Styranec, T. J.; Beckman, E. J. *Ind. Eng. Chem. Res.* **2000**, *39*, 4678-4683.
- (74) Bryukhanova, L. A.; Nikitina, A. K.; Mizinova, T. N. SU 789142, 1980.
- (75) Kazarian, S. G.; Vincent, M. F.; Bright, F. V.; Liotta, C. L.; Eckert, C. A. *Journal of the American Chemical Society* **1996**, *118*, 1729-1736.
- (76) Shen, Z.; McHugh, M. A.; Xu, J.; Belardi, J.; Kilic, S.; Mesiano, A.; Bane, S.; Karnikas, C.; Beckman, E.; Enick, R. *Polymer* **2003**, *44*, 1491-1498.
- (77) Tan, B.; Cooper, A. I. *J. Am. Chem. Soc.* **2005**, *127*, 8938-8939.
- (78) Bie, P.; Yang, H. J.; Bai, Y. *Chin. Chem. Lett.* **2006**, *17*, 743-746.
- (79) Kammermeyer, K.; Sollami, B. J.; (Bendix Corp.). US 3665678, 1972.
- (80) Tsybulevskii, A. M.; Berlin, M. A.; Potapov, V. F.; Stepanova, I. N.; (All-Union Scientific-Research Institute of Petroleum Refining, USSR). SU 975041, 1982.
- (81) Shah, V. M.; Hardy, B. J.; Stern, S. A. *Journal of Polymer Science Part B: Polymer Physics* **1993**, *31*, 313-317.
- (82) Fink, R.; Hancu, D.; Valentine, R.; Beckman, E. J. *J. Phys. Chem. B* **1999**, *103*, 6441-6444.
- (83) Dzielawa, J.; Rubas, A.; Lubbers, C.; Stepinski, D.; Scurto, A.; Barrans, R.; Dietz, M.; Herlinger, A.; Brennecke, J. *Separation Science and Technology* **2008**, *43*, 2520-2536.
- (84) Li, S.; Li, Y.; Wang, J. *Fluid Phase Equilibria* **2007**, *253*, 54-60.
- (85) Blanchard, L. A.; Hancu, D.; Beckman, E. J.; Brennecke, J. F. *Nature* **1999**, *399*, 28-29.
- (86) Anderson, J. L.; Dixon, J. K.; Brennecke, J. F. *Acc. Chem. Res.* **2007**, *40*, 1208-1216.
- (87) Blanchard, L. A.; Gu, Z.; Brennecke, J. F. *The Journal of Physical Chemistry B* **2001**, *105*, 2437-2444.
- (88) Baltus, R. E.; Counce, R. M.; Culbertson, B. H.; Luo, H.; DePaoli, D. W.; Dai, S.; Duckworth, D. C. *Separation Science and Technology* **2005**, *40*, 525 - 541.
- (89) Baltus, R. E.; Culbertson, B. H.; Dai, S.; Luo, H.; DePaoli, D. W. *J. Phys. Chem. B* **2004**, *108*, 721-727.
- (90) Kumelan, J.; Perez-Salado Kamps, A.; Tuma, D.; Maurer, G. *The Journal of Chemical Thermodynamics* **2006**, *38*, 1396-1401.
- (91) Kumelan, J.; Perez-SaladoKamps, D.; Tuma, D.; Maurer, G. *J. Chem. Eng. Data* **2006**, *51*, 1802-1807.
- (92) Aki, S. N. V. K.; Mellein, B. R.; Saurer, E. M.; Brennecke, J. F. *J. Phys. Chem. B* **2004**, *108*, 20355-20365.
- (93) Muldoon, M. J.; Aki, S. N. V. K.; Anderson, J. L.; Dixon, J. K.; Brennecke, J. F. *J. Phys. Chem. B* **2007**, *111*, 9001-9009.
- (94) Shiflett, M. B.; Kasprzak, D. J.; Junk, C. P.; Yokozeki, A. *The Journal of Chemical Thermodynamics* **2008**, *40*, 25-31.
- (95) Tang, J.; Tang, H.; Sun, W.; Radosz, M.; Shen, Y. *Polymer* **2005**, *46*, 12460-12467.
- (96) Blasig, A.; Tang, J.; Hu, X.; Tan, S. P.; Shen, Y.; Radosz, M. *Ind. Eng. Chem. Res.* **2007**, *46*, 5542-5547.
- (97) Hou, Y.; Baltus, R. E. *Ind. Eng. Chem. Res.* **2007**, *46*, 8166-8175.
- (98) Bara, J. E.; Gabriel, C. J.; Lessmann, S.; Carlisle, T. K.; Finotello, A.; Gin, D. L.; Noble, R. D. *Ind. Eng. Chem. Res.* **2007**, *46*, 5380-5386.
- (99) Quinn, R.; Appleby, J. B.; Mathias, P. M.; Pez, G. P. *Separation Science and Technology* **1995**, *30*, 1711 - 1723.
- (100) Xu; Moulijn, J. A. *Energy & Fuels* **1996**, *10*, 305-325.
- (101) Takeshita, K.; Kitamoto, A. *Journal of Chemical Engineering of Japan* **1988**, *21*, 411-417.

- (102) Danckwerts, P. V. *Chemical Engineering Science* **1979**, *34*, 443-446.
- (103) Vaidya, P. D.; Kenig, E. Y. *Chemical Engineering & Technology* **2007**, *30*, 1467-1474.
- (104) Versteeg, G. F.; Van Dijck, L. A. J.; Van Swaaij, W. P. M. *Chemical Engineering Communications* **1996**, *144*, 113 - 158.
- (105) Alvarez-Fuster, C.; Midoux, N.; Laurent, A.; Charpentier, J. C. *Chemical Engineering Science* **1981**, *36*, 1513-1518.
- (106) Littel, R. J.; Versteeg, G. F.; Van Swaaij, W. P. M. *Chemical Engineering Science* **1992**, *47*, 2037-2045.
- (107) Crooks, J. E.; Donnellan, J. P. *J. Chem. Soc., Perkin Trans. 2* **1989**, 331 - 333.
- (108) da Silva, E. F.; Svendsen, H. F. *Ind. Eng. Chem. Res.* **2004**, *43*, 3413-3418.
- (109) Ma'mun, S.; Dindore, V. Y.; Svendsen, H. F. *Ind. Eng. Chem. Res.* **2007**, *46*, 385-394.
- (110) Tomizaki, K.-y.; Shimizu, S.; Onoda, M.; Fujioka, Y. *Chemistry Letters* **2008**, *37*, 516-517.
- (111) Suda, T.; Zhang, Y.; Iwaki, T.; Nomura, M. *Chemistry Letters* **1998**, *27*, 189-190.
- (112) Sartori, G.; Savage, D. W. *Ind. Eng. Chem. Fundam.* **1983**, *22*, 239-49.
- (113) Bishnoi, S.; Rochelle, G. T. *Chemical Engineering Science* **2000**, *55*, 5531-5543.
- (114) Donaldson, T. L.; Nguyen, Y. N. *Ind. Eng. Chem. Fundam.* **1980**, *19*, 260-266.
- (115) Mathonat, C.; Majer, V.; Mather, A. E.; Grolier, J. P. E. *Fluid Phase Equilibria* **1997**, *140*, 171-182.
- (116) Ma'mun, S.; Svendsen, H. F.; Hoff, K. A.; Juliussen, O. *Energy Convers. Manage.* **2006**, *48*, 251-258.
- (117) Ma'mun, S.; Jakobsen, J. P.; Svendsen, H. F.; Juliussen, O. *Ind. Eng. Chem. Res.* **2006**, *45*, 2505-2512.
- (118) Kim, I.; Svendsen, H. F. *Ind. Eng. Chem. Res.* **2007**, *46*, 5803-5809.
- (119) Park, J.-Y.; Yoon, S. J.; Lee, H. *Environmental Science & Technology* **2003**, *37*, 1670-1675.
- (120) Shim, J. G.; Kim, J. H.; Jang, K. R.; Ryu, C. K.; Eum, H. M.; Lim, H. S. US20080125314, 2008.
- (121) Kosaraju, P.; Kovvali, A. S.; Korikov, A.; Sirkar, K. K. *Industrial & Engineering Chemistry Research* **2005**, *44*, 1250-1258.
- (122) Streitberger, H.; Pfueller, O.; Stankowiak, A.; Snell, A.; Mollekopf, N.; Mueller, H.-D.; CLARIANT PRODUKTE DEUTSCHLAND: US7387768, 2008.
- (123) Anders, J.-T.; Melder, J.-P.; Asprien, N.; Brettschneider, O.; Clausen, I.; Eck, B.; Lichtfers, U. US 20080236390, 2008.
- (124) Hook, R. J. *Industrial & Engineering Chemistry Research* **1997**, *36*, 1779-1790.
- (125) Baek, J.-I.; Yoon, J.-H. *Journal of Chemical & Engineering Data* **1998**, *43*, 635-637.
- (126) Hakka, L. E.; Ouimet, M. A. US 20040253159, 2004.
- (127) Chowdhury, F. A.; Okabe, H.; Shimizu, S.; Onoda, M.; Fujioka, Y. *Energy Procedia* **2009**, *in press*, *1*.
- (128) Liao, C.-H.; Li, M.-H. *Chemical Engineering Science* **2002**, *57*, 4569-4582.
- (129) Rinker, E. B.; Ashour, S. S.; Sandall, O. C. *Industrial & Engineering Chemistry Research* **2000**, *39*, 4346-4356.
- (130) Zhang, X.; Zhang, C.-F.; Qin, S.-J.; Zheng, Z.-S. *Industrial & Engineering Chemistry Research* **2001**, *40*, 3785-3791.
- (131) Zhang, X.; Zhang, C.-F.; Liu, Y. *Industrial & Engineering Chemistry Research* **2002**, *41*, 1135-1141.
- (132) Sun, W.-C.; Yong, C.-B.; Li, M.-H. *Chemical Engineering Science* **2005**, *60*, 503-516.
- (133) Nagao, Y.; Hayakawa, A.; Suzuki, H.; Mitsuoka, S.; Iwaki, T.; Mimura, T.; Suda, T.-I. *Chem. Lett.* **1998**, 745-746.
- (134) Zhang, J.; Zhang, S.; Dong, K.; Zhang, Y.; Shen, Y.; Lv, X. *Chem.--Eur. J.* **2006**, *12*, 4021-4026.
- (135) Versteeg, G. F.; Kumar, P. S.; Hogendoorn, J. A.; Feron, P. H. M.; Nederlandse Organisatie Voor Toegepast- Natuurwetenschappelijk Onderzoek TNO: WO 2003095071, 2003.
- (136) Singh, P.; Niederer, J. P. M.; Versteeg, G. F. *International Journal of Greenhouse Gas Control* **2007**, *1*, 5-10.
- (137) Singh, P.; Brilman, D. W. F.; Groeneveld, M. J. *Energy Procedia* **2008**, *in press*.
- (138) Aronu, U. E.; Svendsen, H. F.; Hoff, K.; Juliussen, O. *Energy Procedia* **2008**, *in press*.
- (139) Suzuki, H.; Iwaki, T.; Mimura, T.; Mitsuoka, S.; Tanaka, H.; Iijima, M.; The Kansai Electric Power Co.: US 6051161, 2000.
- (140) Hampe, E. M.; Rudkevich, D. M. *Chem. Commun.* **2002**, 1450 - 1451.

- (141) Hampe, E. M.; Rudkevich, D. M. *Tetrahedron* **2003**, *59*, 9619-9625.
- (142) Dibenedetto, A.; Aresta, M.; Fragale, C.; Narracci, M. *Green Chem.* **2002**, *4*, 439-443.
- (143) Dibenedetto, A.; Pastore, C.; Fragale, C.; Aresta, M. *ChemSusChem* **2008**, *1*, 742-745.
- (144) Aresta, M.; Quaranta, E.; Dibenedetto, A.; Tommasi, I.; Marciniak, B. *Appl. Organomet. Chem.* **2000**, *14*, 871-873.
- (145) Alauzun, J.; Mehdi, A.; Reye, C.; Corriu, R. J. P. *J. Am. Chem. Soc.* **2005**, *127*, 11204-11205.
- (146) Alauzun, J.; Besson, E.; Mehdi, A.; Reye, C.; Corriu, R. J. P. *Chem. Mater.* **2008**, *20*, 503-513.
- (147) George, M.; Weiss, R. G. *Langmuir* **2002**, *18*, 7124-7135.
- (148) Xu, H.; Rudkevich, D. M. *Chem.--Eur. J.* **2004**, *10*, 5432-5442.
- (149) Pérez, E. R.; da Silva, M. O.; Costa, V. C.; Rodrigues-Filho, U. P.; Franco, D. W. *Tetrahedron Letters* **2002**, *43*, 4091-4093.
- (150) Perez, E. R.; Santos, R. H. A.; Gambardella, M. T. P.; de Macedo, L. G. M.; Rodrigues-Filho, U. P.; Launay, J.-C.; Franco, D. W. *The Journal of Organic Chemistry* **2004**, *69*, 8005-8011.
- (151) Heldebrant, D. J.; Jessop, P. G.; Thomas, C. A.; Eckert, C. A.; Liotta, C. L. *J. Org. Chem.* **2005**, *70*, 5335-5338.
- (152) Kitchens, C. L.; Samanta, S.; John, E.; Pollet, P.; Griffith, K.; Richman, K.; Apkarian, R. P.; Liotta, C.; Eckert, C. A. 2006 AIChE Annual Meeting San Francisco, CA, 2006; p 520f.
- (153) Jessop, P. G.; Heldebrant, D. J.; Li, X.; Eckert, C. A.; Liotta, C. L. *Nature* **2005**, *436*, 1102-1102.
- (154) Heldebrant, D. J.; Yonker, C. R.; Jessop, P. G.; Phan, L. *Energy Environ. Sci.* **2008**, *1*, 487 - 493.
- (155) Heldebrant, D. J.; Yonker, C. R.; Jessop, P. G.; Phan, L. *Energy Procedia* **2009**, *in press*.
- (156) Yamada, T.; Lukac, P. J.; George, M.; Weiss, R. G. *Chem. Mater.* **2007**, *19*, 967-969.
- (157) Yamada, T.; Lukac, P. J.; Yu, T.; Weiss, R. G. *Chem. Mater.* **2007**, *19*, 4761-4768.
- (158) Soutullo, M. D.; Odom, C. I.; Wicker, B. F.; Henderson, C. N.; Stenson, A. C.; Davis, J. H. *Chem. Mater.* **2007**, *19*, 3581-3583.
- (159) Pereira, F. S.; deAzevedo, E. R.; da Silva, E. F.; Bonagamba, T. J.; da Silva Agostíni, D. L.; Magalhães, A.; Job, A. E.; Pérez González, E. R. *Tetrahedron* **2008**, *64*, 10097-10106.
- (160) Blasucci, V.; Dilek, C.; Huttenhower, H.; John, E.; Llopis-Mestre, V.; Pollet, P.; Eckert, C. A.; Liotta, C. L. *Chemical Communications* **2009**, 116-118.
- (161) Brodoway, N.; (du Pont de Nemours, E. I., and Co., USA). Application: US
US, 1978.
- (162) Bates, E. D.; Mayton, R. D.; Ntai, I.; Davis, J. H. *J. Am. Chem. Soc.* **2002**, *124*, 926-927.
- (163) Galán Sánchez, L. M.; Meindersma, G. W.; de Haan, A. B. *Chemical Engineering Research and Design* **2007**, *85*, 31-39.
- (164) Yu, G.; Zhang, S.; Yao, X.; Zhang, J.; Dong, K.; Dai, W.; Mori, R. *Ind. Eng. Chem. Res.* **2006**, *45*, 2875-2880.
- (165) Yu, G.; Zhang, S.; Zhou, G.; Liu, X.; Chen, X. *AIChE J.* **2007**, *53*, 3210-3221.
- (166) Diaf, A.; Garcia, J. L.; Beckman, E. J. *J. Appl. Polym. Sci.* **1994**, *53*, 857-875.
- (167) Radosz, M.; Shen, Y. US 2007/0119302, 2007.
- (168) Lu, Y.; Zhai, S.; Wang, Q.; Fitch, F.; The BOC Group, Inc.: WO2007101397, 2007.
- (169) Knowles, G. P.; Delaney, S. W.; Chaffee, A. L. *Industrial & Engineering Chemistry Research* **2006**, *45*, 2626-2633.
- (170) Hicks, J. C.; Drese, J. H.; Fauth, D. J.; Gray, M. L.; Qi, G.; Jones, C. W. *J. Am. Chem. Soc.* **2008**, *130*, 2902-2903.
- (171) Rinaldi, G. *Industrial & Engineering Chemistry Research* **1997**, *36*, 3778-3782.
- (172) Plaza, M. G.; Pevida, C.; Arenillas, A.; Rubiera, F.; Pis, J. J. *Fuel* **2007**, *86*, 2204-2212.
- (173) SHELL INT RESEARCH GB 972140, 1964.
- (174) Brok, T. J.; Groenen, R. J. M.; Klinkenbijn, J. M.; Knaap, M. C.; Shell Internationale Research Maatschappij BV: WO 2003057348, 2003.
- (175) Filburn, T.; Helble, J. J.; Weiss, R. A. *Ind. Eng. Chem. Res.* **2005**, *44*, 1542-1546.
- (176) Lee, S.; Filburn, T. P.; Gray, M.; Park, J.-W.; Song, H.-J. *Ind. Eng. Chem. Res.* **2008**, *47*, 7419-7423.
- (177) Al-Juaied, M.; Rochelle, G. T. *Chemical Engineering Science* **2006**, *61*, 3830-3837.
- (178) Navaza Dafonte, J. M.; Gomez Diaz, D.; Vazquez Orgeira, L.; Universidade de Santiago de Compostela Edificio CACTUS- Sur: ES2301394 2006.
- (179) Gómez-Díaz, D.; Navaza, J. M.; Sanjurjo, B.; Vázquez-Orgeira, L. *Chemical Engineering Journal* **2006**, *122*, 81-86.

- (180) Chakravarti, S.; Gupta, A.; PRAXAIR TECHNOLOGY INC: US 6165433, 2000.
- (181) Notz, R.; Asprion, N.; Clausen, I.; Hasse, H. *Institution of Chemical Engineers Symposium Series* **2006**, 152, 132-141.
- (182) Choi, W.-J.; Cho, K.-C.; Lee, S.-S.; Shim, J.-G.; Hwang, H.-R.; Park, S.-W.; Oh, K.-J. *Green Chem.* **2007**, 9, 594 - 598.
- (183) Siminiceanu, I.; Tataru-Farmus, R.-E.; Bouallou, C. *Environmental Engineering and Management Journal* **2007**, 6, 555-561.
- (184) Asprion, N.; Clausen, I.; Lichtfers, U.; Wagner, R. WO 2007134994, 2007.
- (185) Menzel, J.; Snell, A.; Uhde G.m.b.H.: WO2007101585, 2007.
- (186) Inoue, Y.; Taura, M.; Wataru, N.; Fujii, S.; Sakano, M.; Ichihara, T.; Mitsubishi Heavy Industries, Ltd.: JP 2006150298, 2006.
- (187) Erga, O.; Juliussen, O.; Lidal, H. *Energy Conversion and Management* **1995**, 36, 387-392.
- (188) Kumar, P. S.; Hogendoorn, J. A.; Versteeg, G. F.; Feron, P. H. M. *AIChE Journal* **2003**, 49, 203-213.
- (189) van Holst, J.; Politiek, P. P.; Niederer, J. P. M.; Versteeg, G. F. Eight International Conference on Greenhouse Gas Control Technologies (GHGT-8), Trondheim, Norway, 2006.
- (190) Yoshimura, H.; Teramoto, M.; Matsuyama, H.; Tosoh Corp.: JP 2001293340, 2001.
- (191) Rooney, P. C.; The Dow Chemical Company: US 6207121, 2001.
- (192) Iijima, M.; Mitsuoka, S.; Mitsubishi Jukogyo Kabushiki Kaisha: EP 776687, 2002.
- (193) Yamada, R.; Murakami, K.; Oda, N.; Tanaka, Y.; Takahashi, N.; Babcock Hitachi Kk.; Toho Chem. Ind. Co. Ltd.: JP 3739437, 2006.
- (194) Draxler, J.; Stevens, G.; Kentish, S.; Rubin, E. S.; Keith, D. W.; Gilboy, C. F.; Wilson, M.; Morris, T.; Gale, J.; Thambimuthu, K. In *Greenhouse Gas Control Technologies 7*; Elsevier Science Ltd: Oxford, 2005.

A Computational Study of the Heats of Reaction of Substituted Monoethanolamine with CO₂

Hong-Bin Xie,^{†,‡} J. Karl Johnson,^{*,†,‡} Robert J. Perry,[§] Sarah Genovese,[§] and Benjamin R. Wood[§]

Department of Chemical and Petroleum Engineering, University of Pittsburgh, Pittsburgh, Pennsylvania 15261, United States, National Energy Technology Laboratory, Pittsburgh, Pennsylvania 15236, United States, and GE Global Research, 1 Research Circle, Niskayuna, New York 12309, United States

Received: August 27, 2010; Revised Manuscript Received: November 29, 2010

Various amines have been considered as materials for chemical capture of CO₂ through liquid-phase reactions to form either carbamate or carbamic acid products. One of the main challenges in these CO₂-amine reactions lies in tuning the heat of reaction to achieve the correct balance between the extent of reaction and the energy cost for regeneration. In this work, we use a computational approach to study the effect of substitution on the heats of reaction of monoethanolamine (MEA). We use ab initio methods at the MP2/aug-cc-pVDZ level, coupled with geometries generated from B3LYP/6-311++G(d,p) density functional theory along with the conductor-like polarizable continuum model to compute the heats of reaction. We consider two possible reaction products: carbamate, having a 2:1 amine:CO₂ reaction stoichiometry, and carbamic acid, having a 1:1 stoichiometry. We have considered CH₃, NH₂, OH, OCH₃, and F substitution groups at both the α - and β -carbon positions of MEA. We have experimentally measured heats of reaction for MEA and both α - and β -CH₃-substituted MEA to test the predictions of our model. We find quantitative agreement between the predictions and experiments. We have also computed the relative basicities of the substituted amines and found that the heats of reaction for both carbamate and carbamic acid products are linearly correlated with the computed relative basicities. Weaker basicities result in less exothermic heats of reaction. Heats of reaction for carbamates are much more sensitive to changes in basicity than those for carbamic acids. This leads to a crossover in the heat of reaction so that carbamic acid formation becomes thermodynamically favored over carbamate formation for the weakest basicities. This provides a method for tuning the reaction stoichiometry from 2:1 to 1:1.

Introduction

The capture (separation) and sequestration (long-term storage) of carbon dioxide is seen as a critical near-term strategy for mitigating the effects of greenhouse gas emissions. Generation of electricity from fossil fuels (coal, oil, and gas) accounts for approximately 25% of global CO₂ emissions.¹ Moreover, this fraction could increase drastically in the next 25 years.² The U.S. Department of Energy (DOE) has set a target for the capture and sequestration of 90% of the CO₂ in flue gas with a no more than 35% increase in the cost of electricity.³ No technologies that achieve these targets are currently being implemented. Therefore, development of technologies that facilitate the cost-effective and energy-efficient capture of CO₂ from power plant flue gas is of paramount importance.

Postcombustion capture of CO₂ produced by conventional coal combustion in air presents technical challenges because the flue gas is at atmospheric pressure and the CO₂ concentration is 10–15 vol %, resulting in a low CO₂ partial pressure and a large volume of gas to be treated. One approach to postcombustion CO₂ capture is to use a regenerable solvent. Both physical and chemical solvents have been considered for CO₂ capture; however, chemical solvents (such as amines) are

considered to be a more viable option for treating flue gases because of their ability to capture CO₂ at low partial pressures.^{4–11}

Alkanolamine systems have been studied as possible materials for postcombustion capture of CO₂ from flue gas.^{12–20} Among these alkanolamines, aqueous monoethanolamine (MEA) is the most widely used solvent, having been used for more than 60 years for natural gas purification and food-grade CO₂ production,^{21–23} and has recently received attention as a candidate for the capture of CO₂ from flue gas.^{4,5,7,9,24–33} However, there are several challenges associated with the use of aqueous MEA for capture of CO₂ from flue gas.^{21,22} (1) The reaction of MEA with CO₂ to form carbamate is highly exothermic (approximately –17 kcal/mol), which means that more energy is required in the solvent regeneration step compared to what is optimal.^{27,28,34} We note that a sizable fraction of the energy required to regenerate the solvent goes into vaporization of water in the aqueous solution.³⁵ (2) A non-negligible fraction of the MEA is lost due to vaporization and decomposition during regeneration.^{29,30,36} (3) Aqueous MEA has been shown to be highly corrosive to carbon steels,^{31,37} which increases the capital and maintenance costs of the process. As a result of these and other issues, the use of MEA to capture CO₂ is estimated to require an ~80% increase in the cost of electricity and a ~30% decrease in power plant efficiency,³ making MEA not economically acceptable by the DOE standards.³ There has therefore been a significant effort to identify other amine-based solvents that perform better than MEA.^{1,38–45}

* To whom correspondence should be addressed. E-mail: karlj@pitt.edu.

[†] University of Pittsburgh.

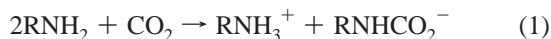
[‡] National Energy Technology Laboratory.

[§] GE Global Research.

TABLE 1: Electronegativities⁶⁹ of Substituent Groups

	H	CH ₃	NH ₂	OH	OCH ₃	F
electronegativity	2.20	2.555	3.117	3.542	3.606	3.938

The generally expected reaction stoichiometry for the reaction between primary or secondary amines and CO₂ is 2:1, resulting in the formation of a carbamate anion and an ammonium cation as shown in eq 1:⁴⁶



However, Mindrup and Schneider⁴⁷ used gas-phase quantum mechanical calculations to qualitatively predict that reactions between negatively charged amines in ionic liquids (i.e., the anions in the ionic liquid) and CO₂ could produce carbamic acid instead of carbamate



Their calculations indicated that a 1:1 amine:CO₂ stoichiometry is achieved because the heat of reaction for the carbamic acid reaction is more exothermic than for the carbamate reaction. These predictions were later experimentally verified.⁴⁵

We postulate that in general, the reaction of CO₂ with an amine will involve both reactions given in eqs 1 and 2. Moreover, the carbamate and carbamic acid species should be in thermodynamic equilibrium if the proton transfer step is facile, which could be the case for aqueous-phase reactions. Hence, carbamate will be the main product if its heat of reaction is more exothermic than that of carbamic acid, and vice versa. It may therefore be possible to change the reaction product distribution by modifying the relative heats of reaction for carbamate and carbamic acid products. Furthermore, we suggest that the relative heats of reaction may be changed via addition of substituent groups onto an amine.

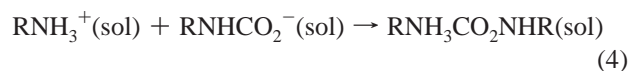
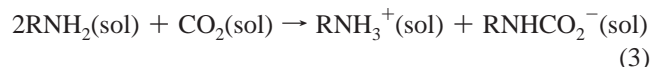
There has been limited computational work describing the effect of substituent groups on the heats of reaction of CO₂ with amines. The only study of which we are aware is that of Chakraborty et al.⁴⁸ They used molecular orbital theory to investigate how methyl substitution at the α -carbon of MEA decreased the basicity of MEA and therefore also decreased the heat of reaction for carbamate formation. The goal of this work is to investigate how substituent groups on the α - and β -carbons of MEA affect the heats of reaction for both carbamate and carbamic acid reactions. We have used the following substituent groups in this study: CH₃, NH₂, OH, OCH₃, and F (listed in Table 1, along with their electronegativities). Our shorthand notation for the substituted amines and the IUPAC chemical names are listed in Table 2. Our work provides general guidelines for tuning the heat of reaction for carbamate formation through the use of substituent groups. This could be useful for designing amines with heats of reaction more favorable than that of MEA. Lower heats of reaction should result in lower operating costs for CO₂ capture, although this is only one consideration.³⁵ We also investigate how substituents can be used to tune the reaction stoichiometry between amine and CO₂ by shifting the equilibrium from the carbamate 2:1 ratio toward the carbamic acid 1:1 ratio.

Methods

Heat of Reaction Calculations. We used a two-step approach to compute the heats of reaction for the various carbamates:

TABLE 2: Naming Conventions for Substituted MEAs Used in This Study

shorthand name	chemical name
MEA	2-aminoethanol
α -CH ₃ -MEA	2-aminopropan-1-ol
β -CH ₃ -MEA	1-aminopropan-2-ol
α -NH ₂ -MEA	2,2-diaminoethanol
β -NH ₂ -MEA	1,2-diaminoethanol
α -OH-MEA	1-aminoethane-1,2-diol
β -OH-MEA	2-aminoethane-1,1-diol
α -OCH ₃ -MEA	2-amino-2-methoxyethanol
β -OCH ₃ -MEA	2-amino-1-methoxyethanol
α -F-MEA	2-amino-2-fluoroethanol
β -F-MEA	2-amino-1-fluoroethanol



This two-step approach uses a thermodynamic path to separate the chemical steps, involving bond breaking and formation as given in eq 3, from the process of bringing the two ions together to form a complex, given in eq 4. The second step involves electrostatic and dispersion interactions between solvated RNH₃⁺ and RNHCO₂⁻ species. The total heat of reaction, ΔH , is the sum of ΔH_1 , the enthalpy change for eq 3, and ΔH_2 , the enthalpy change for eq 4. We split the carbamate heat of reaction calculations for the sake of computational convenience. The carbamic acid heats of reaction are computed in a single direct step.

The reactants, intermediates, and products investigated in this work all have conformational degrees of freedom that may influence the calculated heats of reaction. We used ab initio molecular dynamics (AIMD) to generate reasonable gas-phase conformations for amines, RNH₃⁺, RNHCO₂⁻, and carbamic acids. We used density function theory (DFT) with the B88-PW86 functional⁴⁹ along with a triple- ζ valence polarized basis set (TZVP) within the RI approximation⁵⁰ to conduct the AIMD calculations. The temperature was set to 800 K to sample a large number of different configurations. A time step of 1.451 fs was used. The total length of each AIMD simulation was 7.256 ps (5000 time steps). Calculations were conducted using TURBOMOLE.⁵¹ We selected configurations from the AIMD run and used these as starting points to obtain an average of 6 (range of 3–11) different local minimum structures for each species at the B3LYP/6-311++G(d,p) level using Gaussian 03.⁵² Single-point energy calculations were then performed at the MP2/aug-cc-pVDZ//B3LYP/6-311++G(d,p) level to obtain accurate total energies for each of the sample configurations. In all geometry optimizations, harmonic vibrational frequency calculations, and single-point energy calculations, implicit solvent effects were considered by using the conductor-like polarizable continuum model (CPCM) formalism.^{53,54} We used water as the solvent in these calculations even though the experiments were conducted in neat amines, because amines were not available as a solvent choice within Gaussian 03. However, additional test calculation using methanol and aniline as solvents gave results that were almost the same as those for the water solvent case, indicating that the heats of reaction are not dramatically dependent upon the solvent used, as long as the dielectric constant is high. The CPCM method was initially devised by Tomasi and co-workers^{55–57} and extended for geometry optimizations to converge efficiently.

UAHF⁵⁸ atomic radii were used in the construction of the solute cavity for all calculations. A similar computational approach has successfully been used to calculate the kinetics of MEA-CO₂ reactions.⁵⁹ The enthalpy for each species in the liquid is calculated using the equation

$$H^s = H^s(\text{g}) + E_{\text{sol}} + \text{ZPE} \quad (5)$$

where H^s is the enthalpy of species s in the liquid phase, $H^s(\text{g})$ is enthalpy of species s in the gas phase, ZPE is the zero-point energy, and E_{sol} is the solvation free energy of species s , which includes electrostatic interaction, cavitation, dispersion, and repulsion energies.⁵⁵⁻⁵⁷

To account for the different conformations in a physically reasonable way, we generated a Boltzmann-weighted distribution to compute the conformational averaged energy of each species s :

$$\bar{H}^s = \sum_i w_i H_i^s \quad (6)$$

where the Boltzmann weight w_i is given by

$$w_i^s = \frac{e^{-H_i^s/k_B T}}{\sum_i e^{-H_i^s/k_B T}} \quad (7)$$

and k_B is the Boltzmann constant and T is the absolute temperature, taken to be 298 K in our calculations. Note that it is not possible to sample conformations of the bound carbamate, [RNH₃⁺][⁻CO₂NHR], because it will transform to neutral species RNH₂ and RNHCOOH in our gas-phase AIMD simulations. Therefore, we used the configurations for RNH₃⁺ and RNHCO₂⁻ having the highest Boltzmann weight to evaluate electrostatic and dispersion interactions in eq 4.

As discussed in the Introduction, carbamate formation is expected to dominate for primary and secondary amines.⁴⁶ In addition, a small amount of a bicarbonate product can also be formed in aqueous solutions. We have not considered the bicarbonate product in our computations because the experiments were conducted in the absence of water (neat amine). However, we expect that our computational results will still be valid for aqueous amine solutions because bicarbonate is a minor product.

Relative Amine Basicity Calculations. In general, the basicity of a compound can be evaluated by calculating the $\text{p}K_a$ value of the conjugate base of the compound using the reaction



The $\text{p}K_a$ value can be calculated from

$$\text{p}K_a = \frac{1}{2.303RT} \Delta G \quad (9)$$

where ΔG is the Gibbs free energy of the reaction in eq 8, R is the gas constant, and T is the absolute temperature. According to this definition, the greater the $\text{p}K_a$ value, the stronger the basicity of the amine and the more endothermic the reaction in eq 8. In this work, we are concerned only with the trends in

basicity and not the absolute values. The free energy of the proton is constant for all amines, so one just needs to calculate the free energy difference between the protonated and unprotonated amine to calculate the relative basicity of an amine. The free energy calculation involves computing the solvation free energy for the cations. However, the implicit solvent model is known to be inadequate for predicting the solvation free energy for cations.⁶⁰ We therefore used the cluster-continuum model in these solvation free energy calculations. This model has given excellent results for calculating $\text{p}K_a$ values of acids and conjugate bases.⁶⁰⁻⁶² The solvation free energy of a cation is calculated in the cluster-continuum model as

$$\Delta G_{\text{solv}}^*(\text{A}^+) = \Delta G_{\text{clust}}^\circ(\text{A}^+(\text{S})_n) + \Delta G_{\text{solv}}^*(\text{A}^+(\text{S})_n) + n\Delta G_{\text{vap}}(\text{S}) \quad (10)$$

where $\Delta G_{\text{solv}}^*(\text{A}^+)$ is the solvation free energy of A^+ at a concentration of 1 mol/L, $\Delta G_{\text{clust}}^\circ(\text{A}^+(\text{S})_n)$ is the gas-phase clustering free energy at 1 atm, $\Delta G_{\text{solv}}^*(\text{A}^+(\text{S})_n)$ is the solvation free energy of a cluster containing A^+ and solvent S , and $\Delta G_{\text{vap}}(\text{S})$ is the vaporization free energy of the solvent. The computational details of the cluster-continuum model are given by Pliego and Riveros.⁶⁰ In this section, geometry optimizations in the gas phase were performed at the B3LYP/6-311++G(d,p) level of theory, and single-point energy calculations utilized the MP2/aug-cc-pVDZ level of theory. Solvation free energies were obtained at the MP2/aug-cc-pVDZ level within the CPCMC model with UAHF radii. The idea of the cluster-continuum model is to represent the ion as a cluster formed by the ion and an optimal number of solvent molecules and then to solvate the cluster using the continuum model. The optimal number of solvent molecules is chosen in such a way as to achieve a minimum in the solvation free energy.⁶² In Table S1 (see the Supporting Information), we show that the optimal number of water molecules is one for all amines except $\alpha\text{-F-MEAH}^+$. The calculated Gibbs free energies for the unprotonated and protonated amines in aqueous solution are presented in Table S2 of the Supporting Information.

Experimental. Monoethanolamine, 2-aminopropanol ($\alpha\text{-CH}_3\text{-MEA}$), and 2-hydroxypropylamine ($\beta\text{-CH}_3\text{-MEA}$) were purchased from Aldrich and used as received. Research grade CO₂ was purchased from Airgas Specialty Gases and used as received. The heats of reaction were measured using an OmniCal Inc. ReactMax-Z3-UL calorimeter. Hasteloy-C reactor vessels (25 mL) supplied by the calorimeter manufacturer that can withstand pressures of up to 34.5 bar were used. An additional stainless steel vessel was added adjacent to the calorimeter to supply heated CO₂ to the reactor vessel. This additional vessel was placed in a heated box fitted with a circulating fan. A Sierra Instruments Smart-Trak2Model C100L mass flow controller was installed between the reactor vessel and the additional stainless steel CO₂ storage vessel to measure the amount of CO₂ added to the reactor. This mass flow controller has an integrated totalizer to measure the total flow of a gas over a user-defined time.

The reactor vessel was filled with ~ 1.5 g of sample, and a magnetic stir bar was added. The exact volume of the sample was calculated using the exact weight and density of each sample. The total volume of the reactor system was 27.7 mL. The reactor was sealed and placed inside the calorimeter, with stirring set to ~ 530 rpm, and the temperatures of the calorimeter and the CO₂ storage vessel were set to 40 °C. The CO₂ storage vessel was filled with CO₂ from the supply tank. The system was then allowed to come to equilibrium for 1–2 h. When both

TABLE 3: Relative Basicities (kilocalories per mole) of Substituted MEA

species	relative basicity	species	relative basicity
MEA	279.0	α -OH-MEA	275.5
α -CH ₃ -MEA	277.9	β -OH-MEA	281.3
β -CH ₃ -MEA	278.9	α -OCH ₃ -MEA	273.4
α -NH ₂ -MEA	277.8	β -OCH ₃ -MEA	278.7
β -NH ₂ -MEA	279.5	α -F-MEA	266.7
		β -F-MEA	275.9

the heat flow and the calorimeter temperature achieved steady state, the system was considered to be at equilibrium.

The totalizer on the mass flow controller was reset to zero, and the reactor was filled with approximately 430 standard cm³ of CO₂. A large excess of CO₂ was added to the reactor to ensure complete reaction of the sample. The value on the mass flow controller totalizer was recorded, and the reaction was allowed to proceed until the heat flow returned to the baseline value. The total reaction time was approximately 100 min. The baseline value for the heat flow was established and subtracted from the raw data. The baseline-subtracted heat flow was then integrated over the reaction time to determine the total reaction heat. The total amount of CO₂ remaining in the headspace of the reactor was calculated from the pressure, temperature, and headspace volume. The total amount of CO₂ absorbed by the sample was calculated by subtracting the CO₂ remaining in the headspace at the end of the reaction from the total CO₂ added to the system initially. The heat of reaction was then calculated by dividing the total reaction heat by the amount of CO₂ absorbed by the sample.

Results and Discussion

Basicity of Substituted MEA. There is some debate in the literature about the exact details of the mechanism for the reaction between MEA and CO₂. Several different mechanisms have been proposed, including a single-step reaction mechanism,⁴⁶ a two-step mechanism that proceeds via zwitterion formation,^{59,63,64} and a two-step mechanism involving carbamic acid as an intermediate.⁶⁵ However, there is general agreement that Lewis acid–base interactions between amine and CO₂ are important in both carbamate and carbamic acid reactions. Therefore, the basicity of an amine should have a significant influence on the heat of reaction. We have calculated the relative basicity of each of the substituted MEAs; these values are listed in Table 3. We note that the substitution site has an important influence on the change in basicity. The relative basicities of NH₂-MEA and OH-MEA for α site substitution are 277.8 and 275.5 kcal/mol, respectively, which is lower than that of the parent molecule MEA (279.0 kcal/mol). However, relative basicities of the corresponding β site substituted species are 279.5 and 281.3 kcal/mol, respectively, which are higher than the basicity of MEA. We have plotted the relative basicity of substituted MEA as a function of the electronegativity of the substituent group (taken from Table 1) in Figure 1. The α - and β -substituted compounds are plotted separately to avoid convolution with the site effects noted above. We see that α -substituted MEA shows a monotonic decrease in basicity with increasing electronegativity, but the decrease is highly nonlinear. Conversely, the basicity of β -substituted compounds initially increases and then decreases with increasing electronegativity. Hence, there is no simple relationship between electronegativity and basicity. Our findings are in agreement with the observation that several factors affect the basicity of a molecule in solution, including inductive or polarization effects, solvation free energy, the ability to form intramolecular hydrogen bonds, etc.⁶⁶

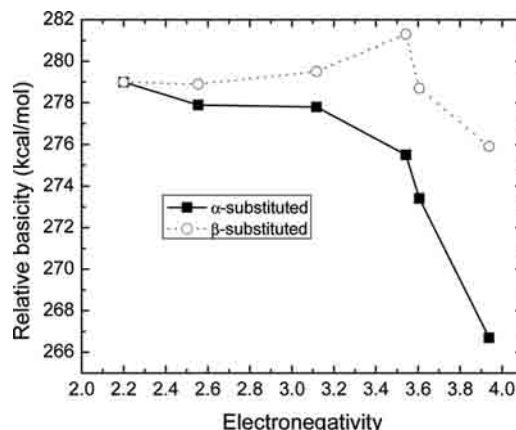


Figure 1. Relative basicity plotted as a function of the electronegativity of the substituent group for α -substituted (■) and β -substituted (○) MEA. Lines are drawn as a guide to the eye.

Heats of Reaction of Carbamic Acid. The geometries of the lowest-energy carbamic acid conformations are given in Figure 2, along with N–C bond lengths for the C atom of the COO group and some key intramolecular hydrogen bonds. The N–C bond length for the unsubstituted MEA is 1.34 Å. This bond length lies between typical N–C single (1.47 Å) and double (1.27 Å) bond lengths. We also note that the four atoms (NCOO) lie in the same plane. The bond length and the coplanarity of the NCOO group indicate that π conjugation is formed between the lone pair of electrons of N, the O atom of OH in COOH, and the CO π bond. We have examined the molecular orbitals to verify the existence of π conjugation in the carbamic acid product. Inspection of the orbitals revealed that the 10th highest occupied molecular orbital (HOMO-9) is the highest occupied orbital that has characteristics of π conjugation bonding between the COO group and the N atom. We have plotted the HOMO-9 orbitals in Figure 3. The formation of π conjugation orbitals increases the stability of the compound. In addition, an intramolecular hydrogen bond is formed between the H atom of the OH group connected to the CH₂ group and the O atom of the CO carboxylic acid group in the lowest-energy conformer. This hydrogen bond also increases the stability of the carbamic acid product. This is illustrated in Figure 2a. We have found that other higher-energy conformations typically have intramolecular hydrogen bonds with different groups of atoms. For example, an MEA carbamic acid conformer was found having a hydrogen bond involving the H atom of the OH group connected to the CH₂ group and the O atom of the OH group in COOH. The energy of this conformer is ~ 2 kcal/mol higher than that of the lowest-energy conformer. This indicates that there is a wide range of energies associated with intramolecular hydrogen bonds. The Boltzmann averaged heat of reaction for forming carbamic acid from MEA and CO₂ is calculated to be -8.9 kcal/mol at the MP2/aug-cc-pVDZ//B3LYP/6-311++G(d,p) level.

The lowest-energy conformers of carbamic acids formed from substituted MEA all share the same planar core among four atoms (COO and N) as discussed above for the parent compound. However, some of the substituted compounds do not have intramolecular hydrogen bonds discussed above and shown in Figure 2a for the parent compound as their lowest-energy conformers. See conformers e, f, and h–k in Figure 2. This may be a result of increased ring strain for the formation of seven-membered ring hydrogen bonds or a decrease in the formation energy of the hydrogen bond due to chemical effects. By way of illustration, the lowest-energy conformations in

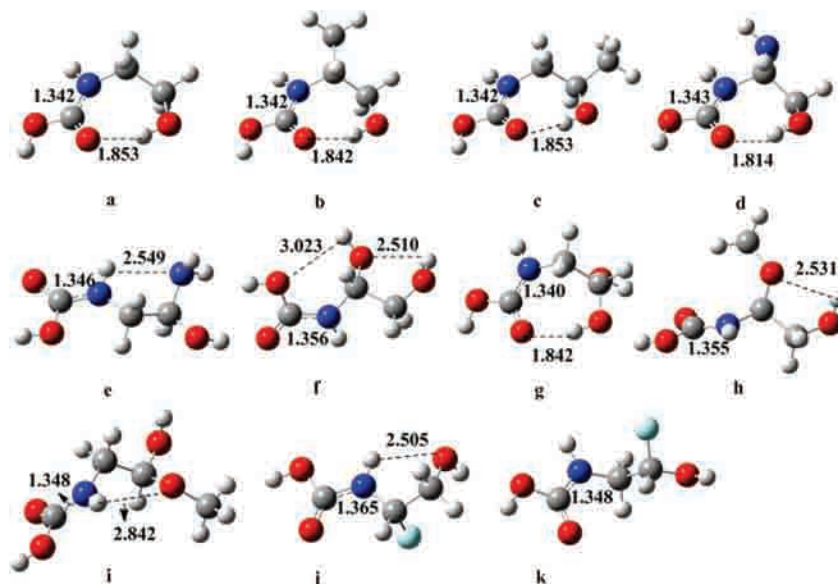


Figure 2. Lowest-energy conformers of carbamic acids formed from reactions of CO₂ with (a) MEA, (b) α -CH₃-MEA, (c) β -CH₃-MEA, (d) α -NH₂-MEA, (e) β -NH₂-MEA, (f) α -OH-MEA, (g) β -OH-MEA, (h) α -OCH₃-MEA, (i) β -OCH₃-MEA, (j) α -F-MEA, and (k) β -F-MEA. C-N bond lengths and hydrogen bond (dashed lines) lengths are given in angstroms. Red spheres denote oxygen, blue spheres nitrogen, gray spheres carbon, and white spheres hydrogen.

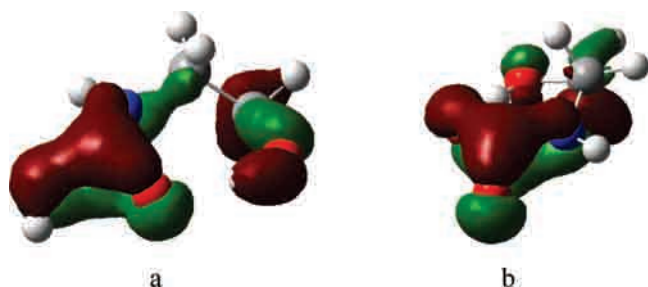


Figure 3. Tenth highest occupied molecular orbitals (HOMO-9) of the lowest-energy conformations of MEA-based carbamic acid (a) and MEA-based carbamate anion (b). The molecular orbitals plotted are associated with π conjugation bonding between the lone pair of electrons of the N atom and the O atom of the COO group, and the CO π bond.

TABLE 4: Computed Heats of Reaction (kilocalories per mole) for Carbamic Acid

species	ΔH	species	ΔH
MEA	-8.9	α -OH-MEA	-6.7
α -CH ₃ -MEA	-7.6	β -OH-MEA	-9.8
β -CH ₃ -MEA	-8.8	α -OCH ₃ -MEA	-7.1
α -NH ₂ -MEA	-7.0	β -OCH ₃ -MEA	-9.0
β -NH ₂ -MEA	-8.9	α -F-MEA	-4.1
		β -F-MEA	-8.4

panels e, f, h, and i of Figure 2 involve intramolecular NH \cdots NH₂, HO \cdots HO \cdots HO, CH₃O \cdots HO, and NH \cdots OCH₃ hydrogen bonds, respectively. We see from inspection of Table 4 that the carbamic acid heats of reaction do not change a great deal as the substituent group is changed, except for α -F-MEA. The heat of reaction is 4.8 kcal/mol less exothermic for α -F-MEA than for MEA; the next largest change is a 2.2 kcal/mol less exothermic value for α -OH-MEA.

We have plotted the heat of reaction for carbamic acid as a function of amine basicity in Figure 4. We observe a roughly linear relationship between the heat of reaction and the relative basicity of the substituted amine with a correlation coefficient (R^2) of 0.85. Notwithstanding the scatter about the linear fit to the data, it is clear from inspection of the data that in general, the stronger the base the more exothermic the heat of reaction.

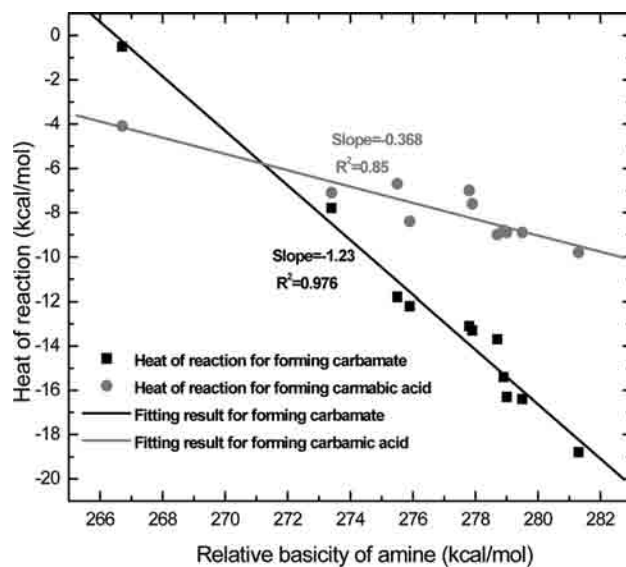


Figure 4. Heats of reaction for forming carbamate and carbamic acid as a function of the relative basicity of the substituted MEA.

Carbamate Heats of Reaction. We now consider the geometries and energetics of carbamates. The lowest-energy conformations of the ammonium cations formed from substituted MEA are presented in Figure 5. Hydrogen bonds are also identified for each cation in Figure 5. We note that for all cations except β -NH₂-MEA (Figure 5e), the lowest-energy conformers involve the formation of intramolecular HO \cdots HNH₂ hydrogen bonds. The ground state conformer for the β -NH₂-MEA-based cation has a H₂N \cdots HNH₂ hydrogen bond and is 1.7 kcal/mol lower in energy than the conformation with a HO \cdots HNH₂ hydrogen bond. The preference for the H₂N \cdots HNH₂ hydrogen bond can be rationalized by noting that in general, the H₂N lone pair of electrons is a stronger hydrogen bond acceptor (electron donor) than the O atom of the OH group. We also note from Figure 5 that several of the ammonium cations form double hydrogen bonds. This is the case for α -NH₂-MEA, α -OH-MEA, β -OH-MEA, and β -OCH₃-MEA, as seen in panels d, f, g, and i of Figure 5, respectively.

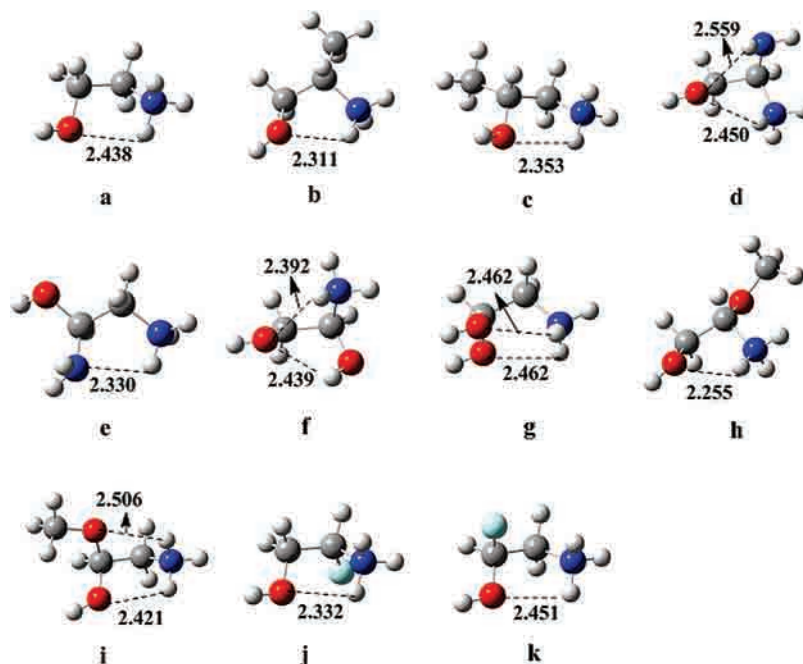


Figure 5. Lowest-energy conformers of ammonium cations formed from reactions of CO_2 with (a) MEA, (b) $\alpha\text{-CH}_3\text{-MEA}$, (c) $\beta\text{-CH}_3\text{-MEA}$, (d) $\alpha\text{-NH}_2\text{-MEA}$, (e) $\beta\text{-NH}_2\text{-MEA}$, (f) $\alpha\text{-OH-MEA}$, (g) $\beta\text{-OH-MEA}$, (h) $\alpha\text{-OCH}_3\text{-MEA}$, (i) $\beta\text{-OCH}_3\text{-MEA}$, (j) $\alpha\text{-F-MEA}$, and (k) $\beta\text{-F-MEA}$. Hydrogen bonds are indicated by dashed lines, and bond lengths are given in angstroms. Atom definitions are as in Figure 2.

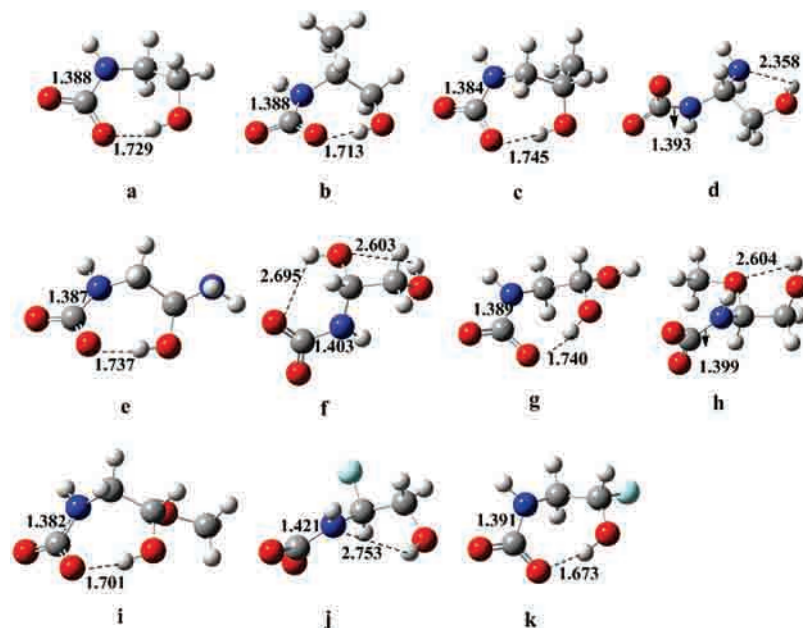


Figure 6. Lowest-energy conformers of carbamate anions formed from reaction of CO_2 with (a) MEA, (b) $\alpha\text{-CH}_3\text{-MEA}$, (c) $\beta\text{-CH}_3\text{-MEA}$, (d) $\alpha\text{-NH}_2\text{-MEA}$, (e) $\beta\text{-NH}_2\text{-MEA}$, (f) $\alpha\text{-OH-MEA}$, (g) $\beta\text{-OH-MEA}$, (h) $\alpha\text{-OCH}_3\text{-MEA}$, (i) $\beta\text{-OCH}_3\text{-MEA}$, (j) $\alpha\text{-F-MEA}$, and (k) $\beta\text{-F-MEA}$. C–N and hydrogen bond (dashed lines) lengths are given in angstroms. Atom definitions are as in Figure 2.

The lowest-energy conformations of the carbamate anions, along with N–C bond lengths and hydrogen bond lengths, are shown in Figure 6. Similar to the cations, the anions also involve the formation of different types of intramolecular hydrogen bonds. The lowest-energy conformers for most of the carbamate anions involve hydrogen bonds between the O atom of the COO^- group and the H atom of the OH group (see Figure 6a–c,e,g,i,k). However, the anions based on $\alpha\text{-NH}_2\text{-MEA}$, $\beta\text{-OH-MEA}$, $\alpha\text{-OCH}_3\text{-MEA}$, and $\alpha\text{-F-MEA}$ involve formation of other types of hydrogen bonds. Perhaps the most striking thing about the anions shown in Figure 6 is that the four atoms (COO and N) lie in the same plane for all of the conformers. This is also the case for the carbamic acid conformers shown

in Figure 2, as discussed previously. This indicates that the NCOO group of the anions also involves π conjugation. We here discuss the MEA-based carbamate anion as an example. The N–C bond length is 1.39 Å (Figure 6a), which lies between the N–C single and double bond lengths of 1.47 and 1.27 Å, respectively. The π conjugation character of the NCOO group can also be seen by plotting the molecular orbitals, as shown in Figure 3b.

The total and stepwise (eqs 3 and 4, respectively) heats of reaction for carbamate formation are listed in Table 5. We observe that the heats of reaction for the first step, ΔH_1 given by eq 3, are very sensitive to the substituent group, changing from 7.4 kcal/mol for $\alpha\text{-F-MEA}$ to -11.6 kcal/mol for $\beta\text{-OH-}$

TABLE 5: Heats of Reaction (kilocalories per mole) for the First Step, ΔH_1 from eq 3, the Second Step, ΔH_2 from eq 4, and the Total Reaction for Formation of Carbamate with Substituted MEA

species	ΔH_1	ΔH_2	ΔH
MEA	-9.7	-6.6	-16.3
α -CH ₃ -MEA	-7.1	-6.2	-13.3
β -CH ₃ -MEA	-8.9	-6.5	-15.4
α -NH ₂ -MEA	-7.9	-5.2	-13.1
β -NH ₂ -MEA	-10.7	-5.7	-16.4
α -OH-MEA	-6.1	-5.7	-11.8
β -OH-MEA	-11.6	-7.2	-18.8
α -OCH ₃ -MEA	-2.3	-5.5	-7.8
β -OCH ₃ -MEA	-7.8	-5.9	-13.6
α -F-MEA	7.4	-7.9	-0.5
β -F-MEA	-5.3	-6.9	-12.2

TABLE 6: Comparison of Calculated and Experimentally Determined Heats of Reaction (kilocalories per mole) for Carbamate Formation with Substituted MEA

species	calculated ΔH	experimental ΔH
MEA	-16.3	-17.3 \pm 1.3
α -CH ₃ -MEA	-13.3	-12.9 \pm 1.2
β -CH ₃ -MEA	-15.4	-15.6 \pm 1.3

MEA. In contrast, heats of reaction in the second step, ΔH_2 from eq 4, range from -5.2 kcal/mol for α -NH₂-MEA to -7.9 kcal/mol for α -F-MEA. Total heats of reaction vary by more than 18 kcal/mol, from -0.5 kcal/mol for α -F-MEA to -18.8 kcal/mol for β -OH-MEA. We note that the implicit solvent model is known to be inaccurate for computing solvation free energies of ions. This affects the calculations in both eqs 3 and 4. However, the errors in these calculations, caused by inaccurate calculation of the solvation free energy for the ions, will largely cancel out because the isolated solvated ions are intermediate products in the thermodynamic path. Hence, we expect the total heats of reaction to be fairly accurate. We have plotted the carbamate heats of reaction as a function of the basicity of the amine in Figure 4. We see that the heats of reaction are a linear function of the amine basicity. The correlation coefficient (R^2) equals 0.976, indicating a good fit of the data. Hence, we can say with a good deal of confidence that the more basic the amine, the more exothermic the heat of reaction. This observation gives us both a design tool for modifying ΔH and a method for screening candidate amines.

We have experimentally determined the total heats of reaction for the parent MEA molecule as well as the two commercially available α - and β -methyl derivatives. The measured ΔH values are listed in Table 6. Our measured heat of reaction for MEA is -17.3 \pm 1.1 kcal/mol. This value is in reasonably good agreement with the value reported by Kim and Svendsen⁶⁷ of -19.1 kcal/mol at 313 K. Our value is also in very good agreement with the value we calculated by fitting the equilibrium constants reported by Jou et al.⁶⁸ to an Arrhenius equation. The linear fit to their data gave an R^2 of 0.9935, and the slope yielded a heat of reaction of -16.5 kcal/mol. We also report the predicted values of ΔH for MEA, α -CH₃-MEA, and β -CH₃-MEA in Table 6 for comparison. The calculated and experimentally measured values are in remarkable agreement. Not only are the trends predicted by our calculations verified by the experimental data, but our predicted ΔH values agree with the experiments within the estimated experimental errors. This level of agreement is certainly fortuitous, given the approximations we have made. However, we have a high degree of confidence that the trends predicted from the calculations are correct. We

note that the experimental data were measured at 313 K while the calculations were performed at 298 K. We do not expect ΔH to vary significantly with temperature over this small temperature range. As a test, we have computed ΔH for MEA at 313 K, obtaining a value of -16.2 kcal/mol, in excellent agreement with the value of -16.3 kcal/mol at 298 K.

Tuning the Amine:CO₂ Stoichiometric Ratio. We note that the linear relationships between the heats of reaction and the basicity for carbamic acid and carbamate formation have very different slopes, as seen from Figure 4. The carbamic acid reaction displays a weak dependence on the basicity, having a slope of -0.368 (Figure 4). In contrast, the slope of the linear fit of the carbamate heats of reaction to the amine basicity is -1.23. Hence, there is a crossing point in the heats of reaction that is apparent from the plot shown in Figure 4. The heats of reaction should be equal, according to the linear fits, for an amine with a relative basicity of 271 kcal/mol, and the corresponding ΔH for both products should be -6 kcal/mol. This prediction is consistent with the observation that the heats of reaction for α -OCH₃-MEA, having a basicity of 273.4 kcal/mol, are -7.1 and -7.8 kcal/mol for the formation of carbamic acid and carbamate, respectively. Our simple model predicts that carbamic acid formation will be thermodynamically favored for amines having relative basicities of <271 kcal/mol. Indeed, the calculated heats of reaction for α -F-MEA are -4.1 and -0.5 kcal/mol for the formation of carbamic acid and carbamate, respectively. Assuming no kinetic limitations, our calculations predict that the relative amounts of carbamic acid and carbamate would be \sim 440:1 in solution at room temperature. This offers the possibility of tuning the stoichiometry of the reaction between the 2:1 carbamate and 1:1 carbamic acid amine:CO₂ ratios.

Conclusions

We have investigated the influence of various substituent groups on the heats of reaction of substituted MEA with CO₂ using ab initio calculations at the MP2/aug-cc-pVDZ level, coupled with geometries generated from B3LYP/6-311++G(d,p) density functional theory, in both cases using conductor-like polarizable continuum model formalism to account for solvent effects. Two reaction products were considered: carbamate, having a 2:1 amine:CO₂ reaction stoichiometry, and carbamic acid, having a 1:1 stoichiometry. We have considered five different substituent groups on both the α - and β -carbons of MEA, namely, CH₃, NH₂, OH, OCH₃, and F. We have taken experimental measurements of the heats of reaction for MEA and the α - and β -substituted MEA with CH₃ as the substituent. The predicted values of ΔH are in excellent agreement with the experimentally measured values, giving us confidence in our predictions for the other substituent groups. We have also computed the relative basicities of the various substituted amines. Our results indicate that heats of reaction for forming both carbamic acid and carbamate are linear functions of the relative basicities of substituted MEA: stronger basicity leads to more exothermic heats of reaction. Hence, a general strategy for reducing the heat of reaction for carbamate formation is to decrease the basicity of the amine. Importantly, the carbamate heats of reaction are much more sensitive to changes in the basicity than carbamic acid heats of reaction. Our linear models predict that carbamic acid formation will be thermodynamically favored over carbamate formation for amines with a relative basicity of <271 kcal/mol. Assuming no kinetic limitations, we predict that carbamic acid will be formed almost exclusively for α -F-MEA, which has a relative basicity of 266.7 kcal/mol.

Acknowledgment. Calculations were performed at the University of Pittsburgh Center for Simulation and Modeling. This material is based upon work supported by the Department of Energy, National Energy Technology Laboratory, under Award number DE-NT0005310. This report was prepared as an account of work sponsored by an agency of the United States Government. Neither the United States Government nor any agency thereof, nor any of their employees, makes any warranty, express or implied, or assumes any legal liability or responsibility for the accuracy, completeness, or usefulness of any information, apparatus, product, or process disclosed, or represents that its use would not infringe privately owned rights. Reference herein to any specific commercial product, process, or service by trade name, trademark, manufacturer, or otherwise does not necessarily constitute or imply its endorsement, recommendation, or favoring by the United States Government or any agency thereof. The views and opinions of authors expressed herein do not necessarily state or reflect those of the United States Government or any agency thereof.

Supporting Information Available: Solvation free energies for univalent cations calculated by the cluster-continuum model and Gibbs free energies for unprotonated and protonated substituted MEA in aqueous solution. This material is available free of charge via the Internet at <http://pubs.acs.org>.

References and Notes

- Puxty, G.; Rowland, R.; Allport, A.; Yang, Q.; Bown, M.; Burns, R.; Maeder, M.; Attalla, M. *Environ. Sci. Technol.* **2009**, *43*, 6427–6433.
- CSIRO. *The heat is on: The Future of Energy in Australia*; Commonwealth Scientific and Industrial Research Organisation: Canberra, Australia, 2006.
- Murphy, J. T.; Jones, A. P. DOE/NETL's Carbon Capture R&D Program for Existing Coal-Fired Power Plants, DOE/NETL-2009/1356, February 2009.
- Rao, A. B.; Rubin, E. S. *Environ. Sci. Technol.* **2002**, *36*, 4467–4475.
- Singh, D.; Croiset, E.; Douglas, P. L.; Douglas, M. A. *Energy Convers. Manage.* **2003**, *44*, 3073–3091.
- Aaron, D.; Tsouris, C. *Sep. Sci. Technol.* **2005**, *40*, 321–348.
- Veltman, K.; Singh, B.; Hertwich, E. G. *Environ. Sci. Technol.* **2010**, *44*, 1496–1502.
- Schach, M. O.; Schneider, R.; Schramm, H.; Repke, J. U. *Ind. Eng. Chem. Res.* **2010**, *49*, 2363–2370.
- Pellegrini, G.; Strube, R.; Manfrida, G. *Energy* **2010**, *35*, 851–857.
- Korre, A.; Nie, Z. G.; Durucan, S. *Int. J. Greenhouse Gas Control* **2010**, *4*, 289–300.
- MacDowell, N.; Florin, N.; Buchard, A.; Hallett, J.; Galindo, A.; Jackson, G.; Adjiman, C. S.; Williams, C. K.; Shah, N.; Fennell, P. *Energy Environ. Sci.* **2010**, *3*, 1645–1669.
- Al-Juaied, M.; Rochelle, G. T. *Chem. Eng. Sci.* **2006**, *61*, 3830–3837.
- Al-Juaied, M.; Rochelle, G. T. *Ind. Eng. Chem. Res.* **2006**, *45*, 2473–2482.
- Pacheco, M. A.; Kaganoi, S.; Rochelle, G. T. *Chem. Eng. Sci.* **2000**, *55*, 5125–5140.
- Oyekan, B. A.; Rochelle, G. T. *Ind. Eng. Chem. Res.* **2006**, *45*, 2457–2464.
- Goff, G. S.; Rochelle, G. T. *Ind. Eng. Chem. Res.* **2004**, *43*, 6400–6408.
- Abu-Zahra, M. R. M.; Schneiders, L. H. J.; Niederer, J. P. M.; Feron, P. H. M.; Versteeg, G. F. *Int. J. Greenhouse Gas Control* **2007**, *1*, 37–46.
- Derks, P. W. J.; Hogendoorn, J. A.; Versteeg, G. F. *J. Chem. Thermodyn.* **2010**, *42*, 151–163.
- Hartono, A.; da Silva, E. F.; Svendsen, H. F. *Chem. Eng. Sci.* **2009**, *64*, 3205–3213.
- Kim, I.; Hoff, K. A.; Hessen, E. T.; Haug-Warberg, T.; Svendsen, H. F. *Chem. Eng. Sci.* **2009**, *64*, 2027–2038.
- Ciferno, J. P.; Fout, T. E.; Jones, A. P.; Murphy, J. T. *Chem. Eng. Prog.* **2009**, *105*, 33–41.
- Liu, Y. D.; Zhang, L. Z.; Watanasiri, S. *Ind. Eng. Chem. Res.* **1999**, *38*, 2080–2090.
- Veawab, A.; Tontiwachwuthikul, P.; Chakma, A. *Ind. Eng. Chem. Res.* **1999**, *38*, 3917–3924.
- Freguia, S.; Rochelle, G. T. *AIChE J.* **2003**, *49*, 1676–1686.
- Alie, C.; Backham, L.; Croiset, E.; Douglas, P. L. *Energy Convers. Manage.* **2005**, *46*, 475–487.
- Jassim, M. S.; Rochelle, G. T. *Ind. Eng. Chem. Res.* **2006**, *45*, 2465–2472.
- Idem, R.; Wilson, M.; Tontiwachwuthikul, P.; Chakma, A.; Veawab, A.; Aroonwilas, A.; Gelowitz, D. *Ind. Eng. Chem. Res.* **2006**, *45*, 2414–2420.
- McCann, N.; Maeder, M.; Attalla, M. *Ind. Eng. Chem. Res.* **2008**, *47*, 2002–2009.
- Abu-Zahra, M. R. M.; Niederer, J. P. M.; Feron, P. H. M.; Versteeg, G. F. *Int. J. Greenhouse Gas Control* **2007**, *1*, 135–142.
- Abu-Zahra, M. R. M.; Schneiders, L. H. J.; Niederer, J. P. M.; Feron, P. H. M.; Versteeg, G. F. *Int. J. Greenhouse Gas Control* **2007**, *1*, 37–46.
- Soosairakasam, I. R.; Veawab, A. *Int. J. Greenhouse Gas Control* **2008**, *2*, 553–562.
- Zhang, Y.; Chen, H.; Chen, C. C.; Plaza, J. M.; Dugas, R.; Rochelle, G. T. *Ind. Eng. Chem. Res.* **2009**, *48*, 9233–9246.
- Plaza, J. M.; Van Wagener, D.; Rochelle, G. T. *Int. J. Greenhouse Gas Control* **2010**, *4*, 161–166.
- Sartori, G.; Savage, D. W. *Ind. Eng. Chem. Fundam.* **1983**, *22*, 239–249.
- Oexmann, J.; Kather, A. *Int. J. Greenhouse Gas Control* **2010**, *4*, 36–43.
- Nguyen, T.; Hilliard, M.; Rochelle, G. T. *Int. J. Greenhouse Gas Control* **2010**, *4*, 707–715.
- Kittel, J.; Idem, R.; Gelowitz, D.; Tontiwachwuthikul, P.; Parrain, G.; Bonneau, A. *Energy Procedia* **2009**, *1*, 791–797.
- Teramoto, M.; Nakai, K.; Ohnishi, N.; Huang, Q. F.; Watari, T.; Matsuyama, H. *Ind. Eng. Chem. Res.* **1996**, *35*, 538–545.
- Khatiri, R. A.; Chuang, S. S. C.; Soong, Y.; Gray, M. *Ind. Eng. Chem. Res.* **2005**, *44*, 3702–3708.
- Serna-Guerrero, R.; Da'na, E.; Sayari, A. *Ind. Eng. Chem. Res.* **2008**, *47*, 9406–9412.
- Harlick, P. J. E.; Sayari, A. *Ind. Eng. Chem. Res.* **2007**, *46*, 446–458.
- Hicks, J. C.; Drese, J. H.; Fauth, D. J.; Gray, M. L.; Qi, G. G.; Jones, C. W. *J. Am. Chem. Soc.* **2008**, *130*, 2902–2903.
- Vaidhyanathan, R.; Iremonger, S. S.; Dawson, K. W.; Shimizu, G. K. H. *Chem. Commun.* **2009**, 5230–5232.
- Gray, M. L.; Soong, Y.; Champagne, K. J.; Pennline, H.; Baltrus, J. P.; Stevens, R. W.; Khatiri, R.; Chuang, S. S. C.; Filburn, T. *Fuel Process. Technol.* **2005**, *86*, 1449–1455.
- Gurkan, B. E.; de la Fuente, J. C.; Mindrup, E. M.; Ficke, L. E.; Goodrich, B. F.; Price, E. A.; Schneider, W. F.; Brennecke, J. F. *J. Am. Chem. Soc.* **2010**, *132*, 2116.
- da Silva, E. F.; Svendsen, H. F. *Ind. Eng. Chem. Res.* **2004**, *43*, 3413–3418.
- Mindrup, E. M.; Schneider, W. F. *Computational Comparison of Tethering Strategies for Amine Functionalised Ionic Liquids*; ACS Symposium Series; American Chemical Society: Washington, DC, 2010; Vol. 27.
- Chakraborty, A. K.; Bischoff, K. B.; Astarita, G.; Damewood, J. R., Jr. *J. Am. Chem. Soc.* **1988**, *110*, 6947–6954.
- Perdew, J. P. *Phys. Rev. B* **1986**, *33*, 8822–8824.
- Ahlich, R.; Bär, M.; Häser, M.; Horn, H.; Kölmel, C. *Chem. Phys. Lett.* **1989**, *162*, 165–169.
- Eichkorn, K.; Treutler, O.; Ohm, H.; Häser, M.; Ahlich, R. *Chem. Phys. Lett.* **1995**, *240*, 283–289.
- Frisch, M. J.; Trucks, G. W.; Schlegel, H. B.; Scuseria, G. E.; Robb, M. A.; Cheeseman, J. R.; Gaussian 03, revision C.02; Gaussian, Inc.: Wallingford, CT, 2004.
- Cossi, M.; Rega, N.; Scalmani, G.; Barone, V. *J. Comput. Chem.* **2003**, *24*, 669–681.
- Barone, V.; Cossi, M. *J. Phys. Chem. A* **1998**, *102*, 1995–2001.
- Cances, E.; Mennucci, B.; Tomasi, J. *J. Chem. Phys.* **1997**, *107*, 3032–3041.
- Miertz, S.; Scrocco, E.; Tomasi, J. *J. Chem. Phys.* **1981**, *55*, 117–125.
- Tomasi, J.; Persico, M. *Chem. Rev.* **1994**, *94*, 2027–2094.
- Barone, V.; Cossi, M.; Tomasi, J. *J. Chem. Phys.* **1997**, *107*, 3210–3221.
- Xie, H.-B.; Zhou, Y.; Zhang, Y.; Johnson, J. K. *J. Phys. Chem. A* **2010**, *114*, 11844–11852.
- Pliego, J. R.; Riveros, J. M. *J. Phys. Chem. A* **2001**, *105*, 7241–7247.
- Ding, F. Z.; Smith, J. M.; Wang, H. B. *J. Org. Chem.* **2009**, *74*, 2679–2691.

(62) Pliego, J. R.; Riveros, J. M. *J. Phys. Chem. A* **2002**, *106*, 7434–7439.

(63) Danckwerts, P. V. *Chem. Eng. Sci.* **1979**, *34*, 443–446.

(64) Caplow, M. *J. Am. Chem. Soc.* **1968**, *90*, 6795–6803.

(65) Arstad, B.; Blom, R.; Swang, O. *J. Phys. Chem. A* **2007**, *111*, 1222–1228.

(66) Kawata, M.; Ten-no, S.; Kato, S.; Hirata, F. *Chem. Phys.* **1996**, *203*, 53–67.

(67) Kim, I.; Svendsen, H. F. *Ind. Eng. Chem. Res.* **2007**, *46*, 5803–5809.

(68) Jou, F.-Y.; Mather, A. E.; Otto, F. D. *Can. J. Chem. Eng.* **1995**, *73*, 140–147.

(69) Suresh, C. H.; Koga, N. *J. Am. Chem. Soc.* **2002**, *124*, 1790–1797.

JP1081627

Appendix 4

Solvents for CO₂ Capture: Fatty Acids and Silicones

Larry N. Lewis, Robert J. Perry, Michael O'Brien, Hubert Tunchiao Lam, Malgorzata Rubinsztajn and Grigorii L. Soloveichik

Abstract

Modified low-cost, high volume fluids were modified and then investigated for their ability to react with CO₂. Reaction of ethylene diamine with either epoxidized linolenic acid methyl ester, 1, or epoxidized flax oil gave viscous products that did not react with CO₂. Use of half-hindered diamine, Dytex (hexane-1,4-diamine) in place of ethylene diamine did give products that had some low-level reactivity with CO₂. An alternative synthetic sequence to form amino-functionalized hydrocarbons was created. 1, was reacted with sodium azide to make the azido-functionalized hydrocarbon, 5, that was then reduced to the amine with LiAlH₄ to give the amino-functionalized hydrocarbon 6 where the ester group was also reduced. Alternatively 5 was catalytically reduced with H₂ to give the amino-substituted hydrocarbon methyl ester, 7. Neither 5 nor 7 were reactive with CO₂.

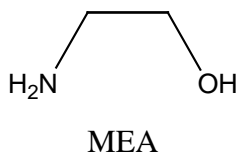
To further understand these results the reactivity of CO₂ with monoethanolamine (MEA) was compared to that of decenyl-functionalized derivatives bearing amines and with free OH or ethoxy-capped units. Reactivity with CO₂ appeared to be controlled by reactivity of the NH₂ group with CO₂ or intramolecular hydrogen bonding to the free OH. Long chain hydrocarbons also seem to limit amine amine-CO₂ reactivity.

Finally attempts to synthesize some amino-functionalized silanes via the processes developed for the long-chain hydrocarbons, were unsuccessful.

Introduction

Carbon capture and storage (CCS) is one strategy under consideration to mitigate high levels of CO₂ emitted during the burning of fossil fuels (1). GE Global research and their partners are currently working on a Department of Energy-funded program to investigate

new materials for CCS (2). In particular the DOE program is focusing on emissions from pulverized coal-fired power plants. The current benchmark material for CCS is monoethanolamine (MEA).



MEA is typically used as a 30% aqueous solution. In order to effectively decompose the MEA-CO₂ adduct (carbamate), the water must be removed in an energy-intensive process.

Thus the goals for the current program were:

- A non-aqueous, CO₂ capture solvent
- A pumpable fluid for capture of CO₂ and for transport of the CO₂-adduct for CO₂ release
- A relatively low cost solvent, available in large volumes
- Rapid kinetics for CO₂ uptake at low temperature and rapid release of CO₂ at about 100°C.

The focus of the current program was to use amine-substituted silicones. The choice of the silicone-based capture solvent was based in part on the likelihood that the carbamate product of silicone amine and carbon dioxide would have low viscosity. In general, for most amines, the reaction product with carbon dioxide is a solid. One notes the white solid deposit found on most organic amine reagents is the carbamate reaction product with CO₂.

Fatty-acid-based CO₂ Capture Solvent

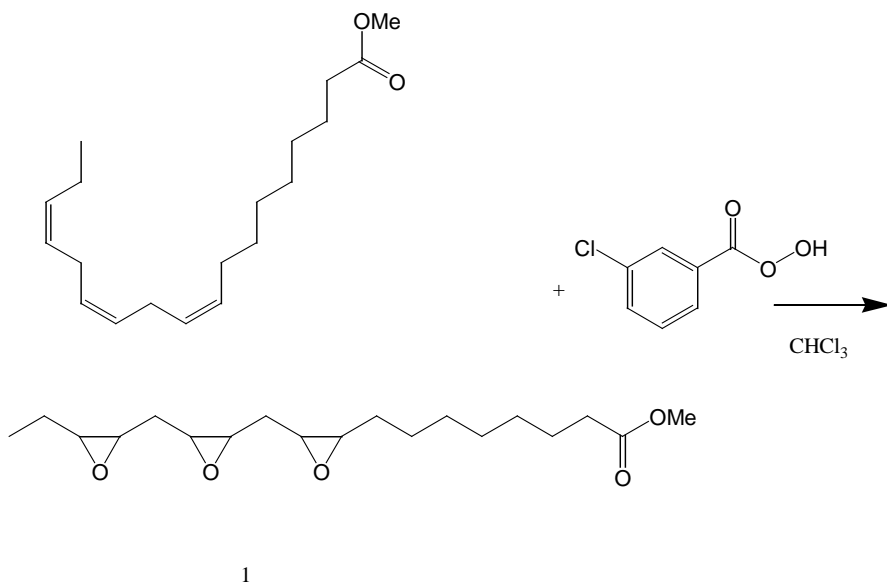
Other than water and petroleum there are no larger liquid sources on earth than plant and animal fats (3). The strategy adopted in the current approach was to prepare amine-containing derivatives of large volume plant oils. Two general approaches were considered. Plant oils with the highest degree of unsaturation were converted to their corresponding epoxide. The epoxidized oil was then reacted directly with a diamine to produce hydroxyl amine derivatives (4) or the epoxide was reacted in two steps to

produce amine by first converting the epoxide to an azide and then reducing to produce the amine (5).

Results & Discussion

Epoxidized oils. Typical plant oils are C18 triglycerides with one, two or three unsaturated groups per chain. For the present purposes, a high degree of unsaturation is desired in order to maximize the final amine content. Thus flax oil, with as many as three double bonds per chain (linolenic acid residue) was selected for study. The double bonds could be converted to epoxide in one step with *m*-Cl-perbenzoic acid (*m*CIBPA). Fortunately epoxidized flax oil (EFO) was commercially available as well. Furthermore the individual carboxylic acid or ester with olefin units (linolenic acid or linolenic acid methylester) was also commercially available and likewise these could be converted to the corresponding epoxide using *m*CIBPA.

The epoxidized linolenic acid methyl ester, 1, was prepared via the reaction of equation 1. Figures 1 and 2 show the ¹H NMR and IR spectra.



Equation 1

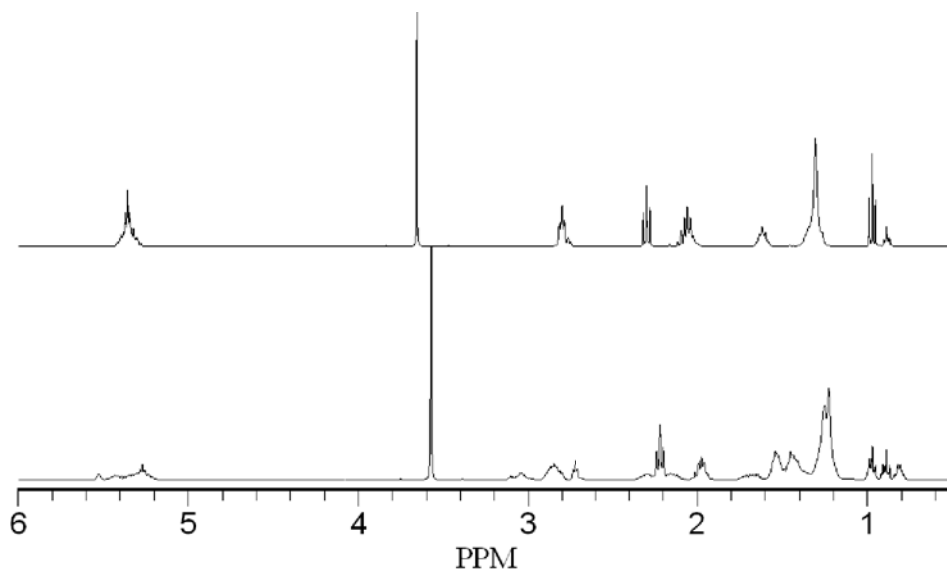


Figure 1. ^1H NMR spectrum of linolenic acid methylester (top) and 1 (bottom)

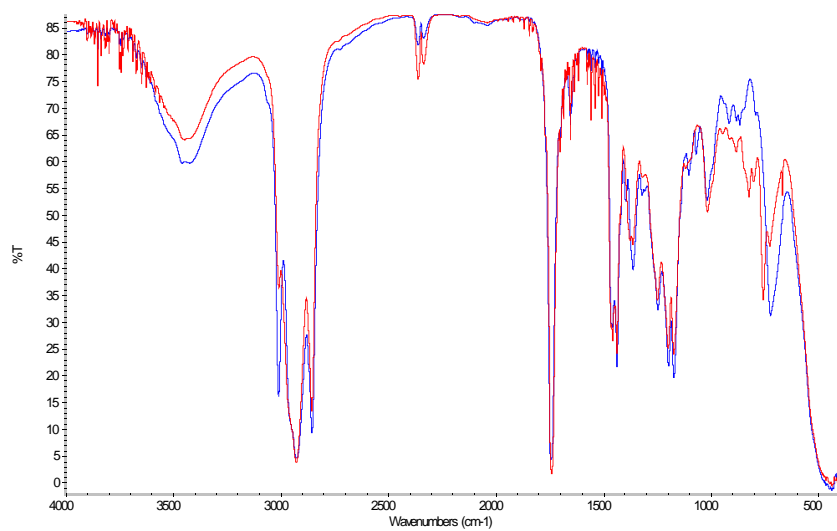
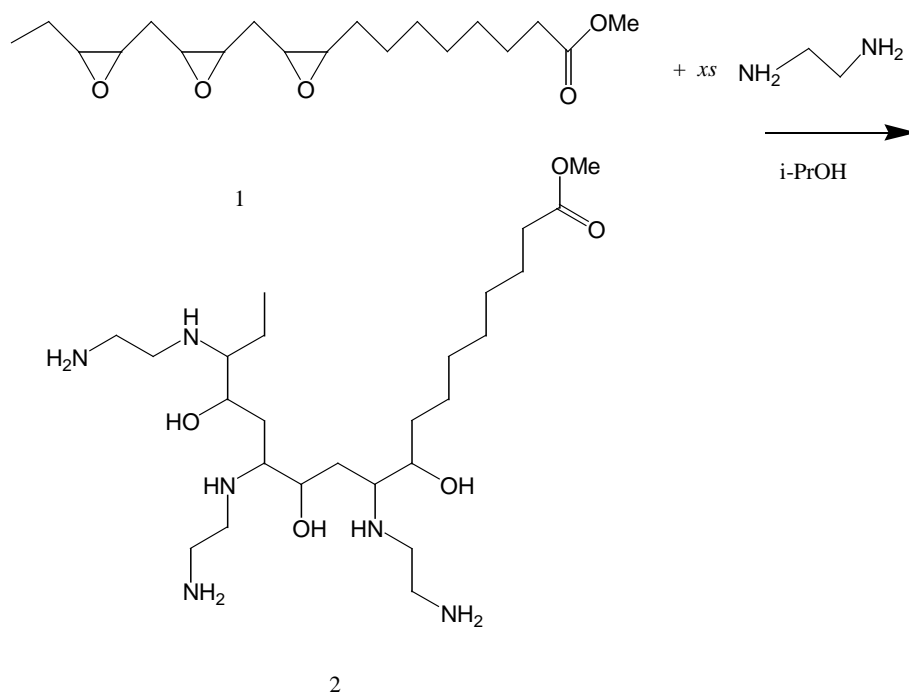


Figure 2. IR spectra for linolenic acid methylester (blue) and 1 (red)

The simplest route to preparation of amine containing species was reaction of epoxidized fatty acids or esters with diamines like ethylene diamine. The key issue with the direct diamine reaction approach is the likelihood of crosslinking leading to highly viscous or gelled product. In fact, virtually all direct reactions of diamines with epoxidized fatty acids or esters led to viscous products. Analysis of products by NMR and IR did show consumption of epoxide and likely amine reaction. Even using slow addition of epoxide to a great excess of amine led to viscous products. Epoxide 1 was reacted with excess ethylene diamine with the plan to convert 1 to 2 as shown in equation 2.



Equation 2

A very viscous semi-solid was obtained whose viscosity decreased when heated to around 100°C . Conversion of the epoxide to the amino hydroxide, 2 is likely, based on the NMR (figure 3) and, more convincingly, the IR as shown in figure 4. Figure 4 shows the consumption of the resonance due to epoxide at 1740 cm^{-1} and growth of the OH resonance in 2 at 3445 cm^{-1} .

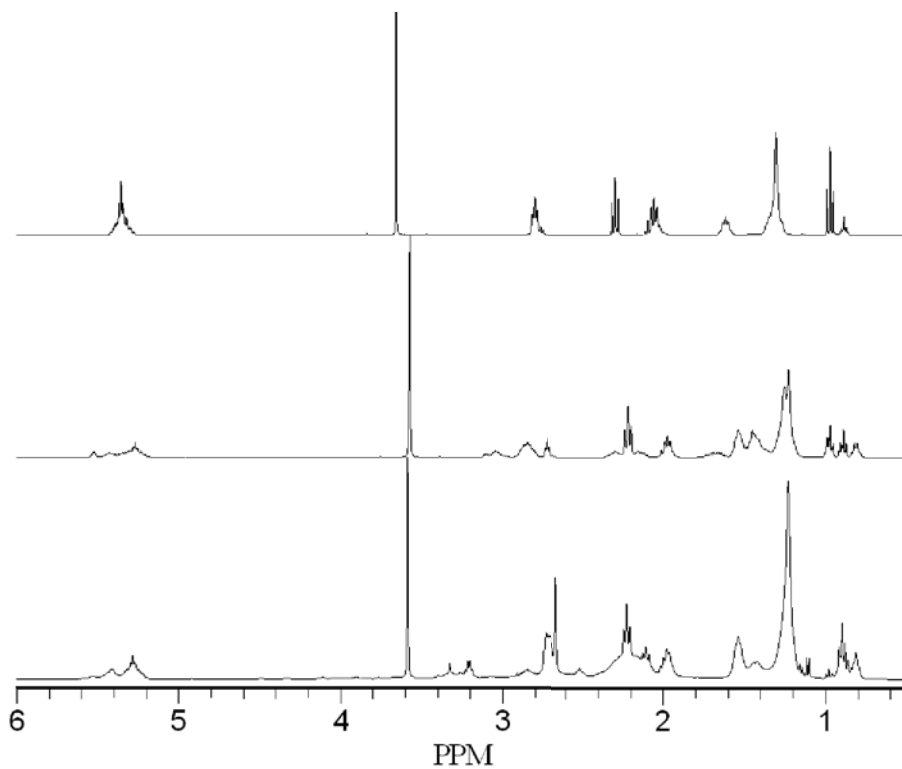


Figure 3. ^1H NMR spectra for linolenic acid methylester (top), 1 (middle) and the product of 1 with excess ethylene diamine 2 (bottom).

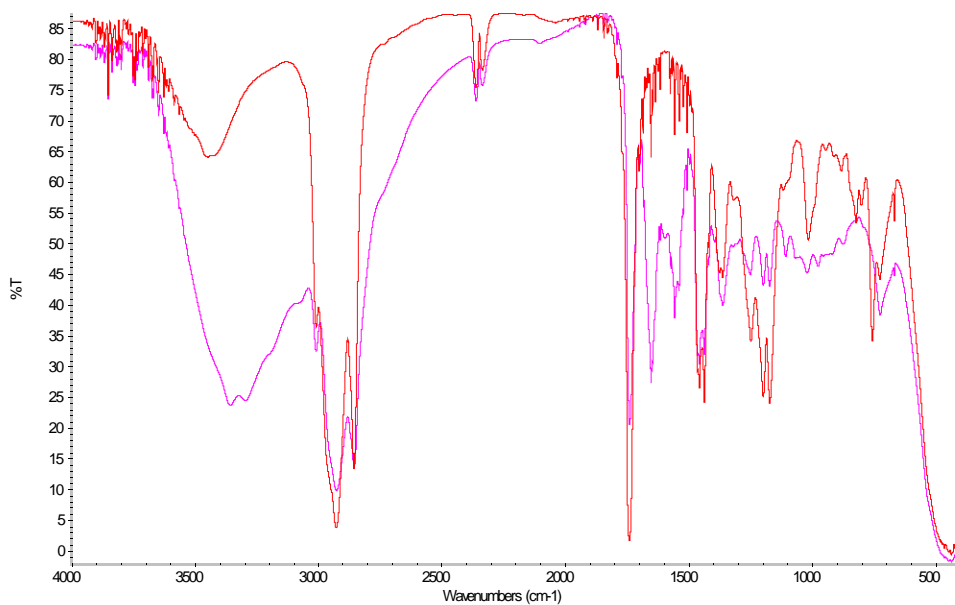
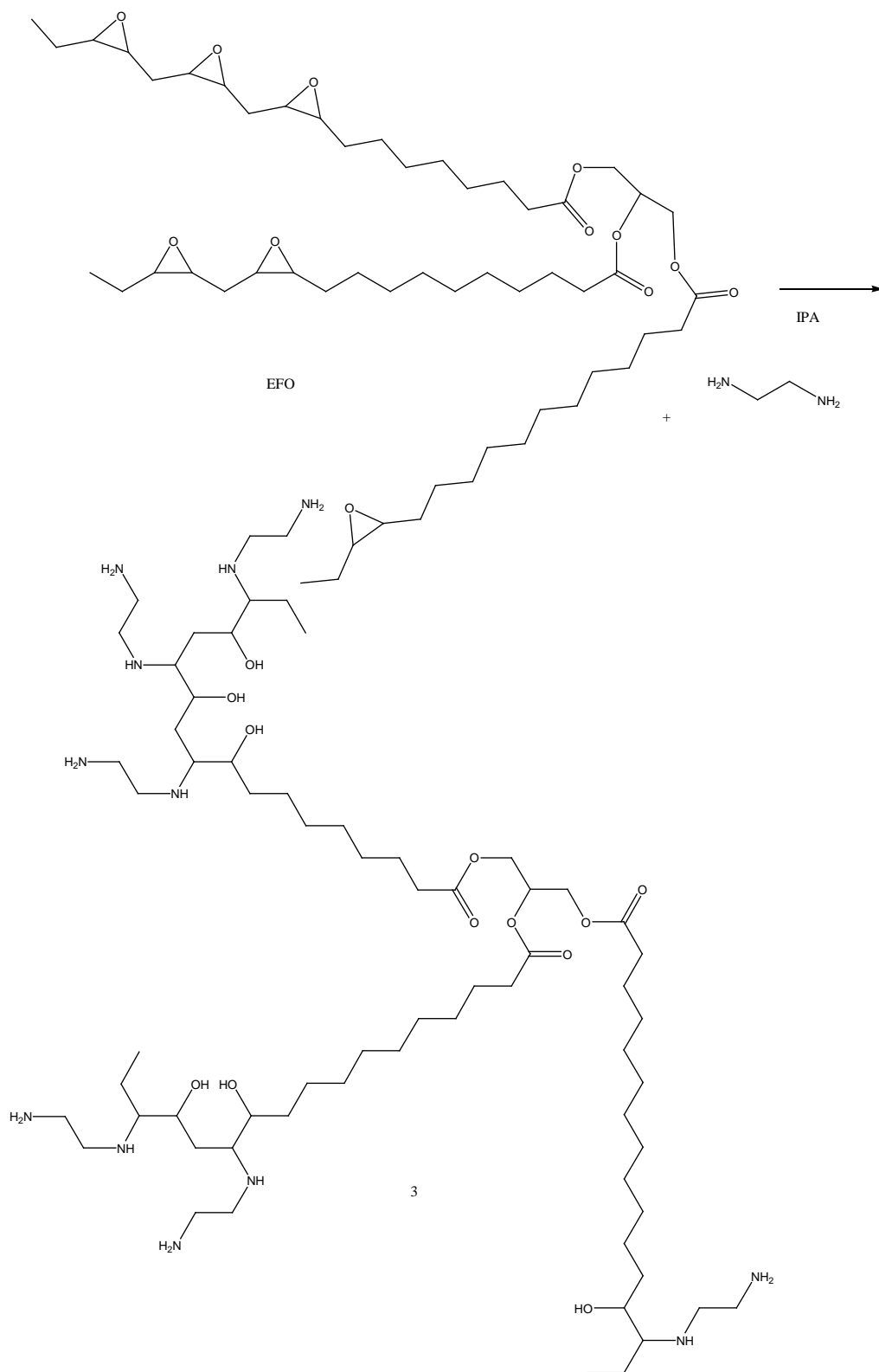


Figure 4. IR spectra for 1 (red) and 2 (pink).



Equation 3

Epoxidized flax oil (EFO) was also reacted with excess ethylene diamine, equation 3. All attempts gave viscous products. Figure 5 shows the ^1H NMR spectra for EFO and 3. In an effort to prevent crosslinking a diamine with one end hindered was used in place of ethylene diamine, Dytek, equation 4.

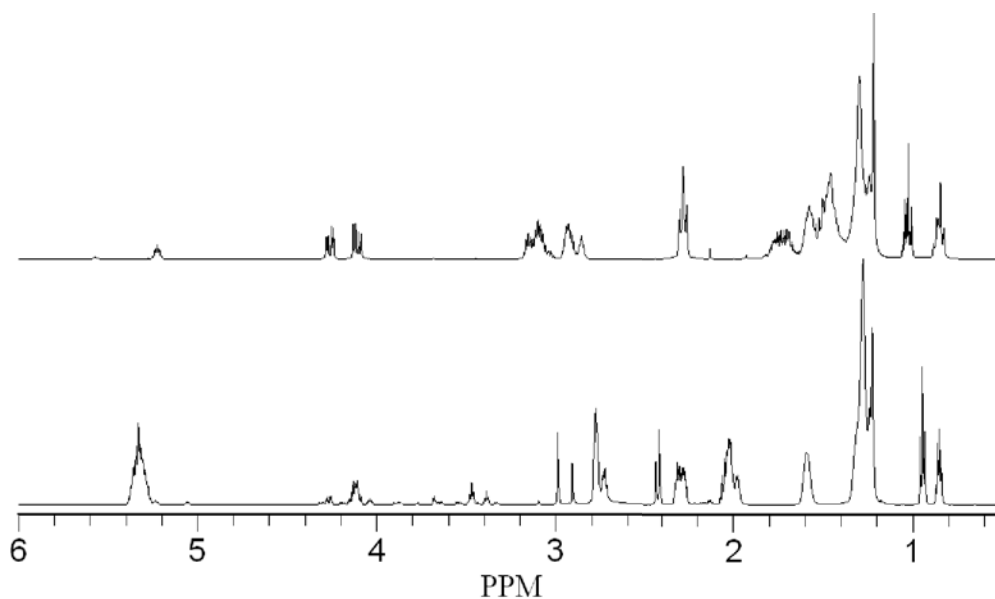
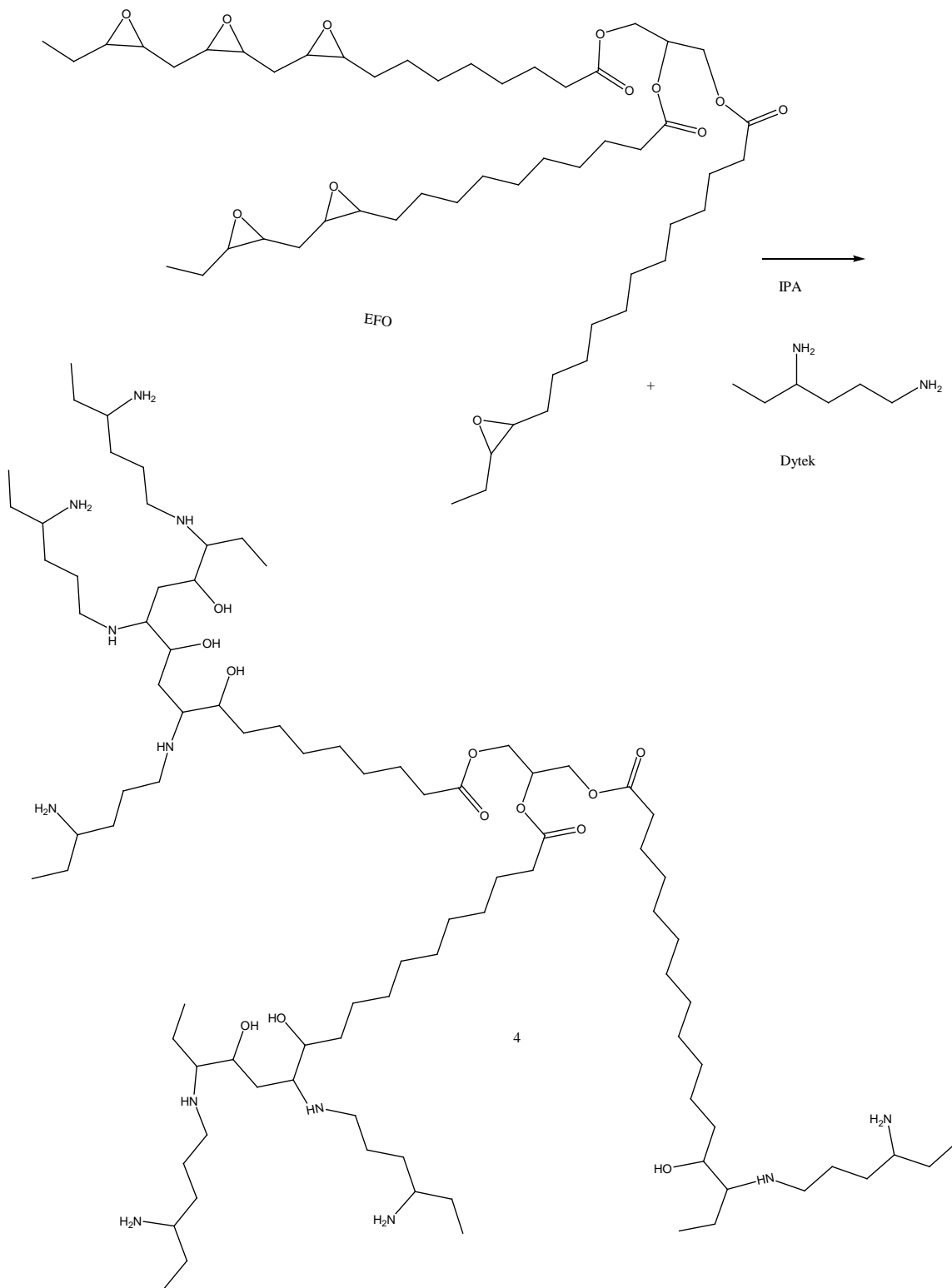


Figure 5. ^1H NMR of EFO (top) and reaction product of EFO with excess ethylene diamine, 3, (bottom).



Equation 4.

Figure 6 shows the comparison of the ^1H NMR of EFO and its product with Dytek and figure 7 shows the IR comparison. Neat 4 after 2 hr at 40°C absorbed 6.6 % by weight of CO_2 which was 38% of theory (assuming that the MW of the material was 1543). The product was a pseudo solid. A 50/50 mix with triethyleneglycol gave only 2.3 % weight gain after exposure to CO_2 that was 28% of theory but remained flowable.

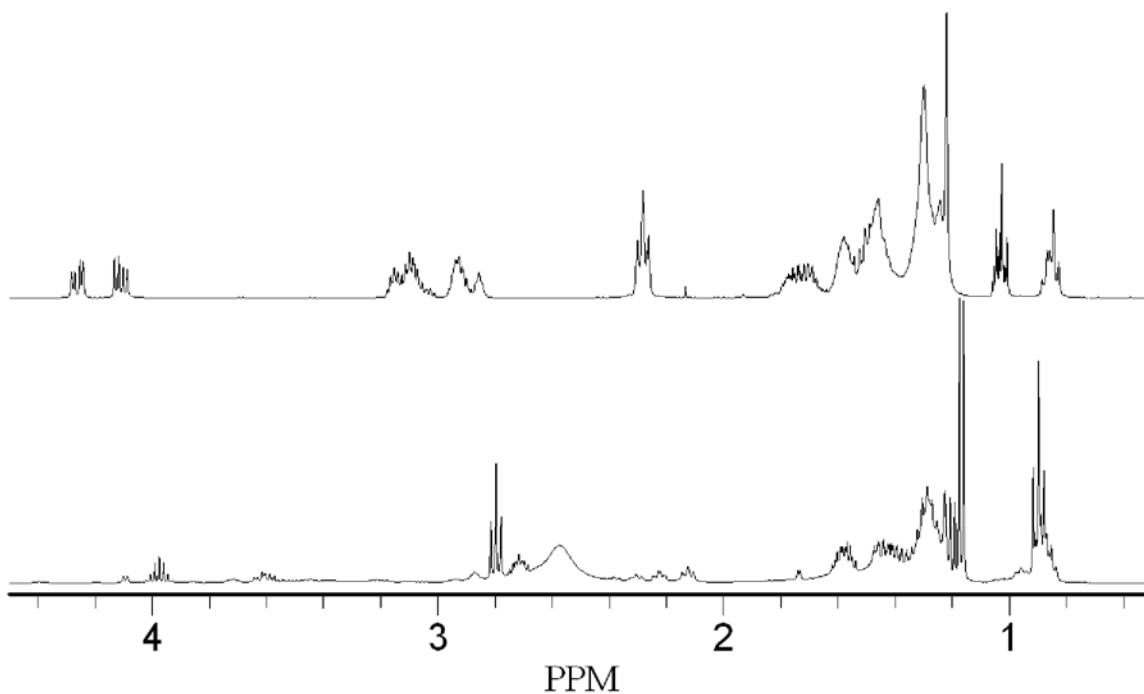


Figure 6. ^1H NMR of EFO (top) and 4, product of EFO and Dytek (bottom).

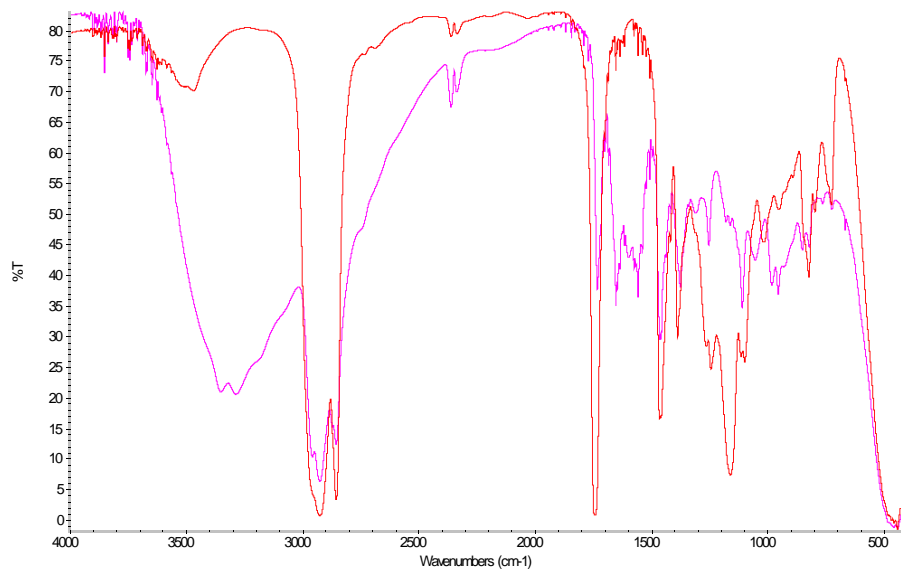
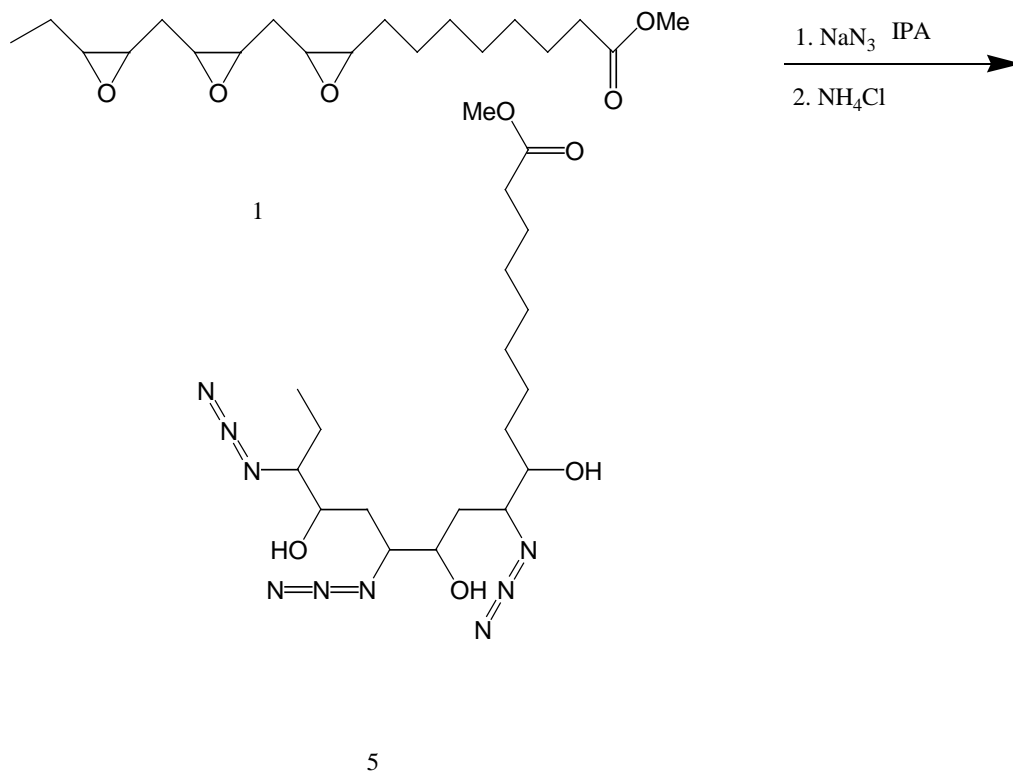


Figure 7. IR of EFO (red) and 4 (pink).

Reaction of Epoxides with Azides. An alternative strategy to obtain amine products based on fatty acids, was reaction of epoxidized fatty acids or esters with sodium azide followed by reduction. NMR and IR analysis showed that epoxides reacted with sodium azide to give the azido-substituted product. We considered two options for reduction of the azido-substituted fatty acids. Reduction with hydrogen and a catalyst or reduction with a hydride, like lithium aluminum hydride, should give the desired amine. Note that the two-step approach gives amine without the problem of cross-linking from the diamine + epoxide approach. NMR and IR analysis did support formation of amine-containing product in several cases. However subsequent reactions with CO₂ showed very poor uptake. It is reasoned that hydrogen bonding from the amine hydroxide products competes with reaction with CO₂.

The epoxidized linolenic acid methylester, 1, was reacted sodium azide and then ammonium chloride in iso-propanol as shown in equation 5. Figure 8 shows the ¹H NMR for 1 and 5 and figure 9 shows the IR comparison. Note the formation of the azido resonance at 2104 cm⁻¹ and the OH resonance at 3450 cm⁻¹.



Equation 5.

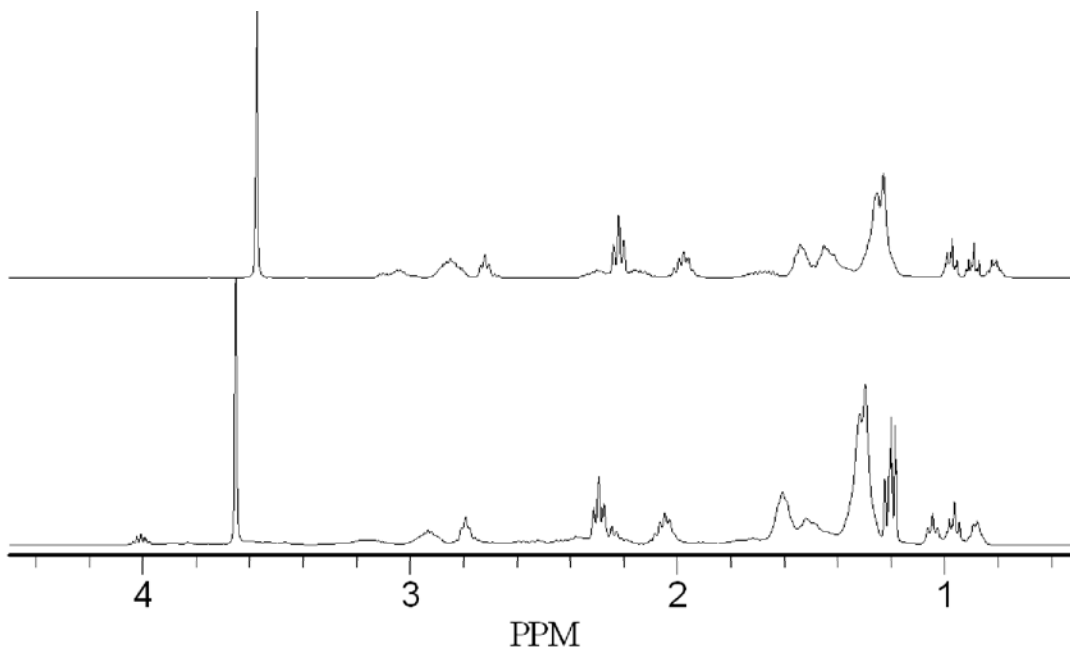


Figure 8. $^1\text{H NMR}$ epoxidized linolenic acid methylester, 1 (top) and product of 1 and sodium azide, 5 (bottom)

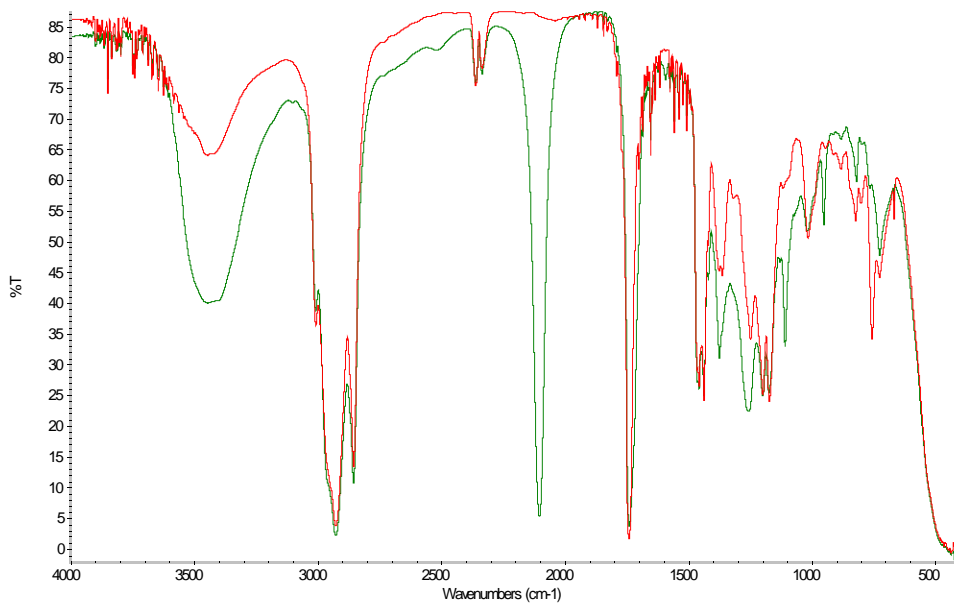
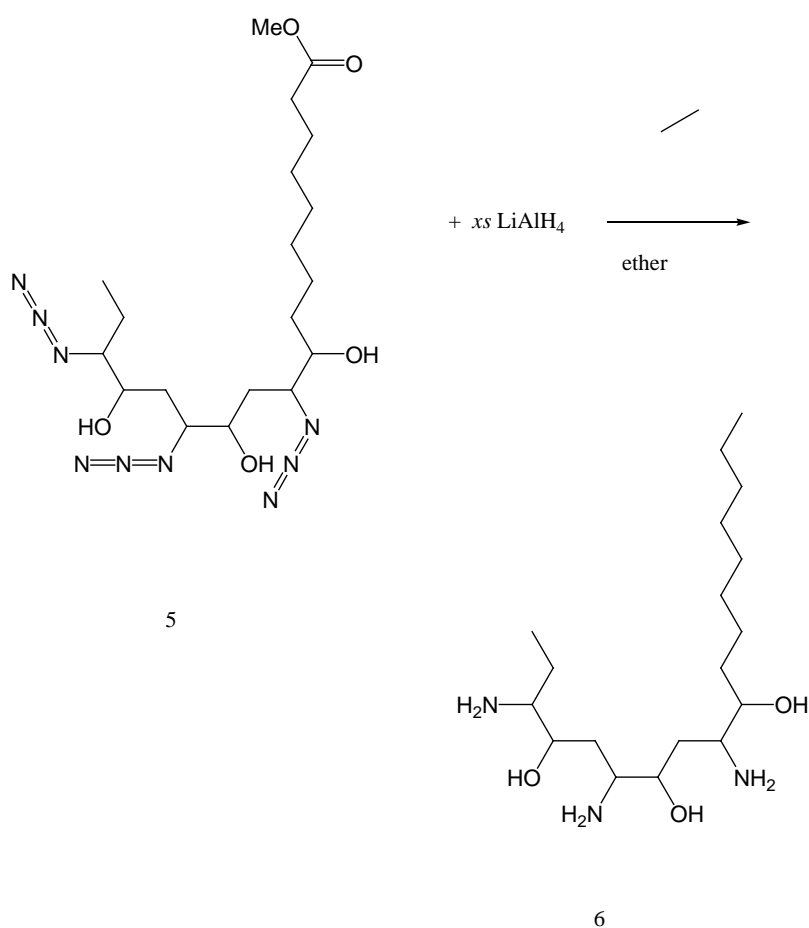


Figure 9. IR for epoxidized linolenic acid, 1, (red) and product of 1 with sodium azide, 5 (green).

Conversion of the azido-substituted linolenic acid methyl ester, 5 to the amine was accomplished via reduction with LiAlH_4 , equation 6. The hydride reacted with the azide and with the ester to give amine product as indicated by both the ^1H NMR, figure 10 and the IR, figure 11. The IR shows consumption of the azido peak at 2104 cm^{-1} and formation of the broad amine peak at 3345 cm^{-1} . There was virtually no CO_2 uptake by neat 6 or with 6 diluted with triethylene glycol.



Equation 6

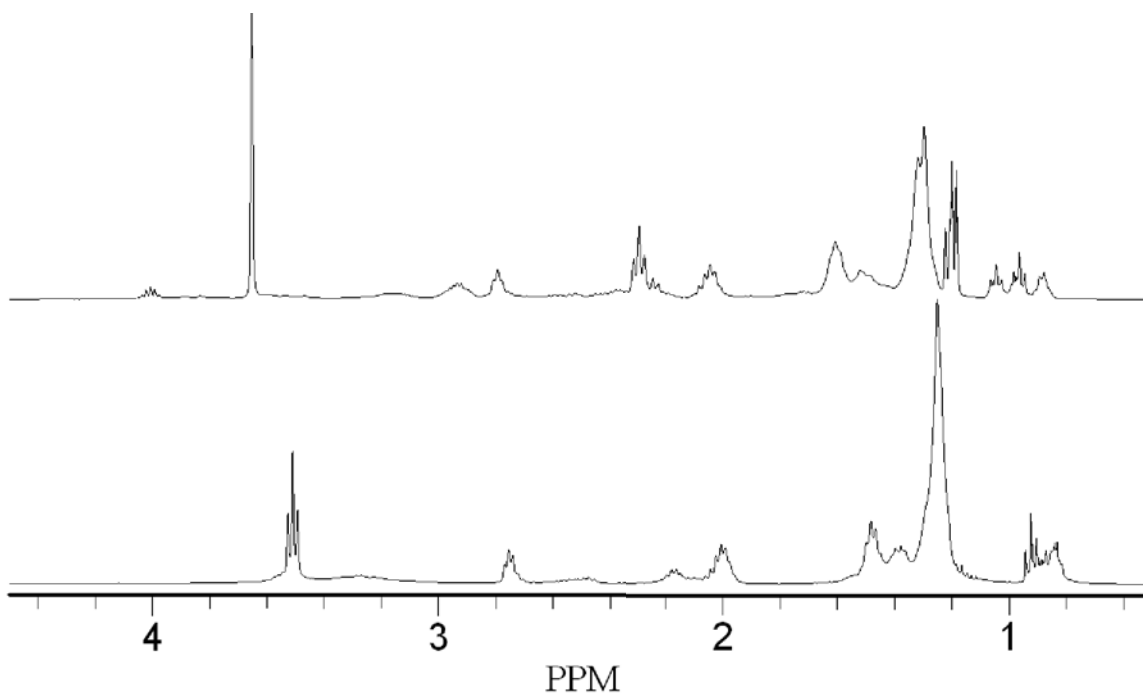


Figure 10. ¹H NMR of azido linolenic acid methylester, 5 (top) and product of 5 with LiAlH₄, 6 (bottom).

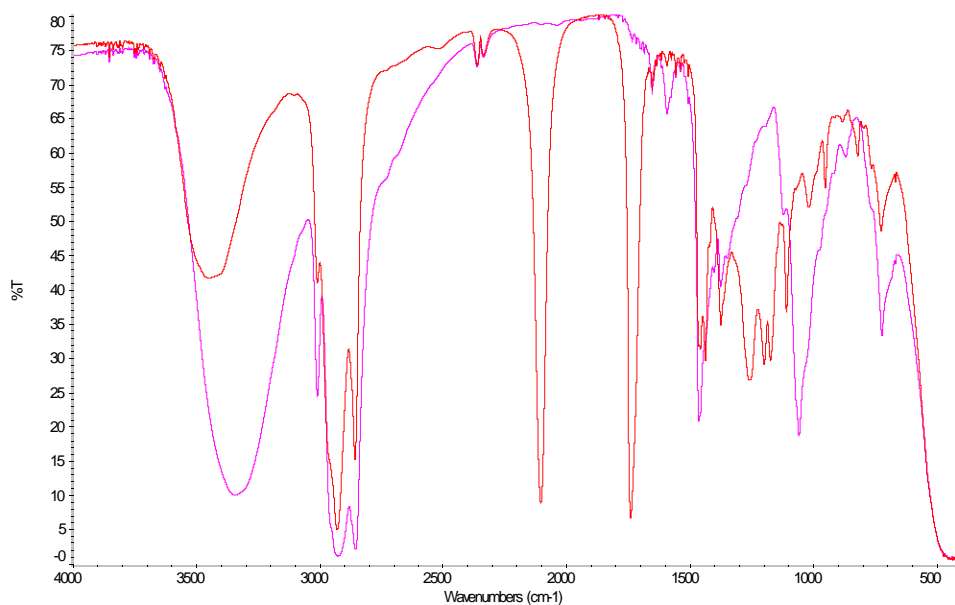
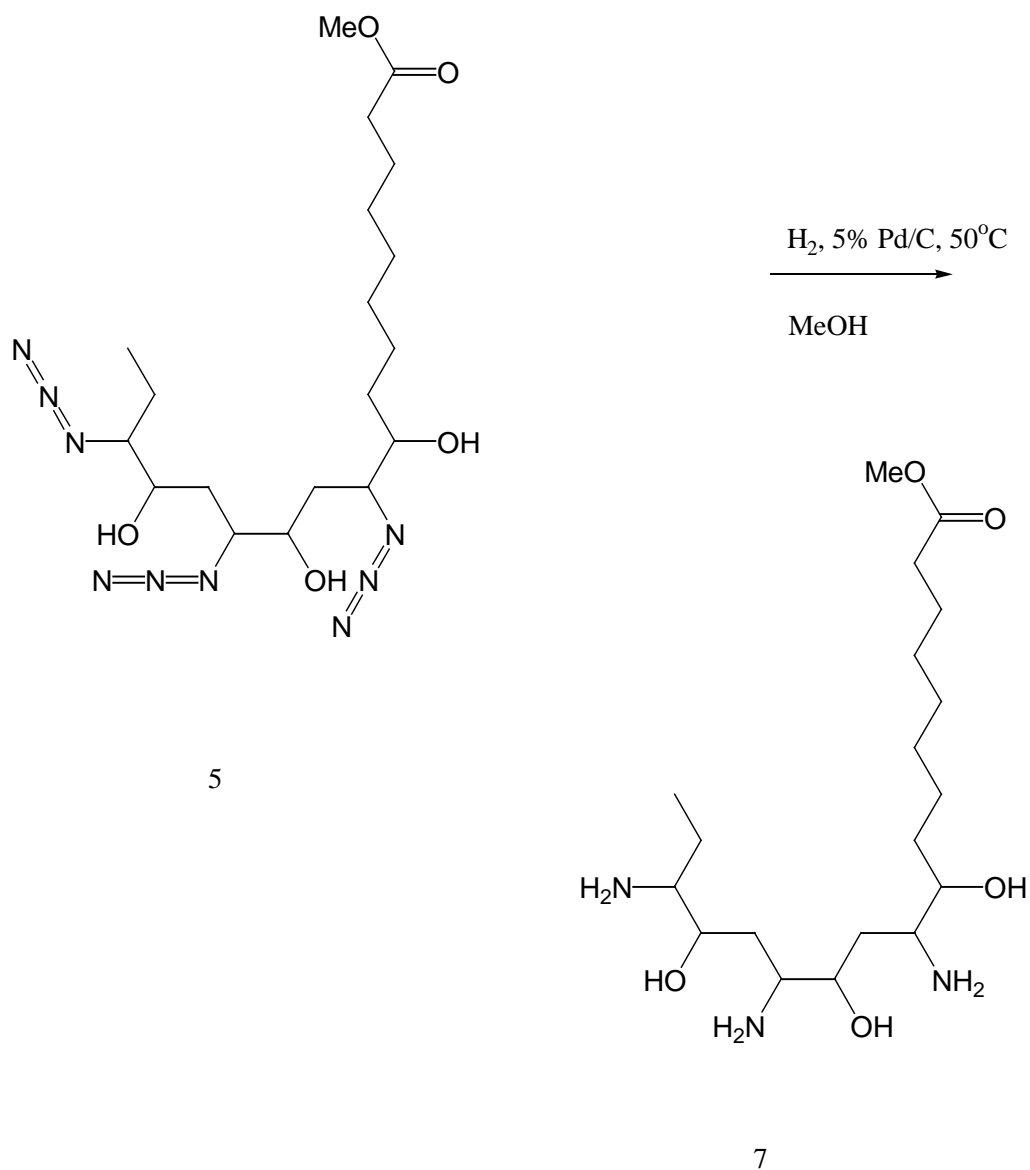


Figure 11. IR spectra for azido-functionalized linolenic acid methylester 5 (red) and product of 5 with LiAlH₄, 6 (pink).

Reduction with hydrogen was a gentler technique than reduction with LiAlH_4 . Whereas LiAlH_4 led to both azide reduction and ester reduction, reaction of 5 with hydrogen and a Pd/C catalyst led to azide reduction to form amine with the ester intact, 7, equation 7.



Equation 7

A working hypothesis of the poor CO₂ uptake of the amine-hydroxy materials was that intra-molecular hydrogen bonding of the amine to the hydroxide competes with reaction of CO₂ with the amine. To test this hypothesis, we added a step whereby we capped the hydroxide. To further determine why the amino alcohol derivatized plant oils performed poorly in reactions with CO₂, several model compounds were made. These were designed to separate the effects of potential H-bonding between adjacent OH and NH₂ groups and the influence of a hydrocarbon chain. To this end, MEA, aminododecane and compounds 10 and 12 were examined for their reactivity in 50% TEG (triethylene glycol) and as neat materials.

1-Decene was used as a model compound in light of the following discoveries:

- Formation of the epoxide was straightforward using mCIPBA
- The azide process was a better path for formation of amino products so as to avoid crosslinked, high viscosity products formed by direct reaction with diamine.
- The azido hydroxyl compound could be ethyl-capped using NaH and ethyl iodide
- Reduction of the azide to amine was straightforward using H₂ reduction and a Pd/C catalyst.

MEA was commercially available as was 1-aminododecane. Compounds 10 and 12 were synthesized as shown in Scheme 1. Epoxidation of 1-decene gave epoxide 8, which was followed by ring opening with sodium azide to give a 9:1 mixture of azido alcohols 9. These azides were either reduced directly to the corresponding amines (10) or the alcohol groups capped with an ethyl group and then reduced to 12.

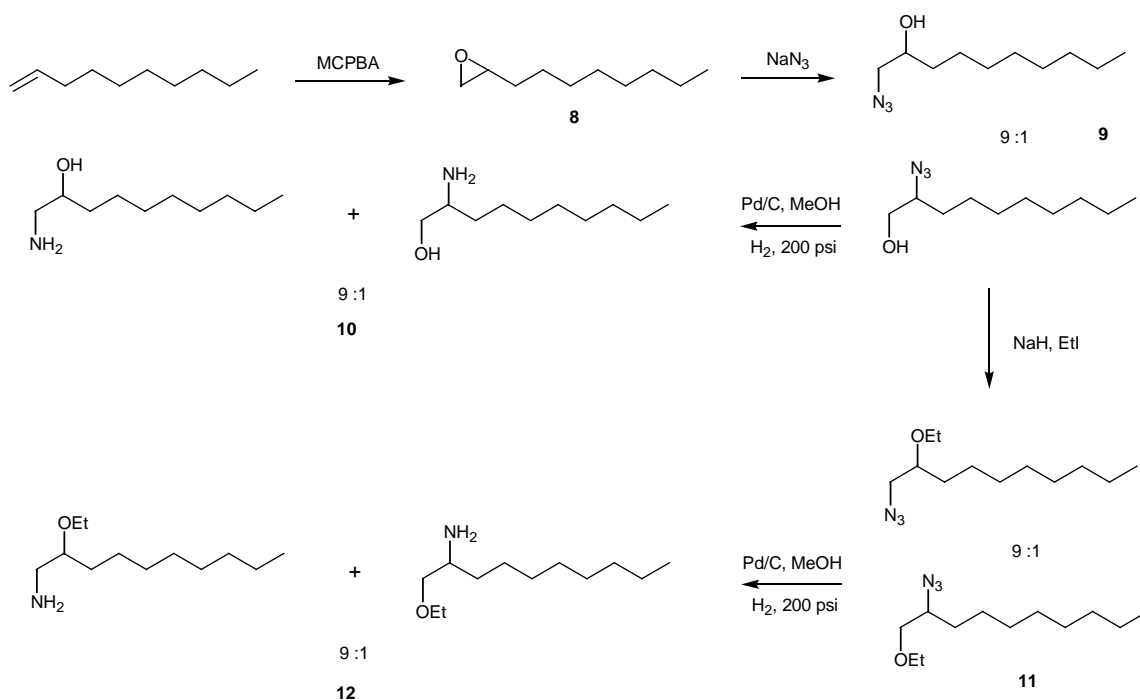
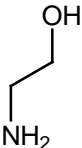
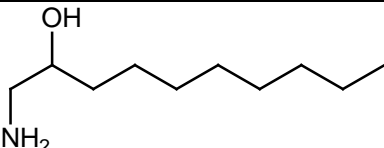
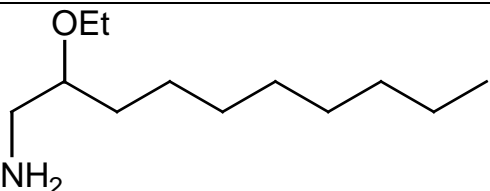
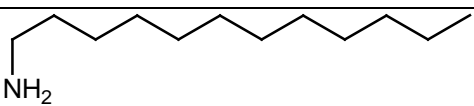


Table 1 shows the results of exposure of these compounds to CO₂. As expected, MEA readily reacted with CO₂ both neat and as a 50% solution in TEG. When a hydrocarbon rich chain was added to MEA, as in compound 10, there was a significant decrease in the CO₂ capture ability of the molecule. This result suggested that the non-polar tail of 10 prevented efficient reaction of CO₂ with the polar amino alcohol; perhaps in a fashion similar to micelle formation with non-polar tails surrounding a core of polar groups.

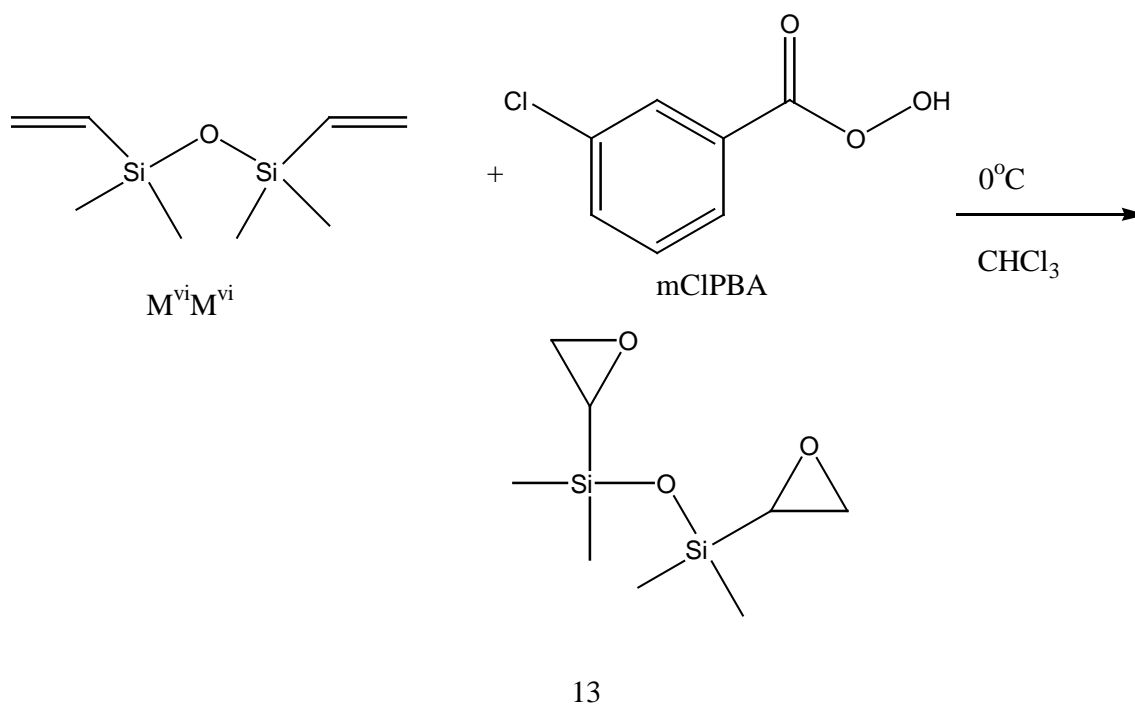
When the hydrogen-bonding ability of the hydroxy group was removed by forming the ethoxy derivative 12, CO₂ capture efficiency increased significantly over 10. The results comparing 10 and 12 also intimated that the potential for H-bonding between adjacent amine and hydroxyl functionalities could suppress reaction with CO₂. The proposed micelle effect was still present when aminododecane was allowed to react with CO₂. A CO₂ loading higher than 10 but less than 12 was observed. These results support the theory that the long hydrocarbon rich chains of the plant oils may hinder the ability of CO₂ to access the polar amine groups. In addition, the potential for H-bonding in the amino alcohols present also suppress the reactivity of the entire system towards CO₂ absorption.

Table 1. Reactivity of MEA Derivative with CO₂.

Compound	Structure	% CO ₂ Weight Gain	
		Neat	50% TEG
MEA		105	104
<u>10</u>		81	72
<u>12</u>		95	91
aminododecane		86	85

Silicon-based CO₂ Solvents. One of the simplest unsaturated silicones was the divinyltetramethyldisiloxane ($M^{vi}M^{vi}$) and vinyltrimethylsilane. Both silicon compounds were easily converted to the corresponding epoxide with mCIBPA. The approach for conversion of the silicon-containing epoxides into silicon-containing amines was the same as described for the fatty acids.

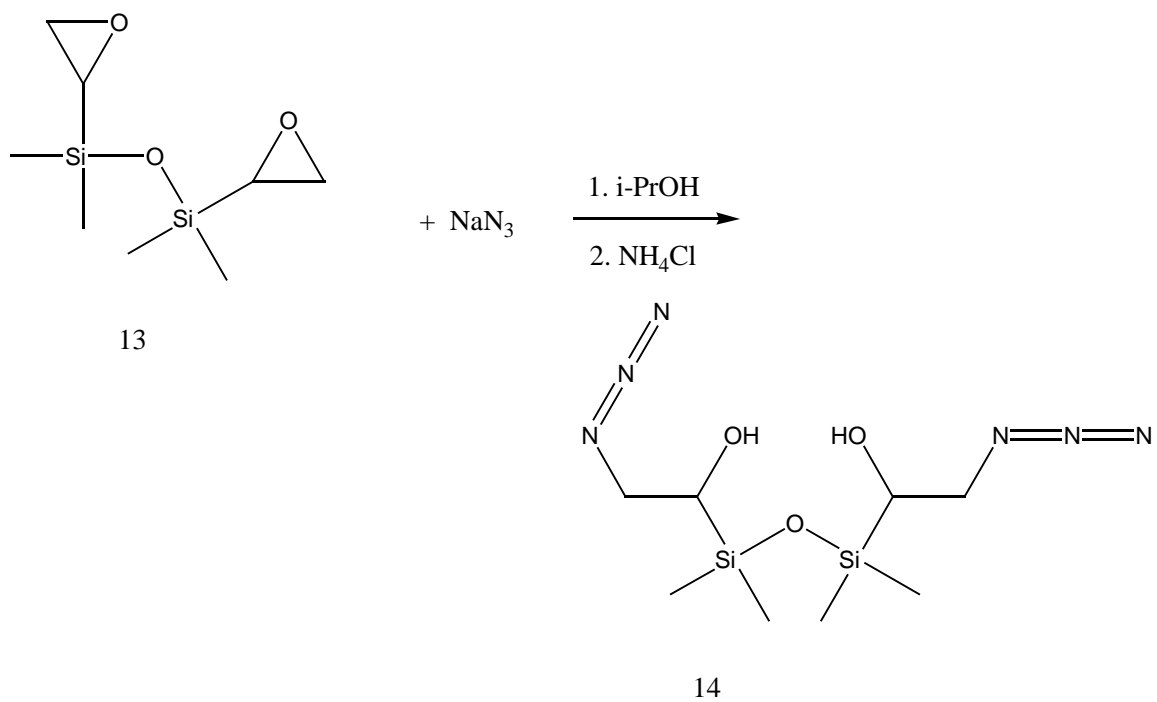
$M^{vi}M^{vi}$ was converted to the diepoxidetramethyldisiloxane, 13 as shown in equation 8.



Equation 8

The reaction of diepoxide 13 with excess ethylene diamine led to products indicating that breakage of the silicon-carbon bond occurred. Work up the reaction between ethylene diamine and 13 gave two layers where one layer had silicon and no amine and the other layer had amine-containing compounds without and silicon.

Given that reaction of diepoxide 13 with diamine led to decomposition, the reaction sequence described above using azide was attempted. The reaction of 13 with sodium azide gave the azido hydroxide, 14, as shown in equation 9. The structure of 14 is confirmed by the ^1H NMR and IR spectra, figures 12 & 13 respectively which shows disappearance of the epoxide-derived resonances for 13 in the NMR and appearance in the IR for peaks due to OH at 3356 cm^{-1} and due to azide at 2114 cm^{-1} .



Equation 9.

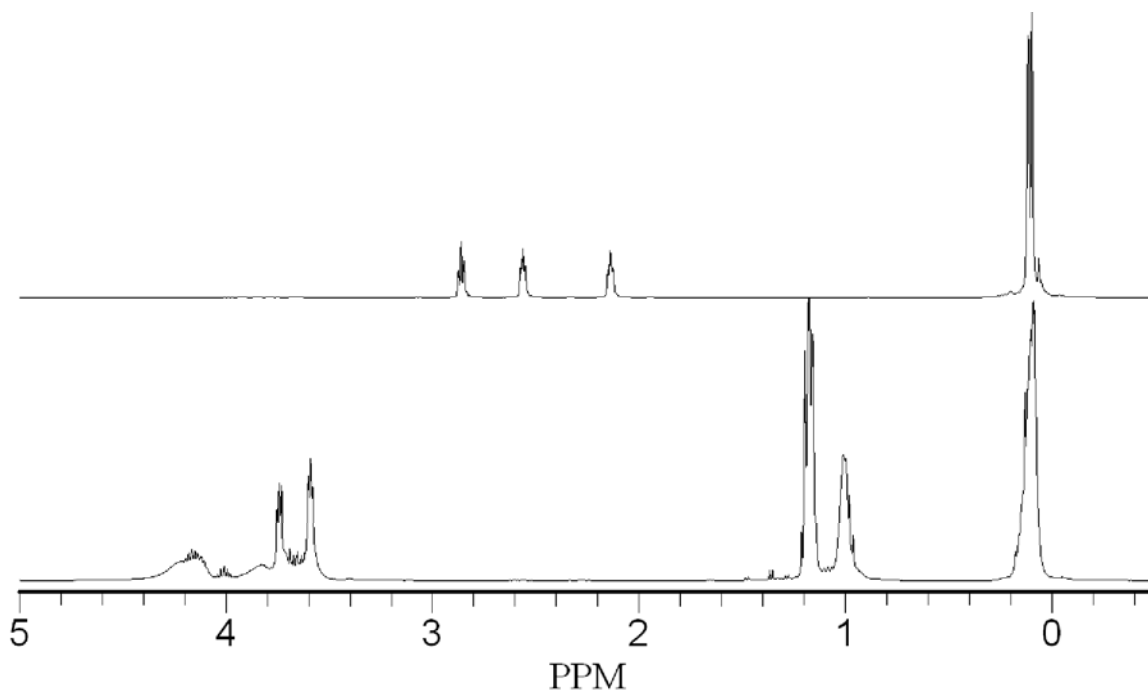


Figure 12. ^1H NMR spectra for 13 (top) and 14 (bottom).

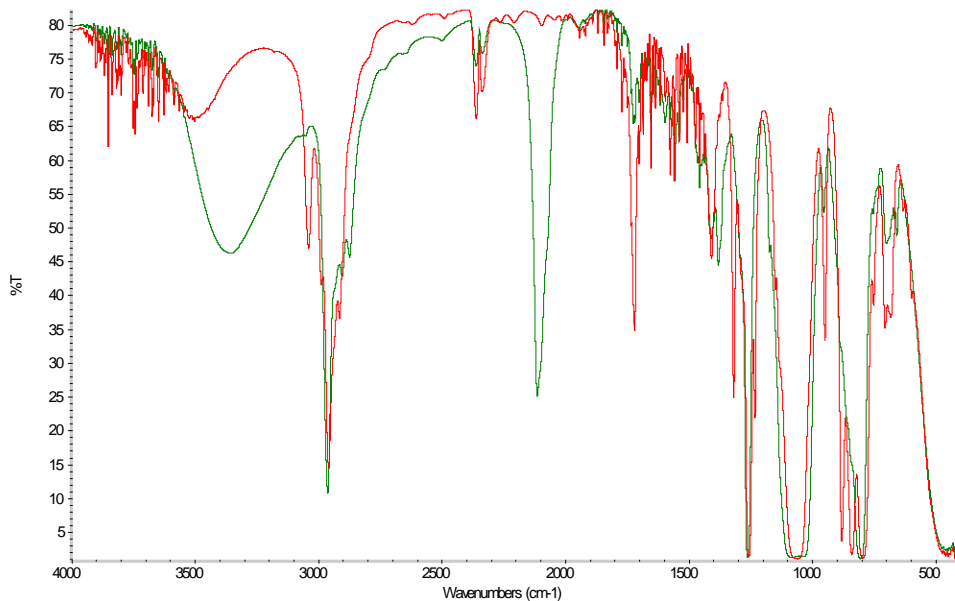
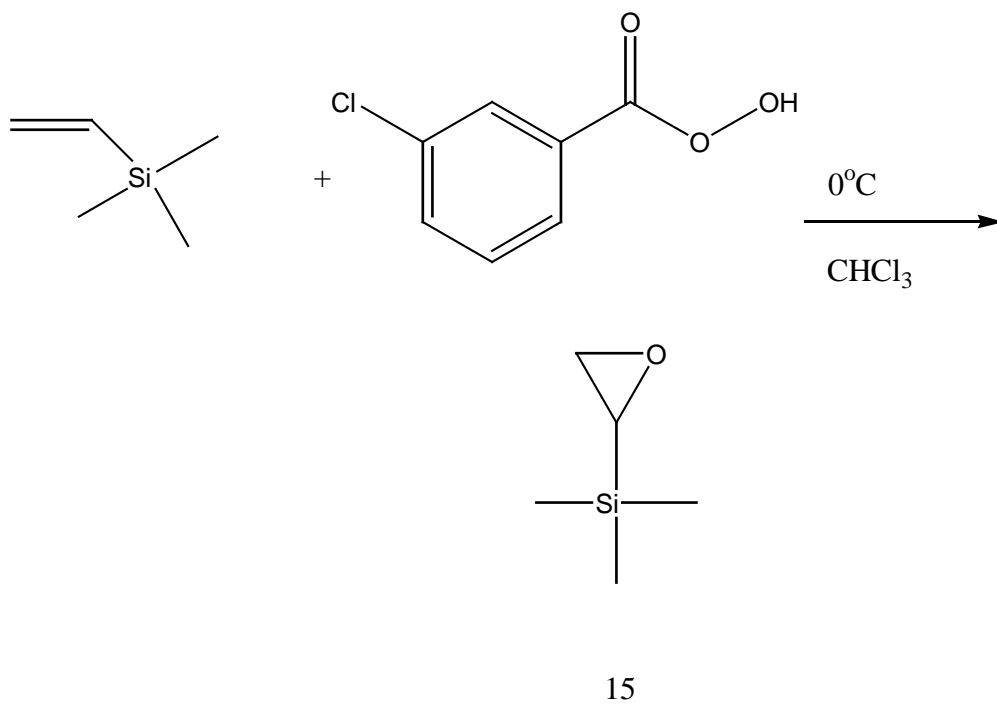


Figure 13. IR spectra for 13 (red) and 14 (green).

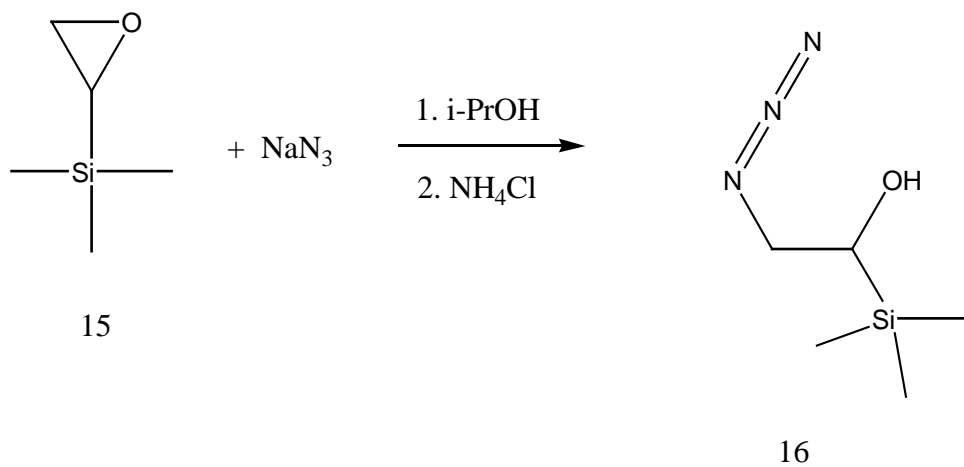
Reduction of the azide in 14 was carried out using hydrogen and Pd/C. IR and NMR analysis of the product of hydrogen reduction of 14 did show consumption of the azide by IR but NMR was equivocal for the anticipated product. Attempts to ethyl-cap the hydroxides in 14 led to apparent breakage of the silicon-carbon bond. Without a viable method to hydroxy-cap the disiloxane, the approach was abandoned and a mono-silane compound was investigated.

Vinyl trimethylsilane was commercially available and converted to the epoxide, 15, as shown in equation 10.



Equation 10

Reaction of **15** with excess ethylene diamine led to products where the Si-C bond was broken. Thus the same plan of attack going through the azide as described above was attempted for **15**, equation 11.



Equation 11

Confirmation of the conversion of epoxide 15 to azide 16 was provided by ^1H NMR and IR, figures 14 and 15 respectively. ^1H NMR shows complete consumption of the epoxide 15 occurred. The spectrum is unusual because there is an apparent 1 ppm downfield shift of the silicon methyls at 1.15 ppm. The IR spectrum does show that 16 had the azide peak at 2100 cm^{-1} and a strong OH peak at 3400 cm^{-1} . Given the equivocal nature of the assignment of the product for the silane reaction, the silane method was not further evaluated.

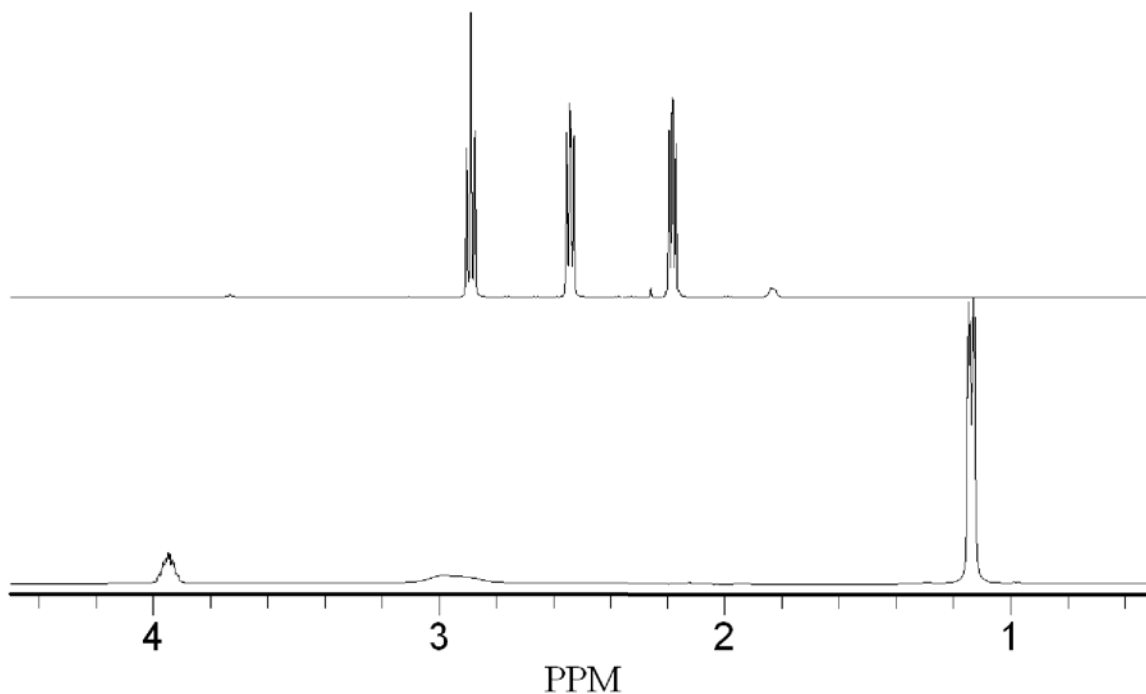


Figure 14a. ^1H NMR of epoxide 15 (top) and azido-silane, 16 (bottom).

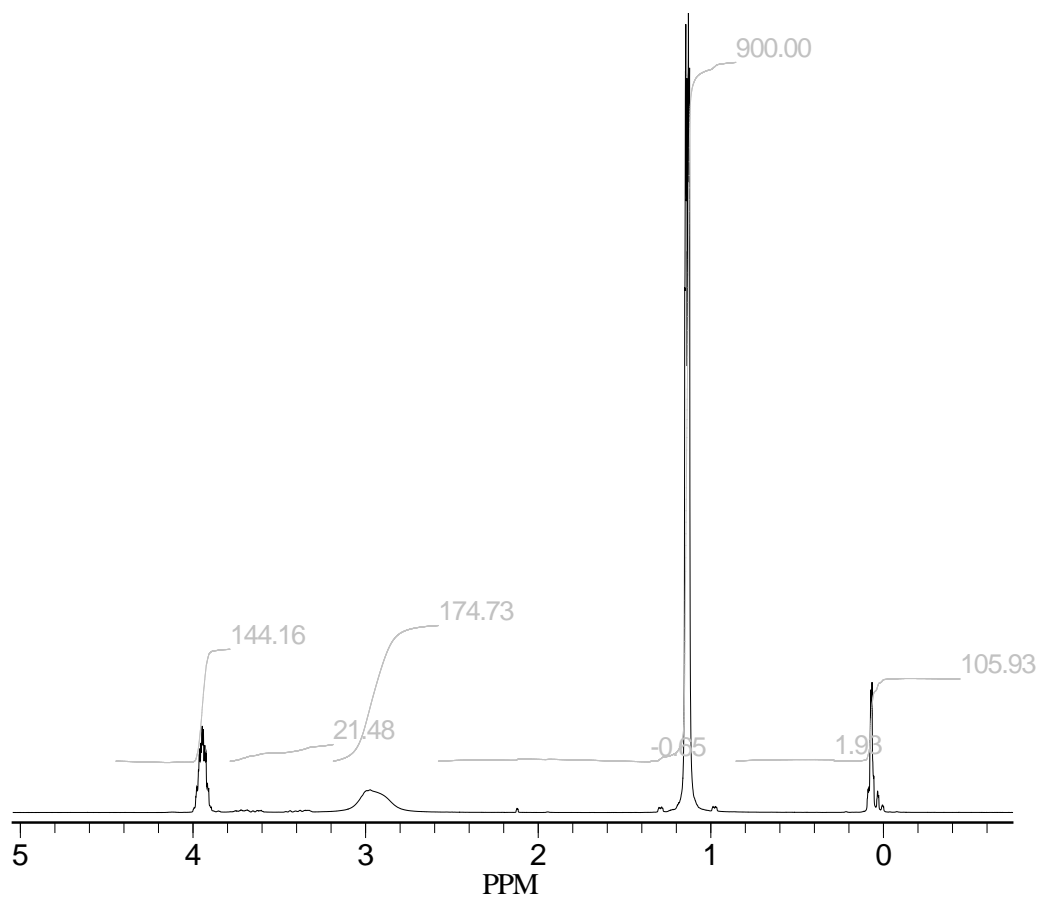


Figure 14b. ¹H NMR of 16

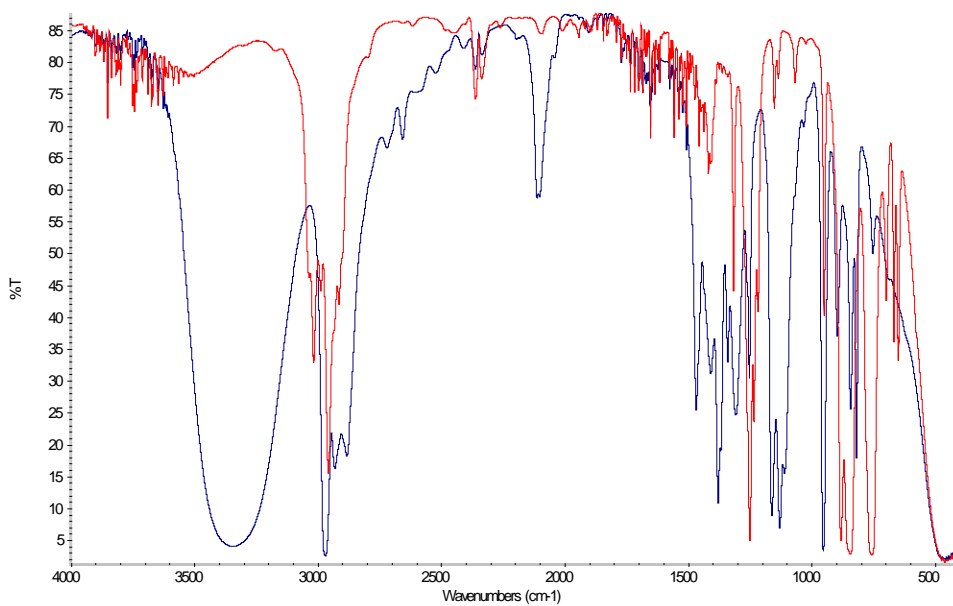


Figure 15. IR spectra for red: 15 and blue 16.

Conclusions

Efficient methods were found for modification of plant oils or their corresponding acids or esters. The olefin functional groups were converted to the epoxides. Reactions with diamines led to highly viscous products except when a sterically bulky diamine was used. An alternative synthetic route to amino-functionalized fatty acid was developed. Epoxidized fatty acids were converted to the azido-functionalized material by reaction with sodium azide. The azide was subsequently reduced either by reaction with hydride or by metal-catalyzed hydrogenation. Nevertheless, no amino functionalized fatty acid or ester examined reacted with CO₂ to any large degree. We hypothesized that the poor reactivity of CO₂ with amino-functionalized oils was due to decreased reactivity of the amine functional groups. This arose from intramolecular hydrogen bonding between free OH and NH₂ units and from the inaccessibility of the amine groups due to formation of a micellular structure with the non-polar hydrophobic alkyl chains protecting the polar amino core. Support for this hypothesis came from examining the CO₂ reactivity of amino-functionalized oils where the free OH groups were ethoxy-capped. However even ethoxy-capped, amino-functionalized hydrocarbons reacted poorly with CO₂ and this effect was likely due to some emulsion-like property of the long hydrocarbon chains. Two amino-functionalized silanes were also examined but none of these materials were useful in this study.

Other approaches employing primary aminosilicones as capture solvents appear more promising from the CO₂ capture standpoint.

Experimental

Formation of 1, epoxidized linolenic acid methylester.

m-CIPBA (70%) (50g) was combined with 600 mL of chloroform and stirred and then filtered. Linolenic acid methyl ester (44.6g, 0.153 mol) was dissolved in 200 mL of CHCl_3 and charged to a 2L, 3-neck flask equipped with a stir bar, addition funnel and cooled with ice. The mCIPBA solution was slowly added over the course of about 1h and the contents were allowed to warm to ambient temperature. The solution was washed with 1.5L of 5% Na_2CO_3 and then dried with MgSO_4 to obtain 53.8 g oil. $^1\text{H NMR}$ (CDCl_3): 0.81 (m), 0.90 (m), 0.97 (t), 1.25 (br m), 1.43 (br, m), 1.54 (br, m), 1.68 (br, m), 1.97 (m), 2.16 (m) 2.2 (t), 2.30 (m), 2.72 (m), 2.86 (br), 3.6 (s).

Reaction of 1 with ethylene diamine, formation of 2.

Ethylene diamine (35.3g, 0.59 mol) was charged to a 3-neck, 500 mL flask with 200 mL of iso-propanol and 10 mL of water. Then 1 (19.94g) in 150 mL of isopropanol was slowly added and the contents heated at reflux for 17h. The volatiles were then removed in vacuo to obtain 23.3g of oil. $^1\text{H NMR}$ (CDCl_3): 0.81 (br), 0.91 (t), 0.98(t), 1.11(d), 1.23 (large, br), 1.44(br), 1.54 (br), 1.98 (m), 2.11 (t), 2.23 (t), 2.67 (s), 2.72 (m), 3.6 (s).

Reaction of epoxidized flax oil (EFO) with ethylene diamine, formation of 3.

Ethylene diamine (925g) was charged to a 3-neck 500 mL flask with 250 mL of isopropanol. EFO (20g) was dissolved in 80 mL of isopropanol and then slowly added to the ethylenediamine solution and then refluxed for 4.5 h. The volatiles were removed in vacuo to obtain 26.6g of an oil. $^1\text{H NMR}$ (CDCl_3): 0.86 (br), 0.96 (br), 1.21 (t), 1.29 (br), 1.47 (br), 1.58 (br), 2.15 (m), 2.22 (m), 2.72 (s), many broad multiplets from 2.8-5.0.

Reaction of epoxidized flax oil with Dytek, formation of 4.

EFO (10g) was dissolved in 50 mL of isopropanol and slowly added to a solution of Dytek (6.8g) in 50 mL of isopropanol and then heated to reflux for 20h. The volatiles including excess Dytek were removed in vacuo to obtain an oil. $^1\text{H NMR}$ (CDCl_3): 0.90

(m), 1.18 (m), 1.22 (m), 1.29 (br), 1.35-1.5 (m), 1.58 (m), 2.1-2.5 (apparent t), 2.57 (br), 2.72 (m), 2.80 (m), 2.87-4.1 (many multiplets).

Reaction of 1 with sodium azide to form 5.

Product 1 (20.14g, 59.2 mmol) was dissolved in 200 mL of isopropanol. NaN₃ (12g, 0.185mol) was added and the mixture heated for 17h at reflux. Then NH₄Cl (11g) was added and stirring was continued for 7h. The entire slurry was filtered through a bed of Celite and carbon black and the filtrate was subjected to rotary evaporation to remove volatiles. An oil was obtained, 21.8g. ¹H NMR (CDCl₃): 0.88 (m), 0.97 (t), 1.04 (t), 1.19 (m), 1.30 (br), 1.52 (br), 1.61 (br), 2.05 (m), 2.29 (t), 2.80 (m), 2.93, br, m), 4 (m)

Reduction of azide 5 with LiAlH₄ to form 6.

LiAlH₄ (11g, 0.289 mol) was added to 200 mL dry ether in a dried 500 mL flask. Compound 5 (14.9g, 31.9 mmol) was dissolved in dry ether and added to an addition funnel and then slowly added to the stirring suspension of LiAlH₄ under argon over the course of 1h. The contents were poured into ice and then extracted with ether, dried with MgSO₄ to obtain 7.8g of an oil. ¹H NMR (CDCl₃): 0.83 (m), 0.92 (t), 1.25 (br), 1.38 (m), 1.48 (m), 2.00 (m), 2.17 (m), 2.75 (m), 3.51 (t).

Hydrogenation of 5 to form 7.

A 90 mL Fisher Porter thick-walled bottle was charged with 5 (4.8g, 10.2 mmol) and 10 mL ethanol. 5% Pd/C (0.1g) was added and then the tube was charged with 65 psi H₂ and then stirred at ambient pressure. The tube was re-pressurized three times total after hydrogen consumption occurred. The contents were then filtered through Celite and the volatiles removed from the filtrate in vacuo to obtain 3.8g of an oil. ¹H NMR (CDCl₃): 0.84 (br), 0.91 (br), 0.99 (m), 1.18 (m), 1.25 (br), 1.46 (br), 1.57 (br), 1.95 (br), 2.25 (m), 2.86 (br), 3.44 (br) and 3.62 (s).

1,2-epoxydecane, 8. *m*-CPBA (50.8 g, 0.21 moles) was slurried with CHCl₃ (400 mL), filtered to remove any undissolved solid and decanted to remove separated water and then added over 1 h to 1-decene (26 g, 0.17 moles) in CHCl₃ (100 mL) at ~ 5 °C. The

reaction was allowed to proceed for 17 h after which time the mixture was filtered, washed with aq NaHCO₃, then water, then dried over MgSO₄, filtered, concentrated, filtered, refluxed with hexanes and cooled. The solid was isolated by filtration then distilled to give 23.0 g (85%) product as a clear, colorless liquid. bp 51-53 °C/0.8 mm Hg. (lit. 94 °C/20 mm Hg). ¹H NMR (CDCl₃) δ: 2.93 (m, 1H); 2.77 (dd, J = 5.0, 5.0 Hz, 1H); 2.48 (dd, J = 5.0, 5.0 Hz, 1H); 1.53 (m, 2H); 1.46 (m, 2H); 1.25-1.37 (m, 10H); 0.90 (t, J = 7.1 Hz, 3H). ¹³C{¹H}NMR (CDCl₃): 52.4, 47.1, 32.5, 31.9, 29.5, 29.4, 29.2, 26.0, 22.7, 14.1 ppm.⁶

1-Azido-2-hydroxydecane, 9. In a 500 mL, 1-neck flask were placed NaN₃ (5.0 g, 77 mmol), NH₄Cl (4.1g, 77 mmol), water (125 mL), EtOH (125 mL) and 1,2-epoxydecane (10.0 g, 64 mmol). The mixture was heated to reflux with stirring in air for 16 h after which time the EtOH was removed in vacuo and the aqueous solution extracted 3 x Et₂O (100 mL), the Et₂O layers combined, washed with water, dried over MgSO₄ and concentrated to give 11.5 g crude product.⁷ Distillation at 75-77 °C/0.15 mm Hg gave 8.8 g (69%) product as a mixture of 87% desired product and 13% 1-hydroxy-2-azidodecane. Major isomer: ¹H NMR (CDCl₃) δ: 3.78 (m, 1H); 3.40 (dd, J = 12.4, 3.3 Hz, 1H); 3.26 (dd, J = 12.4, 7.6 Hz, 1H); 1.49 (m, 2H); 1.29 (m, 12H); 0.90 (t, J = 7.1 Hz, 3H). ¹³C{¹H}NMR (CDCl₃): 70.9, 57.2, 34.3, 31.8, 29.52, 29.47, 29.2, 25.4, 22.6, 14.1 ppm. Minor isomer: ¹H NMR (CDCl₃) δ: 3.72 (dd, J = 11.1, 3.5 Hz, 1H); 3.57 (dd, J = 11.3, 7.3 Hz, 1H); 3.48 (m, 1H); 1.96 (br s, 1H); 1.50 (m, 2H); 1.29 (m, 12H); 0.90 (t, J = 7.1 Hz, 3H).

1-Amino-2-hydroxydecane, 10. Azide 9 (5.75 g, 28.8 mmol) was dissolved in MeOH (50 mL) in a Parr Bomb and then 10% Pd/C (300 mg) was added. (Care should be taken to exclude oxygen!) The mixture was pressurized with 200 psi H₂ and stirred at ambient temperature for 18 h. The reaction mixture was filtered, concentrated and distilled (80 °C/0.15 mm Hg) to give 4.1 g (82%) product as a 9:1 mixture of regio-isomers. Major isomer: ¹H NMR (CDCl₃) δ: 3.49 (m, 1H); 2.85 (dd, J = 12.4, 3.3 Hz, 1H); 2.52 (dd, J = 12.4, 8.5 Hz, 1H); 1.7 (br s, 1H); 1.42 (m, 2H); 1.29 (m, 12H); 0.89 (t, J = 6.8 Hz, 3H). ¹³C{¹H}NMR (CDCl₃): 72.1, 47.4, 34.8, 31.9, 29.7, 29.6, 29.3, 25.7, 22.7, 14.1 ppm.

Minor isomer: ^1H NMR (CDCl_3) δ : 3.59 (dd, $J = 10.4, 3.9$ Hz, 1H); 3.26 (dd, $J = 12.4, 7.8$ Hz, 1H); 2.83 (m, 1H); 1.7 (br s, 1H); 1.42 (m, 2H); 1.29 (m, 12H); 0.90 (t, $J = 6.8$ Hz, 3H).

1-Azido-2-ethoxydecane, 11. 100% dry NaH (1.07 g, 44 mmol) dispersed in dry THF (40 mL) was treated with a solution of alcohol 9 (8.5 g, 42.7 mmol) in THF (10 mL) over 10 min at ambient temperature. After 15 min, substantial gas evolution was noted which slowed after 30 min. A yellow suspension was formed which was allowed to stir at ambient temperature for 24 h under N_2 . EtI (8.5 g, 54.5 mmol) was added and stirred for 24 h. The reaction mixture was diluted with water (30 mL), washed 2 x with water, organic layer concentrated, dissolved in CHCl_3 , washed 2 x water, dried over MgSO_4 , filtered, concentrated and distilled to give 5.7 g (63%) product as ~ a 9:1 mixture of isomers.

1-Amino-2-ethoxydecane, 12. Azide 11 (5.7 g, 25 mmol) was dissolved in EtOH (50 mL) in a Parr Bomb and then 10% Pd/C (~1 g) was added. The mixture was pressurized with 200 psi H_2 and stirred at ambient temperature for 24 h. An additional 10 mL EtOH and 0.5 g 10% Pd/C was added and the vessel re-pressurized to 240 psi H_2 and heated at 50 $^\circ\text{C}$ for an additional 24 h. The reaction mixture was filtered, concentrated and distilled (85-95 $^\circ\text{C}/0.15$ mm Hg) to give 1.83 g (36%) product as a 8:2 mixture of regio-isomers. Major isomer: ^1H NMR (CDCl_3) δ : 3.54 (m, 2H); 3.22 (m, 1H); 2.78 (dd, $J = 13.4, 3.8$ Hz, 1H); 2.66 (dd, $J = 13.1, 6.6$ Hz, 1H); 1.25-1.52 (m, 14H); 1.22 (t, $J = 7.1$ Hz, 3H); 0.89 (t, $J = 7.1$ Hz, 3H). $^{13}\text{C}\{^1\text{H}\}$ NMR (CDCl_3): 81.1, 64.6, 45.2, 32.0, 31.9, 29.9, 29.6, 29.3, 25.5, 22.7, 15.7, 14.1 ppm. DART MH^+ Calc'd for $\text{C}_{12}\text{H}_{28}\text{NO}$: 202.2171; Found: 202.2165. Minor isomer: ^1H NMR (CDCl_3) δ : 3.49 (m, 2H); 3.40 (dd, $J = 9.2, 3.6$ Hz, 1H); 3.16 (dd, $J = 17.8, 9.4$ Hz, 1H); 2.94 (m, 1H); 1.25-1.52 (m, 14H); 1.22 (t, $J = 7.1$ Hz, 3H); 0.89 (t, $J = 7.1$ Hz, 3H).

Epoxidized $\text{M}^{\text{vi}}\text{M}^{\text{vi}}$, 13.

meta-CIPBA (140g) was dissolved in 1L CHCl_3 and charged to an addition funnel. A 2L 3-necked flask was charged with divinyltetramethyldisiloxane (50g, 0.269 mol) in 200

mL of CHCl_3 cooled with ice. mCIPBA was added over the course of 1h and then the contents were stirred an additional 14h while warming to ambient temperature. The solution was extracted with 1.5L of 5% Na_2CO_3 and then the chloroform layer was dried with MgSO_4 to obtain 64.1g of an oil. Residual mCIPBA byproduct was removed by dissolving the oil in a minimum of hexanes and then cooling in a freezer. White solid aromatic-containing byproduct was removed by filtration. ^1H NMR (CDCl_3): 0.11 (m, 12H), 2.14 (m, 2H), 2.56 (m, 2H) and 2.87 (m, 2H).

Reaction of 13 with azide, formation of 14.

Diepoxide 13 (15.11g, 81.2 mmol) was combined with sodium azide (10.8g, 0.166 mol) in 150 mL isopropanol and heated to reflux with stirring for 6h. At this point NH_4Cl (9g) was added and stirring and heating was continued for 17h at ambient temperature. The slurry was filtered through Celite/carbon black and the volatiles removed in vacuo to obtain 14.4g of an oil. ^1H NMR (CDCl_3): 0.09 (m), 1.01 (m), 1.18 (m), 3.60 (m), 3.75 (m) and 4.14 (br, m).

Reaction of vinyltrimethylsilane with mCIPBA, formation of 15.

In a 3-neck, 2L flask was placed vinyltrimethylsilane (25g) was dissolved in 100 mL of CHCl_3 and cooled with ice. An addition funnel was charged with mCIPBA (67g) in 500 mL CHCl_3 and mCIPBA was added over the course of 1h. Stirring was continued an additional 17h and then the contents were extracted with 1.6 L of 5% Na_2CO_3 . The chloroform layer was dried with MgSO_4 . After filtration the solution was subjected to ambient pressure distillation to remove chloroform and unreacted vinyltrimethylsilane. The product 16 was distilled at ambient pressure at 116°C to obtain 23.5g, 80% yield. ^1H NMR (CDCl_3): 0.02 (s, 9H), 2.18 (m, 1H), 2.55 (m, 1H) and 2.89 (t, 1H).

Reaction of 15 with sodium azide, formation of 16.

Epoxytrimethylsolane 15 (9.97g, 85.9 mmol) was dissolved in 100 mL of isopropanol and combined with sodium azide (6g, 92.3 mmol) and heated at reflux for 7h. NH_4Cl (5g) was added and heating and stirring was continued for 17h. The solution was filtered

through Celite/carbon black and the volatiles removed in vacuo to obtain 9g of an oil. ^1H NMR (CDCl_3): 0.07 (s, 1H), 1.14 (m, 9H), 2.97 (br, 1.5H) and 3.94 (m, 1.5H).

References

1. *IPCC special report on Carbon Dioxide Capture and Storage*. Prepared by working group III of the Intergovernmental Panel on Climate Change. Metz, B., O. Davidson, H. C. de Coninck, M. Loos, and L.A. Meyer (eds.). Cambridge University Press, Cambridge, United Kingdom and New York, NY, USA, 442 pp. Available in full at www.ipcc.ch
2. Current DOE Contract DE-NT0005310.
3. M.R. Meier, J.O. Metzger, U.S. Schubert, *Chem. Soc. Rev.* "Plant oil renewable resources as green alternatives in polymer science," **36** (2007).1788-1802.
4. G.L. Tellez, E. Viguera-Santiago, S. Hernandez-Lopez, B. Bilyeu, "Synthesis and Thermal Cross-linking Study of Partially-Aminated Epoxidized Linseed Oil," *Designed Monomers and Polymers*, **11** (2008) 435-445.
5. T. Momose, O. Muraoka, N. Shimada, C. Tsujimoto, T. Minematsu, *Chem. Pharm. Bull.*, "Bicyclo[3.3.1]nonanes as Synthetic Intermediates. XVI. On the Selectivity in the Ring Enlargement of the Bicyclo[3.3.1]nonan-2-one System," **37** (1989) 1909-1912.
6. Imada, Y.; Kitagawa, T.; Ohno, T.; Iada, H.; Naota, T. *Org. Lett.* **2010**, *12*, 32.
7. Mullen, L. B.; Sutherland, J. D. *Angew Chem. Int. Ed.* **2007**, *46*, 4166.

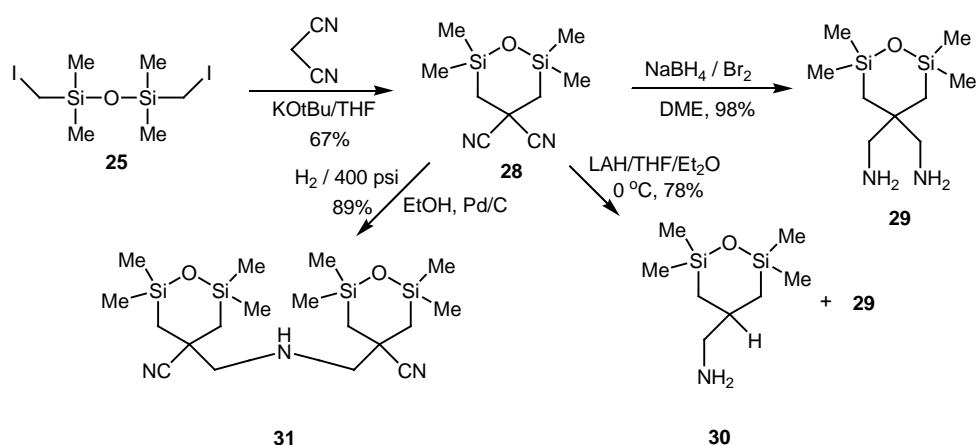
Appendix 5

Amino Disiloxanes for CO₂ Capture.

Robert J. Perry*, Michael J. O'Brien

GE Global Research, 1 Research Circle, Niskayuna, NY 12309

robert.perry@crd.ge.com



Abstract

A series of aminodisiloxanes were synthesized with varying degrees of functionality and steric hindrance, and screened as CO₂-capture solvents. Compounds with unhindered primary amine groups were found to come closest to reaching their theoretical CO₂ uptake values. In contrast, materials containing either hindered primary amines or secondary amine functionality were less efficient. Addition of a co-solvent, triethylene glycol, was found in most cases to maintain solution liquidity and thereby minimize mass transfer limitations on exposure to CO₂.

Introduction

Coal is an important source of global energy with nearly 1500 generators in the US alone producing 315 GW of electricity in 2007.¹ However, it was also estimated that nearly 2.8 billion tons of CO₂ were released to the atmosphere from these same plants.² Given the elevated concern over global warming and the role CO₂ may play in such a scenario, numerous pieces of legislation have been proposed and enormous amounts of funding have been provided to design processes that will capture CO₂ from coal-fired

power plants.³ The United States Department of Energy (DOE) has set a target for processes and materials that demonstrate 90% CO₂ capture efficiency and show less than a 35% increase in the cost of electricity (COE) versus plants with out carbon capture.⁴

Capture of CO₂ produced from conventional coal combustion in air presents several technical challenges in the form of low CO₂ concentration (10-15 volume percent), resulting in a low CO₂ partial pressure, and a large volume of gas to be treated. Post-combustion CO₂ capture processes have been demonstrated at various scales using chilled ammonia,⁵ cryogenics,⁶ carbonates,⁷ organic amines,⁸ and ionic liquids.⁹ However, all suffer from one or more deficiencies including high energy costs for cooling, poor regeneration, low working capacity or slow kinetics.

A variety of silicon-based materials have been examined as CO₂-capture media. Silicon oils were patented as an absorbent in 1972,¹⁰ and changing the side chains in PDMS altered the gas solubility of the polymers.¹¹ Diphosphate substitution was found to increase CO₂ solubility¹² and hydroxy-terminated PDMS solvents were superior to methyl-capped.¹³

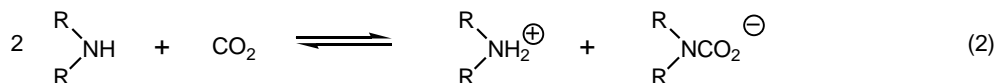
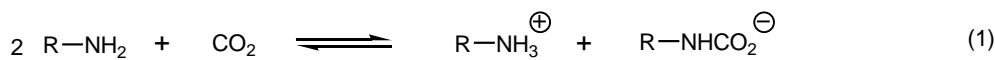
Amino-substituted alkoxy-silanes have also been explored. Glassy carbamic acid dimers have been formed at low temperatures from monoamine derivatives¹⁴ while diaminosilanes formed intramolecular complexes.¹⁵ Sol-gel reactions of the carbamates could be undertaken without decomposition of the carbamate.¹⁶ The intermolecular reaction product of two aminosilanes and CO₂ have been described as ionic liquids.¹⁷

Mesoporous silica derivitized with aminopropyltrimethoxysilane has also been used as a CO₂-capture adsorbants¹⁸ as has silica functionalized by ring-opening polymerization of aziridine.¹⁹

This paper describes the syntheses of a number of amino disiloxanes that are under study as CO₂ capture solvents and their capture capacities. The anticipated thermal stability, higher capture capacity, lower heats of reaction and rapid regeneration are expected to provide a lower overall COE than previous methods.

Results and Discussion

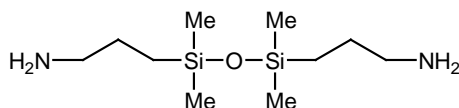
It is well established that primary and secondary amines react with CO₂ to form carbamates as shown in equations 1 and 2 and, under anhydrous conditions, two moles of amine are required to neutralize one mole of CO₂.



Appending these functional groups to a siloxane core was predicted to offer several advantages. These included increased thermal stability from the Si-O-Si linkage, lower volatility and greater bond flexibility and therefore lower viscosity. In addition, it was

hoped that these materials could be used neat as opposed to in an aqueous solution. This would significantly decrease the energy needed to heat the mixture and reclaim the solvent upon CO₂ release.

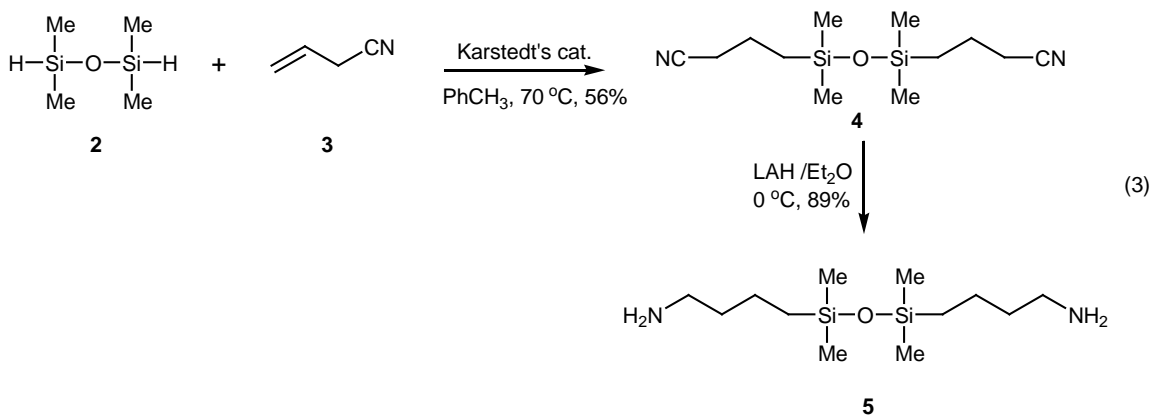
Preliminary results of CO₂ capture using diaminosiloxanes were recently reported.²⁰ That paper examined a variety of core siloxane architectures with pendant amines and reported capture capacities and the effect of a co-solvent on CO₂ absorption. In addition, continuous absorption data, heats of reaction measurements and absorption isotherms were generated for one readily available aminodisiloxane, 1,3-bis(3-aminopropyl)-1,1,3,3-tetramethyldisiloxane, **1**.



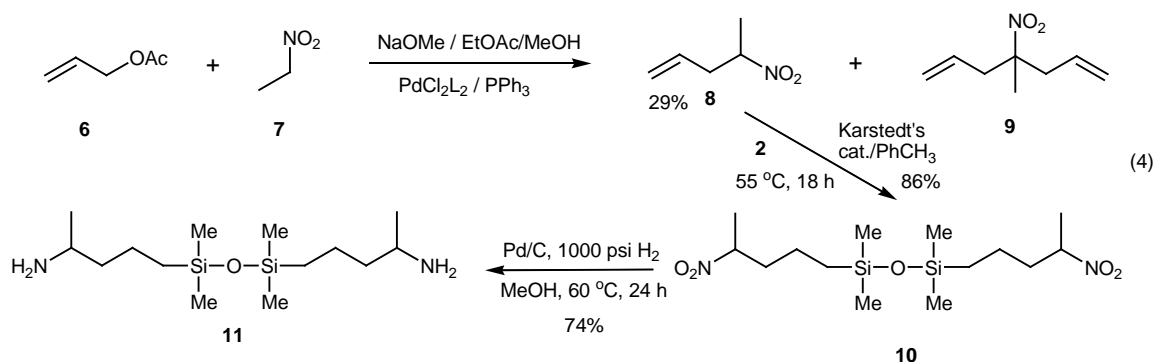
1

Syntheses

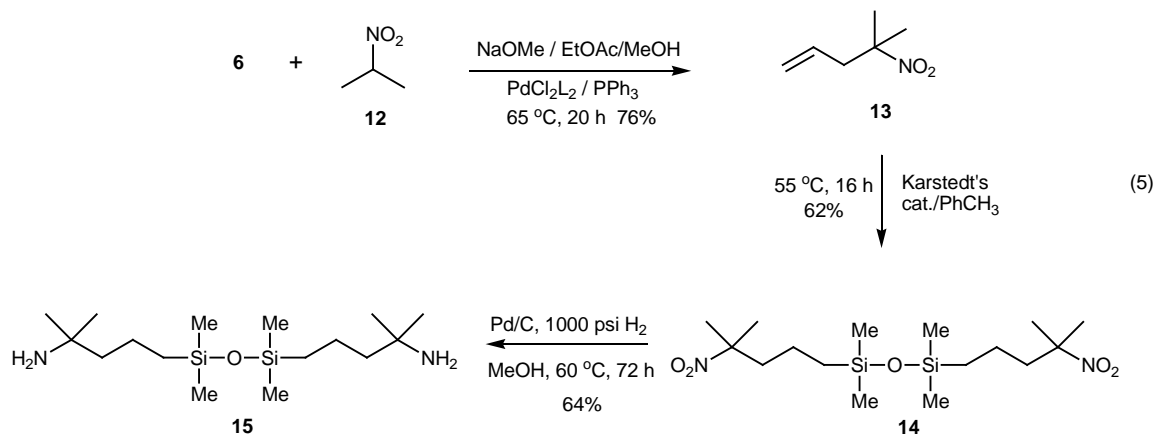
Few aminodisiloxanes are commercially available and we wished to explore a wider range of structural variants in order to gauge their efficacy in CO₂ capture. Hindered amines have been reported to be more effective in capturing CO₂ than their unhindered counterparts.^{8b, 21} To test this concept in this system, a series of compounds **5**, **11** and **15** were synthesized with increasing steric bulk. Aminobutyl derivative **5** was made as shown in equation 3. Hydrosilylation of tetramethyldisiloxane **2** with allyl cyanide **3** gave dinitrile **4**, which was subsequently reduced with lithium aluminum hydride (LAH).



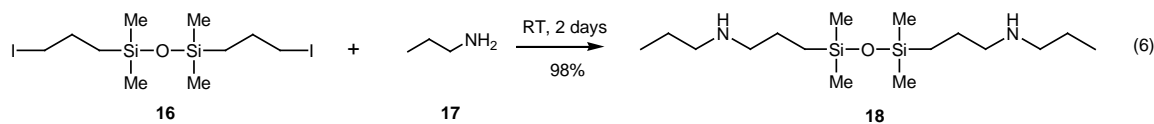
Synthesis of the methyl-substituted derivative **11** proceeded through a nitro functional disiloxane intermediate as shown in equation 4. Nitronate anion reaction with a palladium- π -allyl complex generated in situ provided 2-nitro-4-pentene **8** in 29% isolated yield. A substantial amount of the bis-allylated by-product **9** was also formed in this reaction. Pt catalyzed hydrosilylation gave the dinitro intermediate **10**, which was readily reduced by hydrogenation at 1000 psi using palladium on carbon to give the methylamino derivative **11**.



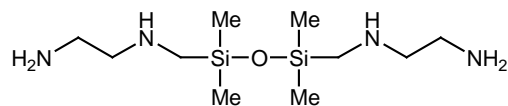
A similar approach was taken for the dimethyl analog **15**. Olefin **13** was produced in substantially better yield than was compound **8**, as bis-allylation was not possible with the 2-nitropropane anion. This compound was readily converted into the desired disiloxane as in equation 5.



To this point, the aminosiloxanes synthesized contained only primary amino groups. Compound **18** was made to determine what effect a purely secondary amine containing disiloxane would have on CO₂ capture. N-Propylamine readily displaced iodide from **16** to give the propylaminopropyl derivative in nearly quantitative yield.

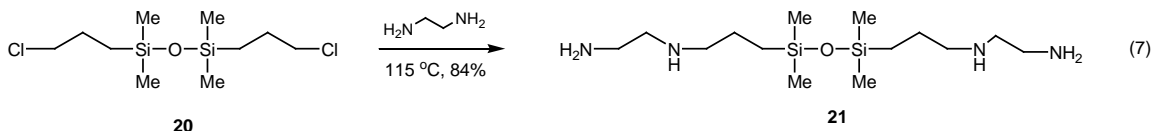


In addition to simple structural variants, some multi-functional derivatives were prepared designed to determine whether higher CO₂ capacity could be obtained. The first approach was to explore compounds with multiple amines in the side chains. These materials contained a mixture of primary and secondary amine functionality.



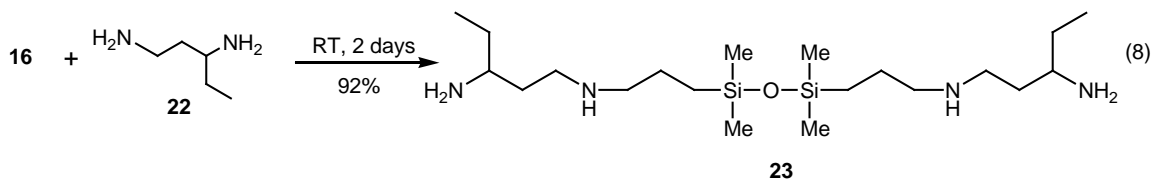
19

The aminoethylaminomethyl derivative **19** was commercially available but the corresponding aminoethylaminopropyl disiloxane, **21**, required preparation as shown in equation 7.



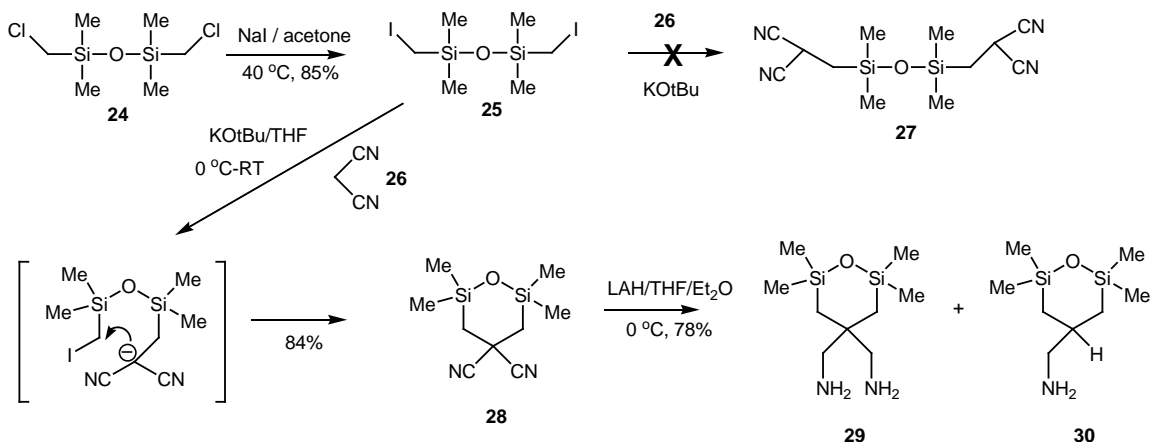
Reaction of the chloropropyl disiloxane **20** with excess ethylenediamine gave a mixture of multiply aminated compounds rich in the desired product. Fractional distillation provided pure **21**.

A tetrafunctional hindered amine disiloxane **23** was prepared via the reaction of 1,3-diaminopentane **22** with **16**. Aqueous washing removed the excess unreacted amine.



Next, another series of tetraamino derivatives were targeted where all of the amines were primary. These were envisioned to be available via reaction of haloalkyl disiloxanes with the anion of malononitrile, followed by reduction of the subsequent tetranitriles. As a first example, synthesis of a malononitrile derivative **27** was targeted (Scheme 1). However, it was quickly determined that reaction of malononitrile **26** with bis(iodomethyl)tetramethyl disiloxane **25** using potassium *t*-butoxide as base, did not give the anticipated product **27**, but rather the solid cyclic compound **28**, via intramolecular cyclization. Interestingly this result was obtained even with excess malononitrile. In fact, it was subsequently determined that when the reaction was done on-stoichiometry, that lower yields were obtained. This was due to the formation of more side products, which appeared to arise from attack by potassium *t*-butoxide on the siloxane linkage.

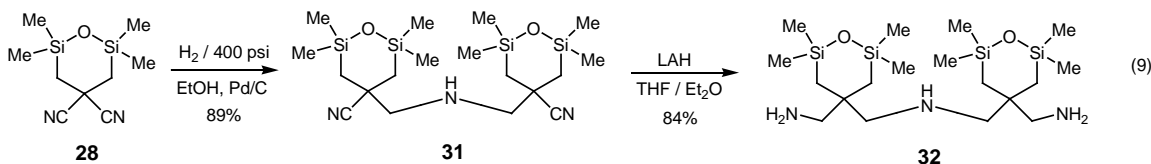
Scheme 1. Preparation of Malononitrile Derivatives.



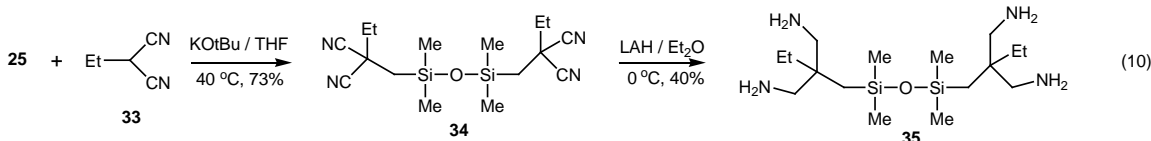
Although not the targeted structure, dinitrile **28** was deemed interesting enough to merit further exploration. Thus, the material was reduced using lithium aluminum hydride. A mixed solvent system composed of ether and THF was used to overcome the poor miscibility of **28** in ether. The overall isolated yield of aminosiloxanes was typically around 78%. However this was found to be composed of a mixture of the expected diamine **29** along with a monoamine **30**. Proton NMR indicated that the molar ratio of these two compounds was approximately 60:40. Separation of the two was accomplished via fractional distillation.

Reductive decyanation of one of the nitriles of malononitrile derivatives is known^{22a-c} and in this case, this reaction followed by subsequent reduction of the remaining CN would give the monoamine. While reductive decyanation of this type is usually performed under free-radical conditions, the related reaction of α -aminonitriles can be accomplished using aluminos and borohydrides.^{22d}

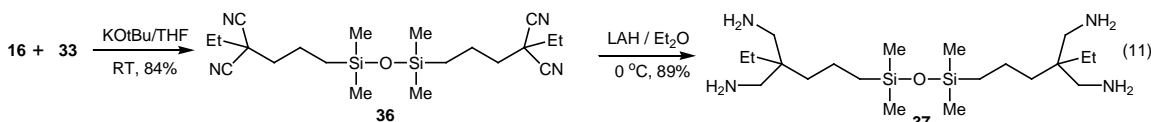
Hydrogenation was examined as an alternate route to reduce **28**. Treatment of the dinitrile with Pd/C at 65 °C and 400 psi H₂ gave the partially reduced dimeric compound **31** in 89% yield (equation 9). While unexpected, the formation of secondary amines during catalytic hydrogenation of nitriles have been reported.²³ Reduction of **31** with LAH proceeded cleanly to give dicyclic triamine **32**.



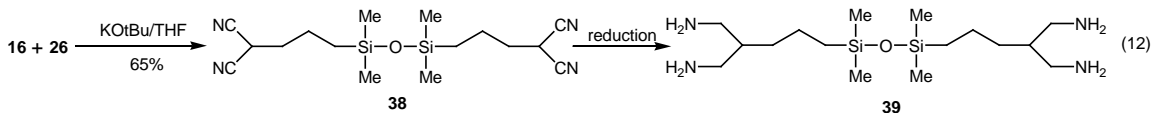
The intramolecular cyclization that led to **28** could be eliminated by using monoalkylated 2-ethyl malononitrile anion as nucleophile as shown in equation 10. Bisalkylation of iodomethyl functional **25** at 40°C resulted in 73% isolated yield of the solid tetracyano compound **34**. LAH reduction allowed for isolation of the final tetraamine, **35** in 40% yield. In this case, no trace of products derived from reductive decyanation was observed.



2-Ethyl malononitrile was also reacted with bis(3-iodopropyl) tetramethyldisiloxane to give tetranitrile **36** (equation 11). The reaction in this case was more facile than with the iodomethyl disiloxane, and excellent yields of product were obtained after reaction for a couple of hours at room temperature. Subsequent reduction with LAH in ether provided tetraamine **37** in high yield and good purity.

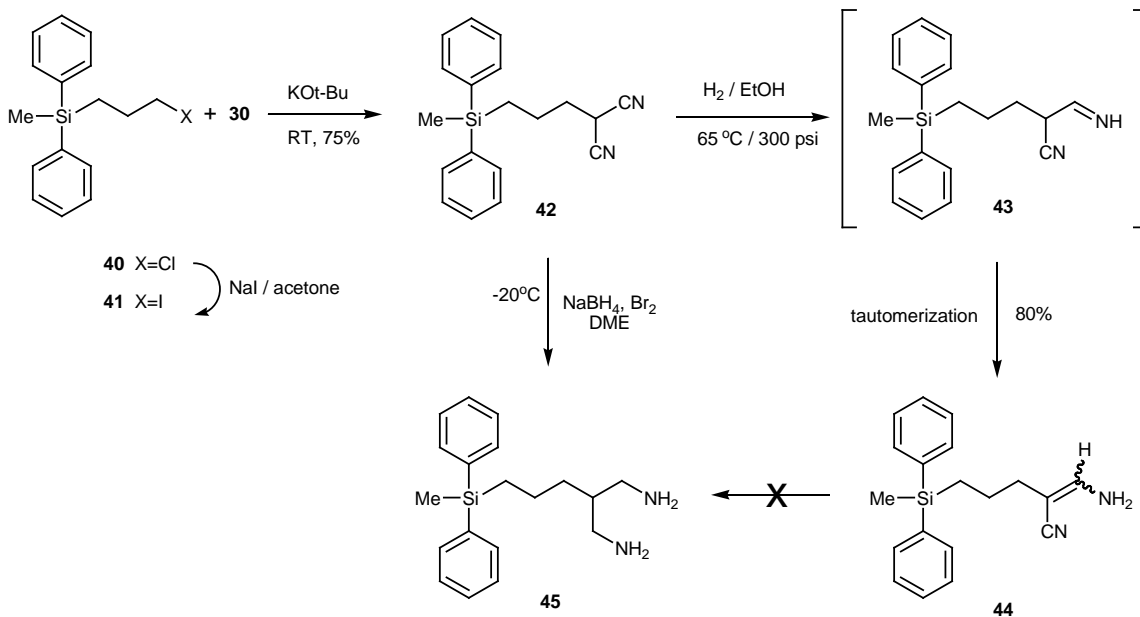


A final tetraamine synthesis was attempted as shown in equation 12. Reaction of the malononitrile anion with **16** gave tetracyano disiloxane **38**. Clean reduction of this material to the corresponding tetraamine **39** proved to be difficult. The acidic methine protons of unsubstituted or monoalkylated malononitrile derivatives have been reported to be the cause of poor yields during reduction.²⁴ Chemical reductions using $\text{NaBH}_4/\text{BF}_3\text{-Et}_2\text{O}$ ²⁵, $\text{NaBH}_4/\text{NiCl}_2$ ²⁶, LAH²⁷ or LAH/AlCl_3 ²⁸ did not proceed cleanly, nor did catalytic reduction using PtO_2 in $\text{EtOH}/\text{CHCl}_3$.²⁹ Hydrogenations with Pd/C in EtOH or in an acidic medium³⁰ were also unsuccessful; even with the possibility of side reactions of amines with partially reduced imine intermediates³¹ being suppressed.



To further explore this problem, model reductions of the dinitrile silane **42** were examined. This material, which was readily prepared via reaction of malononitrile with the iodopropyl compound **41**, was chosen as it possessed aromatic rings for more efficient visualization during chromatography, eliminated the potentially labile siloxane linkage and served as a surrogate of a mono-substituted dinitrile containing an acidic proton.

Scheme 2. Reduction of Model Compound **42**.



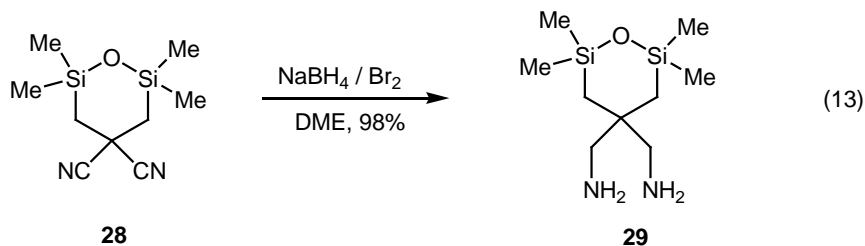
As expected, hydrogenation of **42** did not provide any of the desired product **45**. Instead it gave a good yield of a pair of partially reduced enamino nitrile compounds **44** (Scheme 3). These were presumably formed from initial hydrogenation of one of the nitrile groups, giving cyano imine **43**, that subsequently tautomerized to **44**. Interestingly like the previously described hydrogenation of **28** (equation 9), further reduction was not observed under these reaction conditions. ^1H NMR showed two distinct sets of triplets corresponding to the vinyl proton, which were coupled to the amine H's (broadened doublets). Exchange with D_2O collapsed the triplets into singlets with concomitant disappearance of the NH_2 resonances. Analysis of the crude reaction mixture showed that the E and Z isomers were formed in a roughly 1:1 ratio. It should be noted that these types of materials have also been reported to be formed during the LAH reduction of malononitriles.³²

Recently a mild route for the reduction of monoalkylated malonate esters has been reported, using borane-dimethoxyethane prepared from the reaction of bromine with sodium borohydride.³³ Adaptation of this procedure to dinitrile **42** resulted in the formation of the desired diamine **45** in 58% yield, after purification by column chromatography.

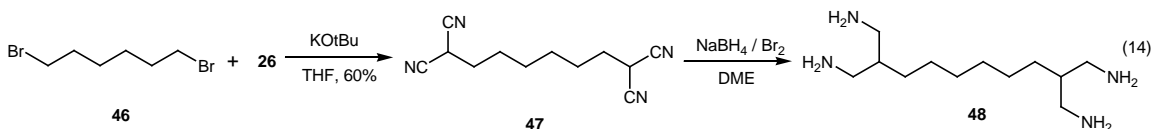
Application of this technique to **38** provided the sought after tetraamine **39** but in significantly lower yield (ca. 20%) and moderate purity. A large amount of aqueous HCl insoluble solid by-products were obtained in this case. In addition, purification proved to be difficult- the disiloxane did not survive the chromatographic conditions like those used for **45**.

In order to obtain further insight into these results, this reaction protocol was run on the cyclic dinitrile **28**. Like **38**, this material contained a potentially labile siloxane linkage. Interestingly, reduction of **28** with $\text{NaBH}_4/\text{Br}_2$ was found to proceed in excellent yield (98% crude) and purity (>95%) (Equation 13). Thus, the disiloxane portion of this molecule seemed to be stable under these reaction conditions.

Furthermore, in contrast to the previously described LAH reduction of this compound (see Scheme 1), only diamine **29** was obtained in this case.



Finally, a hydrocarbon based tetranitrile **47** was synthesized via reaction of 1,6-dibromohexane with malononitrile, and was then reduced with $\text{NaBH}_4/\text{Br}_2$. As was the case with tetranitrile **38**, the results were poor- very little material was isolated on workup and acid-insoluble solid was observed. In addition, proton NMR provided scant evidence to support formation of tetraamine **48**. Thus while this reduction procedure worked well for dinitriles **28** and **42**, it was not particularly successful for tetranitriles containing either a siloxane or hydrocarbon skeleton.



Testing

Preliminary evaluation of these aminodisiloxanes proceeded by exposing the neat materials at 40°C in a flask with mechanical stirring, to a stream of dry CO_2 . Mechanical agitation was necessary to improve the mass transfer of the gas through the reaction medium and 40°C is the approximate temperature that flue gas would enter a CO_2 absorber column. The first column of Table 1 shows the weight gain recorded for the neat compounds after 2 h exposure to CO_2 . The second column indicates the percentage of theoretical pickup to which this weight gain corresponds. Theoretical weight gain values were calculated based on the amine equivalent weight of each compound and the assumption that two amines were required per carbon dioxide molecule as shown in Equations 1 and 2. As can be seen, few of the materials reached their theoretical capacity in the neat state. However, many were in the 70-90% range. This was especially encouraging as almost all the aminodisiloxanes turned into solids during reaction with CO_2 . Significantly, the only exception was the monoamine **30**, which remained liquid during CO_2 uptake, and as such was the only neat material to exceed 100% of the theoretical uptake value. This higher than theoretical value was presumably due to some physi-sorption of gas, as well as formation of bicarbonate salts from adventitious water present in the system.³⁴

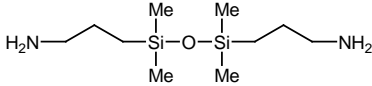
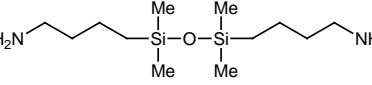
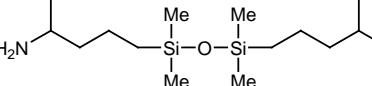
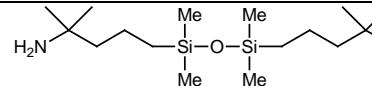
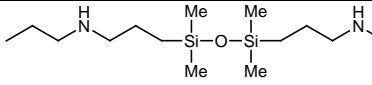
A closer look at the structural variations and their effect of CO_2 absorption revealed that the best materials were the linear primary amine containing solvents **1**, **5**, **11** and **30**. Increased steric hindrance around the primary amine with alkyl groups (compounds **15**,

23, 35 and **37**) or a ring (**29**) substantially reduced the CO₂ capture capability. Multiple amines on a chain as seen in aminoethyl derivatives **19** and **21** did enhance CO₂ pickup on a weight % basis, but were less impressive on a molar or theoretical basis. Presumably, the secondary amines were less reactive than the primary ones. This latter supposition was born out by the relatively poor reactivity of secondary amine functional disiloxane **18**.

To further facilitate the mass transfer of CO₂ to the reactive amine sites, use of a co-solvent was also explored. Triethylene glycol (TEG) was found to be a suitable candidate for this purpose.²⁰ First, it has low volatility and thus did not readily evaporate during testing. Furthermore, it solubilizes most carbamate salts formed from the reaction of the aminodisiloxanes with CO₂. Exposure of 50/50 mixtures of each of the disiloxanes with TEG for 2 h at 40 °C generated the results seen in column 3 of Table 1. Theoretical CO₂ uptake increased significantly and in several cases exceeded 100%. In all cases of increased weight gain, the reaction mixtures were homogeneous liquids. Secondary amine **18** did not show any improvement in CO₂ weight gain and compound **29** showed a decrease. In the latter case, the carbamate mixture in TEG was a waxy gel that suppressed rapid CO₂ reaction. The dicyclic triamine **32** was only tested in TEG as it was a solid at 40 °C. Even diluted, the reaction product with CO₂ gave a very thick waxy solid that only absorbed 63% of the theoretical amount of CO₂. Again, poor reactivity was likely a result of poor mass transfer.

Interestingly, the stability of the absorbed CO₂ was evidenced by the fact that no appreciable loss of weight was seen with samples absorbing over 100% even after standing at ambient temperature for several days.

Table 1. CO₂ Absorption of Aminodisiloxanes.

Cmpd	Structure	% CO ₂ Wt Gain (Neat)	% of Theoretical	% CO ₂ Wt Gain (1/1 TEG)	% of Theoretical
1		17.3	98	10.2	115
5		14.6	92	8.6	108
11		13.5	94	8.2	116
15		9.5	72	5.4	84
18		7.1	54	3.3	50

19		21.8	69	15.9	101
21		16.7	64	11.8	90
23		16.5	79	9.9	95
29		15.5	82	6.5	69
30		12.7	117	6.1	111
32		NT	NT	4.6	63
35		4.8	20	11.4	90
37		13.4	64	9.9	95

Conclusion

A variety of amino-substituted disiloxanes were synthesized and tested for their efficacy in CO₂ absorption. Three basic reaction schemes were pursued in this work. First, a series of alkyl amine functional disiloxanes with varying degrees of steric hindrance, **5**, **11**, and **15**, were prepared via hydrosilylation of either allyl cyanide or

nitroalkenes **8** and **13** with tetramethyldisiloxane, followed by reduction. Each of these derivatives contained two primary amine groups.

A second scheme involved the reaction of halopropyl disiloxane derivatives with amines. When propyl amine was used as nucleophile, a secondary amine containing derivative **18**, was obtained. Reactions with ethylenediamine and 1,3-diaminopentane produced tetramines **21** and **23** respectively. These latter compounds each had two primary and two secondary amino groups.

Tetraamine derivatives with all primary amino functionality (**35** and **37**) were prepared via the reaction of iodoalkyl functional disiloxanes with the anion of 2-ethyl malononitrile, followed by reduction with lithium aluminum hydride. Extension of this protocol to derivatives of malononitrile itself proved to be more challenging. First, reaction of the potassium salt of malononitrile with bis(iodomethyl) tetramethyl-disiloxane did not form the desired tetranitrile **27**, but instead underwent intramolecular reaction of the intermediate monomalononitrile derivative to provide cyclic dinitrile **28**. Reaction of bis(iodopropyl) tetramethyldisiloxane with excess malononitrile anion did provide the desired tetranitrile **38** in excellent yield. However, clean reduction of this compound to the tetraamine was not entirely successful. The best results were obtained using a modification of a procedure reported by Tudge et. al. for the reduction of malonate ester derivatives.³³ However, low yields were obtained along with moderate purity.

Reduction of cyclic dinitrile **28** also provided interesting results. When LAH was used as reductant, an approximate 60:40 mixture of the desired diamine **29** with monoamine **30** was obtained. Hydrogenation using palladium on carbon led to partial reduction and formation of a secondary amine dinitrile **31** that was readily reduced with LAH to triamine **32**. In contrast to this, when NaBH₄/Br₂ was used to reduce **28**, only the diamine **29** was obtained, in both excellent yield and purity.

Unhindered, primary linear amine groups were found to be the most efficient on a molar basis at absorbing carbon dioxide, with more hindered primary amines being less effectual. Tetraamine functional disiloxane compounds reacted with CO₂ to give higher overall weight increases but demonstrated uptake values significantly lower than predicted based on their overall amine content. In some cases this was due to less effective reactions of the secondary amino groups that were present. Mass transfer was another important factor. Materials or mixtures that remained liquid during absorption experiments gave higher CO₂ uptake values (relative to theoretical levels) than those that became solids. Furthermore, in most cases addition of triethylene glycol allowed for the formation of liquid carbamate salt solutions, which led to improved performance.

Acknowledgments

This material is based upon work supported by the Department of Energy, National Energy Technology Laboratory under Award Number DE-NT0005310. We thank T. Early for assignments of the E and Z isomers of compound **44** and H. Grade for mass spectrometry measurements.

Disclaimer

This report was prepared as an account of work sponsored by an agency of the United States Government. Neither the United States Government nor any agency thereof, nor any of their employees, makes any warranty, express or implied, or assumes any legal liability or responsibility for the accuracy, completeness, or usefulness of any information, apparatus, product, or process disclosed, or represents that its use would not infringe privately owned rights. Reference herein to any specific commercial product, process, or service by trade name, trademark, manufacturer, or otherwise does not necessarily constitute or imply its endorsement, recommendation, or favoring by the United States Government or any agency thereof. The views and opinions of authors expressed herein do not necessarily state or reflect those of the United States Government or any agency thereof.

Experimental

General. All chemicals were used as received unless otherwise noted. The disiloxane starting materials were obtained from Gelest. Solvents were purchased from Fisher Scientific and all other chemicals were obtained from Sigma-Aldrich. ^1H and ^{13}C NMR spectra were obtained on a Bruker 400 MHz instrument. FTIR spectra were recorded on a Perkin Elmer Spectrum 100 Spectrometer. Mass spectra were acquired on a JEOL AccuTofF JMS T100 LC-MS instrument retrofitted with an Ionsense DART (Direct Analysis in Real Time) ion source in place of the normal Electrospray source used for LCMS. Helium (2.4 l/min) was used as the DART gas. The gas heater (post glow discharge) of the DART source was set to 240°C. The analytes experience temperatures far below this during analysis. Melting points were measured on an Electrothermal® Melting Point Apparatus and are uncorrected.

1,3-bis(3-cyanopropyl)-1,1,3,3-tetramethyldisiloxane (4) Tetramethyldisiloxane **2** (10.0 g, 74 mmol) in toluene (15 mL) was treated dropwise with allyl cyanide **3** (10.1 g, 151 mmol) in toluene (10 mL) containing 10 μL of Karstedt's catalyst (4.7 wt % Pt in xylenes) over 5 min. An exotherm was observed from 23 to 29 °C after a few minute induction period. When addition was complete, the reaction mixture was heated to 70 °C for 48 h during which time 5 additional aliquots of Karstedt's catalyst were added. After this time, the solvent was removed and the product 11.14 g (56%) collected by distillation at 105-111 °C/0.16 torr. ^{35}H NMR (CDCl_3) δ : 2.39 (t, $J = 7.0$ Hz, 4H); 1.69(m, 4H); 0.70 (m, 4H); 0.10 (s, 12H). $^{13}\text{C}\{^1\text{H}\}$ NMR (CDCl_3): 119.8, 20.6, 20.0, 17.8, 0.2 ppm. FT-IR (neat): 2958, 2903, 2881, 2246, 1494, 1452, 1427, 1414, 1344, 1259, 1176, 1050, 825, 798 cm^{-1} .

1,3-bis(4-aminobutyl)-1,1,3,3-tetramethyldisiloxane (5) A solution of 1,3-bis(3-cyanopropyl)-1,1,3,3-tetramethyldisiloxane **4** (9.9 g, 36.9 mmol) in Et_2O (50 mL) was added slowly over 25 min to a mechanically stirred, pre-cooled slurry of LAH (6.7 g, 176 mmol) in Et_2O (450 mL) at -5 °C under N_2 so as to keep the temperature below 5 °C. The mixture was stirred for 1.5 h then water (20 mL), 20% NaOH (40 mL) and then water (100 mL) were added carefully in that order with vigorous stirring. Additional Et_2O was added (100 mL) and the Et_2O was decanted from the 2-phase slurry. The white sludge was extracted with Et_2O (2 x 50 mL) and the Et_2O layers combined, dried with MgSO_4 ,

filtered and concentrated to a light orange liquid which was fractionally distilled at 85-87 °C/0.16 torr to give 9.1 g (89%) product as a colorless liquid.³⁶ ¹H NMR (CDCl₃) δ: 2.94 (br s, 4H); 2.75 (m, 4H); 1.38 (m, 4H); 0.55 (m, 4H); 0.05 (s, 12H). ¹³C{¹H} NMR (CDCl₃): 41.8, 37.1, 20.6, 18.2, 0.4 ppm. FT-IR (neat): 3368, 3289, 2954, 2922, 2855, 1598, 1455, 1409, 1252, 1059, 940, 795, 704 cm⁻¹.

4-Nitro-1-pentene (8) A solution of NaOMe in MeOH (60 g, 0.27 mole of 25 wt%) was added to a MeOH solution (500 mL) of nitroethane (102 g, 1.35 mole) and heated until dissolved. Then PdCl₂(PPh₃)₂ (1.5 g, 2.1 mmol), PPh₃ (1.5 g, 5.7 mmol) and EtOAc (24 g, 0.27 mole) were added and heated to reflux under N₂ with magnetic stirring for 15 min. After this time, the homogeneous reaction mixture was cooled to 5-10 °C and allyl acetate (27 g, 0.27 mole) was added in one portion and the mixture allowed to react for 18 h at 10-15 °C. The reaction mixture was poured into water (600 mL) then extracted with hexanes (1 x 400 mL). The aqueous layer was acidified to pH 7 and further extracted with hexanes (2 x 300 mL). The organic layers were combined, washed with water, dried over MgSO₄, concentrated in vacuo and fractionally distilled at 45-47 °C/9-10 torr to give 9.1 g product (29% yield).³⁷ Various other fractions were contaminated with substantial amounts of bis-allylated product (**9**). ¹H NMR (CDCl₃) δ: 5.73 (m, 1H); 5.15 (m, 2H); 4.62 (m, 1H); 2.74 (m, 1H); 2.54 (m, 1H); 1.56 (d, J = 6.7 Hz, 3H). ¹³C{¹H}NMR (CDCl₃): 131.4, 119.5, 82.6, 39.1, 18.6 ppm. FT-IR (neat): 3089, 2993, 2949, 2923, 1861, 1648, 1552, 1457, 1442, 1420, 1394, 1362, 1321, 1274, 1229, 1163, 1118, 1034, 998, 935, 857, 645 cm⁻¹.

4-Nitro-4-methyl-1,6-heptadiene (9): ¹H NMR (CDCl₃) δ: 5.68 (m, 2H); 5.15 (m, 4H); 2.74 (m, 2H); 2.56 (m, 2H); 1.54 (s, 3H). ¹³C{¹H} NMR (CDCl₃): 130.8, 120.6, 90.6, 43.4, 21.9 ppm. FT-IR (neat): 3083, 2985, 2944, 2922, 2880, 1858, 1742, 1643, 1539, 1452, 1438, 1388, 1351, 1291, 1164, 1049, 996, 926, 855 cm⁻¹.³⁷

1,3-bis(4-nitropentyl)-1,1,3,3-tetramethyldisiloxane (10) 1,1,3,3-Tetramethyldisiloxane (4.19 g, 31 mmol) in toluene (40 mL) was treated dropwise with 2-nitro-4-pentene **8** (9.0 g, 78 mmol) in toluene (10 mL) containing 10 μL of Karstedt's catalyst (4.7 wt % Pt in xylenes). An exotherm was observed from 24 to 44 °C after a few minute induction period. When addition was complete, the reaction mixture was heated to 55 °C for 18 h. After this time, the solvent was removed and the product 9.7 g (86%) collected by distillation at 133-136 °C/0.16 torr. ¹H NMR (CDCl₃) δ: 4.63 (m, 2H); 2.07 (m, 2H); 1.74 (m, 2H); 1.55 (d, J = 6.6 Hz, 6H); 1.36(m, 4H); 0.55 (m, 4H); 0.05 (s, 12h). ¹³C{¹H} NMR (CDCl₃): 83.3, 38.6, 19.7, 19.2, 17.7, 0.3 ppm. FT-IR (neat): 2991, 2955, 2903, 2881, 1553, 1495, 1451, 1389, 1358, 1312, 1260, 1191, 1059, 849, 805, 709 cm⁻¹. Exact mass MS: Calc'd for: C₁₄H₃₃N₂O₄Si₂ (M+H⁺); 349.1979. Found; 349.1961.

1,3-bis(4-aminopentyl)-1,1,3,3-tetramethyldisiloxane (11) 1,3-bis(4-nitropentyl)-1,1,3,3-tetramethyldisiloxane **10** (7.75 g, 21.2 mmol) and 10% Pd/C (1.0g) were heated to 60 °C in MeOH (78g) under 1000 psi H₂ for 24 h. The catalyst was removed by filtration, the solvent removed in vacuo and the product (4.8 g, 74%) collected by distillation at 75-77 °C/0.2 torr. ¹H NMR (CDCl₃) δ: 2.84 (m, 2H); 1.68 (br s, 4H); 1.30 (m, 8H); 1.02 (d, J = 6.4 Hz, 6H); 0.46 (m, 4H); 0.00 (s, 12H). ¹³C{¹H} NMR (CDCl₃):

46.6, 43.8, 23.8, 20.1, 18.4, 0.4 ppm. FT-IR (neat): 3363, 3285, 2955, 2921, 2874, 1597, 1460, 1413, 1376, 1255, 1181, 1060, 843, 799, 766, 707 cm^{-1} . Exact mass MS: Calc'd for $\text{C}_{14}\text{H}_{37}\text{N}_2\text{OSi}_2$ ($\text{M}+\text{H}^+$); 305.2444. Found; 305.2422.

4-Nitro-4-methyl-1-pentene (13) 2-nitropropane **12** (36 g, 0.41 mole), NaOMe in MeOH (88.2 g, 0.41 mole of 25 wt%), MeOH (500 mL) and EtOAc (36 g, 0.41 mole) were added together and heated at 60–65 °C under N_2 . Then $\text{PdCl}_2(\text{PPh}_3)_2$ (1.5 g, 2 mmol), PPh_3 (1.5 g, 5 mmol) were added and stirred for 2 h at 65 °C. After this time, allyl acetate **6** (61 g, 0.61 mole) was added and the mixture allowed to react for 20 h. The reaction mixture was diluted with water (600 mL), extracted with hexanes (3 x 250 mL), the organic layers were combined, washed with water, dried over MgSO_4 , concentrated in vacuo and fractionally distilled at 30–32 °C/0.3 torr to give 40.0 g product (76% yield) as a colorless liquid.³⁸ ^1H NMR (CDCl_3) δ : 5.69 (m, 1H); 5.18 (m, 2H); 2.65 (d, $J = 7.3$ Hz, 2H); 2.56 (m, 2H); 1.59 (s, 6H). $^{13}\text{C}\{^1\text{H}\}$ NMR (CDCl_3): 131.1, 120.4, 87.8, 45.0, 25.5 ppm. FT-IR (neat): 3084, 2987, 2944, 2876, 1861, 1643, 1539, 1471, 1457, 1445, 1396, 1373, 1348, 1274, 1230, 1137, 1088, 997, 928, 857 cm^{-1} . Exact mass MS: Calc'd for $\text{C}_6\text{H}_{12}\text{NO}_2$ ($\text{M}+\text{H}^+$); 130.0868. Found; 130.0869.

1,3-bis(4-nitro-4-methylpentyl)-1,1,3,3-tetramethyldisiloxane (14) 1,1,3,3-Tetramethyldisiloxane (4.9 g, 36 mmol) in toluene (50 mL) was treated dropwise with 2-nitro-4-methyl-4-pentene **13** (9.5.0 g, 74 mmol) in toluene (25 mL) containing 30 μL of Karstedt's catalyst (4.7 wt % Pt in xylenes). An exotherm was observed after a few minute induction period. Addition over 5 min resulted in an exotherm to 32 °C. When addition was complete, the reaction mixture was heated to 60 °C for 16 h. After this time, an additional aliquot of Karstedt's catalyst was added (20 μL) and the reaction allowed to continue for a total of 26 h. The solvent was removed and the product 10.9 g (77%) collected by distillation at 138–145 °C/0.18–0.24 torr. ^1H NMR (CDCl_3) δ : 1.90 (m, 4H); 1.59 (s, 12H); 1.28 (m, 4H); 0.49 (m, 4H); 0.85 (s, 12H). $^{13}\text{C}\{^1\text{H}\}$ NMR (CDCl_3): 88.3, 44.6, 25.8, 18.2, 18.0, 0.3 ppm. FT-IR (neat): 2993, 2955, 2899, 2875, 1539, 1472, 1455, 1397, 1373, 1348, 1255, 1208, 1188, 1059, 844, 803, 764, 706 cm^{-1} . Exact mass MS: Calc'd for $\text{C}_{10}\text{H}_{24}\text{NO}_2\text{Si}_2$ ($\text{M}-\text{C}_6\text{H}_{12}\text{NO}_2^+$); 262.1295. Found; 262.1293.

1,3-bis(4-amino-4-methylpentyl)-1,1,3,3-tetramethyldisiloxane (15) 10% Pd/C (1 g) was added to a solution of 1,3-bis(4-nitro-4-methylpentyl)-1,1,3,3-tetramethyldisiloxane **14** (9.6 g, 24.4 mmol) in MeOH (75 mL) and heated to 60 °C for 3 days under 1000 psi H_2 . After this time, the catalyst was removed by filtration, the solvent was removed in vacuo and the product isolated by vacuum distillation at 95–97 °C/0.2 torr to give 5.16 g (64%) colorless liquid. ^1H NMR (CDCl_3) δ : 2.35 (br s, 4H); 1.37 (m, 8H); 1.13 (s, 12H); 0.51 (m, 4H); 0.06 (s, 12H). $^{13}\text{C}\{^1\text{H}\}$ NMR (CDCl_3): 50.2, 48.7, 29.8, 19.1, 18.1, 0.5 ppm. FT-IR (neat): 3350, 3281, 3178, 2959, 2926, 2908, 2875, 1601, 1495, 1469, 1411, 1381, 1363, 1253, 1198, 1063, 847, 807 cm^{-1} . Exact mass MS: Calc'd for: $\text{C}_{16}\text{H}_{41}\text{N}_2\text{OSi}_2$ ($\text{M}+\text{H}^+$); 333.2757. Found; 333.2747.

1,3-bis(3-iodopropyl)-1,1,3,3-tetramethyldisiloxane (16). To a solution of 1,3-bis(3-chloropropyl)-1,1,3,3-tetramethyldisiloxane **20** (30.0 g, 209 mmols RCl) in acetone (125 mL) was added sodium iodide (47.0 g, 314 mmols). The result was heated to reflux

under nitrogen for 4 days. At the end of this time, the mixture was cooled to room temperature and the solids were removed by filtration. The filtrate was then stripped on a rotary evaporator and the resulting residue was partitioned between heptane and water. The aqueous layer was discarded and the organics were washed with water, dilute sodium hydrosulfite, another portion of water, and saturated sodium chloride. After drying over anhydrous sodium sulfate, the solvent was stripped under reduced pressure yielding 45.5 g (93%) of product as a colorless oil.⁴⁰ ¹H NMR (CDCl₃) δ: 3.19 (t, J = 8 Hz, 4H), 1.82 (m, 4H), 0.61 (m, 4H), 0.06 (s, 12H).

1,3-bis(propylaminopropyl)-1,1,3,3-tetramethyldisiloxane (18) A 50 mL round bottom flask was charged with n-propylamine **17** (16.1 mL, 196 mmol) and placed in a room temperature water bath. 1,3-bis(3-iodopropyl)-1,1,3,3-tetramethyldisiloxane (7.7 g, 38 mmol) was added dropwise under nitrogen. The mixture was then allowed to stir at room temperature for 2 days. At this point, the bulk of excess propylamine was stripped off under vacuum. The residue was then partitioned between chloroform and 10% sodium hydroxide. The organic layer was then washed four times with deionized water and once with saturated sodium chloride. After drying over anhydrous sodium sulfate, the solvent was removed on a rotary evaporator yielding 5.3 g (98%) product as a colorless oil. ¹H NMR (CDCl₃) δ: 2.55 (q, J = 8 Hz, 8H), 1.48 (m, 8H), 0.90 (t, J = 8 Hz, 6H), 0.48 (m, 4H), 0.02 (s, 12H). ¹³C{¹H}NMR (CDCl₃): 53.28, 51.90, 23.90, 23.32, 15.88, 11.82, 0.29 ppm. FT-IR (neat): 3286, 2956, 2926, 2875, 2806, 1459, 1410, 1378, 1340, 1252, 1174, 1130, 1051, 839, 795 cm⁻¹. Exact mass MS: Calc'd for C₁₆H₄₁N₂OSi₂ (M+H⁺); 333.2757. Found; 333.2755.

1,3-bis(3-(2-aminoethyl)aminopropyl)-1,1,3,3-tetramethyldisiloxane (21) Ethylenediamine (155 g, 2.58 moles) was charged to a 500 mL three-necked flask equipped with a magnetic stirbar, reflux condenser, addition funnel and nitrogen sweep. It was then heated using an oil bath. Once the temperature reached about 95 °C, 1,3-bis(3-chloropropyl)-1,1,3,3-tetramethyldisiloxane, **20**, (73 g, 254 mmols) was added dropwise over about 2 hours. During this time the temperature of the oil bath was allowed to increase to about 110-115 °C. Once addition was complete, the reaction mix was allowed to continue at this temperature for 2 more hours at which time proton NMR indicated that the reaction was complete. The mix was cooled, and then some of the excess ethylene diamine was stripped off. At this point the material was cooled to room temperature, partitioned between chloroform and 10% NaOH, and then the organic phase was washed with deionized water and saturated sodium chloride and dried over anhydrous potassium carbonate. After filtration, solvent was removed on a rotary evaporator yielding 71.2 g (84%) crude product which was purified by fractional distillation at 130-135 °C/0.18-0.25 mm Hg.⁴⁰ ¹H NMR (CDCl₃) δ: 2.79 (t, J = 6.0 Hz, 4H); 2.65 (t, J = 6.0 Hz, 4H); 2.58 (t, J = 7.3 Hz, 4H); 1.49(m, 4H); 1.31 (br 6H); 0.49 (m, 4H); 0.03 (s, 12H). ¹³C{¹H}NMR (CDCl₃): 53.1, 52.7, 41.9, 23.9, 15.8, 0.3 ppm. FT-IR (neat): 3366, 3285, 2929, 2877, 2807, 1604, 1495, 1455, 1345, 1301, 1257, 1176, 1127, 1054, 841, 795 cm⁻¹.

1,3-bis(3-(2-aminobutyl)aminopropyl)-1,1,3,3-tetramethyldisiloxane (23) A 50 mL round bottom flask was charged with 1,3-diaminopentane **26** (15.3 g, 150 mmol) and

placed in a room temperature water bath. 1,3-bis(3-iodopropyl)-1,1,3,3-tetramethyldisiloxane **22** (7.0 g, 30 mmol) was added dropwise under nitrogen. The mixture was then allowed to stir at room temperature for 2 days. At this point, the solution was partitioned between chloroform and 10% sodium hydroxide. The organic layer was then washed four times with deionized water and once with saturated sodium chloride. After drying over anhydrous sodium sulfate, the solvent was removed on a rotary evaporator yielding 5.7 g (92%) product as a colorless oil. ^1H NMR (CDCl_3) δ : 2.1-2.6 (m, 10H), 1.06-1.5 (m, 12H), 1.04 (br s, 6H), 0.72 (t, $J = 8$ Hz, 6H), 0.30 (m, 4H), -0.16 (s, 12H). $^{13}\text{C}\{^1\text{H}\}$ NMR (CDCl_3): 53.4, 51.6, 47.5, 37.7, 31.3, 23.8, 15.9, 10.3, 0.3 ppm. FT-IR (neat): 3363, 3286, 2956, 2924, 2874, 2810, 1607, 1460, 1409, 1357, 1252, 1176, 1125, 1051, 839, 795 cm^{-1} . Exact mass MS: Calc'd for: $\text{C}_{20}\text{H}_{51}\text{N}_4\text{OSi}_2$ ($\text{M}+\text{H}^+$); 419.3601. Found; 419.3597.

1,3-bis(iodomethyl)-1,1,3,3-tetramethyldisiloxane (25) 1,3-Bis(chloromethyl)-1,1,3,3-tetramethyldisiloxane **24** (20.0 g, 173 mmols RCl) was combined with acetone (80mL) and sodium iodide (39.0 g, 260 mmol). The mixture was then heated to 35-40°C overnight. At this point it was cooled and filtered to remove salts. The acetone was then stripped on a rotary evaporator. The residue, which was a mix of solid and liquid, was then partitioned between heptane and water. The organic layer was washed with dilute sodium hydrosulfite, water, and saturated sodium chloride. After drying over anhydrous sodium sulfate, the solvent was removed on a rotary evaporator yielding 30.3 g (85%) product as a colorless oil.^{39, 41} ^1H NMR (CDCl_3) δ : 2.01 (s, 4H), 0.28 (s, 12H). $^{13}\text{C}\{^1\text{H}\}$ NMR (CDCl_3): -0.29, -12.49.

2,2,6,6-tetramethyl-1,2,6-oxadisilinane-4,4-dicarbonitrile (28) Malononitrile (9.8 g, 148 mmol) in THF (85 mL) was cooled in an ice bath under nitrogen. Solid potassium t-butoxide (14.7 g, 131 mmol) was added causing the mixture to turn milky pink. After approximately 15 minutes, a solution of 1,3-bis(iodomethyl)1,1,3,3-tetramethyldisiloxane (25.0 g, 121 mmols RI) in THF (25 mL) was added dropwise over 2 minutes. An additional portion of THF (5 mL) was used to rinse the addition funnel. The ice bath was removed and the reaction mixture was allowed to warm to room temperature where it was kept overnight. As time passed the color of the solution changed from pink to orange. At this point, the solution was filtered to remove solids and then the solvent was removed under reduced pressure. The residue was dissolved in chloroform and washed three times with deionized water, once with dilute sodium hydrosulfite, and once with saturated sodium chloride. After drying over anhydrous sodium sulfate, the solution was filtered and stripped on a rotary evaporator. The crude solid product was then recrystallized from a mixture of heptane and isopropanol (45mL/9mL). This provided 11.4 g of product (84% yield) as off-white needles. The melting point was determined to be 132-134 °C. ^1H NMR (CDCl_3) δ : 1.46 (s, 4H) 0.32 (s, 12 H). $^{13}\text{C}\{^1\text{H}\}$ NMR (CDCl_3): 118.08, 28.77, 26.42, 1.47. FT-IR (neat): 2966, 2240, 1425, 1252, 1023, 1001, 968, 817, 762, 695 cm^{-1} . Exact mass MS: Calc'd for: $\text{C}_9\text{H}_{17}\text{N}_2\text{OSi}_2$ ($\text{M}+\text{H}^+$); 225.0879. Found; 225.0870.

(2,2,6,6-tetramethyl-1,2,6-oxadisilinane-4-4-diyl)dimethanamine (29) and (2,2,6,6-tetramethyl-1,2,6-oxadisilinane-4-4-diyl) methanamine (30) A solution of 2,2,6,6-

tetramethyl-1,2,6-oxadisilinane-4,4-dicarbonitrile **28** (13.0 g, 57.9 mmol) in THF (90mL) was added slowly over 45 min to a stirred slurry of LAH (5.80 g, 153 mmol) in Et₂O (190 mL) under N₂. The mixture was stirred overnight then cooled to ca. 0°C and water (31 mL) was added carefully, followed by 0.8 mL 50% NaOH. After warming to room temperature the solid was filtered off and washed with fresh THF. The combined organics were dried over K₂CO₃ and then concentrated under reduced pressure to give 11.3 g of crude product. Purification was accomplished via fractional distillation. Three cuts were isolated. The first (3.1 g, 15 mmol) with a boiling point of 43-55°C/0.9 mm Hg was found to be monoamine **30** with a purity of >98%. ¹H NMR (CDCl₃) δ: 2.51 (d, J = 8 Hz, 2H); 1.73 (m, 1H); 1.08 (br s, 2H); 0.67 (dm, J = 12 Hz, 2H), 0.25 (t, J = 12 Hz, 2H), 0.11 (s, 6H), 0.10(s, 6H). ¹³C{¹H} NMR (CDCl₃): 54.11, 34.10, 20.95, 1.35, 0.24 ppm. FT-IR (neat): 3386, 3303, 2956, 2898, 2870, 1615, 1447, 1415, 1337, 1296, 1252, 1222, 1173, 1140, 1113, 1067, 1049, 986, 939, 880, 809, 720, 703, 685, 634, 590 cm⁻¹. Exact mass MS: Calc'd for: C₈H₂₂NOSi₂ (M+H⁺); 204.12399. Found; 204.12359. The second (0.9 g) with a boiling point of 55-76°C/0.9 mm Hg was a 53:47 mix of the mono and diamines. Finally the third cut (4.6 g, 19.8 mmol) had a boiling point of 76-84°C/0.8 mm Hg and was determined to be 99% pure diamine **29**. ¹H NMR (CDCl₃) δ: 2.70 (s, 4H); 1.93 (br s, 4H); 0.58 (s, 4H); 0.15 (s, 12H). ¹³C{¹H} NMR (CDCl₃): 54.2, 40.7, 22.7, 2.7 ppm. FT-IR (neat): 3385, 3305, 2961, 2899, 2869, 1603, 1460, 1417, 1314, 1259, 1189, 1058, 988, 853, 816, 761, 644, 601 cm⁻¹. Exact mass MS: Calc'd for: C₉H₂₅N₂OSi₂ (M+H⁺); 233.1505. Found; 233.1495.

Alternate preparation of (2,2,6,6-tetramethyl-1,2,6-oxadisilinane-4-4-

diyl)dimethanamine (29) Sodium borohydride (2.36 g, 62.4 mmol) was mixed with dimethoxyethane (DME, 40 mL) and cooled to -78°C under nitrogen. At this point, a freshly prepared solution of bromine (1.42 mL g, 27.7 mmol) in DME (20 mL) was added dropwise over approximately 30 minutes. The reaction mixture was stirred for an additional 30 minutes after all of the bromine had been added, and then it was warmed to ~0°C using an ice bath. At this point, a solution of 2,2,6,6-tetramethyl-1,2,6-oxadisilinane-4,4-dicarbonitrile **28** (2.00 g, 8.93 mmol) in DME (15mL) was added. Once addition was complete, the reaction was maintained at ~0°C for a couple of hours, and then it was allowed to slowly warm to room temperature where it was kept overnight. The mixture was then carefully added to 80 mL of ice cold 10% HCl. Next, it was allowed to warm to room temperature and was concentrated by stripping off about half the volume of liquid on a rotary evaporator. After cooling back down in an ice bath, the solution was made strongly basic by the addition of 10% NaOH. The result was extracted four times with chloroform and then the combined organics were dried over anhydrous sodium sulfate and stripped under reduced pressure. The result was 2.04 g (98% yield) of product as a light yellow oil. ¹H NMR showed it to be >95% pure.

4,4'-(azanediylbis(methylene))bis(2,2,6,6-tetramethyl-1,2,6-oxadisilinane-4-carbonitrile (31). A slurry of EtOH (100 mL), **28** (3.65 g, 16.3 mmol) and 10% Pd/C (300 mg) was added to a pressure reactor, sealed, degassed 3x and charged with 350 psi H₂ and heated to 65 °C for 48h. The reaction mixture was cooled, filtered through Celite® and allowed to stand. A white crystalline solid formed which was collected by filtration and dried to give 1.09 g product. Further product was collected from the concentrated

filtrate for a total of 3.2 g (89%). Mp 169-171 °C. ¹H NMR (CDCl₃) δ: 2.88 (d, J = 5.5 Hz, 4H), 1.6 (br, 1H); 1.24 (d, J = 14.7 Hz, 4H), 0.72 (d, J = 14.7 Hz, 4H), 0.38 (s, 12H), 0.19 (s, 12H). ¹³C{¹H}NMR (CDCl₃): 124.9, 63.6, 37.3, 24.6, 2.2, 1.3 ppm. FT-IR (neat): 2962, 2937, 2906, 2832, 2226, 1469, 1419, 1331, 1247, 1197, 1124, 1074, 986, 932, 906, 846, 812, 792, 764, 691 cm⁻¹. Exact mass MS: Calc'd for: C₁₈H₃₈N₃O₂Si₄ (MH⁺): 440.2041. Found: 440.2049.

Bis((4-(aminomethyl)-2,2,6,6-tetramethyl-1,2,6-oxadisilinan-4-yl)methyl)amine (32). A solution of **31** (1.0 g, 2.3 mmol) in dry THF (10 mL) was added slowly to a slurry of LAH (250 mg, 6.4 mmol) in dry Et₂O (10 mL) at room temperature. A slight exotherm and gas evolution was observed and after 24 hours, the reaction mixture was quenched with water (2 mL) followed by 0.5 mL of 10% NaOH. The mixture was stirred at room temperature, filtered, the solid washed with THF (10 mL), the filtrates combined, dried with Na₂SO₄, filtered and concentrated to give 0.84 mg (84%) product as a colorless oil that crystallized on standing to a waxy solid mp 68-70 °C. ¹H NMR (CDCl₃) δ: 2.66 (s, 4H), 2.53 (s, 4H), 1.2 (br, 5H), 0.62 (d, J = 4.6 Hz, 4H), 0.58 (d, J = 4.6 Hz, 4H), 0.16 (s, 12H); 0.15 (s, 12 H). ¹³C{¹H}NMR (CDCl₃): 60.3, 53.2, 40.7, 23.6, 2.8, 2.7 ppm. FT-IR (neat): 3376, 3307, 2955, 2893, 2863, 2808, 1591, 1459, 1413, 1249, 982, 844, 806, 749, 636 cm⁻¹. Exact mass MS: Calc'd for: C₁₈H₄₆N₃O₂Si₄ (MH⁺): 448.2667. Found: 448.2643.

1,3-bis(2,2-dicyanobutyl) -1,1,3,3-tetramethyldisiloxane (34) To an ice cold solution of 2-ethylmalononitrile **33** (4.2 g, 44.7 mmol) in THF (20 mL) was added potassium t-butoxide (3.68 g, 32.8 mmol). This caused the mixture to turn clear brown. Once all of the KOtBu had dissolved (10-15 minutes), a solution of 1,3-bis(iodomethyl)1,1,3,3-tetramethyldisiloxane (6.15 g, 29.7 mmol RI) in THF (12 mL) was added dropwise. Once the addition was complete, another portion of fresh THF (3 mL) was used to rinse the addition funnel. At this point the reaction mixture was allowed to first warm to room temperature and then it was further heated to 40 °C. As the reaction proceeded, the solution became milky yellow. After heating overnight, the reaction mixture was filtered and the solids washed with THF. The solution was concentrated on a rotary evaporator and the residue thus obtained was partitioned between chloroform and water. The organics were then washed with water, dilute sodium hydrosulfite, another portion of water and finally with saturated sodium chloride solution. After drying over anhydrous potassium carbonate, the solvent was stripped under reduced pressure yielding 5.34 g of crude material as a yellow oil. Purification was accomplished via column chromatography (200-400 mesh silica gel, 4:1 heptane:ethyl acetate as eluent). The result was 3.60g (73%) of product as a white solid. Further purification could be accomplished by recrystallization from heptane:acetone. The melting point of the material was determined to be 39-41 °C. ¹H NMR (CDCl₃) δ: 2.03 (q, J = 8 Hz, 4H), 1.39 (s, 4H), 1.26 (t, J = 8 Hz, 6H), 0.35 (s, 12H). ¹³C{¹H}NMR (CDCl₃): 116.61, 35.33, 33.96, 27.03, 9.94, 1.44 ppm. FT-IR (neat): 2982, 2944, 2885, 2245, 1580, 1462, 1410, 1392, 1329, 1311, 1256, 1239, 1116, 1082, 959, 935, 844, 809, 791 cm⁻¹. Exact mass MS: Calc'd for C₁₆H₂₇N₄O₂Si₂ (M+H⁺); 347.1723. Found; 347.1730.

1,3-bis(2,2-bis(aminomethyl)butyl) -1,1,3,3-tetramethyldisiloxane (35) A solution of 1,3-bis(2,2-dicyanobutyl) -1,1,3,3-tetramethyldisiloxane **34** (2.45 g, 7.1 mmol) in Et₂O

(25 mL) was added slowly over 15 min to a mechanically stirred, pre-cooled slurry of LAH (2.49 g, 65.7 mmol) in Et₂O (275 mL) at 0 °C under N₂ so as to keep the temperature below 5 °C. The mixture was stirred for 6 h then water (10 mL), 1 M NaOH (40 mL) and then water (50 mL) were added carefully in that order with vigorous stirring. Additional Et₂O was added (100 mL) and the mixture was extracted with Et₂O (4 x 100 mL). The Et₂O layers combined, dried with Na₂SO₄, filtered and concentrated to an oil. The aqueous layer was further extracted with CHCl₃ (3 x 30 mL) and treated as above. All crude product was dissolved in Et₂O, acidified with conc HCl and the salt isolated as a white solid. The solid was isolated, dissolved in water, neutralized with 1N NaOH, extracted with CHCl₃, dried with Na₂SO₄, and concentrated to give 1.02 g (40%) product as a colorless liquid. ¹H NMR (CDCl₃) δ: 2.39 (s, 8H), 1.14 (q, J = 7.6 Hz., 8H), 1.08 (br s, 8H), 0.64 (t, J = 7.6 Hz, 6H), 0.41 (s, 4H), -0.02 (s, 12H). ¹³C{¹H}NMR (CDCl₃): 48.1, 41.0, 27.2, 23.6, 7.8, 3.0 ppm. FT-IR (neat): 3377, 3296, 2959, 2852, 1604, 1463, 1408, 1379, 1253, 1044, 836, 802, 750 cm⁻¹. Exact mass MS: Calc'd for C₁₆H₄₃N₄OSi₂ (M+H⁺); 363.2975. Found; 363.2949.

1,3-bis(4,4-dicyanohexyl) -1,1,3,3-tetramethyldisiloxane (36). To an ice cold solution of 2-ethylmalononitrile (4.5 g, 47.8 mmol) in THF (25 mL) was added potassium t-butoxide (4.3 g, 38.3 mmol). This caused the mixture to turn clear brown. Once all of the KOtBu had dissolved (10-15 minutes), a solution of 1,3-bis(iodopropyl)1,1,3,3-tetramethyldisiloxane (7.48 g, 31.8 mmol RI) in THF (8 mL) was added dropwise. Once the addition is complete, another portion of fresh THF (3 mL) was used to rinse the addition funnel. At this point the reaction mixture was allowed to warm to room temperature. As the reaction proceeded, the color changed from clear brown to milky yellow. After 2 hours at room temperature, the reaction was judged to be complete by proton NMR. Thus, the reaction mixture was filtered and the solids were washed with more THF. The resulting THF solution was stripped under reduced pressure, and the residue was then partitioned between chloroform and water. Next, the organic phase was washed with two more portions of water, once with dilute sodium hydrosulfite, and finally with saturated sodium chloride solution. After drying over anhydrous potassium carbonate, the chloroform was stripped off under reduced pressure. Purification was then accomplished via column chromatography (200-400 mesh silica gel, 3:1 heptane:ethyl acetate as eluent). The result was 5.38 g (84%) of product as a slightly yellow oil. ¹H NMR (CDCl₃) δ: 1.98 (q, J = 8Hz, 4H), 1.93 (m, 4H), 1.69 (m, 4H), 1.26 (t, J = 8Hz, 6H), 0.61 (m, 4H), 0.10 (s, 12H). ¹³C{¹H}NMR (CDCl₃): 115.67, 40.54, 38.67, 31.59, 19.82, 17.74, 9.88, 0.34. FT-IR: 2979, 2957, 2884, 2247, 1461, 1412, 1303, 1255, 1193, 1063, 843, 801, 765cm⁻¹. Exact mass MS: Calc'd for: C₂₀H₃₅N₄OSi₂ (M+H⁺); 403.2349. Found; 403.2362.

1,3-bis(4,4-di(aminomethyl)hexyl) -1,1,3,3-tetramethyldisiloxane (37). To an ice cold mixture of lithium aluminum hydride (1.80 g, 47.4 mmols, 190 mmols H) in ether (100 mL) was added dropwise under nitrogen a solution of 1,3-bis(4,4-dicyanohexyl) -1,1,3,3-tetramethyldisiloxane (3.16 g, 7.8 mmols, 31.4 mmols CN) in ether (50 mL). Once addition was complete, the reaction mixture was allowed to slowly warm to room temperature where it was kept for three hours. At this point the mix was cooled back down to ca. 0°C and 10 mL of water was added carefully over approximately 15 minutes.

This was followed by 0.5 mL of 50% NaOH. After the reaction mixture warmed to room temperature, it was filtered to remove the salts. After drying over anhydrous potassium carbonate, the solution was stripped under reduced pressure. This gave 2.92 g (89%) of product as a slightly yellow oil. ^1H NMR (CDCl_3) δ : 2.51 (s, 8 H), 1.22 (q, J = 8 Hz, 4H), 1.17-1.20 (m, 8H), 1.00 (br s, 8H), 0.79 (t, J = 8 Hz, 6H), 0.49 (m, 4H), 0.03 (s, 12H, $\text{CH}_3\text{-Si}$). $^{13}\text{C}\{^1\text{H}\}$ NMR (CDCl_3): 45.65, 40.61, 36.23, 24.53, 19.42, 16.58, 7.42, 0.46. FT-IR: 3377, 3298, 2957, 2926, 2865, 1606, 1462, 1252, 1062, 840, 802, 723 cm^{-1} . Exact mass MS: Calc'd for: $\text{C}_{20}\text{H}_{51}\text{N}_4\text{OSi}_2$ ($\text{M}+\text{H}^+$); 419.3601. Found; 419.3596.

1,3-bis(4,4-dicyanobutyl) -1,1,3,3-tetramethyldisiloxane (38) To an ice cold solution of malononitrile (8.42 g, 127 mmols) in THF (35 mL) was added potassium t-butoxide (5.15 g, 45.9 mmols). The resulting milky pink solution was stirred under nitrogen for 15 minutes and then 1,3-bis(3-iodopropyl)-1,1,3,3-tetramethyldisiloxane (10.0 g, 42.5 mmol) in THF (10 mL) was added dropwise over 20 minutes. A small amount (5 mL) of fresh THF was used to rinse the addition funnel. At this point, the reaction mixture was allowed to warm to room temperature where it was kept overnight. Next, the THF was stripped on a rotary evaporator and the residue was partitioned between chloroform and 10% HCl. The organics were then washed twice with DI water and once each with dilute sodium hydrosulfite and saturated sodium chloride. After drying over anhydrous sodium sulfate, the solvent was removed on a rotary evaporator yielding 7.2 g (98% crude) product as a red oil. Further purification was accomplished via column chromatography (200-400 mesh silica gel, 3:1 hexanes:ethyl acetate as eluent). In this way 6.26 g (85%) product was obtained as a light yellow oil. ^1H NMR (CDCl_3) δ : 3.78 (t, J = 8 Hz, 2H), 2.04 (q, J = 8 Hz, 4H), 1.63 (m, 4H), 0.57 (m, 4H), 0.09 (s, 12H). $^{13}\text{C}\{^1\text{H}\}$ NMR (CDCl_3): 113.02, 33.67, 22.27, 20.66, 17.05, 0.27 ppm. FT-IR (neat): 2958, 2923, 2882, 2258, 1578, 1460, 1412, 1349, 1314, 1260, 1180, 1066, 849, 798, 767, 706 cm^{-1} . Exact mass MS: Calc'd for $\text{C}_{16}\text{H}_{27}\text{N}_4\text{OSi}_2$ ($\text{M}+\text{H}^+$); 347.1723. Found; 347.1714.

1,3-bis(4,4-di(aminomethyl)butyl) -1,1,3,3-tetramethyldisiloxane (39). To a mixture of sodium borohydride (0.60 g, 15.9 mmol) in dimethoxyethane (DME, 8 mL) at -78°C under nitrogen was added dropwise a freshly made solution of bromine (1.12 g, 7.0 mmol) in DME (6 mL). Once addition was complete the reaction mixture was stirred another 15-20 mins at this temperature and then the dry ice/acetone bath was replaced with a water ice bath. Once the temperature of the mix approached $\sim 0^\circ\text{C}$, a solution of 1,3-bis(4,4-dicyanobutyl) -1,1,3,3-tetramethyldisiloxane (0.50 g, 5.8 mmol) in DME (1.5 mL) was added. The resulting mixture was allowed to slowly warm to room temperature as the ice melted. It was then kept at this temperature overnight. The reaction was worked up by first carefully adding it to 24 mL of ice cold 10% HCl. Next, it was allowed to warm to room temperature, the solid that had formed was filtered off, and the solution was concentrated by stripping off about half the volume of liquid on a rotary evaporator. After cooling back down in an ice bath, the solution was made strongly basic by the addition of 10% NaOH. The result was extracted four times with chloroform and then the combined organics were dried over anhydrous sodium sulfate and stripped under reduced pressure. The result was 0.10 g (19% yield) of crude **39** as a light yellow oil. ^1H NMR (CDCl_3) δ : 2.62 (d, J = 6 Hz, 8H), 2.26 (br s, 8H), 1.18-1.45 (m, 10H), 0.52 (t, J = 8 Hz, 4H), 0.03 (s, 12H). $^{13}\text{C}\{^1\text{H}\}$ NMR (CDCl_3): 43.68, 42.86,

32.86, 20.42, 17.90, 0.08 ppm. FT-IR (neat): 3365, 3295, 2952, 2920, 2868, 1600, 1458, 1408, 1251, 1059, 951, 890, 840, 793, 703 cm^{-1} . Exact mass MS: Calc'd for $\text{C}_{16}\text{H}_{43}\text{N}_4\text{OSi}_2$ ($\text{M}+\text{H}^+$); 363.2975. Found; 363.2961.

(4,4-Dicyanobutyl)diphenylmethylsilane (42). To an ice cold solution of malononitrile (6.87 g, 104 mmols) in THF (25 mL) was added potassium t-butoxide (4.20 g, 37 mmols). The resulting milky pink solution was stirred under nitrogen for 15 minutes and then 3-iodopropyl-diphenylmethylsilane (12.7 g, 35 mmol) in THF (15 mL) was added dropwise over 20 minutes. A small amount (5 mL) of fresh THF was used to rinse the addition funnel. At this point, the reaction mixture was allowed to warm to room temperature where it was kept overnight. Proton NMR at this point showed the reaction to be approximately 95% complete. The reaction was then heated to 40°C for 3.5 hours to drive it to completion. Next, the THF was stripped on a rotary evaporator and the residue was partitioned between chloroform and 10% HCl. The organics were then washed twice with DI water and once each with dilute sodium hydrosulfite and saturated sodium chloride. After drying over anhydrous sodium sulfate, the solvent was removed on a rotary evaporator yielding 10.6 g product as a red oil (100% crude yield). Purification was accomplished via column chromatography (200-400 mesh silica gel, 4:1 hexanes:ethyl acetate as eluent). In this way 8.02 g (75%) product was obtained as a light yellow oil. ^1H NMR (CDCl_3) δ : 7.52 (m, 4H), 7.40 (m, 6H), 3.65 (t, $J = 8$ Hz, 1H), 2.04 (q, $J = 8$ Hz, 2H), 1.70 (m, 2H), 1.13 (m, 2H), 0.61 (s, 3H). $^{13}\text{C}\{^1\text{H}\}$ NMR (CDCl_3): 136.02, 134.38, 129.62, 128.11, 112.54, 33.97, 22.11, 21.35, 13.43, -4.59 ppm. FT-IR (neat): 3070, 3021, 2922, 2256, 1589, 1488, 1458, 1427, 1303, 1253, 1180, 1111, 998, 787, 732, 699 cm^{-1} . Exact mass MS: Calc'd for: $\text{C}_{19}\text{H}_{20}\text{N}_2\text{Si}$; 304.1396. Found; 304.1396.

2-(Aminomethylene)-5-(methyl-diphenylsilane)pentanenitrile (44). (4,4-Dicyanobutyl)diphenylmethylsilane (**42**) (2.08 g, 6.83 mmol), EtOH (30 mL) and 10% Pd/C (0.25 g) were added together in a pressure reactor equipped with a stir-bar and thermocouple, purged with H_2 and pressurized to 300 psi H_2 with stirring for 18 h at 60 °C. The reaction mixture was cooled, concentrated in vacuo and subjected to silica gel chromatography, eluting with 2:1 hexanes/EtOAc. 1.55 g of a mixture of two products (E and Z isomers) was obtained (73% yield). This mixture was further chromatographed to separate the two isomers. **(Z)-2-(aminomethylene)-5-(methyl-diphenylsilane)-pentanenitrile (44Z)**. ^1H NMR (CDCl_3) δ : 7.56 (m, 4H), 7.42 (m, 6H), 6.53 (t, $J = 10.3$ Hz, 1H), 4.35 (br d, $J = 10.1$ Hz, 2H), 2.10 (t, $J = 7.2$ Hz, 2H); 1.57 (m, 2H); 1.11 (m, 2H); 0.62 (s, 3H). $^{13}\text{C}\{^1\text{H}\}$ NMR (CDCl_3): 146.1, 137.1, 134.5, 129.3, 127.9, 119.6, 79.8, 33.6, 24.0, 13.4, -4.4 ppm. FT-IR (neat): 3480, 3365, 3287, 3241, 2068, 3048, 3020, 2926, 2858, 2188, 1647, 1607, 1427, 1298, 1252, 1193, 1111, 788, 733, 701 cm^{-1} . Exact mass MS: Calc'd for: $\text{C}_{19}\text{H}_{22}\text{N}_2\text{Si}$; 306.1552. Found; 306.1555. **(E)-2-(aminomethylene)-5-(methyl-diphenylsilane)pentanenitrile (44 E)**. ^1H NMR (CDCl_3) δ : 7.56 (m, 4H), 7.41 (m, 6H), 6.75 (t, $J = 10.6$ Hz, 1H), 4.08 (br d, $J = 10.1$ Hz, 2H), 2.02 (t, $J = 7.3$ Hz, 2H); 1.65 (m, 2H); 1.17 (m, 2H); 0.62 (s, 3H). $^{13}\text{C}\{^1\text{H}\}$ NMR (CDCl_3): 144.6, 137.0, 134.5, 129.3, 128.0, 123.1, 81.2, 28.6, 22.2, 13.8, -4.4 ppm. FT-IR (neat): 3480, 3359, 3443, 3068, 3049, 3020, 2925, 2861, 2188, 1651, 1611, 1427, 1253, 1112, 789, 733, 701 cm^{-1} . Exact mass MS: Calc'd for: $\text{C}_{19}\text{H}_{22}\text{N}_2\text{Si}$; 306.1552. Found; 306.1554.

(4,4-Bis(aminomethyl)butyl)diphenylmethylsilane (45). Sodium borohydride (0.43 g, 11 mmol) was mixed with dimethoxyethane (DME, 6 mL) and cooled to -20°C under nitrogen. At this point a solution of bromine (0.81 g, 5.1 mmol) in DME (5 mL) was added dropwise over approximately 30 minutes. As each drop was added the red-orange color of bromine faded almost instantly. In addition, a small amount of gas evolution was observed as each drop reached the NaBH_4 suspension. The reaction mixture was stirred for an additional 15 minutes after all of the bromine had been added and then it was warmed to $\sim 0^{\circ}\text{C}$ using an ice bath. A solution of (4,4-dicyanobutyl)diphenylmethylsilane (0.50 g, 1.6 mmol) in DME (2 mL) was then added. The reaction mixture was then allowed to slowly warm to room temperature where it was kept overnight. At this point the reaction was cooled back down to 0°C and 15 mL 10% HCl was carefully added in order to quench the excess hydride. After the resulting solution was allowed to warm to room temperature, it was concentrated on a rotary evaporator and then cooled back down in an ice bath and the pH was made strongly basic via the addition of 10% NaOH. After warming to room temperature the solution was then extracted three times with ether. The combined organics were then washed with saturated sodium chloride solution, dried over anhydrous potassium carbonate, and then stripped on a rotary evaporator. The result was 0.46 g of crude product as a hazy, light yellow oil. Purification was accomplished via column chromatography (200-400 mesh silica gel, 80:20:2 chloroform:methanol:concentrated ammonium hydroxide as eluent). In this way 0.29 g (58%) product was obtained as a light yellow oil. ^1H NMR (CDCl_3) δ : 7.51 (m, 4H), 7.34 (m, 6H), 2.63 (m, 4H), 1.48 (br s, 4H), 1.26-1.46 (m, 5H), 1.08 (m, 2H), 0.56 (s, 3H). $^{13}\text{C}\{^1\text{H}\}$ NMR (CDCl_3): 137.26, 134.45, 129.17, 127.85, 43.79, 42.80, 33.91, 21.33, 14.51, -4.37 ppm. FT-IR (neat): 3370, 3068, 3047, 3020, 2917, 2858, 1588, 1487, 1457, 1427, 1303, 1250, 1111, 998, 786, 730, 699 cm^{-1} . Exact mass MS: Calc'd for: $\text{C}_{19}\text{H}_{29}\text{N}_2\text{Si}$ ($\text{M}+\text{H}^+$); 313.2100. Found; 313.2090.

1,1,8,8-Tetracyanooctane (47). To an ice cold solution of malononitrile (4.9 g, 74 mmols) in THF (20 mL) was added potassium t-butoxide (3.4 g, 30 mmols). The resulting milky pink solution was stirred under nitrogen for 15 minutes and then 1,6-dibromohexane (3.0 g, 28 mmol RBr) in THF (3 mL) was added dropwise over 20 minutes. A few mLs of fresh THF was used to rinse the addition funnel. At this point, sodium iodide (0.70 g, 4.7 mmol) was added and the reaction mixture was heated to $40\text{--}45^{\circ}\text{C}$ for 16 hours. Next, the solvent was stripped on a rotary evaporator and the resulting residue was partitioned between chloroform and 10% HCl. The organic layer was washed three times with DI water, and then once with saturated sodium chloride solution. It was then dried using anhydrous sodium sulfate. After addition of the drying agent, a few grams of silica gel (200-400 mesh) were added as well, in order to remove a large amount of the color (red) in the solution. After filtration, the resulting yellow solution was concentrated under reduced pressure yielding 1.94 g (74%) crude product as a yellow oil. Isopropanol (9 mL) was added and the mixture was heated until the product dissolved. It was then allowed to cool to room temperature and then further to $\sim 0^{\circ}\text{C}$. Initially the product oiled out, but on standing on ice, it solidified. The resulting material was collected by vacuum filtration and washed with ice-cold isopropanol (10 mL). After drying, 1.58 g (60%) of yellow solid was obtained. Further recrystallization was used to prepare samples for analysis. The melting point of the material was determined to be 53--

55°C. ^1H NMR (CDCl_3) δ : 3.74 (t, $J = 8$ Hz, 2H), 2.05 (q, $J = 8$ Hz, 4H), 1.66 (m, 4H), 1.46 (m, 4H). $^{13}\text{C}\{^1\text{H}\}$ NMR (CDCl_3): 112.88, 30.42, 27.86, 26.25, 22.63 ppm. FT-IR (neat): 2925, 2858, 2257, 1470, 1379, 1331, 1310, 1281, 1245, 1214, 1131, 1042, 992, 966, 940, 844, 729 cm^{-1} . Exact mass MS: Calc'd for $\text{C}_{12}\text{H}_{15}\text{N}_4$ ($\text{M}+\text{H}^+$); 215.1297. Found 215.1292.

General procedure for measuring CO_2 uptake: Samples of the aminodisiloxane or solvent blend were charged to a 25 mL three-necked flask and the mass was determined using an analytical balance. The flask was then equipped with an overhead stirrer, a CO_2 inlet terminating with a glass pipette aimed slightly above the surface of the liquid, and another tube connected to a bubbler filled with silicone oil. Each sample was heated to 40°C (oil bath) for two hours with gentle stirring. The CO_2 flow was produced via charging 250-270 g of dry ice to a 1000mL three necked-flask equipped with a stopper, a plastic tube connected through a drying tube (filled with blue Indicating Drierite) to the CO_2 inlet on the 25 mL flask, and finally a stopcock that was used to control the rate of gas flow through the test system. The rate was adjusted so that a steady stream of bubbles was observed in the bubbler. Care was taken to keep the flow from being excessive.

Once the test was complete, the CO_2 flow was discontinued as was stirring. The sample was then cooled to room temperature and the outside of the flask was washed with chloroform to remove any silicone oil remaining from the oil bath. After drying the outside of the flask, the combined weight of aminodisiloxane, carbamate (and TEG if used) was determined using an analytical balance. The weight gain was then compared to the theoretical weight gain based on the amount of aminodisiloxane charged, the number of amines per molecule, and the molecular weight of the material. It was assumed that two amines are required to react with each CO_2 molecule ($\text{MW} = 44.01$) via the classic primary amine- CO_2 reaction.

Supporting information available: ^1H and ^{13}C NMR spectra for all compounds synthesized. This information is available free of charge via the Internet at <http://pubs.acs.org>.

References

1. Energy Information Administration, Existing Capacity by Energy Source, January 2009. <http://www.eia.doe.gov/cneaf/electricity/epa/epat2p2.html>.
2. Science Daily, <http://www.sciencedaily.com/releases/2007/11/071114/63448.htm>.
3. American Clean Energy and Security Act of 2009.
4. Murphy, J. T.; Jones, A. P. DOE/NETL's Carbon Capture R&D Program for Existing Coal-Fired Power Plants, DOE/NETL-2009/1356 February 2009.
5. (a) Valenti, G.; Bonalumi, D.; Macchi, E. *Energy Procedia* **2009**, *1*, 1059. (b) Gal, E.; Bade, O. M.; Jataweera, I.; Krishnan, G. US Pat Appl. US200/9148930, **June 11, 2009** to Alstom Power, Inc. (c) Peltier, R. *Power* **2008** *152*(2), 38.
6. "Cryogenic Carbon Capture Technology," *Carbon Capture Journal*, **2009**, (10), 18.
7. (a) Nelson, T. O.; Green, D. A.; Coleman, L. J. I.; Gupta, Raghbir P.; Figueroa, J. D. Proceedings - Annual International Pittsburgh Coal Conference **2008**, 25th, 411/1-411/2. (b) Anthony, E. J. *Ind. Eng. Chem. Res.* **2008**, *47*, 1747.
8. (a) Reddy, S.; Johnson, D.; Gilmartin, J. "Fluor's Econamine FG PlusSM Technology for CO₂ Capture at Coal-fired Power Plants," Power Plant Air Pollutant Control "Mega" Symposium, August 25-28, 2008. (b) Sartori, G.; Savage, D. W., *Ind. Eng. Chem. Fundam.* **1983**, *22*, (2), 239-49.
9. (a) Camper, D.; Bara, J. E.; Gin, D. L.; Noble, R. D. *Ind. Eng. Chem. Res.* **2008**, *47*, 8496. (b) Bates, E. D.; Mayton, R. D.; Ntai, I.; Davis, J. H. Jr. *J. Am. Chem. Soc.* **2002**, *124*, 926. (c) Muldoon, M. J.; Aki, S. N. V. K.; Anderson, J. L.; Dixon, J. K.; Brennecke, J. F., *J. Phys. Chem. B* **2007**, *111*, (30), 9001-9009.
10. Kammermeyer, K.; Sollami, B. J. Recovering carbon dioxide from a gaseous fluid. US 3665678, 19700914., 1972.
11. Shah, V. M.; Hardy, B. J.; Stern, S. A., *Journal of Polymer Science Part B: Polymer Physics* **1993**, *31*, (3), 313-317.
12. Dzielawa, J.; Rubas, A.; Lubbers, C.; Stepinski, D.; Scurto, A.; Barrans, R.; Dietz, M.; Herlinger, A.; Brennecke, J., *Separation Science and Technology* **2008**, *43*, 2520-2536.
13. Li, S.; Li, Y.; Wang, J., *Fluid Phase Equilibria* **2007**, *253*, (1), 54-60.

14. Dibenedetto, A.; Aresta, M.; Fragale, C.; Narracci, M., *Green Chem.* **2002**, 4, (5), 439-443.
15. Dibenedetto, A.; Pastore, C.; Fragale, C.; Aresta, M., *ChemSusChem* **2008**, 1, (8-9), 742-745.
16. (a) Alauzun, J.; Mehdi, A.; Reye, C.; Corriu, R. J. P., *J. Am. Chem. Soc.* **2005**, 127, (32), 11204-11205. (b) Alauzun, J.; Besson, E.; Mehdi, A.; Reye, C.; Corriu, R. J. P., *Chem. Mater.* **2008**, 20, (2), 503-513.
17. Blasucci, V.; Dilek, C.; Huttenhower, H.; John, E.; Llopis-Mestre, V.; Pollet, P.; Eckert, C. A.; Liotta, C. L., *Chemical Communications* **2009**, (1), 116-118.
18. Knowles, G. P.; Delaney, S. W.; Chaffee, A. L., *Industrial & Engineering Chemistry Research* **2006**, 45, (8), 2626-2633.
19. Hicks, J. C.; Drese, J. H.; Fauth, D. J.; Gray, M. L.; Qi, G.; Jones, C. W., *J. Am. Chem. Soc.* **2008**, 130, (10), 2902-2903.
20. Perry, R. J.; Grocela-Rocha, T. A.; O'Brien, M. J.; Genovese, S.; Wood, B. R.; Lewis, L. R.; Lam, H.; Soloveichik, G.; Rubinsztajn, M.; Kniajanski, S.; Draper, S.; Enick, R. M.; Johnson, J. K.; Xie, H.-b.; Tapriyal, D. *ChemSusChem*, **2010**, 3, 919.
21. (a) Yoshida, K.; Mimura, T.; Shimojo, S.; Karasaki, M.; Iijima, M.; Mitsuoka, S. US 6689332 to Kansai Electric Power Co., Inc and Mitsubishi Jukogyo Kabashika Kaisha, **Feb 10, 2004**. (b) Yoshida, K.; Mimura, T.; Shimojo, S.; Karasaki, M.; Iijima, M.; Mitsuoka, S. EP 588178 to Kansai Electric Power Co., Inc and Mitsubishi Jukogyo Kabashika Kaisha, **Jan. 21, 1998**. (c) Yoshida, K.; Mimura, T.; Shimojo, S.; Karasaki, M.; Iijima, M.; Seto, T.; Mitsuoka, S. EP 588175 to Kansai Electric Power Co., Inc and Mitsubishi Jukogyo Kabashika Kaisha, **Aug. 6, 1997**. (d) Tontiwachwuthikul, P.; Wee, A. G. H.; Idem, R.; Maneeintr, K.; Fan, G.-J.; Veawab, A.; Henni, A.; Aroonwilas, A.; Chakma, A. US 20080050296 to University of Regina, Ca., **Feb. 28, 2008**.
22. (a) Curren, D.P.; Seong, C.M.; *J. Am. Chem. Soc.* **1990**, 112, 9401. (b) Curren, D.P.; Seong, C.M.; *Synlett* **1991**, 107. (c) Kang, H-Y; Hong, W.S.; Cho, Y.S.; Koh, H.Y.; *Tetrahedron Lett.* **1995**, 36, 7661. (d) Mattalia, J-M; Marchi-Delapierre, C.; Hazimeh, H.; Chanon, M.; *ARKIVOC* **2006**, 90.
23. Smith, M. B.; March, J. in "March's Advanced Organic Chemistry, 6th Ed.," John Wiley & Sons, New York, **2007**, pg 1814.
24. (a) Haddenham, D.; Pasamansky, L.; DeSoto, J.; Eagon, S.; Singaam, B., *J. Org. Chem.* **2009**, 74, 1964. (b) Ohsawa, T.; Kobayashi, T.; Mizaguchi, Y.; Saitoh, T.; Oishi, T. *Tetrahedron Lett.* **1985**, 26, 6103. (c) Sieveking, H. U.; Luttke, W. *Angew. Chem. Int. Ed Engl.* **1969**, 8, 458.

25. Hutchins, R. O.; Maryanoff, B. E., *Org. Syn.*, **1973**, *53*, 21.
26. Xie, X.; Liotta, C. L.; Eckert, C. A. *Ind. Eng. Chem. Res.* **2004**, *43*, 7907
27. Takiguchi, T.; Amagai, K.; Kawabata, H., *Bull. Chem. Soc. Jpn.*, **1979**, *52*, 1871.
28. Kida, T.; Isogawa, K.; Morishima, H.; Zhang, W.; Masatuma, A.; Nakatsuji, Y.; Ikeda, I., *J. Jpn. Oil. Chem. Soc.*, **1998**, *47*, 41.
29. Mikata, Y.; Inaba, Y.; Morioka, M.; Yano, S., *Tetrahedron Lett.*, **2004**, *45*, 8785.
30. Yu, S.-B.; Droege, M.; Downey, S.; Segal, B.; Newcomb, W.; Sanderson, T.; Crofts, S.; Suravajjala, S.; Bacon, E.; Earley, W.; Delecki, D.; Watson, A. D. *Inorg. Chem.*, **2001**, *40*, 1576.
31. Rylander, P. N. in "Catalytic Hydrogenation in Organic Syntheses," Academic Press, New York, **1979**, pgs 138-145.
32. Matsumoto, T.; Yoshida, D.; Tomita, H. *Agric. Biol. Chem.* **1981**, *45*, 2031.
33. Tudge, M.; Mashima, H.; Savarin, C.; Humphrey, G.; Davies, I. *Tetrahedron Lett.* **2008** *49*, 1041.
34. ¹³C NMR spectra of the carbamate from **1** showed evidence of a bicarbonate resonance at ~160 ppm vs carbamate resonance at ~164.5 ppm. See Tomizaki, K.-y.; Kanakubo, M.; Nanjo, H.; Shimizu, S.; Onoda, M.; Fujioka, Y. *Ind. Eng. Chem. Res.* **2010**, *49*, 1222.
35. Boutevin, B.; Guida-Pietrasanta, F.; Robin, J.-J. *Makromolec. Chem.* **1989**, *190*, 2437.
36. Takiguchi, T.; Amagai, K.; Kawabata, H., *Chem. Soc. Bull. Jpn.*, **1979**, *52*, 1871.
37. Ono, N.; Zinsmeister, K.; Kaji, A., *Bull. Chem. Soc. Jpn.*, **1985**, *58*, 1069.
38. Aleksandrowicz, P.; Piotrowska, H.; Sas, W., *Tetrahedron*, **1982**, *38*, 1321.
39. Rimniceanu, C.; Cazacu, M.; Marcu, M.; Rimniceanu, I. *Rev. Roum. Chim.* **2002**, *47*, 551.
40. Hu, C.; He, J.; O'Brien, D. H.; Irgolic, K. J. *J. Organomet. Chem.* **1984**, *268*, 31.
41. Reyx, D.; Guillaume, P. *Makromol. Chem.* **1983**, *184*, 1179.

Appendix 6

A computational study on the heat of reaction for amino silicones with CO₂

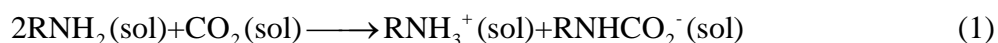
3. Selection of Computational Model and Computational Details

3.1. Selection of computational model

For the silicon amine systems, it at least includes 43 atoms for GAP-0. For the system with so many atoms, it is computationally expensive to perform high-level calculations such as MP2 level of theory. We have therefore developed a computational model for silicon amines that retain the important functional moieties while reducing the number of atoms in the calculation. Computation model is obtained via (as shown in Figure 1): firstly cutting the silicon amine into two parts at Si-O bond and the part with O-atom is taken; then, replacing the methyls connected to Si-atom by hydrogens; at last, H-atom is used to saturate O-atom. The reliability of computational model is discussed in the Section 3.3.

3.2 Computational details

Heat of reaction for forming carbamate was calculated using two-step scheme (eq. 1 and 2). Reliability of the two-step scheme was tested in our previous paper¹.



Ab initio molecular dynamics is used to sample conformation space for amines, RNH₃⁺ and RNHCO₂⁻ in the gas phase. The same sampling scheme was used in our previous paper¹. The density function theory (DFT) with the B88-PW86 functional² along with a triple zeta valence polarized basis set (TZVP) within the RI approximation³ was used throughout ab initio molecular dynamics calculation. The NVT ensemble was used. The temperature was set to 800K in order to sample a large number of different configurations. A time step of 1.451 fs was used. Total length of the ab initio MD simulation was 7.256 ps. The calculations were carried out using

TURBOMOLE package.⁴ Then, several local minima for each species were located at B3LYP/6-311++G(d,p) level within Gaussian03 package⁵ based on initial configurations from MD trajectory. Single point energy calculations were performed at the MP2/aug-cc-pVDZ//B3LYP/6-311++G(d,p) level. In geometry optimizations, harmonic vibrational frequencies for all structures and single point energy calculations, implicit solvent effects were taken into account by exploiting the conductor-like polarizable continuum model (CPCM) formalism.^{6,7} This method was initially devised by Tomasi and co-worker,⁸⁻¹⁰ and extended for geometry optimizations to converge efficiently. To consider the effect of solute cavity on calculated result, two different atom radii UAHF and BODNI were used in the construction of the solute cavity for the most of calculations, respectively. In the experiment, the heats of reaction were measured in the pure silicon amines or mixture between silicon amine and triethylene glycol (TEG) solvent. To consider the influence of solvent on the heat of reaction, heats of reaction for test compounds GAP-0 and MEA were calculated using three different implicit solvents: water, aniline and methanol. Aniline solvent is assumed to be similar to pure silicon amine and methanol to triethylene glycol in the view of dielectric constant. For other silicon amines, just water implicit solvent was used. All calculations except ab initio molecular dynamics calculation were performed using Gaussian 03 program package.⁵

At last, a Boltzmann distribution is used to average over the conformer at 298K; the Boltzmann-weighted enthalpy of species S is given by

$$\overline{H}^s = \sum_i w_i H_i^s \quad (3)$$

Where the Boltzmann weight w_i is given by:

$$w_i^s = \frac{e^{-H_i^s/k_B T}}{\sum_i e^{-H_i^s/k_B T}} \quad (4)$$

Note that it is not possible to sample conformations of the bound carbamate, $[\text{RNH}_3^+][\text{CO}_2\text{NHR}]^-$, because it will transform to neutral species RNH_2 and RNHCOOH in our AIMD simulations in gas phase. Therefore, we used the configurations for RNH_3^+ and RNHCO_2^- having the highest Boltzmann weight to evaluate electrostatic and dispersion interactions in eq. (5).

3.3 Reliability of the computational model

To inspect the reliability of computational model, a test was performed. At the B3LYP/6-311++G(d,p) level within CPCM model with UAHF radii, we calculated heat of reaction for forming inter-molecular carbamate for both real GAP-0 and its model. We randomly constructed the initial configurations for real GAP-0 and optimized to a local minimum. We constructed the initial configurations for carbamate by keeping the backbone of real GAP-0 unchanged. Then, the initial configurations for computational models of GAP-0 are obtained by trimming the optimized configurations of real GAP-0, and GAP-0 carbamate using the scheme in Figure 1. Heat of reaction for forming inter-molecular carbamate from computational model is calculated to be -11.8 kcal/mol, which is very close to that (-12.1 kcal/mol) from real GAP-0. This indicates that chemical environment of reactive center (amino group) in the computational model is kept. This can be easily understood because losing group is far away from the reactive center NH_2 group. In addition, heat of reaction for forming inter-molecular carbamate for real GAP-0 is -12.1 kcal/mol at the B3LYP/6-311++G(d,p) level with UAHF radii, which is more favorable than that for forming intra-molecular carbamate (-7.2 kcal/mol). This provides further support for rationality that remains half molecule of real silicon amine (reactive center of silicon amine) in the computational model.

4. Results and discussion

4.1. Effect of solvents on the heat of reaction

In the experiment, the heats of reaction were measured in the pure silicon amines or mixture between silicon amine and triethylene glycol (TEG) solvent. However, we cannot find completely corresponding implicit solvent model in ab initio program package as ones the experiment used. To reasonably consider the solvent effect, we have to find a good implicit solvent to present the experimental solvent. To realize it, three different implicit solvents including water, aniline and methanol are selected to calculate heats of reaction for test amines GAP-0 and MEA. From Table 1, it is seen that total heats of reaction for test amines are very similar in three different implicit solvent, e.g. heats of reaction for MEA are -16.3, -15.5 and -15.2 kcal/mol in water, methanol and aniline, respectively; the corresponding values for GAP-0 are -14.5, -14.6 and -14.8 kcal/mol, respectively. The calculated heats of reaction for GAP-0 and MEA are close to corresponding experimental data. Also, the trend for these two amines from

calculation is in good agreement with experimental data. It is found that heats of reaction both in the first step and second step are different from each other in three different implicit solvents for either GAP-0 or MEA. This phenomenon could result from the difference in dielectric constant of three different solvents. High dielectric constant solvents such as water and methanol lead to stronger electrostatic interaction between ions and solvent than that of low dielectric constant solvent aniline. This therefore makes ions more stable in the high dielectric constant solvent relative to that in low dielectric constant solvent. However, product in the second step is kind of neutral, dielectric constant of solvent should have a little influence on its stability. So, heat of reaction in the second step in lower dielectric constant solvent aniline is more exothermic than that in higher dielectric constant solvent water and methanol as shown in Table 1. We note that the implicit solvent model is known to be inaccurate for computing solvation free energies of ions. This affects the calculations in both eqns. (6) and (7). However, the errors in these calculations will largely cancel out because the solvated ions are intermediate products in the thermodynamic cycle. Hence, we expect the total heats of reaction to be fairly accurate. It is concluded based on above discussions, solvent has a little influence on the heat of reaction. So, for other silicon amines, just water implicit solvent was used to predict their heats of reaction.

4.2. Heats of reactions

To easily present our results, we divide the silicon amines into two groups: the first one includes GAP-0, DAB-0, DAB-Me, and DAB-diMe, which belongs to primary amines; the second one just includes one member GAP-AEAM that contains both primary and secondary amino group.

4.2.1 Primary silicon amines

For ammonium cations forming from primary silicon amines, all the lowest energy conformers involve the formation of intra-molecular hydrogen bond between O-atom of OH and H-atom of $-NH_3$ group except one forming from DAB-diMe (Figure 2d). This is similar to substituted MEA system¹. For DAB-diMe ammonium cation, the lowest energy conformer does not involve the formation of intra-molecular hydrogen bond between O-atom of OH and H-atom of $-NH_3$ group. This indicates that introducing two methyl groups on α -C of silicon amine could increase the ring strain for forming seven-membered ring H-bond and therefore forming conformer with H-bond in energy is not favorable as the others anymore. In all lowest energy conformers for carbamate anion, the N-C bond length between N-atom and C-atom of $-COO$ is between typical N-C single

and double bond lengths of 1.47 and 1.27 Å, respectively. The four atoms –COO and N-atom are in the same plane. All these including bond length character and coplanarity of NCOO atoms indicate that π conjugation is formed between lone pair of electrons of N, O-atom of –COO and CO π bond, which feature is the same as substituted MEA system.¹ However, there is one difference between substituted MEA and primary silicon system. In the most of lowest energy conformers for carbamate anion forming from substituted MEA system, intra-molecular H-bond is formed between H-atom of OH and O-atom of –COO. For silicon amine system, the conformer with this kind of H-bond was not considered because H-atom of OH is introduced in the process of constructing computational model and therefore it is artificial.

The heats of reaction for GAP-0, DAB-0, DAB-Me and DAB-diMe are -14.5, -15.0, -13.0 and -11.5 kcal/mol at MP2/aug-cc-PVDZ//B3LYP/6-311++G(d,p) with UAHF radii, respectively, which is a less exothermic than corresponding values -16.7, -16.7, -14.6 and -12.6 kcal/mol at MP2/aug-cc-PVDZ//B3LYP/6-311++G(d,p) level with Bondi radii. At both levels, order of the heats of reaction for primary silicon amine is GAP-0 \approx DAB-0 > DAB-Me > DAB-diME. This is in good agreement with our previous conclusion that the substitution of methyl group at α -site makes the basicity of amino group weaker and therefore makes the heat of reaction less exothermic.¹ From GAP-0 to DAB-0, it just increases one more CH₂ spacer, which will have little influence on the heat of reaction and therefore heat of reaction almost did not change. From DAB-Me to DAB-diME, one more methyl group is introduced into α -site, which will further decrease the basicity of amino group and make the heat of reaction less exothermic relative to DAB-Me. More importantly, heats of reaction for these silicon amines are less exothermic than that of MEA, which could decrease the energy cost of regeneration process in the CO₂ capture.

4.2.2 GAP-AEAM

GAP-AEAM includes two different amino groups –NH and –NH₂. Therefore, when CO₂ reacts with GAP-AEAM, the product could be inter-molecular or intra-molecular carbamate. Firstly, we discuss heat of reaction for forming inter-molecular carbamate. It could form two types of ammonium cations and carbamate anions in the process of forming inter-molecular carbamate. Figure 3a and 3b show the lowest energy conformers of two types of ammonium cations, respectively. The lowest energy conformer of ammonium cation forming from –NH group as

shown in Figure 3b in energy is 1.3 kcal/mol lower than that forming from the -NH_2 group in Figure 3a. This means that the conformer Figure 3b should be the most populated ammonium cation. Figure 3c and 3d shows the lowest energy conformers for two types of carbamate anions, respectively. One in Figure 3c is formed from -NH_2 group of GAP-AEAM; the other in Figure 3d is formed from -NH group of GAP-AEAM. The conformer in Figure 3d in energy is 7.7 kcal/mol lower than that in Figure 3c at MP2/aug-cc-pVDZ//B3LYP/6-311++G(d,p) level with UAHF radii. From Figure 3d, it is seen that Si-O distance is 2.024 Å, which is not much longer than typical Si-O single bond length 1.67 Å. This indicates that there is strong interaction between Si-atom and O-atom. However, in the real system, the group connecting to Si-atom is methyl, not H-atom in the computational model. Steric effect of methyl could weaken the interaction between Si-atom and O-atom. To investigate it, the methyl substituted conformers in Figure 3c and Figure 3d are calculated. It is seen in Figure 3f that Si-O distance becomes 2.158 Å once methyl has connected to Si-atom instead of H-atom, which is longer than that 2.024 Å obtained from original computational model. This means that methyl substitution do weaken the interaction between Si-atom and O-atom. As far as the energy is concerned, the conformer in Figure 3f is just 0.6 kcal/mol higher than that in Figure 3e. They are almost isoenergetic. So, our computational model overestimates the energy gap between conformers in Figure 3c and Figure 3d relative to the real system. In the process of calculation for heat of reaction for forming inter-molecular carbamate, the conformer of ammonium cation in Figure 3b and the conformer of carbamate anion in Figure 3c are used. As shown in Table 2 and Table 3, the heats of reaction of GAP-AEAM are -14.5 and -15.4 kcal/mol at MP2/aug-cc-pVDZ//B3LYP/6-311++G(d,p) level with UAHF and BODNI radii, respectively.

We also consider the possibility for forming intra-molecular carbamate. As shown in Figure 4, two types of intra-molecular carbamate could be formed once CO_2 reacts with GAP-AEAM. It is worth mentioning that we did not consider the conformer like Type II in Figure 4 while there is an artificial interaction between O-atom and Si-atom. The heat of reaction for forming intra-molecular carbamate Type II is -9.9 kcal/mol, which is 3.1 kcal/mol lower than that (-6.8 kcal/mol) forming Type I at MP2/aug-cc-pVDZ//B3LYP/6-311++G(d,p) level with UAHF radii. However, heat of reaction for forming intra-molecular carbamate still less exothermic than forming inter-molecular carbamate. So, if GAP-AEAM in the reaction is excess, main product

could be inter-molecular carbamate from the view of thermodynamics; if CO_2 is excess, intra-molecular carbamate could be main product because CO_2 will continue to react with another vacant $-\text{NH}$ or $-\text{NH}_2$ group in ammonium cations and carbamate anions to form intra-molecular carbamate, even though inter-molecular carbamate is firstly formed. Surely, there is also a possibility to form ammonium dication and carbamate dianion. However, it should be unfavorable relative to form neutral intra-molecular carbamate because ammonium dication and carbamate dianion are generally unstable as Brennecke et al. suggested in their recent paper.¹¹

Table 1: Heats of reaction for MEA and GAP-0 for forming inter-molecular carbamate obtained at MP2/aug-cc-pVDZ//B3LYP/6-311++G(d,p) level in water, methanol and aniline implicit solvent with UAHF radii.

Heat of reaction	MEA			GAP-0		
	Water	Methanol	Aniline	Water	Methanol	Aniline
The first step	-9.7	-6.5	17.4	-9.0	-5.9	16.4
The second step	-6.6	-9.0	-32.6	-5.5	-8.7	-31.2
Total heat of reaction	-16.3	-15.5	-15.2	-14.5	-14.6	-14.8

Table 2: Heat of reaction for forming inter-molecular carbamate obtained at MP2/aug-cc-pVDZ//B3LYP/6-311++G(d,p) level with UAHF radii.

Heat of reaction (kcal/mol)	GAP-0	DAB-0	DAB-Me	DAB-diMe	GAP-AEAM	MEA
First step	-9.0	-8.6	-7.2	-3.1	-10.8	-9.7
Second step	-5.5	-6.4	-5.8	-8.4	-3.7	-6.6
Total	-14.5	-15.0	-13.0	-11.5	-14.5	-16.3
Exp	-16.8	-13.7	-12.8	-11.6	-12.3	-17.2

Table 3: Heat of reaction for forming inter-molecular carbamate obtained at MP2/aug-cc-pVDZ//B3LYP/6-311++G(d,p) level with Bondi radii.

Heat of reaction (kcal/mol)	GAP-0	DAB-0	DAB-Me	DAB-diMe	GAP-AEAM	MEA
First step	-12.0	-11.9	-10.1	-6.9	-10.0	-13.7
Second step	-4.7	-4.8	-4.5	-5.7	-5.4	-4.1
Total	-16.7	-16.7	-14.6	-12.6	-15.4	-17.8
Exp	-16.8	-13.7	-12.8	-11.6	-12.3	-17.2

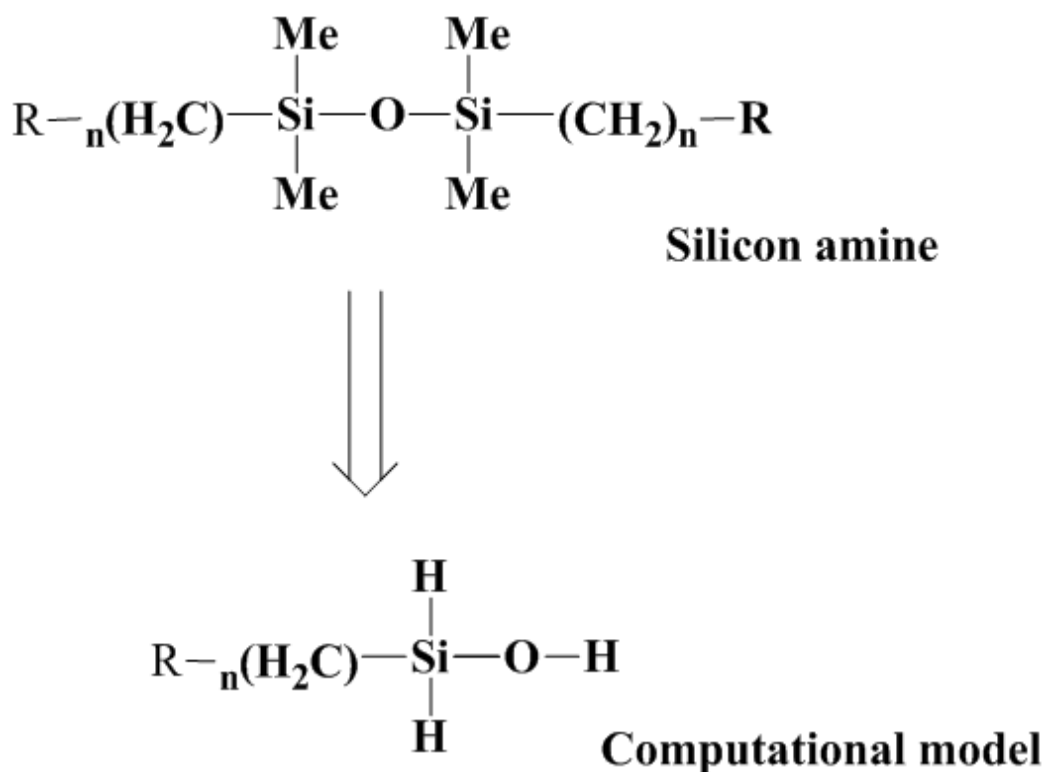


Figure 1: Schematic illustration of selection of computational model. Sign “**R**” presents the groups that include the amino groups, e.g. For GAP-0 and DAB-0, **R** presents NH₂- group; for GAP-AEAP, **R** presents NH₂(CH₂)₃NH- group; and for DAB-Me and DAB-diMe, **R** presents the NH₂CH(CH₃)- and NH₂C (CH₃)₂- group, respectively.

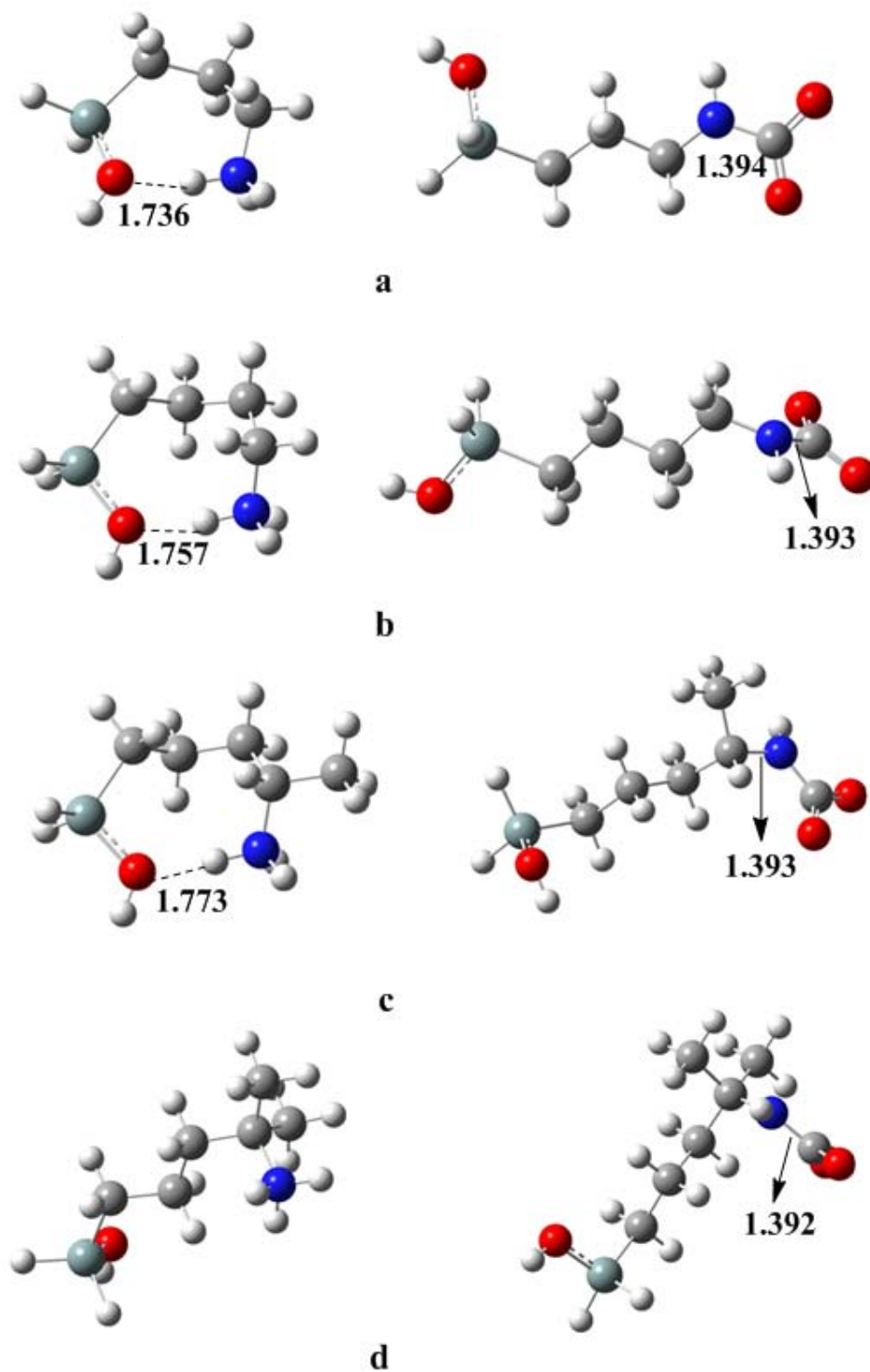


Figure 2. The lowest energy conformers of ammonium cations (left) and carbamate anions (right) formed from reaction of CO₂ with **a.** GAP-0, **b.** DAB-0, **c.** DAB-Me and **d.** DAB-diMe. The unit for bond length is Å. The red balls are for oxygen, blue ones for nitrogen, gray ones for carbon, green ones for silicon and smallest white ones for hydrogen.

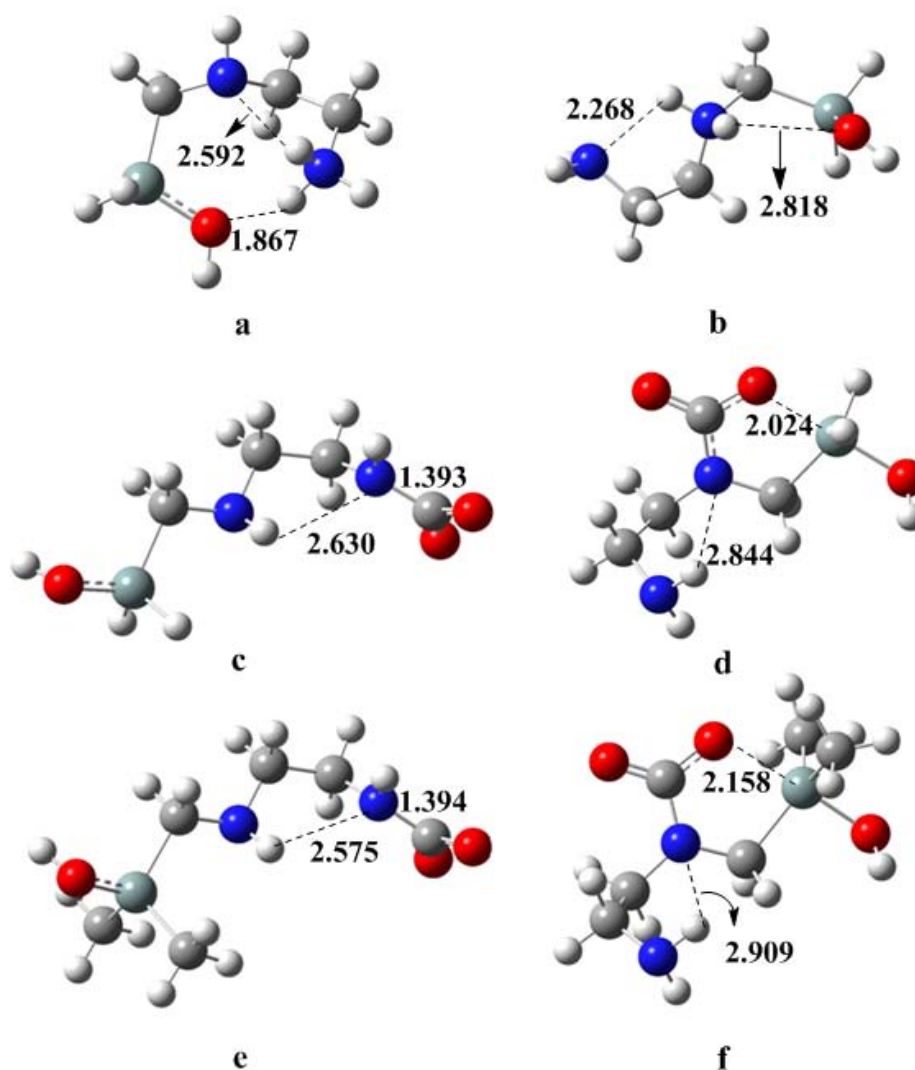


Figure 3. The lowest energy conformers of ammonium cations (first line) and carbamate anions (the second line) formed from reaction of CO_2 with primary amine (left hand) and secondary amine (right) of GAP-AEAM, and the CH_3 substituted carbamate anions at Si-site. The unit for bond length is Å. The red balls are for oxygen, blue ones for nitrogen, gray ones for carbon, green ones for silicon and smallest white ones for hydrogen.

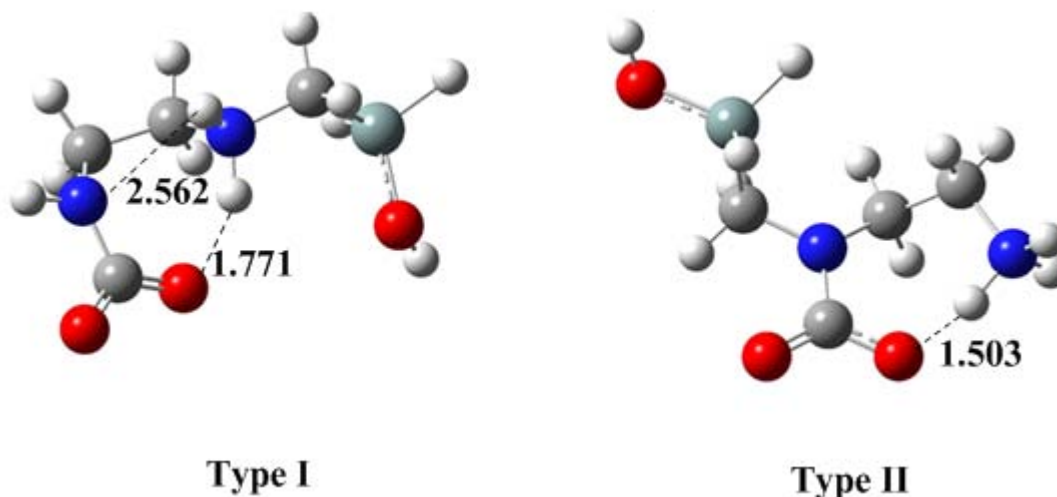


Figure 4. Two type of intra-molecular carbamate formed from the reaction of CO₂ with GAP-AEAM. The unit for bond length is Å. The red balls are for oxygen, blue ones for nitrogen, gray ones for carbon, green ones for silicon and smallest white ones for hydrogen.

References:

- (1) H. B., X.; J. K., *J. J. Phys. Chem. A*, submitted
- (2) Perdew;, J. P. *Phys. Rev. B*, **1986**, 33, 8822.
- (3) Ahlrichs, R.; Bär, M.; Häser, M.; Horn, H.; Kölmel, C. *Chem.Phys.Lett*, **1989**, 162 165.
- (4) Eichkorn, K.; Treutler, O.; Ohm, H.; Haser, M.; Ahlrichs, R. *Chem.Phys.Lett*, **1995**, 240, 283.
- (5) Frisch, M. J.; Trucks, G. W.; Schlegel, H. B.; Scuseria, G. E.; Robb, M. A.; Cheeseman, J. R., et.al. Gaussian 03 revision C.02 ed.; Gaussian, Inc: Wallingford, CT 2004,.
- (6) Cossi, M.; Rega, N.; Scalmani, G.; Barone, V. *J. Comput.Chem*, **2003**, 24, 669.
- (7) Barone, V.; Cossi, M. *J.Phys.Chem. A* **1998**, 102, 1995.
- (8) Cancès, E.; Mennucci, B.; Tomasi, J. *J. Chem. Phys.* **1997**, 107, 3032.
- (9) Miertz, S.; Scrocco, E.; Tomasi, J. *J. Chem. Phys* **1981**, 55, 117.
- (10) Tomasi, J.; Persico, M. *Chem.Rev* **1994**, 94, 2027.
- (11) Gurkan, B. E.; de la Fuente, J. C.; Mindrup, E. M.; Ficke, L. E.; Goodrich, B. F.; Price, E. A.; Schneider, W. F.; Brennecke, J. F. *J. Am.Chem.Soc*, **2010**, 132, 2116.

Appendix 7. Optimization

The baseline MEA process is similar to the Fluor's Econamine process reported in the 2004 IEA report and the 2007 DOE report. The process has four process variables that dominate the performance with a given solvent and they are:

- Absorber Temperature
- Desorber Reboiler Temperature
- Desorber Pressure
- Rich/Lean Heat Exchanger Approach Temperature

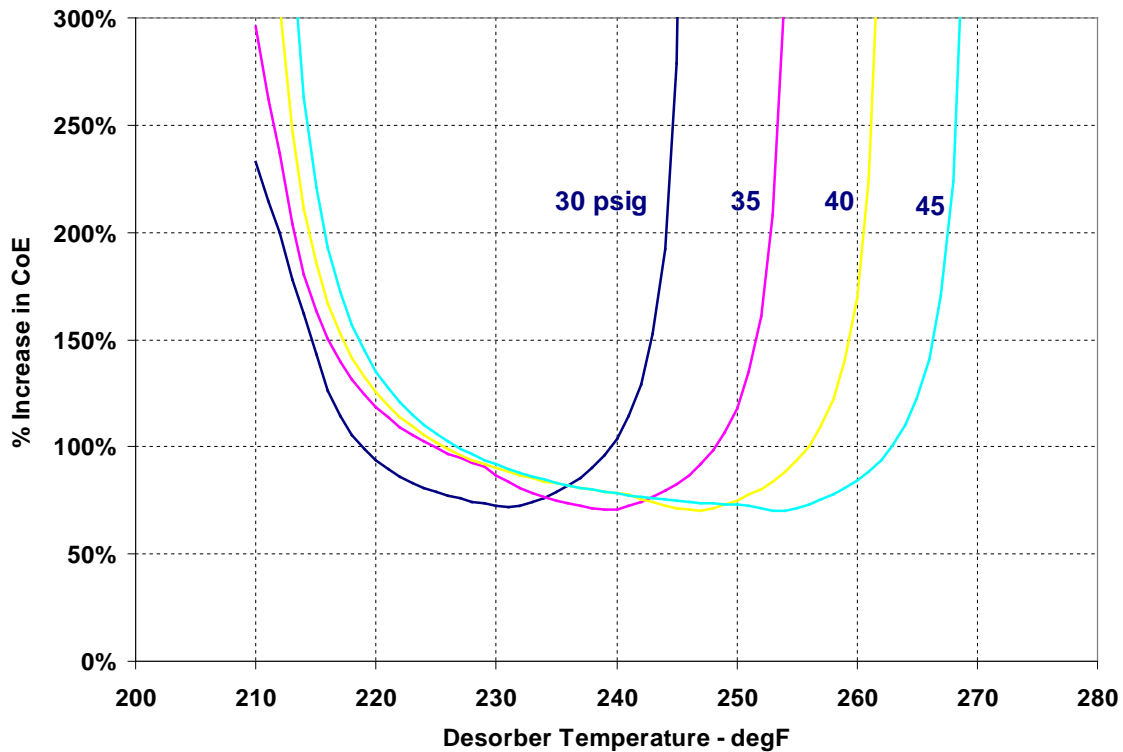


Figure A1. MEA System ISO Bars at 140F absorption temperature.

Figure A1 shows the effect of varying the temperature in the desorber reboiler and pressures in the desorber on the cost of electricity (CoE). In an aqueous system (30% by weight MEA in water), the desorber operation is dominated by optimization of the water-boiling and steam-condensation processes. At the high-temperature of the desorber reboiler, water vaporizes with the CO₂. The steam at the bottom of the desorber serves to suppress the partial pressure of CO₂, aiding in CO₂ desorption. As the CO₂ and steam gas flow up the desorber, they exchange heat with the solvent passing down the desorber column, and the steam is condensed.

As the temperature in the desorber reboiler increases, the solvent desorption increases which in turn increases the solvent net loading. This reduces the sensible heat since less solvent is recirculated and this in turn reduces the cost of electricity. This behavior of decreasing COE with increasing temperature is shown on the left side of the isobar curves shown in Figure. As the desorber reboiler temperature is further increased, the solvent does not have sufficient heat capacity to condense the steam to maintain the temperature at the top of the desorber. So, the top of the desorber temperature rises as the desorber reboiler temperature increases, and significant amount of water vaporizes, which

in turn increases the desorber load. This behavior of increasing COE with increasing temperature is shown on the right side of the isobar curves shown in figure. These competing effects result in an optimum temperature for each pressure.

As total pressure is increased, the ideal operating temperature also increases. This increased temperature drives an increase in thermal degradation of solvent, and an increase in the water vaporization, creating an optimum temperature in the desorber of approximately 230F at 30 psia. Literature studies show that amine desorbers are operated at approximately 240F and 30 psia in practice.

Rich-Lean Heat Exchanger Temperature Approach

The rich-lean heat exchanger reduces the sensible heat requirement for the capture process by exchanging heat from the hot lean solvent leaving the desorber to the cool rich solvent leaving the absorber. Practically, heat exchangers cannot transfer all the heat from the cold stream to the hot stream, and in practice, an approach temperature between 10 and 50 F is common. Figure A2 shows that the sensible heat requirement of the system increases linearly as the approach temperature increases. The figure also shows that as the approach temperature increases, the heat capacity of the solvent falling in the desorber also increases, decreasing the amount of water that is vaporized. The presence of steam in the desorber creates an optimum approach temperature in the desorber of 50F.

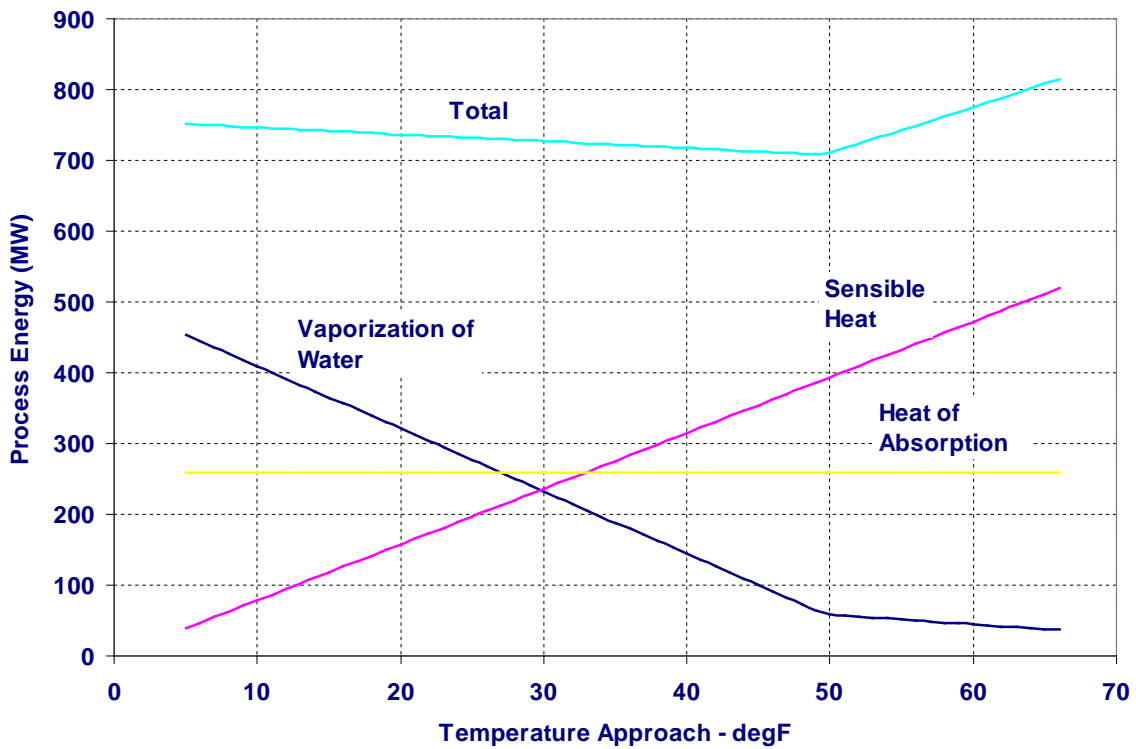


Figure A2. MEA System effect of reduced R/L HX approach.

Reaction Mechanism of Monoethanolamine with CO₂ in Aqueous Solution from Molecular Modeling

Hong-Bin Xie,^{†,‡} Yanzi Zhou,[§] Yingkai Zhang,^{*,§} and J. Karl Johnson^{*,†,‡}

Department of Chemical and Petroleum Engineering, University of Pittsburgh, Pittsburgh, Pennsylvania 15261, United States, National Energy Technology Laboratory, Pittsburgh, Pennsylvania 15236, United States, and Department of Chemistry, New York University, New York, New York 10003, United States

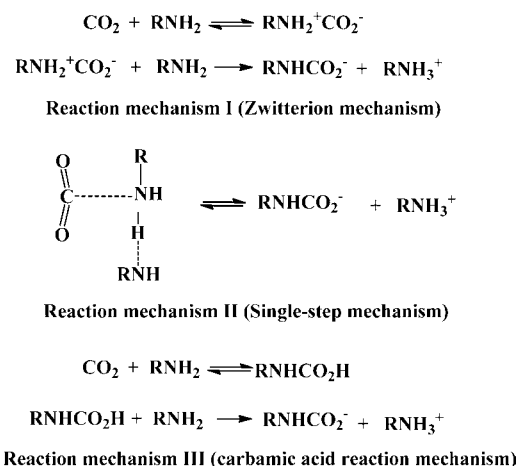
Received: August 9, 2010; Revised Manuscript Received: September 24, 2010

We present a theoretical study of the reaction mechanism of monoethanolamine (MEA) with CO₂ in an aqueous solution. We have used molecular orbital reaction pathway calculations to compute reaction free energy landscapes for the reaction steps involved in the formation of carbamic acids and carbamates. We have used the conductor-like polarizable continuum model to calculate reactant, product, and transition state geometries and vibrational frequencies within density functional theory (DFT). We have also computed single point energies for all stationary structures using a coupled cluster approach with singles, doubles, and perturbational triple excitations using the DFT geometries. Our calculations indicate that a two-step reaction mechanism that proceeds via a zwitterion intermediate to form carbamate is the most favorable reaction channel. The first step, leading to formation of the zwitterion, is found to be rate-determining, and the activation free energies are 12.0 (10.2) and 11.3 (9.6) kcal/mol using Pauling (Bondi) radii within the CPCM model at the CCSD(T)/6-311++G(d,p) and CCSD(T)/6-311++G(2df,2p) levels of theory, respectively, using geometries and vibrational frequencies obtained at the B3LYP/6-311++G(d,p) level of theory. These results are in reasonable agreement with the experimental value of about 12 kcal/mol. The second step is an acid–base reaction between a zwitterion and MEA. We have developed a microkinetic model to estimate the effective reaction order at intermediate concentrations. Our model predicts an equilibrium concentration for the zwitterion on the order of 10⁻¹¹ mol/L, which explains why the existence of the zwitterion intermediate has never been detected experimentally. The effective reaction order from our model is close to unity, also in agreement with experiments. Complementary ab initio QM/MM molecular dynamics simulations with umbrella sampling have been carried out to determine the free energy profiles of zwitterion formation and proton transfer in solution; the results confirm that the formation of the zwitterion is rate-determining.

1. Introduction

Monoethanolamine (MEA) has been used commercially for many decades to separate CO₂ from natural gas. It is also considered as a prototype for amine-based capture of CO₂ from fossil fuel power plant flue gas.^{1–3} It is typically used as a 30% by weight aqueous mixture in an absorption column,⁴ where it reacts to form a carbamate solution, and is then regenerated in a stripping column by heating the solution with low pressure steam to produce a stream of nearly pure CO₂. The MEA process is able to capture 90% of the CO₂ in flue gas.⁵ The increase in the cost of electricity due to CO₂ capture using aqueous MEA is estimated to be about 80% and the decrease in power plant efficiency is estimated to be about 30%.⁵ Hence, the high cost and low efficiency of the MEA process makes this an unattractive technology for CO₂ capture in coal-fired power plants. Nevertheless, fundamental understanding of the MEA/CO₂ reaction mechanism is needed in order to help design more cost-effective amine-based solvents. Despite a number of different experimental and theoretical studies on the reaction mechanism of the MEA + CO₂ system,^{6–15} there is still a controversy regarding the details of the reaction mechanism. Three reaction

SCHEME 1p



mechanisms have been proposed for the MEA/CO₂ system. These are summarized in Scheme 1. Several experimental studies published in the 1980s supported the zwitterion-mechanism proposed by Caplow¹⁶ and reintroduced by Danckwerts.¹⁴ There is consensus from experiments that the intrinsic reaction order of MEA in the reaction is close to unity.¹⁵ Recently, Ali et al. reinvestigated the reaction of MEA with CO₂ using stopped-flow techniques in the concentration range

* To whom correspondence should be addressed. E-mail: yingkai.zhang@nyu.edu (Y.Z.) and karlj@pitt.edu (J.K.J.).

[†] University of Pittsburgh.

[‡] National Energy Technology Laboratory.

[§] New York University.

of MEA from 0.005 to 0.040 mol/L.⁸ They measured the reaction rate coefficient and from that estimated an activation free energy of 12.4 kcal/mol at 298 K, which is in good agreement with previous studies.^{6,7,9,10} The reaction order of MEA deduced from their experiment is 1.2. However, none of the experiments have been able to detect the presence of the predicted zwitterion intermediate.

We are aware of three published theoretical studies^{11–13} on the MEA/CO₂ system. Da Silva and Svendsen¹² studied the formation process of carbamate from CO₂ and MEA by scanning the potential energy curve at the HF/3-21G(d) level. They suggested that the processes of CO₂ attacking MEA to form zwitterion intermediates and the subsequent hydrogen abstraction process between a zwitterion and another MEA to form carbamate had no intrinsic energy barrier. They therefore concluded that no stable zwitterion species was formed and a single-step reaction mechanism, e.g., mechanism II in Scheme 1, was most feasible. At first glance, a single-step reaction mechanism will result in a reaction order of 2 in MEA, which does not agree with experiments. They explain this discrepancy by introducing a water molecule as proton acceptor. That is, a water molecule acts as a proton acceptor instead of MEA. However, a recent study by Shim et al.¹¹ indicated that MEA is more suitable as a base than water in the reaction. In contrast to their studies, Arstad et al.¹³ found that the proton abstraction process between zwitterions and MEA has an energy barrier of 9.3 kcal/mol at the G3MP2B3 level of theory and concluded that reaction mechanism III in Scheme 1, via a carbamic acid intermediate catalyzed by another MEA, is the most likely reaction pathway. Their studies, to some extent, supported a zwitterion description of the starting complex. Their results appear to be in good agreement with experiments in view of the activation energy and order of the reaction. However, they did not consider the mechanism for forming the zwitterion intermediate from the reactants. Also, they did not explain why experiments have not been able to detect the zwitterion intermediate. It is worth mentioning that most of the calculations from da Silva and Svendsen and Astrad et al. were performed using single-point energy calculations based on gas-phase configurations of the molecules. They used implicit solvation models only in the single-point calculations, not the geometry optimizations. We expect that geometries of the intermediates and products will be quite sensitive to the presence of a solvent, which means that the results of these studies may not be completely reliable.

To get a clearer picture of the reaction mechanism and further explain experimental observations, we have reinvestigated this reaction mechanism using more reliable theoretical methods compared to previous studies. Specifically, we have included implicit solvent effects in both the geometry optimizations and frequency calculations for this reaction in the *ab initio* calculations. We have examined the influence of different atomic radii for constructing the solute cavity on the reaction energy barrier. High-level single-point energy calculations are performed to test the convergence of the energies. We have used potential of mean force (PMF) calculations to investigate the free energy landscape at finite temperatures and to account for the entropy of the solution-phase reaction. In this work we focus on the reaction mechanisms I and III (Scheme 1) because only these two reaction mechanisms are consistent with the experimentally observed reaction order.

2. Computational Details

2.1. *Ab Initio* Electronic Structure Calculations. The Gaussian 03 package¹⁷ was used for the molecular orbital and

density functional theory calculations in this work. One may reasonably ask whether single reference methods are appropriate for the MEA + CO₂ system. We have tested the MEA/CO₂ zwitterion for evidence of multireference character by computing a T1 diagnostic¹⁸ within the CCSD/6-311++G(d,p) treatment. The T1 diagnostic is defined for use with self-consistent-field molecular orbitals and is invariant to the same orbital rotations as the coupled cluster energy.¹⁸ A value of the T1 diagnostic larger than 0.02 indicates that the degree of multireference character in the system is large enough to cast doubt on the reliability of a single reference correlation treatment.¹⁸ We obtained a value 0.01 for the zwitterion, indicating a negligible degree of multireference character. Hence, we believe that a single reference correlation treatment is justified.

In da Silva and Svendsen's study,¹² they found that the zwitterion is not a local minimum in the gas phase, but it is a minimum when solvent effect are included. This indicates that solvent effects are of critical importance in the stabilization of zwitterions. Therefore, solvent effects must be carefully accounted for when studying the reaction of MEA with CO₂. Accordingly, implicit solvent effects were taken into account in this study by exploiting the conductor-like polarizable continuum model (CPCM) formalism^{19,20} with the dielectric constant of water (ϵ) equal to 78.39. We used the CPCM model for all geometry optimizations, vibrational frequency calculations, and single-point energy calculations. This method was initially devised by Tomasi and co-workers^{21–23} and extended for geometry optimizations to converge efficiently. UAHF atom radii were initially used in the construction of the solute cavity for all calculations. We note that the definition of the cavity is one of the important factors in determining the accuracy of the continuum solvation model.²⁴ Therefore, we also used UFF, UA0, UAKS, Bondi, and Pauling atomic radii in computing energies and other properties as a comparison. Unless otherwise indicated, the UAHF radii were used in calculations reported here.

The optimized geometries and harmonic frequencies of the reactants, products, isomers, and transition states were obtained at the B3LYP/6-311++G(d,p) level. Single-point energy calculations for important configurations were performed at the CCSD(T)/B1//B3LYP/B1 and CCSD(T)/B2//B3LYP/B1 level, where B1 = 6-311++G(d,p), B2 = 6-311++G(2df,2p), and //B3LYP/B1 means that the B3LYP/B1-optimized geometries were used in the calculations. Connections of the transition states between designated local minima have been confirmed by intrinsic reaction coordinate (IRC) calculations at the B3LYP/B1 level. To determine whether the zwitterion structure is a real minimum, calculations with MP2 and B3LYP methods combined with various basis sets were used to optimize geometry and calculate frequencies.

We have estimated the Gibbs free energy for each of the compounds at 298 K by combining total energy calculations with vibrational frequency calculations. The frequency calculations were computed at the B3LYP/B1 level, including solvent effects within the CPCM model. The Gibbs free energy is given by

$$G = E_{\text{SCF}} + G_{\text{corr}} + \text{ZPE} \quad (1)$$

where E_{SCF} is the total energy from the quantum mechanical calculation, G_{corr} is a correction term, and ZPE is the zero point energy. G_{corr} is given by

$$G_{\text{corr}} = E_{\text{corr}} + k_{\text{B}}T - TS \quad (2)$$

where E_{corr} is the internal energy computed from the molecular partition function (translational, rotational, and vibrational degrees of freedom), k_{B} is the Boltzmann constant, T is the absolute temperature, and S is the entropy, also computed from the molecular partition function. Entropic effects for bimolecular reactions will be overestimated because the molecular partition functions are based on the gas phase. A reaction whereby species A and B react to form a complex C involves conversion of three translational and three rotational degrees of freedom into six vibrational degrees of freedom. This transformation overestimates contributions to the free energy in condensed phases. To avoid this, we have chosen a reference state for bimolecular reactions that fixes the A–B reactive center distance at 10 Å. The total free energy of the reference state is calculated as follows:

$$G_{\text{total}} = E_{\text{A}} + E_{\text{B}} + G_{\text{corr}}(10\text{\AA}) + ZPE_{\text{A}} + ZPE_{\text{B}} \quad (3)$$

2.2. Reaction Rate Coefficient Calculation. The reaction rate coefficients for elementary reaction steps were calculated from transition state theory:

$$k = (c^\circ)^{\Delta n} \frac{k_{\text{B}}T}{h} \exp\left(-\frac{\Delta G}{RT}\right) \quad (4)$$

where c° is the standard-state concentration (1 mol/L), Δn is the change of the number of moles from reactants to the transition state, which is -1 for our case, h is the Planck constant, ΔG is the difference in the Gibbs free energy between reactants and the transition state, and R is the gas constant.

2.3. Potential of Mean Force Calculations. Perhaps the most questionable part of the calculations for the free energy in eq 3 above is the assumption that the reference state is composed of reactants held fixed at a distance of 10 Å apart. This is a rather arbitrary assumption that is needed to prevent overestimation of the entropic part of the free energy. A better approach would be to compute the free energy through a PMF approach using a large system containing many explicit water molecules so that the configurational entropy of the reactants and the solvent can be correctly accounted for. Performing such a calculation using an ab initio molecular dynamics (MD) approach would be the best approach, but at present this is not computationally feasible. We have therefore determined the free energy reaction profile with Born–Oppenheimer MD simulations using the ab initio quantum mechanics/molecular mechanics (QM/MM) method^{25–30} in conjunction with the umbrella sampling technique.^{31–33} The QM subsystem for the first reaction step consists of CO₂ and MEA, described at the B3LYP/B1 level of theory, while all solvent water molecules were treated molecular mechanically with the TIP3P water model.³⁴ The reaction coordinate was chosen as the distance between the C atom of CO₂ and the N atom of MEA. Twenty simulation windows were placed along the reaction coordinate from 5.0 to 1.3 Å, and the total potential energy was biased with a

harmonic constraint of 30–50 kcal mol⁻¹ Å⁻², centered on the successive values of the reaction coordinate. For each simulation window, the initial structure of the QM subsystem obtained from B3LYP/B1 QM calculations was first solvated in a pre-equilibrated water sphere of 25 Å radius, which was centered on the N atom of MEA, and then water molecules within 20 Å were equilibrated for 500 ps with the QM subsystem fixed. Subsequently, simulation windows of 50 ps in length using the B3LYP/B1 QM/MM method were carried out. For each window, the first 10 ps of the simulation were discarded for equilibration and the last 40 ps were used for data analysis. Finally, probability distributions along the reaction coordinate were determined for each window and pieced together with the weighted histogram analysis method (WHAM)^{35–37} to obtain the reaction free energy profile. We have followed a similar approach for the key part of the second reaction step, but using the zwitterion and the additional MEA as the QM subsystem. We have used 20 ps ab initio QM/MM MD simulations for each window for the second step in order to save computational time. This is a reasonable approach because the QM subsystem is larger for the second step and the free energy profile from the 10–20 ps trajectories is reasonably well converged. This computational protocol has been successfully applied to study several enzymes as well as chemical reactions in aqueous solution.^{38–46}

All the ab initio QM/MM calculations were performed with modified Q-Chem⁴⁷ and Tinker programs.⁴⁸ A time step of 1 fs was used, and Newton’s equations of motion were integrated with the Beeman algorithm.⁴⁹ Spherical boundary conditions were applied to atoms beyond 20 Å from the N atom of MEA in our QM/MM simulations. Cutoffs of 18 and 12 Å were employed for electrostatic and van der Waals interactions, respectively. Note that there was no electrostatic cutoff between QM and MM subsystems. The Berendsen thermostat method⁵⁰ was used to maintain the system temperature at 298 K.

2.4. Conformer Selection. MEA has several conformers that could be used as starting points for reaction path calculations. According to a recent study by da Silva et al.,⁵¹ the main (O–C–C–N) dihedral tends to remain in a gauche conformer in pure MEA and aqueous solutions of MEA. Therefore, rather than arbitrarily selecting one conformer as the reactant conformation, we have selected four different conformers in order to test the influence of different conformers on the reactivity of MEA toward CO₂. We selected the two conformers having the highest population (tGg and tGg’) in pure MEA and aqueous solution of MEA, along with another gauche conformer (g’Gg’) and one trans conformer (g’Tt). The results, shown in Table 1, indicate that all conformers except g’Gg’ have similar reactivity toward CO₂. We have selected the tGg’ as the reactant conformer for all further calculations in this work, due to its high population and similar reactivity to tGg.

3. Results and Discussions

3.1. Ab Initio Calculations. Figure 1 depicts the structures of important intermediates and transition states optimized at the B3LYP/B1 level with the CPCM model for the reaction of MEA with CO₂. The schematic free energy surfaces of the carbamate and carbamic acid reactions computed at the B3LYP/B1 level are presented in Figure 2. The first step in the reaction is for

TABLE 1: Relative Free Energies in kcal/mol of TS1 (see Figure 1) at the B3LYP/B1 Level Computed with the CPCM Model Using the UAHF Radii

tGg + CO ₂	0.0	tGg’ + CO ₂	0.0	g’Gg’ + CO ₂	0.0	g’Tt + CO ₂	0.0
TS1	5.1	TS1	4.7	TS1	8.2	TS1	5.0

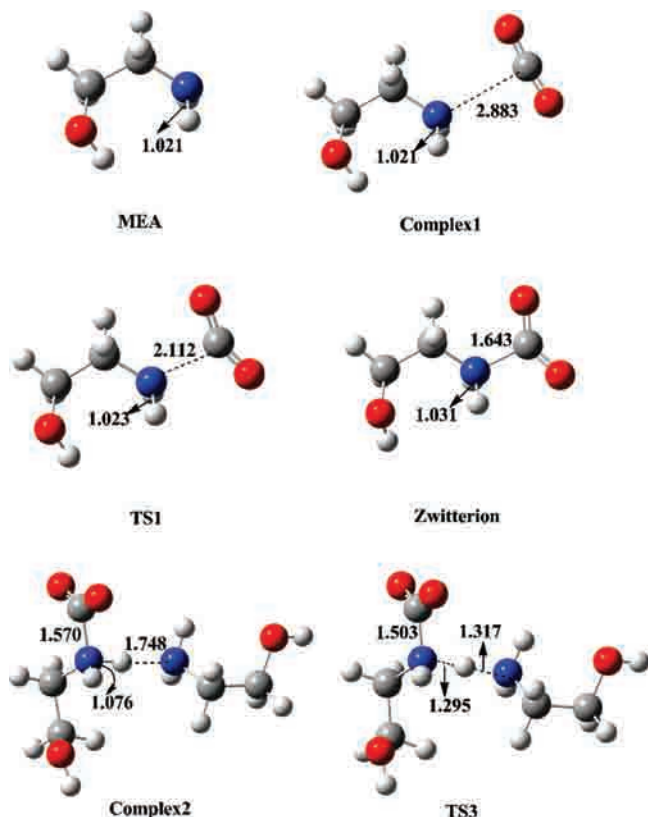


Figure 1. Optimized geometries of important intermediates and transition states computed at the B3LYP/B1 level using the CPCM model with UAHF radii for the reaction of MEA (2MEA) + CO₂. Bond lengths are in angstroms.

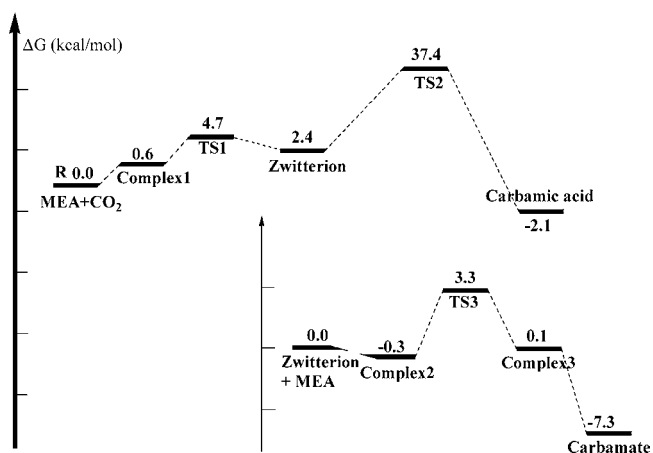


Figure 2. Schematic free energy surface for the MEA + CO₂ reaction to form carbanic acid or carbamate through the addition of an additional MEA molecule. Calculations were performed at the B3LYP/B1 level using the CPCM model with UAHF radii.

MEA + CO₂ to form a complex (complex 1 in Figure 2). The energy of complex 1 is 0.6 kcal/mol higher than that of the reactants in the (arbitrary) reference state we have chosen. There is an activation free energy of 4.1 kcal/mol in going from complex 1 to the zwitterion intermediate. There are (at least) two different reaction channels for the zwitterion: one is for the zwitterion to transform to carbanic acid and the other is to react with another MEA to form carbamate via an H-abstraction process. From Figure 2 we see that the carbamate reaction channel is more favorable than formation of carbanic acid due to its much lower activation free energy. Arstad et al. considered the catalytic effect of MEA for the carbanic acid reaction

channel and estimated a reaction energy barrier of about 10 kcal/mol,¹³ which is much lower than the barrier from our calculations of 35 kcal/mol, but still much higher than the carbamate channel. In their studies, MEA facilitates the proton transfer from the N atom to the O atom of the zwitterion via decreasing the ring-strain in the transition state. However, it is our view that catalysis of the proton transfer process by MEA is highly unlikely. This is because a much lower energy pathway exists for MEA to form the carbamate product by direct abstraction of a proton, as discussed below. In addition to MEA, water molecules could also catalyze the proton transfer process in the carbamic acid reaction. Therefore, we have calculated the activation free energy for carbamic acid formation including explicit water catalysis. We found an activation free energy of 13.4 kcal/mol when proton transfer was catalyzed by two water molecules (at the B3LYP/B1 level with UAHF radii). This barrier is comparable to the value reported by Arstad et al. Note that water will not directly participate in carbamate formation, because the first step does not involve proton transfer and direct proton abstraction by MEA is more facile for the second step. It is therefore sufficient to use the CPCM implicit solvent model to account for environmental effects of water in the carbamate reaction.

Studies by da Silva and Svendsen¹² and Shim et al.¹¹ using the coordinate driving method indicated that the H abstraction process in forming carbamate is reaction energy barrier free. In contrast, Arstad et al.¹³ found that this process has a reaction energy barrier of 9.3 kcal/mol on the basis of gas-phase geometry optimization of the reactants and transition state complex. We believe that the study of Shim et al. is most reliable of these three published studies, because they performed coordinate driving calculations within an effective solvent model (PCM) approach at the B3LYP/6-31+G(d,p) level of theory. In contrast, other groups used geometries optimized in the gas phase and applied effective solvent models for single point calculations only. Our B3LYP/B1 calculations using the UAHF radii within the CPCM model predict an activation free energy barrier of 3.6 kcal/mol for the H abstraction process (see Figure 2). Furthermore, we have explored the sensitivity of the reaction barrier to the choice of the atomic radii in the CPCM model. Different sets of atomic radii, including Bondi, Pauling, UFF, UAKS, and UA0, were used in the CPCM method to locate the transition states starting from the geometry obtained at the B3LYP/B1 level with UAHF atomic radii. Interestingly, we failed to locate a transition state for the H abstraction process using any of these other radii, notwithstanding making several attempts with different starting configurations. This likely means that the process is barrier-free, as Shim et al. and da Silva and Svendsen predicted. It appears that use of the UAHF radii in the CPCM calculations leads to overestimation of the reaction energy barrier for the H abstraction process. Indeed, it has recently been argued that use of UAHF radii overestimates the reaction energy barrier for the process of basic hydrolysis of β -lactams,⁵² which involves the breaking of H-X bonds. We have therefore concluded that the H abstraction process between MEA and the zwitterion likely has a very low intrinsic energy barrier.

From the above discussion, we can conclude that the two-step reaction mechanism via a zwitterion intermediate is more favorable than the channel to form carbanic acid; furthermore, the first step, formation of the zwitterion, is rate-determining.

We have carried out additional calculations in order to obtain more reliable energetic information on the favorable carbamate reaction channel. We have first used the B3LYP/B1 method

TABLE 2: Energies (kcal/mol) of Complex 1, TS1, and Zwitterion (see Figure 1) Relative to the Reactants^a

species	UFF	UAHF	UA0	UAKS	Bondi	Pauling
complex 1	1.1	-1.3	-3.0	0.6	2.2	2.9
TS1	9.4	5.5	5.5	7.0	10.2	12.0
zwitterion	7.4	2.4	2.4	4.5	4.9	7.4

^a Calculations were performed at the CCSD(T)/B1//B3LYP/B1 level of theory with UFF, UAHF, UA0, UAKS, Bondi, and Pauling radii within the CPCM model. The energy of the reactants (defined as a complex composed of MEA and CO₂ at a distance of 10 Å between the C atom of CO₂ and the N atom of MEA) is set to zero for the different radii.

TABLE 3: Energies (kcal/mol) of Complex 1, TS1, and Zwitterion (see Figure 1) Relative to the Reactants as in Table 2, but for Calculations at the CCSD(T)/B2//B3LYP/B1 Level of Theory

species	UFF	UAHF	UA0	UAKS	Bondi	Pauling
complex 1	1.1	-1.3	-2.9	0.7	2.2	2.8
TS1	8.6	5.1	4.9	6.5	9.6	11.3
zwitterion	6.1	0.9	1.1	3.3	3.2	5.6

with the CPCM approach using UFF, UA0, UAKS, Bondi, and Pauling radii to reoptimize the geometries of **R**, complex 1, **TS1**, and zwitterion (see Figure 2) in the rate-determining step. Second, high-level quantum methods, CCSD(T)/B1 and CCSD(T)/B2, were used to calculate the single-point energies based on the geometries obtained at the B3LYP/B1 level of theory. The activation free energies at the CCSD(T)/B1 level are 9.4, 5.5, 5.5, 7.0, 10.2, and 12.0 kcal/mol using UFF, UAHF, UA0, UAKS, Bondi, and Pauling radii, respectively (see Table 2). The corresponding values at the CCSD(T)/B2 are 8.6, 5.1, 4.9, 6.5, 9.6, and 11.3 kcal/mol (Table 3). We conclude that activation free energies predicted by Bondi and Pauling radii at the CCSD(T) method both with B1 and B2 basis sets are in reasonable agreement with experiments (about 12.4 kcal/mol). However, UAHF, UA0, UFF, and UAKS underestimate the activation free energy. The activation free energies for the reverse process (zwitterion to the reactants) are 2.0, 3.1, 3.1, 2.5, 5.3, and 4.6 kcal/mol as computed at the CCSD(T)/B1 level of theory using UFF, UAHF, UA0, UAKS, Bondi, and Pauling radii, respectively (Table 2). The corresponding values at the CCSD(T)/B2 level are 2.5, 4.2, 3.8, 3.2, 6.4, and 5.7 kcal/mol (Table 3). Comparing the results from the two different basis sets, we conclude that the larger basis set involving d and f polarization functions for heavy atoms and d functions for hydrogens increases the stability of the zwitterion; i.e., the relative free energy of the zwitterion is more sensitive to changes in the basis set than TS1.

The second step in the reaction corresponds to the addition of MEA to the zwitterion to form the carbamate, as shown in Figure 2. We have computed activation free energies for the MEA + zwitterion reaction pathway at the CCSD(T)/B1 level of theory using the Bondi and Pauling radii. We use this combination of level of theory and radii because it gives reasonable activation free energies for the formation of the zwitterion and use of the large B2 basis set in the single-point calculations does not appear to change the results substantially. We acknowledge that this is not a rigorous criterion for determining the proper level of theory to use, but this is a reasonable approximation given the size of the systems involved. We have calculated the single point energies at CCSD(T)/B1 for the following complexes (see Figure 2): zwitterion + MEA, complex 2, and **TS3**. It is worth mentioning that geometries and free energy corrections were obtained from B3LYP/B1

TABLE 4: Relative Energies (kcal/mol) of Complex 2, TS3, and Complex 3 (see Figure 1) at the CCSD(T)/B1//B3LYP/B1 level with Bondi and Pauling Radii within the CPCM Model Based on the Geometries at B3LYP/B1 with UAHF Radii^a

radii	complex 2	TS3	complex 3
Bondi	-2.2	-1.7	-6.6
Pauling	-1.6	-1.4	-6.7

^a The reference energies are taken to be those of the zwitterion + MEA complex in each case.

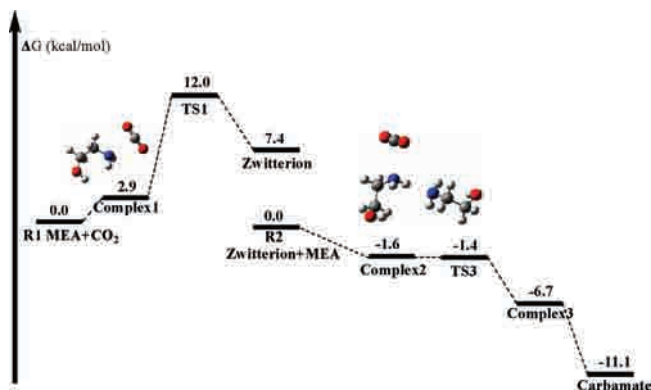


Figure 3. Schematic of the most favorable reaction channel for the MEA(2MEA) + CO₂ reaction obtained at the CCSD(T)/B1//B3LYP/B1 level with Pauling radii. The CCSD(T)/B1 single-point energy calculations for the second step are based on geometries obtained from B3LYP/B1 optimizations using UAHF radii. See the text for details. Note the use of two different reference states: MEA + CO₂ is the reference state for the first step and zwitterion + MEA is the reference state for the second step.

CPCM calculations using the UAHF radii. From Table 4, we can see that free energies of complex 2 and **TS3** are more than 1 kcal/mol lower than that of the zwitterion + MEA starting configuration. Moreover, the free energies of **TS3** are just 0.5 and 0.2 kcal/mol higher than that of complex 2 computed with Bondi and Pauling radii, respectively. From this we conclude that the reaction mechanism for the addition of MEA to the zwitterion occurs with almost no barrier. The diagram in Figure 3 schematically summarizes our findings. Namely, that formation of the zwitterion is the rate-determining step and that subsequent steps occur almost spontaneously.

It is well-known that MEA is a strong base; therefore, deprotonation in solution from MEA is energetically very unfavorable. It is tempting, therefore, to assume that H⁺ abstraction from the MEA/CO₂ zwitterion is the rate-limiting step in carbamate formation. However, our calculations indicate that proton abstraction from MEA in the zwitterion is facile because formation of the zwitterion activates the N–H bond. Evidence of this activation can be seen by the change of the N–H bond length from MEA to zwitterion. The N–H bond length of MEA is 1.021 Å; however, it is lengthened to 1.031 Å in the zwitterion, which is in good agreement with similar calculations of Shim et al.¹¹ In addition, we have calculated the pK_a value of the zwitterion to try to further explain why the H-abstraction step has such a low reaction barrier. The implicit solvent model is not considered to be accurate for predicting pK_a values.⁵³ We therefore use the cluster-continuum model to calculate the pK_a value for the zwitterion; this approach has given excellent results for calculating the pK_a values of acids and conjugate bases.^{53–55} Details of the cluster-continuum model are given by Pliego and Riveros.⁵⁴ We have found that the optimal number of explicit water molecules is three for our

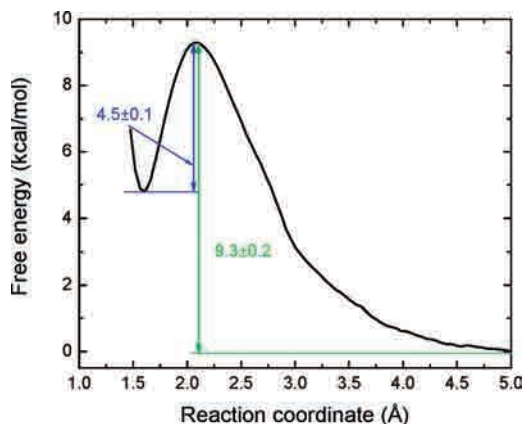


Figure 4. Potential of mean force plot for CO₂ approaching MEA obtained at the B3LYP/6-311++G(d,p) QM/MM level of theory. The distance between the N atom of MEA and the C atom of CO₂ is taken as the reaction coordinate.

system. The pK_a value of the zwitterion is calculated to be 3.3 using the MP2/B1//B3LYP/B1 level of theory with Bondi radii. For comparison, this value is close to the value reported for acetic acid of 4.75.^{54,56} This indicates that the zwitterion is acidic and hence the reaction between MEA and zwitterion is an acid–base reaction, which explains why the kinetics of this process are so fast. To the best of our knowledge, this is the first time that the second step has been identified as an acid–base reaction. Moreover, our calculations provide indirect evidence that the trimolecular reaction mechanism (reaction mechanism II in Scheme 1) is not feasible because the activation of N–H through zwitterion formation is very important for lowering the energy barrier of the reaction. The relatively small pK_a value implies that the zwitterion could dissociate to release a proton, even when there is no other MEA near the zwitterion. The transfer rate of protons in aqueous solutions is fast, which indicates that the second step in carbamate formation is not rate-limiting.

3.2. Potential of Mean Force Calculations. Potential of mean force calculations were performed to estimate the free energy of zwitterion formation in solution. These calculations complement the ab initio molecular orbital free energy calculations using the implicit solvent model. The PMF for CO₂ approaching MEA from 5 to 1.3 Å is plotted in Figure 4. We see from this figure that the free energy increases with decreasing C–N distance from 5 Å to about 2.1 Å, where it reaches a maximum. This maximum in the free energy corresponds to the transition state structure. The free energy decreases from the transition state to a local minimum at a C–N distance of 1.613 Å, which corresponds to the zwitterion intermediate. The C–N distances for the transition state and zwitterion computed from the PMF calculations are in good agreement with those predicted by ab initio calculations with Bondi (2.156 and 1.609 Å for transition state and zwitterion, respectively) and Pauling (2.138 and 1.584 Å) radii. This indicates that the implicit solvent model with the Bondi and Pauling radii can produce reasonable geometries compared with an explicit solvent model. More importantly, the activation free energy predicted from the PMF calculations is 9.3 ± 0.2 kcal/mol, which is in good agreement with values obtained from B3LYP/B1 calculations with Bondi (9.2 kcal/mol) and Pauling (10.9 kcal/mol) radii. The activation free energy of the reverse reaction (zwitterion to MEA + CO₂) predicted by the PMF calculations is 4.5 ± 0.1 kcal/mol, which is also in good agreement with values obtained from B3LYP/B1 with Bondi (4.3 kcal/mol) and

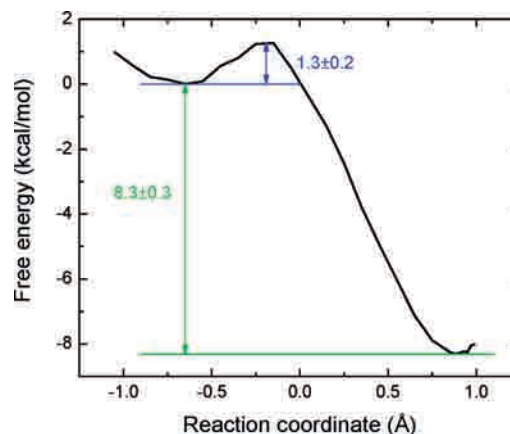


Figure 5. Potential of mean force for complex **2** transforming to complex **3** obtained at the B3LYP/6-311++G(d,p) QM/MM level of theory. The reaction coordinate corresponds to the difference $d_{N-H} - d_{N'-H}$, where d_{N-H} is the N–H bond length in the zwitterion (where the bond is being broken) and $d_{N'-H}$ is the distance between the atoms where bond is being formed, i.e., the N atom on MEA and the H atom leaving the zwitterion. See Figure 1, complex **2** and **TS3**.

Pauling (4.1 kcal/mol) radii. This further indicates that the ab initio scheme we used gives reasonable free energy estimates for the reaction of MEA with CO₂. We note that the activation free energies for zwitterion formation predicted by B3LYP/B1 using the CPCM model with Bondi and Pauling radii are a little lower than those obtained at the CCSD(T)/B1//B3LYP/B1 level with Bondi (10.2 kcal/mol) and Pauling (12.0 kcal/mol) radii. This indicates that use of a higher level of theory increases the activation free energy for the rate-determining step. Moreover, the activation free energies of the reverse reaction (zwitterion to MEA + CO₂) predicted at the CCSD(T)/B1//B3LYP/B1 level with Bondi and Pauling radii are 5.3 and 4.6 kcal/mol, respectively. These values are slightly larger than the corresponding values computed from B3LYP/B1, indicating that use of a higher level of theory increases the kinetic stability of the zwitterion.

We have also carried out additional PMF calculations to estimate the reaction barrier for the second step in the reaction. We have computed the PMF for transforming from complex **2** to **3** (see Figures 2 and 3). The reaction coordinate was chosen to follow the transfer of the proton from the zwitterion complex to the adjacent MEA. We therefore define the reaction coordinate as the difference between the N–H bond length in the zwitterion for the proton being transferred (d_{N-H}) and the bond length between that proton and the N atom in the MEA receiving the proton ($d_{N'-H}$). For example, the reaction coordinate for **TS3** in Figure 1 would be $1.295 - 1.317 = -0.022$ Å, based on B3LYP/B1-optimized geometries. The calculated PMF is presented in Figure 5. The free energy barrier computed from the PMF calculations is 1.3 ± 0.2 kcal/mol at a reaction coordinate of about $d_{N-H} - d_{N'-H} = -0.15$ Å. This value is considerably larger than the free energy barriers computed from CCSD(T)/B1 with the Bondi and Pauling radii, but it is still low enough to be facile at room temperature. As an additional but qualitative probe into the kinetics of the reaction, we have carried out unconstrained QM/MM MD simulations at room temperature starting from complex **2** with initial values of $d_{N'-H}$ between 2 and 3 Å. The proton was observed to transfer in these simulations within about 2 ps. Moreover, similar unconstrained calculations starting from complex **3** resulted in rearrangement of the hydrogen-bonding network to form the carbamate within 3 ps. These calculations indicate that the second reaction step

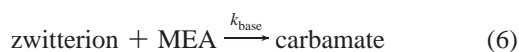
TABLE 5: Smallest Frequency (in cm⁻¹) for the Zwitterion Obtained from the B3LYP and MP2 Methods Using Various Basis Sets^a

method basis set	B3LYP/ 6-311++G(d,p)	B3LYP/ 6-311++G(3df,3pd)	B3LYP/ Aug-cc-pVDZ	B3LYP/ Aug-cc-pVTZ	MP2/ 6-311++G(d,p)	MP2/ Aug-cc-pVDZ
smallest frequency	27.9	25.9	26.3	17.7	58.7	75.7

^a The geometry in each case was obtained at the same level of theory as the frequency calculation.

is essentially spontaneous at room temperature, in agreement with the CCSD(T)/B1 calculations.

3.3. Microkinetic Modeling and Comparison with Experiments. We have developed a microkinetic model using the data from our calculations in order to compare our ab initio calculations with experimental observations. We start from the same assumed reaction scheme as Ali et al.,⁸ noting that this scheme is consistent with our calculations:



Invoking the pseudo-steady-state approximation, the zwitterion concentration can be expressed as

$$[\text{zwitterion}] = \frac{k_2[\text{MEA}][\text{CO}_2]}{k_{-1} + k_{\text{base}}[\text{MEA}]} \quad (7)$$

The overall rate of consumption of CO₂ is therefore

$$r_{\text{CO}_2} = \frac{k_{\text{base}}k_2[\text{MEA}]^2[\text{CO}_2]}{k_{-1} + k_{\text{base}}[\text{MEA}]} \quad (8)$$

We can rewrite eq 8 as

$$r_{\text{CO}_2} = k_o[\text{CO}_2] \quad (9)$$

where the pseudo-first-order reaction rate coefficient k_o is defined as

$$k_o = \frac{k_{\text{base}}k_2[\text{MEA}]^2}{k_{-1} + k_{\text{base}}[\text{MEA}]} \quad (10)$$

In the eqs 7, 8, and 10, the elementary reaction rate coefficients k_2 , k_{-1} , and k_{base} can be calculated using transition state theory as given in eq 4. We have computed k_2 , and k_{-1} using data from our CCSD(T)/B1 calculations with the Pauling radii because the activation free energy with this choice of parameters gave the best agreement with the experimentally measured activation energy. The values of k_2 and k_{-1} at 298 K are calculated from eq 4 to be 1.001×10^5 L/(mol s) and 2.646×10^9 /s. As noted previously, the second step is predicted to be barrier-free so, k_{base} is calculated to be 6.209×10^{12} L/(mol s), independent of temperature. These values can be combined with the concentration of MEA in order to compute k_o and the pseudo-steady-state concentration of the zwitterions.

As discussed in the Introduction, no experiments have been able to detect the presence of zwitterions in the MEA + CO₂

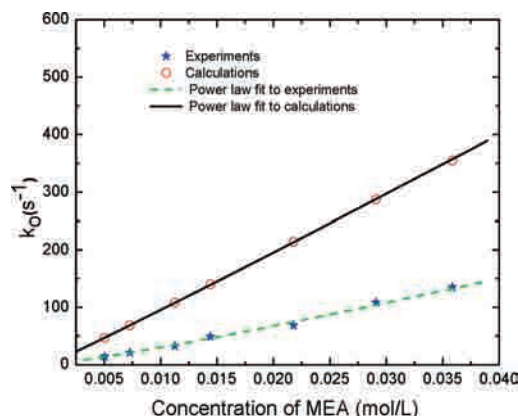


Figure 6. Pseudo-first-order reaction rate coefficient k_o calculated with the use of energetic data at CCSD(T)/B1//B3LYP/B1 with Pauling radii and experimental data from Ali et al.⁸ in the concentration range of MEA from 0.005 to 0.035 mol/L. Power law fits to the formula $k_o = a[\text{MEA}]^n$ are also plotted for the calculated and experimental k_o values. The fitted values are $n = 1.0$ and 1.2 for the calculated and experimental data, respectively.

reaction, despite experimental evidence supporting the zwitterion mechanism (mechanism I in Scheme I). We here apply two different tests to explore possible reasons for the inability to observe the zwitterion during the reactions. First, we investigate whether or not the structure is a real minimum or a metastable configuration. For example, if the zwitterion is actually a transition state, then it would not be experimentally observable due to its very short lifetime. Second, we compute the steady-state concentration of the zwitterion from our microkinetic model. If this concentration is very small, then we would also not expect to be able to observe the zwitterion in experiments. In order to test for stability, we have computed the vibrational frequencies of the zwitterion using the CPCM model. Both the B3LYP and MP2 methods with various basis sets were used to optimize the geometry of the zwitterion, followed by frequency calculations at the same theory of level as the geometry optimizations. The smallest vibrational frequencies computed from each method are listed in Table 5, from which we can see that all frequencies are positive. This indicates that the zwitterion is very likely a stable intermediate. Next, we have computed the concentration of the zwitterion from eq 7 taking concentrations of MEA to be 5 mol/L, in agreement with a recent NMR experiment.⁵⁷ We take the concentration of CO₂ to be 0.03 mol/L, which is the saturation concentration for CO₂ in water at 298 K and 1 bar. These values, along with the values of the reaction rate coefficients give the concentration of zwitterions to be 4.8×10^{-11} mol/L. This exceedingly small concentration would be very difficult to observe experimentally and therefore our model provides a simple explanation for the lack of direct evidence for the zwitterion during the MEA+CO₂ reaction.

We have computed the value of k_o as a function of concentration of MEA at 298 K and have plotted these data in Figure 6 in order to compare our calculations with the experimental data of Ali et al.,⁸ which are also plotted in Figure 6. We see that the calculated values of k_o at the CCSD(T)/B1 level with Pauling radii are about 4 times higher than the

experimental data. We note that the kinetic data are extremely sensitive to the reaction energy surface; e.g., a 1 kcal/mol difference in the activation energy for an elementary reaction step can lead to a factor of 10 difference in the reaction rate coefficient. This problem has been discussed in detail by Miller and Klippenstein for the $C_2H_5 + O_2$ reaction.⁵⁸ Computing the reactant and transition state geometries at a high level of theory, such as CCSD(T), and extrapolating the results to the complete basis set limit would likely improve the agreement with experiments. However, this level of effort exceeds our computational capabilities at present. More importantly, we do not expect the basic mechanism to change if one were to carry out such calculations. Hence, our calculations provide a qualitatively accurate picture of the reaction mechanism at an acceptable level of computational cost.

We have fitted our calculated values of k_0 to an empirical power-law kinetics formula to obtain an estimate of the effective order of rate expression given in eq 10. The reaction order in MEA is calculated to be 1.0, which is in reasonable agreement with the experimental value of about 1 from Blouwhoff et al.¹⁵ and the experimental value of 1.2 from Ali et al.⁸ This result can also be directly obtained from eq 10 by noting that, when $k_{-1} \ll k_{base}[MEA]$, then the reaction will be effectively first-order in the concentration of MEA. The smallest value of $k_{base}[MEA]$ is 3.1×10^{10} , corresponding to $[MEA] = 0.005$ mol/L in Figure 6. This is still more than 1 order of magnitude larger than k_{-1} , confirming that the effective order is unity in [MEA].

We have also used the PMF data to compute the effective reaction order in MEA as a further check of the consistency between our CCSD(T)/B1 calculations and the PMF simulations. We have found that use of the reaction barriers computed from PMF data in the microkinetic model gives a value of 1.26 for the reaction order in MEA, whereas use of just the second step data from PMF with CCSD(T)/B1 data for the first step gives 1.2. These values are in good agreement with the CCSD(T)/B1 predictions, giving further credence to the consistency of our calculations.

4. Conclusion

We have studied the reaction of CO_2 with MEA using both ab initio transition state calculations utilizing an effective solvent model and potential of mean force calculations using B3LYP/B1 QM/MM MD simulations. The results indicate that a two-step reaction mechanism involving a zwitterion intermediate is the most favorable reaction channel for forming carbamate. Our calculations indicate that the formation of the zwitterion is the rate-determining step and the H-abstraction process from zwitterion in the second step is nearly barrier-free. The activation free energies for the rate-determining step are 12.0 (10.2) and 11.3 (9.6) kcal/mol using Pauling (Bondi) radii within the CPCM model at the CCSD(T)/B1//B3LYP/B1 and CCSD(T)/B2//B3LYP/B1 level, respectively. These values are in reasonable agreement with the experimental value of about 12.4 kcal/mol.^{6–10} However, use of other atomic radii such as UFF, UAHF, UA0, and UAKS underestimate the activation free energy for the rate-determining step. The second step is revealed to be an acid–base reaction between the zwitterion and MEA. The calculated pK_a value for the zwitterion is 3.3, which for comparison is similar to acetic acid. We have constructed a microkinetic model for the reaction mechanism that gives qualitative agreement with experiments and predicts an equilibrium concentrations of the zwitterion species to be on the order of 10^{-11} mol/L. This very small concentration of zwitterions explains why experiments

have thus far failed to observe the existence of zwitterions during the reaction. The effective rate coefficient, k_0 , calculated from our model is close to that observed in experiments.⁸ The effective reaction order from our model is close to unity, also in agreement with experiments. The potential of mean force calculations using a B3LYP/B1 QM/MM MD approach verifies that the ab initio scheme we used is reliable for predicting the reaction mechanism of MEA with CO_2 .

Acknowledgment. This material is based upon work supported by the Department of Energy, National Energy Technology Laboratory under Award Number DE-NT0005310. Most of the calculations were performed at the University of Pittsburgh's Center for Simulation and Modeling. This work was performed in support of the National Energy Technology Laboratory's ongoing research in the area of carbon management under the RDS contract DE-AC26-04NT41817. Y.Z. would like to acknowledge the support by NSF (CHE-CAREER-0448156, and TeraGrid computing resources) and NYU-ITS (computing resources). This report was prepared as an account of work sponsored by an agency of the United States Government. Neither the United States Government nor any agency thereof, nor any of their employees, makes any warranty, express or implied, or assumes any legal liability or responsibility for the accuracy, completeness, or usefulness of any information, apparatus, product, or process disclosed, or represents that its use would not infringe privately owned rights. Reference herein to any specific commercial product, process, or service by trade name, trademark, manufacturer, or otherwise does not necessarily constitute or imply its endorsement, recommendation, or favoring by the United States Government or any agency thereof. The views and opinions of authors expressed herein do not necessarily state or reflect those of the United States Government or any agency thereof.

References and Notes

- (1) Ciferno, J. P.; Fout, T. E.; Jones, A. P.; Murphy, J. T. *Chem. Eng. Prog.* **2009**, *105*, 33.
- (2) Liu, Y. D.; Zhang, L. Z.; Watanasiri, S. *Ind. Eng. Chem. Res.* **1999**, *38*, 2080.
- (3) Veawab, A.; Tontiwachwuthikul, P.; Chakma, A. *Ind. Eng. Chem. Res.* **1999**, *38*, 3917.
- (4) IEA. *Prospects for CO_2 capture and storage*; 2004; <http://www.iea.org/textbase/nppdf/free/2004/prospects.pdf>.
- (5) Murphy, J. T.; Jones, A. P. *DOE/NETL's Carbon Capture R&D Program for Existing Coal-Fired Power Plants*; DOE/NETL-2009/1356; February 2009; <http://www.netl.doe.gov/technologies/coalpower/ewr/co2/pubs/EPEC%20CO2%20capture%20program%20overview%20feb09.pdf>.
- (6) Hikita, H.; Asai, S.; Katsuo, Y.; Ikuno, S. *AIChE J.* **1979**, *25*, 793.
- (7) Alper, E. *Ind. Eng. Chem. Res.* **1990**, *29*, 1725.
- (8) Ali, S. H. *Int. J. Chem. Kinet.* **2005**, *37*, 391.
- (9) Penny, B. D. E.; Ritter, T. J. *J. Chem. Soc., Faraday Trans. 1* **1983**, *79*, 2103.
- (10) Hikita, H.; Asai, S.; Ishikawa, H.; Honda, M. *Chem. Eng. J.* **1977**, *13*, 7.
- (11) Shim, J. G.; Kim, J. H.; Jhon, Y. H.; Kim, J.; Cho, K. H. *Ind. Eng. Chem. Res.* **2009**, *48*, 2172.
- (12) da Silva, E. F.; Svendsen, H. F. *Ind. Eng. Chem. Res.* **2004**, *43*, 3413.
- (13) Arstad, B.; Blom, R.; Swang, O. *J. Phys. Chem. A* **2007**, *111*, 1222.
- (14) Danckwerts, P. V. *Chem. Eng. Sci.* **1979**, *34*, 443.
- (15) Blouwhoff, P. M. M. V.; G. E.; Van Swaij, W. P. M. *Chem. Eng. Sci.* **1983**, *38*, 1411.
- (16) Caplow, M. *J. Am. Chem. Soc.* **1968**, *90*, 6795.
- (17) Frisch, M. J.; Trucks, G. W.; Schlegel, H. B.; Scuseria, G. E.; Robb, M. A.; Cheeseman, J. R.; Montgomery, J. J. A.; Vreven, T.; Kudin, K. N.; Burant, J. C.; Millam, J. M.; Iyengar, S. S.; Tomasi, J.; Barone, V.; Mennucci, B.; Cossi, M.; Scalmani, G.; Rega, N.; Petersson, G. A.; Nakatsuji, H.; Hada, M.; Ehara, M.; Toyota, K.; Fukuda, R.; Hasegawa, J.; Ishida, M.; Nakajima, T.; Honda, Y.; Kitao, O.; Nakai, H.; Klene, M.; Li, X.; Knox, J. E.; Hratchian, H. P.; Cross, J. B.; Bakken, V.; Adamo, C.; Jaramillo, J.; Gomperts, R.; Stratmann, R. E.; Yazyev, O.; Austin, A. J.;

- Cammi, R.; Pomelli, C.; Ochterski, J. W.; Ayala, P. Y.; Morokuma, K.; Voth, G. A.; Salvador, P.; Dannenberg, J. J.; Zakrzewski, V. G.; Dapprich, S.; Daniels, A. D.; Strain, M. C.; Farkas, O.; Malick, D. K.; Rabuck, A. D.; Raghavachari, K.; Foresman, J. B.; Ortiz, J. V.; Cui, Q.; Baboul, A. G.; Clifford, S.; Cioslowski, J.; Stefanov, B. B.; Liu, G.; Liashenko, A.; Piskorz, P.; Komaromi, I.; Martin, R. L.; Fox, D. J.; Keith, T.; Al-Laham, M. A.; Peng, C. Y.; Nanayakkara, A.; Challacombe, M.; Gill, P. M. W.; Johnson, B.; Chen, W.; Wong, M. W.; Gonzalez, C.; Pople, J. A. *Gaussian 03*, 2004.
- (18) Lee, T. J.; Taylor, P. R. *Int. J. Quantum Chem.* **1989**, *23*, 199.
- (19) Barone, V.; Cossi, M. *J. Phys. Chem. A* **1998**, *102*, 1995.
- (20) Cossi, M.; Rega, N.; Scalmani, G.; Barone, V. *J. Comput. Chem.* **2003**, *24*, 669.
- (21) Mierts, S.; Scrocco, E.; Tomasi, J. *J. Chem. Phys.* **1981**, *55*, 117.
- (22) Cancès, E.; Mennucci, B.; Tomasi, J. *J. Chem. Phys.* **1997**, *107*, 3032.
- (23) Tomasi, J.; Persico, M. *Chem. Rev.* **1994**, *94*, 2027.
- (24) Barone, V. C., M.; Tomasi, J. *J. Chem. Phys.* **1997**, *107*, 3210.
- (25) Warshel, A.; Levitt, M. *J. Mol. Biol.* **1976**, *103*, 227.
- (26) Singh, U. C.; Kollman, P. A. *J. Comput. Chem.* **1986**, *7*, 718.
- (27) Field, M. J.; Bash, P. A.; Karplus, M. *J. Comput. Chem.* **1990**, *11*, 700.
- (28) Mulholland, A. J. *Drug Discovery Today* **2005**, *10*, 1393.
- (29) Zhang, Y. K. *Theor. Chem. Acc.* **2006**, *116*, 43.
- (30) Hu, H.; Yang, W. T. *Annu. Rev. Phys. Chem.* **2008**, *59*, 573.
- (31) Patey, G. N.; Valleau, J. P. *J. Chem. Phys.* **1975**, *63*, 2334.
- (32) Roux, B. *Comput. Phys. Commun.* **1995**, *91*, 275.
- (33) Boczko, E. M.; Brooks, C. L. *J. Phys. Chem.* **1993**, *97*, 4509.
- (34) Jorgensen, W. L.; Chandrasekhar, J.; Madura, J. D.; Impey, R. W.; Klein, M. L. *J. Chem. Phys.* **1983**, *79*, 926.
- (35) Kumar, S.; Bouzida, D.; Swendsen, R. H.; Kollman, P. A.; Rosenberg, J. M. *J. Comput. Chem.* **1992**, *13*, 1011.
- (36) Souaille, M.; Roux, B. *Comput. Phys. Commun.* **2001**, *135*, 40.
- (37) Ferrenberg, A. M.; Swendsen, R. H. *Phys. Rev. Lett.* **1988**, *61*, 2635.
- (38) Wang, S. L.; Hu, P.; Zhang, Y. K. *J. Phys. Chem. B* **2007**, *111*, 3758.
- (39) Hu, P.; Wang, S. L.; Zhang, Y. K. *J. Am. Chem. Soc.* **2008**, *130*, 16721.
- (40) Hu, P.; Wang, S.; Zhang, Y. *J. Am. Chem. Soc.* **2008**, *130*, 3806.
- (41) Lu, Z. Y.; Zhang, Y. K. *J. Chem. Theory Comput.* **2008**, *4*, 1237.
- (42) Ke, Z. H.; Wang, S. L.; Xie, D. Q.; Zhang, Y. K. *J. Phys. Chem. B* **2009**, *113*, 16705.
- (43) Ke, Z. H.; Zhou, Y. Z.; Hu, P.; Wang, S. L.; Xie, D. Q.; Zhang, Y. K. *J. Phys. Chem. B* **2009**, *113*, 12750.
- (44) Zheng, H.; Wang, S. L.; Zhang, Y. K. *J. Comput. Chem.* **2009**, *30*, 2706.
- (45) Wu, R. B.; Hu, P.; Wang, S. L.; Cao, Z. X.; Zhang, Y. K. *J. Chem. Theory Comput.* **2010**, *6*, 337.
- (46) Zhou, Y. Z.; Wang, S. L.; Zhang, Y. K. *J. Phys. Chem. B* **2010**, *114*, 8817.
- (47) Shao, Y.; Molnar, L. F.; Jung, Y.; Kussmann, J.; Ochsenfeld, C.; Brown, S. T.; Gilbert, A. T. B.; Slipchenko, L. V.; Levchenko, S. V.; O'Neill, D. P.; DiStasio, R. A.; Lochan, R. C.; Wang, T.; Beran, G. J. O.; Besley, N. A.; Herbert, J. M.; Lin, C. Y.; Van Voorhis, T.; Chien, S. H.; Sodt, A.; Steele, R. P.; Rassolov, V. A.; Maslen, P. E.; Korambath, P. P.; Adamson, R. D.; Austin, B.; Baker, J.; Byrd, E. F. C.; Dachsel, H.; Doerksen, R. J.; Dreuw, A.; Dunietz, B. D.; Dutoi, A. D.; Furlani, T. R.; Gwaltney, S. R.; Heyden, A.; Hirata, S.; Hsu, C. P.; Kedziora, G.; Khalliulin, R. Z.; Klunzinger, P.; Lee, A. M.; Lee, M. S.; Liang, W.; Lotan, I.; Nair, N.; Peters, B.; Proynov, E. I.; Pieniazek, P. A.; Rhee, Y. M.; Ritchie, J.; Rosta, E.; Sherrill, C. D.; Simmonett, A. C.; Subotnik, J. E.; Woodcock, H. L.; Zhang, W.; Bell, A. T.; Chakraborty, A. K.; Chipman, D. M.; Keil, F. J.; Warshel, A.; Hehre, W. J.; Schaefer, H. F.; Kong, J.; Krylov, A. I.; Gill, P. M. W.; Head-Gordon, M. *Phys. Chem. Chem. Phys.* **2006**, *8*, 3172.
- (48) Ponder, J. W. *TINKER, Software Tools for Molecular Design, Version 4.2*; June 2004.
- (49) Beeman, D. *J. Comput. Phys.* **1976**, *20*, 130.
- (50) Berendsen, H. J. C.; Postma, J. P. M.; van Gunsteren, W. F.; DiNola, A.; Haak, J. R. *J. Chem. Phys.* **1984**, *81*, 3684.
- (51) da Silva, E. F.; Kuznetsova, T.; Kvamme, B.; Merz, K. M. *J. Phys. Chem. B* **2007**, *111*, 3695.
- (52) Pliego, J. R., Jr.; Riveros, J. M. *J. Phys. Chem. A* **2004**, *108*, 2520.
- (53) Pliego, J. R., Jr.; Riveros, J. M. *J. Phys. Chem. A* **2002**, *106*, 7434.
- (54) Pliego, J. R., Jr.; Riveros, J. M. *J. Phys. Chem. A* **2001**, *105*, 7241.
- (55) Ding, F. Z.; Smith, J. M.; Wang, H. B. *J. Org. Chem.* **2009**, *74*, 2679.
- (56) Pliego, J. R., Jr.; Riveros, J. M. *Phys. Chem. Chem. Phys.* **2002**, *4*, 1622.
- (57) Fan, J. G.; Wee, A. G. H.; Idem, R.; Tontiwachwuthikul, P. *Ind. Eng. Chem. Res.* **2009**, *48*, 2717.
- (58) Miller, J. A.; Klippenstein, S. J. *Int. J. Chem. Kinet.* **2001**, *33*, 654.